



UNIVERSITY OF
BIRMINGHAM

Investigating the Changes in the Geophysical and Geotechnical Properties of Fine-grained Soils when Exposed to Changes in Vertically Applied Loads

by

Anna Farooqy

A thesis submitted to
the University of Birmingham
for the degree of
Doctor of Philosophy

School of Civil Engineering
College of Engineering and Physical Sciences
University of Birmingham
January 2018

UNIVERSITY OF
BIRMINGHAM

University of Birmingham Research Archive

e-theses repository

This unpublished thesis/dissertation is copyright of the author and/or third parties. The intellectual property rights of the author or third parties in respect of this work are as defined by The Copyright Designs and Patents Act 1988 or as modified by any successor legislation.

Any use made of information contained in this thesis/dissertation must be in accordance with that legislation and must be properly acknowledged. Further distribution or reproduction in any format is prohibited without the permission of the copyright holder.

ABSTRACT

Geophysical techniques have the potential to advance understanding of the ground's behaviour by providing spatial and temporal information. However, correlations between the geophysical and geotechnical properties of soil with respect to changing environmental conditions seem to be poorly understood.

Fine-grained soils containing clay minerals are known to have the potential to experience considerable changes in geotechnical properties when exposed to external loads. These could lead to the loss of mechanical performance or the catastrophic failure of geotechnical assets. In order to prevent catastrophic-failure events and/or avoid the costly replacement of infrastructure, the long-term monitoring of geotechnical assets' 'health' should be considered. This can be supported by the implementation of geophysical sensing. Therefore, this research explored simple geophysical sensing techniques, which could enable the monitoring of the condition of the ground over the long term, and provide a warning system, based on correlations between geotechnical and geophysical parameters.

Fine-grained soils of differing plasticities were exposed to changes in vertical loading and unloading in bespoke experimental chambers developed for this study. The monitoring of geotechnical parameters focused on the volumetric water content (VWC), gravimetric water content (GWC), void ratio (e) and pore-water pressure (u). The geophysical properties investigated were apparent permittivity (AP), which was measured using time domain reflectometry (TDR); bulk electric conductivity (BEC), in a kHz frequency range, which was measured using TDR; and bulk electrical conductivity (EC) in a Hz frequency range,

measured with electrical resistivity (ER). The research studied the correlations between the geophysical and geotechnical parameters, and, furthermore, the effect of the orientation of the geophysical instrumentation, in relation to the load, on these relationships. The influence of the pore fluid's electrical conductivity and the measurement technique (ER/TDR) on the BEC was also explored.

For what is believed to be the first time, TDR measurements were carried out continuously, and in both the vertical and horizontal directions during the volumetric changes of the soil samples, which were induced by changes in the loading conditions. In addition, the TDR testing was run simultaneously with taking ER measurements, utilising the capacity of the bespoke test chambers and a custom-built acquisition system.

It is clear from the trends observed that vertically measured AP (AP_v) can detect a decrease in the void ratio with loading, and, to a lesser extent, changes in the void ratio with the swelling associated with unloading. Horizontally monitored AP (AP_h) varied slightly with respect to the AP_v , as it appears to correspond with the pore-water-pressure distribution. The combination of which suggests that TDR could be used for the continuous monitoring of settlement in real time during increased loading, and potentially (further research is required to confirm this) identify swelling and warn of the potential loss of strength that these soils may experience as a result.

Unlike the AP results, the BEC and EC readings were not found to be suitable for continuous monitoring due to inconsistent correlation with the void ratio. Nonetheless, it was concluded that their response is affected more strongly by pore connectivity within the soil

rather than by the void ratio, which indicates that the saturated soil becomes more electrically conductive shortly after the load is applied.

It is envisaged that monitoring the relative changes in AP and BEC over time, in conjunction with spatially distributed ER arrays, would enhance traditional geotechnical monitoring by providing a temporal indication of the soil's response to load under near-saturated conditions. Trigger levels could be set for the geophysical parameters correlated with the geotechnical implications, and, if exceeded, prompt for inspections or interventions.

The AP and BEC responses of the vertical and horizontal TDR probes indicates the potential application of TDR in monitoring during the vertical-loading process, with AP_v readings providing 5% accuracy in VWC prediction and a 10% accuracy in e prediction.

To my Mother; my Husband Yahr; Sadaf; and Hadyah

ACKNOWLEDGEMENTS

First and foremost, I would like to express my sincere gratitude to my supervisors – Professor David Chapman, Doctor Alexander Royal and Doctor Giulio Curioni – for their invaluable guidance, support and understanding, which was provided throughout the course of my research.

I greatly appreciate the financial support provided by Professor Chris Rogers on behalf of the Assessing the Underworld Project (ATU) and the UK's Engineering and Physical Sciences Research Council (EPSRC).

My special thanks go to Mr Phil Atkins for his help and support. I am also very grateful to Mr Phil Atkins and Dr Farzad Hayati for building the electrical-resistivity-acquisition system, and for all their time and patience during the initial trials.

I would also like to express my deep gratitude to Professor Nigel Cassidy for his invaluable advice, enthusiasm and support, and for helping me to see the bigger picture.

I am very grateful to the technical team, particularly Mr Jim Guest for his help, kindness and for building the equipment, and to Mr Luis Portela for his supportive and caring attitude.

My sincere thanks go to Mr David Gunn and Mr Ben Dashwood for introducing me to the electrical-resistivity measurements. Many thanks go to Dr Ali Sadeghioon for providing me with the temperature-acquisition system and for the help in setting it up.

I would also like to thank Dr Eimear Orgill at the School of Geography, Earth Sciences and Environmental Sciences for her help in conducting spectroscopy testing, and Mr Paul Stanley for his assistance in undertaking electron-microscopy scans.

I would like to convey my great thanks to my reviewers – Professor Ian Jefferson and Professor Nicole Metje – for their valued feedback during the annual progress reviews.

I feel fortunate that I have had the chance to visit several scientific institutions during my research. I am grateful to Professor Wojciech Skierucha, Dr Andrzej Wilczek, Dr Agnieszka Szyplowska and Dr Anna Krol at the Institute of Agrophysics in Lublin for the warm welcome, and for introducing me to their research on TDR and soil.

Many thanks to all my friends and colleagues for their support. I would especially like to thank Dr Woroud Melhem and Dr Nesreen Al-Obaidy for their inspiration and support.

My deep and sincere gratitude goes to my family for their love: my Husband Yahr, for his encouragement and support; my Mother for all her help; and my daughters Sadaf and Hadyah for their beautiful hearts.

This thesis was copy-edited for the conventions of language, spelling and grammar by Safis Editing.

TABLE OF CONTENTS

UNIVERSITY OF BIRMINGHAM RESEARCH ARCHIVE.....	I
ABSTRACT	II
ACKNOWLEDGEMENTS.....	VI
TABLE OF CONTENTS	VIII
TABLES	XII
FIGURES	XIV
ABBREVIATIONS, ACRONYMS AND SYMBOLS.....	XX
CHAPTER 1: INTRODUCTION.....	1
1.1 BACKGROUND	1
1.2 AIM AND OBJECTIVES	3
1.3 STRUCTURE OF THE THESIS	5
CHAPTER 2: LITERATURE REVIEW	7
2.1 SCOPE.....	7
2.2 FINE-GRAINED SOILS' GEOTECHNICAL PARAMETERS.....	9
2.2.1 FINE-GRAINED SOILS.....	9
2.2.2 CLAYS AND THEIR INTERACTION WITH PORE FLUID.....	9
2.2.3 FINE-GRAINED-SOIL-VOLUME CHANGE UNDER VERTICAL LOAD APPLICATION.....	13
2.3 GEOPHYSICAL TECHNIQUES AND SOIL-VOLUME-CHANGE INVESTIGATION	16
2.3.1 GEOPHYSICAL TECHNIQUES	16
2.3.2 SELECTED GEOPHYSICAL TECHNIQUES (ER AND TDR), AND THEIR APPLICATION IN FINE-GRAINED-SOIL VOLUME MONITORING	20
2.4 ELECTROMAGNETIC PROPERTIES OF SOIL.....	23
2.4.1 DIELECTRIC PERMITTIVITY.....	24
2.4.2 ELECTRICAL CONDUCTIVITY	30
2.4.3 ELECTRICAL RESISTIVITY.....	32
2.5 FINE-GRAINED-SOIL VOLUME-CHANGE CORRELATIONS WITH AP, BEC AND ρ	36
2.5.1 AP-SOIL WATER CONTENT	36
2.5.1.1 AP-VWC	36
2.5.1.2 AP-VWC TDR-PROBE ORIENTATION.....	39
2.5.1.3 AP-GWC	40
2.5.2 AP-VOID RATIO.....	42
2.5.3 BEC AND EC-VOID RATIO	43
2.5.4 BEC-VWC.....	47
2.6 SUMMARY AND IDENTIFICATION OF KNOWLEDGE GAPS.....	48
CHAPTER 3: OVERARCHING RESEARCH PHILOSOPHY AND METHODS.....	51
3.1 TESTING PROGRAMME OVERVIEW.....	53
3.2 SOIL CHARACTERISATION.....	55
3.2.1 INDEX TESTING	56

3.2.2	PARTICLE DENSITY	58
3.2.3	OEDOMETER	60
3.3	DEVELOPMENT OF THE TESTING EQUIPMENT.....	70
3.3.1	LOADING ARRANGEMENT.....	71
3.3.1.1	PRESSURE SYSTEM 1 (PS1).....	71
3.3.1.2	PRESSURE SYSTEM 2 (PS2).....	74
3.3.1.3	BESPOKE CHAMBER-SAMPLE SIZE	77
3.3.1.4	SAMPLE PREPARATION AND VALIDATION OF SAMPLE UNIFORMITY	79
3.3.2	BESPOKE LOADING-ARRANGEMENT CONSTRAINTS.....	82
3.3.2.1	PRESSURE-HEAD DIFFERENCE.....	82
3.3.2.2	LOAD TRANSFER and FRICTION	84
3.3.2.3	PARTIAL SATURATION.....	86
3.3.3	SHEAR STRENGTH.....	89
3.3.3.1	HAND-SHEAR-VANE SOIL-SHEAR-STRENGTH MEASUREMENTS	89
3.3.3.2	FALL-CONE SOIL-SHEAR-STRENGTH MEASUREMENTS	91
3.3.4	TEMPERATURE	92
3.4	PORE-FLUID TESTING	93
CHAPTER 4:	DEVELOPMENT OF THE BESPOKE TDR ARRANGEMENT	96
4.1	BESPOKE TDR CHAMBER	96
4.2	PORE-WATER-PRESSURE MEASUREMENTS IN THE BESPOKE TDR CHAMBER ..	98
4.3	TDR ACQUISITION SYSTEM.....	100
4.3.1	TDR-PROBE CALIBRATION	102
4.3.1.1	TDR CALIBRATION – AP.....	102
4.3.1.2	TDR CALIBRATION-BEC	105
4.3.1.3	CONTAINER-SIZE EFFECT ON TDR MEASUREMENTS.....	109
4.3.2	TDR DATA QUALITY	111
4.4	INITIAL SOIL-LOADING TESTING IN THE BESPOKE TDR CHAMBER (PS1)	116
4.5	INITIAL SOIL-LOADING TESTING IN THE BESPOKE TDR CHAMBER (PS2)	118
4.6	PORE-WATER-PRESSURE MEASUREMENTS IN A BESPOKE TDR CHAMBER ...	120
4.7	TDR INSTRUMENTATION’S EFFECT ON THE PROGRESS OF SETTLEMENT	123
4.7.1	TDR – FLUORESCIEIN TESTING.....	124
4.7.2	SEM-TDR	125
4.8	PRESSURE EFFECT ON THE TDR MEASUREMENTS IN FLUIDS.....	127
CHAPTER 5:	DEVELOPMENT OF THE BESPOKE ER ARRANGEMENT.....	129
5.1	PRELIMINARY ER TESTING.....	130
5.1.1	ER BOXES	130
5.1.2	ER-ACQUISITION SYSTEM ‘T’	132
5.1.3	ER-ACQUISITION SYSTEM I (ER-ACQ-I).....	132
5.1.4	TEMPERATURE EFFECT ON ρ	134
5.1.5	ER DATA QUALITY.....	138
5.1.6	PRELIMINARY ER-TESTING SUMMARY	139

5.2	ER ARRANGEMENT I (PS1)	139
5.2.1	ER CHAMBER I	139
5.2.2	ER ARRANGEMENT I – CONFIGURATIONS	143
5.2.3	ER ARRANGEMENT I – CALIBRATION.....	145
5.2.4	BESPOKE ER ARRANGEMENT I – SOIL TESTING	149
5.2.5	BESPOKE ER ARRANGEMENT I – INITIAL SOIL TEST RESULTS	150
5.3	ER ARRANGEMENT II (PS2)	153
5.3.1	ER CHAMBER II AND ELECTRODE DESIGN	153
5.3.2	ER-ACQUISITION SYSTEM II.....	155
5.3.3	ER ARRANGEMENT II – CONFIGURATIONS.....	157
5.3.3.1	ER-ACQ-II CONFIGURATION APPROACH 1	157
5.3.3.2	ER-ACQ-II CONFIGURATION APPROACH 2	160
5.3.4	ER ARRANGEMENT II – CALIBRATION.....	161
5.3.5	ER ARRANGEMENT I AND II – SOIL TESTING	163
5.3.6	ER ARRANGEMENT II SUMMARY	164
CHAPTER 6:	RESULTS	165
6.1	INTRODUCTION	165
6.2	ELECTROMAGNETIC RESPONSE TO LOADING AND THE SUBSEQUENT CONSOLIDATION OF THE SOIL SAMPLES	168
6.2.1	INITIAL TDR RESPONSE PRIOR TO THE APPLICATION OF THE LOAD	168
6.2.2	AP_V AND AP_H RESPONSES TO THE APPLICATION OF A LOAD AND THE SUBSEQUENT CONSOLIDATION.....	169
6.2.2.1	AP_H RESPONSE – CONSOLIDATION MECHANISM	174
6.2.2.2	AP_H RESPONSE: SEEPAGE FORCES.....	176
6.2.3	RELATIONSHIP BETWEEN AP AND VOID RATIO.....	181
6.2.4	RELATIONSHIP BETWEEN BEC AND VOID RATIO	183
6.2.5	RELATIONSHIP BETWEEN ρ_v AND VOID RATIO	193
6.2.5.1	CH SAMPLES – PS1 ARRANGEMENT	196
6.2.5.2	CI SAMPLES – PS2 ARRANGEMENT	198
6.2.6	TDR RESPONSE TO PORE-WATER-PRESSURE-INDUCED CHANGES	203
6.3	ELECTROMAGNETIC RESPONSE OF THE SAMPLES TO UNLOADING	208
6.4	CORRELATIONS BETWEEN THE GEOTECHNICAL AND GEOPHYSICAL PARAMETERS	211
6.4.1	VWC’S RELATIONSHIP WITH AP IN SATURATED SOILS	212
6.4.1.1	VWC- AP IN RELATION TO TOPP’S MODEL	212
6.4.1.2	VWC- AP CORRELATION.....	215
6.4.1.3	VWC-REFRACTIVE INDEX CORRELATION.....	216
6.4.2	GWC RELATIONSHIP WITH AP	219
6.4.3	VOID-RATIO RELATIONSHIP WITH AP IN SATURATED SOILS.....	220
6.4.3.1	VOID RATIO- AP CORRELATION	220
6.4.3.2	VOID RATIO-REFRACTIVE INDEX CORRELATION	222
6.4.4	BEC CORRELATION WITH VWC AND VOID RATIO.....	224

6.4.5	ESTIMATING CONSOLIDATION STAGE BASED ON AP, BEC AND ρ	225
6.5	SUMMARY OF THE RESULTS AND DISCUSSION	227
CHAPTER 7:	CONCLUSIONS AND RECOMMENDATIONS FOR FURTHER WORK.....	232
7.1	RESEARCH OUTCOMES AND CONCLUSIONS.....	232
7.2	RECOMMENDATIONS FOR FURTHER WORK.....	238
LIST OF REFERENCES	241

TABLES

Page No.

Table 2.1. Selection of geophysical methods currently used to investigate the ground for engineering purposes	17
Table 2.2. General summary of the correlations between geotechnical and geophysical parameters (Liu, 2007).....	19
Table 2.3. Examples of common electrical-resistivity arrays (Samouëlian et al., 2005)	34
Table 2.4. Typical range of electrical resistivity/conductivity of common earth materials (Samouëlian et al., 2005)	35
Table 3.1. Index test results of the soil mixtures.....	57
Table 3.2. Particle density of selected soils measured in a helium pycnometer	60
Table 3.3. Oedometer test C_c and C_s results.....	63
Table 3.4. Reference soil properties	64
Table 3.5. Oedometer test results – CL	68
Table 3.6. Oedometer test results – CI	69
Table 3.7. Oedometer test results – CH.....	70
Table 3.8. Post-loading sample-uniformity verification (sand content) in four samples (CH.S4.TDR, CI.S6.ER, CH.S5.ER and CI.S10.N)	82
Table 3.9. Samples with a saturation degree below 100%.....	87
Table 4.1. TDR conductivity of calibration solutions	106
Table 4.2. TDR-probe calibration parameters (TDR57600)	109
Table 4.3. The precision of AP and BEC measurements in soil (for the bespoke TDR chamber prior to the load application).....	113
Table 4.4. Accuracy and precision of BEC measurements in a saline solution.....	115
Table 4.5. Testing carried out with TDR (PS2) approach (P - pore-water pressure)	120
Table 4.6. Pressure-sensor specification	121
Table 4.7. TDR measurements for CI.S7.TDR with fluorescein.....	125
Table 5.1. ρ variations in CH and CI, with temperature measured at the LL in the McMiller boxes	136
Table 5.2. ER percentage change per 1 °C measured in CH and CI at their LL in the McMiller Boxes	137

Table 5.3. ER Chamber I electrode configurations	144
Table 5.4. ER Chamber I calibration solutions	145
Table 5.5. ER Chamber I geometric-factor calibration results (vertical Wenner configurations).....	147
Table 5.6. ER Chamber I geometric-factor (K) calibration results (horizontal dipole-dipole configurations).....	147
Table 5.7. Accuracy of vertical and horizontal ρ measurements in ER Chamber I based on the adopted geometric factors	148
Table 5.8. RE estimation based on the ρ measurement in the CH.S02.ER sample during loading in the bespoke ER chamber I	150
Table 5.9. ER-Acq-II reference-resistor (1 k Ω) calibration results	156
Table 5.10. Accuracy of vertical ρ measurements in ER Chamber II based on the adopted geometric factor	162
Table 5.11. Soil-loading ER-testing summary	163
Table 6.1. Summary of the tests carried out in the bespoke ER and TDR chambers	167
Table 6.2. Conductivity of the soil mixtures measured with TDR in relation to the pore-fluid conductivity (measured with low frequency [11 Hz] resistivity method)	187
Table 6.3. Cation concentrations observed in pore fluid diluted in HNO ₃ (measured using ICP-OES, with detection limits of 0.5 mg/l to 200 mg/l).....	188

FIGURES

	Page No.
Figure 2.1. Water in soil (Saarenketo, 1998)	12
Figure 2.2. Variation of the complex permittivity components (Cassidy, 2009)	26
Figure 2.3. Relaxation types with regards to soil type (Zambrano et al., 2006).....	28
Figure 2.4. GWC prediction based on a soil's specific AP/d _d relationship in sandy clay (DCF) and silty sand (DPF) (Thring et al., 2014)	41
Figure 2.5. TDR test in an oedometer soil sample (Liu, 2007)	42
Figure 2.6. Kaolinite's consolidation-void ratio relationship with pressure: (a) vertical conductivity response to loading; and (b) horizontal conductivity response to loading (McCarter et al., 2005).....	43
Figure 2.7. The consolidation-void ratio relationship with resistivity for inactive clay (Fukue et al., 1999)	44
Figure 2.8. The consolidation-void ratio relationship with resistivity for bentonite (Fukue et al., 1999)	44
Figure 2.9. Void ratio-EC relationship during consolidation of sands (Comina et al., 2008)...	45
Figure 2.10. BEC-VWC relationship in sandy clay (DCF) and silty sand (DPF) (Thring et al., 2014)	47
Figure 3.1. Schematic showing the methodology adopted for the research	52
Figure 3.2. Testing programme schematic overview.....	53
Figure 3.3. Soil classification in accordance with the plasticity chart (BSI, 2015)	57
Figure 3.4. Fine-sand particle-size distribution (PSD).....	58
Figure 3.5. Compression index results (standard oedometer)	63
Figure 3.6. Example square-root-of-time method for determining t ₉₀ based on a sample of CL	66
Figure 3.7. Initial loading arrangement for PS1, including lever arms for load transfer to a soil sample.....	73
Figure 3.8. Loading frame design (units in mm)	75
Figure 3.9. Initial (unsuccessful) trials of the PS2 arrangement	76
Figure 3.10. Loading rig PS2: (a) initial stages of development; and (b) final PS2 arrangement	77

Figure 3.11. Bespoke chamber – loading and drainage locations	83
Figure 3.12. GWC variation within the horizontal layers at the end of the loading of the CI samples (b = GWC sample collected at the boundary, and in = sample collected away from the boundary)	85
Figure 3.13. GWC variation (in the vertical plane) within the CL, CI and CH samples at the end of the loading	86
Figure 3.14. Example (CI.N sample) of changes in settlement (δh) and the pore-fluid volume collected from the top and bottom drainage points normalised (r) by the initial reading. The error bars are indicative representations of the approximately 0.5mm error associated with reading the pore-fluid level from a measuring tape.	88
Figure 3.15. GWC- c_u relationship in selected CH and CI samples, measured at the end of the consolidation test	90
Figure 3.16. Shear-strength measurements in a TDR chamber with a fall-cone method	91
Figure 3.17. (a) Automatic temperature-acquisition node; (b) the waterproof temperature sensor DS18B20; and (c) its position in the TDR chamber	93
Figure 3.18. ICP-OES testing: (a) sample filtration; (b) storage of the samples; and (c) sample testing using the Perkin Elmer Optima 8000	95
Figure 4.1. TDR chamber.....	97
Figure 4.2. (a) Pore-water-pressure TDR chamber design; and (b) prototype.....	98
Figure 4.3. TDR acquisition system	100
Figure 4.4. TDR-probe calibration in (a) water and (b) short-circuit on aluminium foil (in air)	103
Figure 4.5. TDR waveforms in air and water (Curioni, 2013)	104
Figure 4.6. Hanna HI8733's conductivity reading drift with time in (a) low- and (b) medium-conductivity solutions, respectively.....	107
Figure 4.7. BEC calibration (step 1) – inverse Kp , represented by the slope of the line reflecting the relationship between the TDR read conductance $1/RL$ and the reference conductivity.....	108
Figure 4.8. Investigation of the effect of the TDR chamber container.....	110
Figure 4.9. Bespoke chamber's effect on TDR-probe readings	110
Figure 4.10. Accuracy of the AP readings with reference to the real permittivity of water values presented in Malmberg and Maryott (1956)	112

Figure 4.11. Investigation of the TDR probes' BEC accuracy	116
Figure 4.12. Initial TDR arrangement (PS1) – AP and correlation with VWC.....	118
Figure 4.13. Bespoke TDR chamber and soil-loading arrangement (PS2)	119
Figure 4.14. (a) Pressure sensor with a de-airing valve; and (b) a data logger	121
Figure 4.15. (a) TDR-pore-pressure bespoke arrangement; and (b) air bubble in the connecting pipe.....	122
Figure 4.16. Fluorescein (a) powder, (b) solution and (c) injection into the CI.S7.TDR soil sample.....	124
Figure 4.17. Location of the SEM samples within the consolidation chamber	126
Figure 4.18. TDR response to pore-water pressure variations measured in a customised triaxial cell; in (a) distilled water, (b) KCl solution trial 1 and (c) KCl solution trial 3	128
Figure 5.1. Schematic representation of the ER-arrangement development process.....	130
Figure 5.2. Preliminary ER arrangement: BGS box, current generator and oscilloscope.....	131
Figure 5.3. ER-Acq-I: a) with the BGS box; and b) with the McMiller soil box, with annotated current injection (C1 and C2) and potential measurement channels (P1 and P2).....	134
Figure 5.4. ER Chamber I: a) schematic design; and b) prototype	142
Figure 5.5. ER Arrangement I: a) vertical; and b) horizontal configurations.....	144
Figure 5.6. ER Chamber I geometric-factor calibration obtained from the ρ_{ref} -R relationship (a, b, c and d correspond to vertical Wenner configurations, vertical_1–4, respectively) ...	146
Figure 5.7. Loading bespoke ER Arrangement I.....	149
Figure 5.8. Preliminary results for 1D loading of ER Arrangement I (CH.S02.ER): a) vertical, horizontal and diagonal ER configurations (open circles on the settlement line show the times the measurements were taken); b) temperature readings in relation to ER-vertical-1	151
Figure 5.9. a) ER Chamber II and b) point electrode design	154
Figure 5.10. ER-Acq-II, including the power supply, automatic switching board the electrical chassis used in ER-Acq-I	155
Figure 5.11. ER Chamber II configurations: a) vertical (view from the side); and b) horizontal (view from the top), with measurements in mm	160
Figure 5.12. ER Arrangement II geometric-factor calibration in the vertical configuration corresponding to the AD soil layer; measurements were carried out in 8 Ohm.m KCl solution	162

Figure 6.1. TDR waveforms: in water; in the pore fluid from CI; and in the three soil mixtures prior to loading	168
Figure 6.2. TDR waveform collected in CI from TDR _v prior to the load application (L0) and at three consecutive points in time (T1-T3), following the application of a 10 kPa load (L1) ...	171
Figure 6.3. TDR waveform collected in CI from TDR _h prior to the load application (L0) and at three consecutive points in time (T1-T3), following the application of a 10 kPa load (L1) ...	171
Figure 6.4. AP _v and AP _h responses to changes in settlement in the CI.S3.TDR sample	172
Figure 6.5. GWC variation with depth in the TDR chambers in CH and CI soil (CH.S01.TDR–CH.S9.TDR correspond to sample numbers; CI.S10.N is a control sample with no instrumentation)	173
Figure 6.6. Post-consolidation SEM image of the clay particles next to one of the TDR _h probe rods	175
Figure 6.7. Post-consolidation SEM image of the clay particles within the top centimetre of the CI sample	175
Figure 6.8. Hydraulic-gradient estimation in relation to change in the sample height (dh) in CH, CI and CL samples	178
Figure 6.9. Relationship between the volume of water expelled through the top and bottom drainage in the CH, CI and CL samples	179
Figure 6.10. AP versus void ratio during the consolidation process, for all load steps; measurements were taken with probes positioned horizontally (TDR _h) and vertically (TDR _v)	181
Figure 6.11. BEC versus void ratio for CH, CI and CL during vertical loading, with measurements taken using both TDR _v and TDR _h ; S1–S9 correspond to the sample numbers	184
Figure 6.12. BEC relationship with the volume of pore fluid draining out of the sample	191
Figure 6.13. BEC _{TDR} (CH.S02.TDR) and EC _b (CH.S02.ER) in relation to void ratio and AP _v	192
Figure 6.14. Relationship between relative void ratio ($e_{(r)} = e/e_0$) and relative vertical electrical resistivity ($\rho_{v(r)} = \rho_v/\rho_{v0}$) in CH and CI at 10 Hz	195
Figure 6.15. Relative (normalised by the initial values) $\rho_{v(r)}$ measured with vertical (1, 2, 3 and 4) and diagonal (24) configurations in relation to the relative void ratio ($e_{(r)}$) in two CH samples (CH.S01.ER and CH.S02.ER)	196

Figure 6.16. Absolute ρ_v (10 Hz) changes in the CH.S01.ER sample (measured with two vertical configurations) during loading in relation to the settlement. The error bars indicate a 3% measurement accuracy.....	197
Figure 6.17. ρ_v (10 Hz) changes in the CH.S02.ER sample (measured with two vertical configurations) during loading in relation to the settlement. The error bars indicate a 3% measurement accuracy.....	198
Figure 6.18. Relative (normalised by the initial values) $\rho_{v(r)}$ (11 Hz) measured at different sample heights in two CI samples (CI.S4.ER and CI.S6.1.ER); plotted with respect to the relative void ratio ($e_{(r)}$).....	200
Figure 6.19. Absolute ρ_v (11 Hz) changes during the consolidation of CI.S4.ER	201
Figure 6.20. Absolute ρ_v (11 Hz) changes during the consolidation of CI.S6.ER	201
Figure 6.21. ρ_v (11 Hz) changes during the consolidation of CI.S6.ER.....	202
Figure 6.22. Responses for a) $AP_{(r)}$ and b) $BEC_{(r)}$, relative to the initial readings taken during the consolidation process in each of the clayey soils. The results are shown for three loading stages (L1, L2 and L3) for each soil, and there is an unload stage for CI.	205
Figure 6.23. AP_h and AP_v changes (normalised by the pre-loading measurement) in relation to the settlement and the pore-water-pressure dissipation recorded at the top (PS-t), in the middle (PS-m) and at the height of the TDR _h (PS-b)	207
Figure 6.24. AP_v -e relationship during the unloading of the CI and CL samples in two steps (Unload_1 and Unload_2).....	210
Figure 6.25. BEC_v -e relationship during the unloading of the CI and CL samples in two steps (Unload_1 and Unload_2).....	210
Figure 6.26. AP_v -VWC relationship in relation to Topp's model (for all TDR samples)	213
Figure 6.27. VWC- AP_v relationship in relation to Topp's model in the CH, CI and CL samples	214
Figure 6.28. Relationship between VWC and AP_v , shown for the CH, CI and CL results	215
Figure 6.29. Comparison between VWC measured during the vertical loading and the estimated VWC based on the AP_v -VWC correlations (Eq.6.3, Eq. 6.4 and Eq.6.5).....	216
Figure 6.30. Correlation between the VWC measured during the consolidation and the refractive index (square root of AP)	217

Figure 6.31. VWC estimation based on the refractive index (square root of AP) correlation, Eq. 6.7 and Eq. 6.6, in relation to the measured VWC	218
Figure 6.32. GWC relationship with AP_v normalised by d_d	219
Figure 6.33. AP_v -void ratio relationship in the CH, CI and CL samples	220
Figure 6.34. The relationship between AP_v and e , shown for the CH, CI and CL samples	221
Figure 6.35. Void-ratio estimation based on the AP_v relationship, from Eq. 6.8, Eq. 6.9 and Eq. 6.10	222
Figure 6.36. Void-ratio estimation based on the SQRT. AP_v relationship, from Eq. 6.11 and Eq. 6.12	223
Figure 6.37. BEC relationship with VWC	224
Figure 6.38. BEC_v - e relationship during loading	225
Figure 6.39. Primary and secondary consolidation in relation to TDR readings during first loading stage (25 kPa) of CI.S3.TDR	227

ABBREVIATIONS, ACRONYMS AND SYMBOLS

Symbol	Unit	Description
AP	-	Apparent permittivity
AP _h	-	Apparent permittivity measured with TDRh
AP _v	-	Apparent permittivity measured with TDRv
AP _(r)	-	Apparent permittivity normalised by an initial reading
BEC	S/m	Bulk electrical conductivity measured with TDR
BEC _h	S/m	Bulk electrical conductivity measured with TDRh
BEC _v	S/m	Bulk electrical conductivity measured with TDRv
C _c	-	Compression index
CH	-	High-plasticity clay
CI	-	Intermediate-plasticity clay
CL	-	Low-plasticity clay
C _s	-	Swelling index
c _u	kPa	Undrained peak shear strength
C _u	-	Uniformity coefficient (C _u =D ₆₀ /D ₁₀)
c _v	m ² /year	Coefficient of consolidation
D ₁₀	mm	Effective size of 10% grains
D ₆₀	mm	Effective size of 60% grains
d _d	Mg/m ³	Dry density
DDL	-	Diffusive double layer

e	-	Void ratio
e_0	-	Initial void ratio
$e_{(r)}$	-	Relative void ratio ($e_{(r)} = e/e_0$)
EC	S/m	Electrical conductivity (in this research, this refers to the electrical conductivity measured with the low-frequency [0.1–500 Hz] ER method)
EC_{dc}	S/m	Direct-current conductivity
EC_f	S/m	Electrical conductivity of pore fluid
EC_{ref}	S/m	Reference electrical conductivity measured with a conductivity meter
e_f	-	Effective void ratio (i.e. the void ratio at the end of each pressure increment)
ER	-	Electrical-resistivity instrumentation
GPR	-	Ground penetrating radar
GWC	%	Gravimetric water content
G_s	-	Particle density
h	mm	Sample height
ICP-OES	-	Inductively coupled plasma optical emission spectrometry
K	m	Geometric factor ($K = ER/R$)
k	m/s	Hydraulic conductivity
LL	%	Liquid limit
m_d	g	Dry mass of the soil (after oven drying at 105 °C)
m_v	m^2/kN	Coefficient of volume compressibility
GWC	%	Gravimetric water content

G_s	-	particle density
ICP-OES	-	inductively coupled plasma optical emission spectrometry
LL	%	Liquid Limit
m_d	Mg	Initial dry mass
PI	%	Plasticity index ($PI = LL - PL$)
PL	%	Plastic limit
PS1	-	Pressure system 1
PS2	-	Pressure system 1
PSD	-	Particle-size distribution
ρ	Ohm.m	Electrical resistivity ($\text{Ohm.m} = 1/EC$)
ρ_h	Ohm.m	Horizontal electrical resistivity – measured in the horizontal plane (normal to the direction of loading)
ρ_{ref}	Ohm.m	$\rho_{ref} = 1/EC_{ref}$
ρ_v	Ohm.m	Vertical electrical resistivity – measured in the vertical plane (in the direction of loading)
$\rho_{v(r)}$	-	Relative vertical electrical resistivity ($\rho_{v(r)} = \rho_v / \rho_{v0}$)
ρ_{v0}	Ohm.m	Initial ρ_v
σ	kPa	Effective stress
SEM	-	Scanning electron microscopy
S_r	%	Saturation degree
SSA	m^2/g	Specific surface area

TDR	-	Time domain reflectometry
TDR _h	-	TDR probe positioned normally to the direction of loading (horizontal plane)
TDR _v	-	TDR probe positioned in the direction of loading (vertical plane)
V	m ³	volume
VWC	m ³ /m ³	Volumetric water content
ω	Hz	Frequency

CHAPTER 1: INTRODUCTION

1.1 BACKGROUND

Geophysical techniques have the potential to advance understanding of the ground's behaviour by providing spatial and temporal information (Arulanandan, 2003). Therefore, there has been a growing interest in developing the geophysical sensing of various ground conditions, and linking geotechnical and geophysical parameters (Drnevich et al., 2001; Liu, 2007; Bryson and Bathe, 2009; Kibria and Hossain, 2012). Whilst advances have undoubtedly been made (Topp et al., 1980; Arulanandan et al., 1983; Abu-Hassanein et al., 1996; Jung et al., 2013b), developments in understanding the relationships between the geophysical and geotechnical parameters of soil in order to monitor geotechnical assets via geophysical monitoring, and potentially warn of a failure before it occurs, as part of long-term asset management processes, appear to have lagged behind these advances. Although the incorporation of electrical resistivity (ER) and time domain reflectometry (TDR) into an early warning ground-monitoring system has been suggested by Gunn et al. (2015) and Curioni et al. (2018), respectively, the interpretation of geophysical responses to changes in geotechnical properties remains challenging. The changes in the fabric of a soil – especially those containing chemically active, fine-grained materials (such as clay minerals) – with the application/removal of external loads can be complex (Sridharan and Rao, 1973). Changing the water content with a volumetric change – i.e. decreasing water contents with an increased load or increasing water contents, with water being drawn into the

soil fabric when unloaded – can result in changes in the nature of the chemical and physical behaviour of the soil, at the pore level, which is expressed in physical behaviour at the macroscale. Whether, in such conditions, the geophysical response can inform about the changes in geotechnical properties remains an active research question. It is suggested that the output of the geophysical testing is not fully understood from a geotechnical-engineering view point and this inhibits the direct translation of its response into geotechnical practice.

This research aims to investigate whether changes in the geophysical properties of various soils are observed during a geotechnical-engineering process and, if so, whether these are correlated with the changes in geotechnical properties. The geotechnical process chosen is the volumetric change of fine-grained soils with respect to changes in the magnitude of vertical loads acting on the soil in saturated and near-saturated conditions (where water is displaced from, or drawn into, the soil with the application/removal of the vertical load, respectively). Furthermore, it explores whether the orientation of the geophysical instrumentation affects the correlations. It focuses on the currently available geophysical techniques, which, if expanded to use on site, could provide an inexpensive and reliable method of monitoring geotechnical assets, complementing the existing geotechnical instrumentation.

Three fine-grained soils (of different plasticities) were exposed to changes in vertical loads (loading and unloading) within a controlled laboratory setting, in bespoke experimental apparatus (based on a modified one-dimensional [1D] consolidation

apparatus) that housed the soil, the loading frame and the geophysical sensors. This enabled the monitoring of the geotechnical parameters, which that included volumetric water content (VWC), gravimetric water content (GWC), void ratio (e) and pore water pressure (u). The geophysical parameters that were monitored are apparent permittivity (AP) and bulk electrical conductivity (BEC), both in a kHz frequency range and measured using the TDR technique; in parallel, bulk apparent resistivity (ρ) measurements in a Hz frequency range were performed utilising the ER method. For what is believed to be the first time, TDR measurements were carried out both continuously, and in both the vertical and horizontal planes. In addition, utilising the custom-built experimental apparatus, and also for the first time, TDR was undertaken simultaneously with ER measurements, and throughout the volumetric change process of the soil (rather than measuring the change in these geophysical properties once the soil had reached an equilibrium and associated movements had ceased).

1.2 AIM AND OBJECTIVES

The aim of this research is to investigate the relationships between changes in the geophysical and geotechnical properties of fine-grained soils during volumetric change with changes in vertical loading, with a view to using the available geophysical techniques to provide an inexpensive and reliable method of monitoring geotechnical assets.

Therefore, the objectives of this research are to:

- identify the gaps in current knowledge by undertaking a comprehensive literature review of the research on the changing geotechnical properties of fine-grained soils during vertical loading, their link with geophysical parameters and available approaches, enabling the identification of the correlation between geotechnical and geophysical parameters;
- produce fine-grained soil mixtures – which include sand, kaolinite and bentonite – that demonstrate a range of geotechnical and geophysical properties;
- identify appropriate (and simple) geophysical techniques, such as TDR and ER, that could be used to monitor the changes in the soil samples (and that, if expanded for use on site, could provide an inexpensive and reliable method of monitoring geotechnical assets such as earth dams, embankments, cuttings and flood levees);
- develop a bespoke experimental apparatus that will allow (i) load changes to be applied to the soil, causing compression or expansion, and the associated real-time geophysical monitoring of AP, BEC and ρ ; (ii) the effect of the positioning of the geophysical instrumentation on the AP, BEC and ρ responses to be investigated; and
- analyse the data resulting from the carefully designed testing programme to (i) identify possible correlations between AP/BEC/ ρ and VWC/GWC/e/u observed in the soil samples during vertical loading; (ii) identify the effect of the

positioning of the geophysical instrumentation in relation to the load direction on the above correlations; (iii) evaluate the benefits of the concurrent application of ER and TDR in geotechnical monitoring; (iv) assess the low (ER) and high (TDR) frequency measurement techniques effects on the BEC.

1.3 STRUCTURE OF THE THESIS

This thesis is organised into seven chapters:

- Chapter 1 – Introduction: This introduces the subject, states the problem and the associated aim and objectives. It also explains the structure of the thesis.
- Chapter 2 – Literature Review: This provides the theoretical background to the research, including identifying the knowledge gaps based on a review of the past research on the geotechnical properties of fine-grained soils subject to loading and unloading in saturated and near-saturated conditions; suitable geophysical parameters and sensing techniques; and the potential links between geotechnical and geophysical parameters when soils are exposed to changing loading conditions.
- Chapter 3 – Overarching Research Philosophy and Methods: This includes details of the background philosophy for the research approach and the justification for the decisions made, including the choice of soil used and its characterisation, the consolidation-chamber arrangement and the testing programme.

CHAPTER 1: INTRODUCTION

- Chapter 4 – Development of the TDR-Consolidation Set-up: This provides details of the design and development of a bespoke TDR-consolidation arrangement. It also includes details of the development of the experimental laboratory-testing programme, calibration, validation and preliminary results.
- Chapter 5 – Development of the ER Chamber and Acquisition System: This provides details of the design, development and modification of a bespoke ER-consolidation arrangement, including the ER chamber and the ER-acquisition system. It also includes details of the development of the experimental laboratory-testing programme, calibration, validation and preliminary results.
- Chapter 6 – Results and Discussion: This reports the results of the soil's response to changes in loading conditions, and the observed changes in geophysical properties using TDR and ER. It considers the observed data, discusses the potential correlations between geotechnical and geophysical changes in properties, and considers the suitability of these sensing technologies for monitoring the relative performance of geotechnical assets.
- Chapter 7 – Conclusions and Recommendations: This draws conclusions regarding the suitability of ER and TDR for the monitoring of fine-grained soils that are subject to changes in loading, and provides recommendations for future work.

CHAPTER 2: LITERATURE REVIEW

This chapter provides an overview of the past research on the relationships between the geotechnical properties of fine-grained soils and the geophysical parameters. Selected ground-sensing techniques are reviewed in the context of their suitability for monitoring changes in the fine-grained soil's response under vertical loading. This chapter is concluded by identifying gaps in the knowledge in the field of geotechnical and geophysical parameter correlation, and the potential for non-intrusive ground-movement monitoring.

2.1 SCOPE

The failure of a geotechnical asset can lead to tragic and costly consequences; therefore, the long-term monitoring of the ground has been the focus of geotechnical engineers in recent years (Basu et al., 2013), who are calling for an improved management strategy and planned intervention systems (Clarke et al., 2016). The long-term monitoring of geotechnical assets is still not common practice (Shah et al., 2014) as it often requires a high initial investment, can delay the start of projects, and requires special expertise for the management of the instrumentation and of the data collected. However, long-term monitoring could be used to provide warnings of potential ground movement before damage is inflicted on the surrounding infrastructure.

Ground movement can be induced by soil volume changes, resulting from stress, water, chemical and temperature variations (Mitchell and Soga, 2005). Damage caused by the volumetric changes of unsaturated fine-grained soils containing expansive clays (identified as problematic soils from a geotechnical standpoint (Jones and Jefferson, 2012)) are taken into consideration by the governing bodies, as their cost can be estimated; for example, based on domestic-subsidence claims (Driscoll and Skinner, 2007). However, the volumetric changes of saturated fine-grained soils that are not covered by domestic policies (Financial Ombudsman, 2018), such as settlement, are often not given enough attention.

Traditional ground investigations measure the conditions at one specific point in time (Rogers et al., 2012) and may not reflect the behaviour of the soil in the future (Pritchard et al., 2013). Given that many physico-chemical factors affecting the engineering behaviour of soils also affect their electrical responses (Schon, 2004), non-intrusive geophysical sensing techniques, which have the potential to save operation time and ultimately reduce costs (McDowell et al., 2002), have been the focus of significant research effort (Lambot et al., 2009; Royal et al., 2011). Geophysical monitoring of the ground offers a sustainable approach for monitoring changes in soil properties over time, which could be used to provide warnings of potential ground movement if the geophysical response to geotechnical changes is understood fully.

2.2 FINE-GRAINED SOILS' GEOTECHNICAL PARAMETERS

2.2.1 FINE-GRAINED SOILS

The definition of soil may differ depending on the context within which it is considered. This thesis focuses on geotechnical parameters; therefore, the engineering behaviour of soil and hence the definition provided in BS6707:1 (British Standards Institution (BSI), 2017) is considered the most relevant, i.e. 'soil' describes mineral material that results from the weathering of rock or the decay of vegetation.

Fine-grained soils, in accordance with BS5930 (BSI, 2015), contain particles below 63 μm , which includes fine sand, silt and clay. Therefore, their behaviour can be controlled by gravitational forces (dominant in sand and silt) and electric-charge interactions (which governs clay behaviour), (Fam and Santamarina, 1995). The presence of clay minerals leads to a complex chemical composition and hence a wide range of engineering properties within any one group (Mitchell and Soga, 2005). The electrostatic interactions are much more difficult to investigate, and, consequently, the behaviour of fine-grained soils, containing clay minerals, is more difficult to predict.

2.2.2 CLAYS AND THEIR INTERACTION WITH PORE FLUID

The term 'clay' refers to both a certain particle size and a type of mineral. The size of clay particles is considered to fall below 2 μm (BSI, 2015); however, some non-clay particles (e.g. rock flour) can also be less than 2 μm , whilst certain clay minerals may

be larger than this. Therefore, to classify soil as clay, its behaviour is also considered in accordance with its cohesiveness and plasticity (Barnes, 2000). In accordance with BS5930 (BSI, 2015), soil is considered to be clay if clay particles make up 35% of the soil mass; however, an even lower percentage of clay is found to be sufficient to control soil behaviour (Norbury, 2010).

Clay minerals are identified based not only on their size but also on their net negative charge, plasticity when mixed with water and high weathering resistance (Mitchell and Soga, 2005).

The structure of clay minerals is dominated by oxygen and hydroxyl ions, which enable the substitution of cations for, for example, silica, (Si^{4+}), aluminium (Al^{3+}), magnesium (Mg^{2+}) or sodium (Na^{1+}). The ability of the clay mineral to exchange the cations within its structure (referred to as the base-exchange or cation-exchange capacity) and the bonding present within clay minerals determines their interaction with water molecules, and therefore their geotechnical behaviour. Most clay soils formed by sedimentation are made of kaolinite, illite and smectite (Barnes, 2000).

Kaolinite minerals are made of alternating silica and octahedral sheets (referred to as 1:1 structure) in an octahedral coordination of ' Al^{3+} and Mg^{2+} ' with oxygens or hydroxyls, and include both hydrogen (strong) and van der Waals (weak) bonds. Strong hydrogen bonds dominate kaolinite behaviour, preventing hydration and leading to a low cation-exchange capacity. Kaolinite particles are quite large (up to $3\text{ }\mu\text{m}$), which

results in a low specific surface area (SSA) within 10–20 m²/g (Mitchell and Soga, 2005).

In contrast, high-SSA clay minerals are represented by smectites (with an SSA up to approximately 840 m²/g) with particles smaller than 1 µm. Smectites are composed of an octahedral sheet bonded between two silica sheets (a 2:1 structure) by van der Waals forces and cations, which balances charge deficiencies in the structure. Weak bonding facilitates a high cation-exchange capacity. As cations are also exchanged between the sheet layers, smectites exhibit high susceptibility to expansion. Due to the higher availability of exchangeable ions, evidenced in the relatively high cation-exchange capacity of smectites when compared to kaolinite, smectites have a dominant influence on the salt content of the pore fluid (Mitchell and Soga, 2005).

The pore fluid (pore water) present in the soils can be encountered in three different forms, including (Craig, 2004):

- i. free – gravitational water, flowing freely between solid particles and responding to gravitational force;
- ii. capillary water – controlled by surface tension and colloidal forces; and
- iii. hygroscopic water – adsorbed (tightly or loosely) to a soil particle by surface forces.

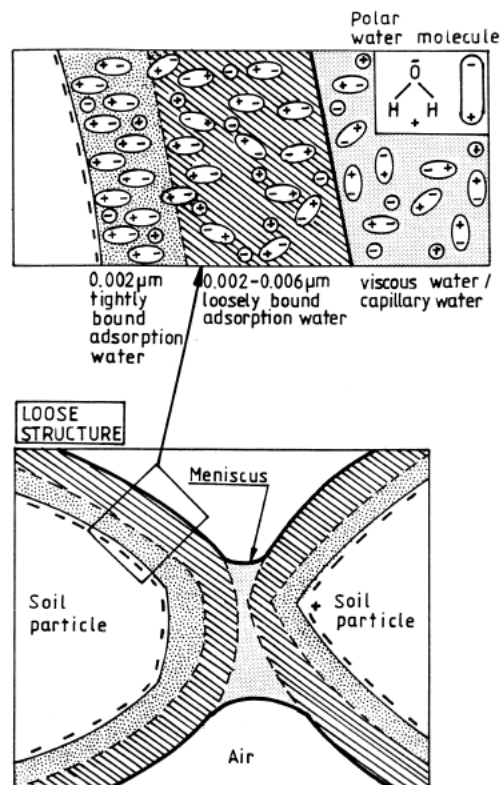


Figure 2.1. Water in soil (Saarenketo, 1998)

The level of water bonding to a clay mineral reflects the interaction between the clay's surface and water. A negatively charged clay surface holds strongly adsorbed cations. The cations that have an excess of the electronegativity neutralisation form salts with associated anions, which travel to the pore fluid. The ions close to the clay's surface are inclined to diffuse away; however, they are restrained by the clay's charges. Therefore, a high concentration of ions is present next to the clay's surface and it decreases outwards. This phenomenon is referred as a diffused double layer (DDL) and attempts have been made to describe it by several models, such as Gouy-Chapman and Stern (Mitchell and Soga, 2005). Following the Stern model, assuming that two layers of cations balance the net negative charge on the clay's surface, the first layer of cations adsorbed onto the clay's surface is referred to as the Stern layer. This DDL is

indicated to affect the load-unload response of smectite-containing soils (Sridharan and Rao, 1973). It also influences the geophysical response, such as the dielectric permittivity (Section 2.4.1) response, which is dependent on the ability of a water molecule to rotate. Whilst free water exhibits a dielectric permittivity of 81 (at 20 °C), in tightly bound water it is close to 4 (Saarenketo, 1998).

2.2.3 FINE-GRAINED-SOIL-VOLUME CHANGE UNDER VERTICAL LOAD

APPLICATION

The mechanical properties of soil depend on the interaction between the solid, liquid and gas phases; therefore, for geotechnical purposes, the soil is often referred to in terms of a three-phase system. The solid phase includes soil particles that differ in shape and size, as well as mineral content; the liquid phase is the pore fluid, which is often water containing various types and amounts of electrolytes; and the gas phase contains a mixture of naturally occurring gases (often air) (Mitchell and Soga, 2005).

The volume change of fine-grained soils depends on the initial water content, initial void ratio/dry density, initial microstructure, vertical stress, and clay type and content (Bell and Culshaw, 2001).

The application of an external vertical load to a given area of saturated fine-grained soil leads to a soil volume change over time, due to the dissipation of excess pore water (and consequently an increase in effective stress), and is referred to as

consolidation (Terzaghi et al., 1996). Consolidation is a time-dependent process governed by the hydraulic conductivity of the soil, and results in soil compression. The removal of the load leads to the 'rebounding' of the soil due to the elasto-plastic nature of soil; however, its magnitude is much lower than the compression (Barnes, 2000).

The compressibility of the soil and the prediction of soil settlement are commonly tested in oedometer tests, based on the one-dimensional (1D) consolidation theory, proposed by Terzaghi (Terzaghi et al., 1996). The theory assumes that, in fully saturated soil, the compression and flow of water take place in a vertical direction only; hence, the volumetric changes (ΔV) are expressed as a change in height ($\Delta H = \Delta V$). Following on from this, the void ratio (e) is estimated for each loading step. For each pressure increment, the final equilibrium void ratio (e_f) is calculated, and the compression index (C_c) is estimated for normally consolidated soils by applying the void ratio versus log effective pressure (σ') correlation. This procedure allows the estimation of the coefficient of volume compressibility (m_v) (m^2/kN); the rate at which the consolidation proceeded; the coefficient of consolidation (c_v) (m^2/yr); and the coefficient of hydraulic conductivity (k) (m/s).

Given that consolidation is carried out in saturated soils, based on the e estimation, other geotechnical parameters can be calculated, including VWC (Eq. 2.1), GWC (Eq. 2.2) and dry density (d_d) (Eq. 2.3):

$$\text{VWC} = \frac{e}{1 + e} \quad (\%) \quad \text{Eq. 2.1}$$

$$\text{GWC} = \text{VWC} \frac{\rho_w}{d_d} \quad (\%) \quad \text{Eq. 2.2}$$

$$d_d = \frac{m_s}{V} \quad (\text{Mg/m}^3) \quad \text{Eq. 2.3}$$

Where ρ_w – the density of water – is assumed to be 1 Mg/m^3 , and d_d is calculated based on the initial dry mass solids (m_s) and the sample volume (V).

The 1D theory also assumes that Darcy's law describes the fluid flow, and the permeability and compressibility are constant. Limitations resulting from these assumptions are known, as permeability decreases faster in the soil layers close to the drainage outlet and this reduces the flow rate of the excess pore water flowing from the interior of the sample (Terzaghi et al., 1996). Nonetheless, the 1D consolidation approach continues to be the most common method of predicting fine-grained soil settlement (Barnes, 2000).

It is implied that the prediction of the settlement from the void ratio versus the log effective provides an estimate within 10–15% of the values measured in laboratory conditions. It is noted, however, that in the case of soft or very soft soils, which exhibit a large settlement, the chance of a successful prediction falls dramatically (Bowles, 1984). It is therefore prudent to explore whether geophysical techniques could provide further assistance in predicting and monitoring the fine-grained soil settlement and volumetric changes resulting from vertical load application.

2.3 GEOPHYSICAL TECHNIQUES AND SOIL-VOLUME-CHANGE INVESTIGATION

2.3.1 GEOPHYSICAL TECHNIQUES

Geophysical methods respond to the physical properties of the subsurface media (Reynolds, 1997), and their success depends on there being a significant variation in the physical property to which the method is sensitive, the depth of penetration, the resolution and the signal-to-noise ratio (McDowell et al., 2002). Since the various geophysical methods rely on different physical parameters, it is crucial that an appropriate technique is selected for a given application (Reynolds, 1997).

Within recent decades, the geophysical methods for investigating the subsurface of shallow ground have become more popular, since they can provide the data for larger areas in a shorter time than intrusive methods (McDowell et al., 2002). Additionally, they eliminate the need for obtaining soil samples and conducting laboratory analyses, as they can provide the information about the *in situ* conditions at the time of investigation (Arulanandan, 2003).

A brief summary of the geophysical methods currently used to investigate the ground for engineering purposes is presented in Table 2.1, based on the Reynolds (1997) and current industrial practices (RSK, 2018). The most recent UK industry standard for underground-utilities detection (BSI, 2014) lists the geophysical methods most frequently used in this field.

Table 2.1. Selection of geophysical methods currently used to investigate the ground for engineering purposes

Geophysical Method	Dependent Physical Property	Application
Resistivity	Resistivity	Determining depth to bedrock Water-content monitoring Locating voids, fissures, faults, buried foundations, etc. Assessing landslides Assessing aquifer heterogeneity
Electromagnetic (EM)	Conductance, reactance	Locating sinkholes and subsurface voids Locating buried structures and utilities Determining layer thickness Mapping water-filled fractures and fissures
Ground-Penetrating Radar (GPR)	Permittivity, conductivity	Determining depth to bedrock and depth to water table Locating buried structures and utilities
Time-Domain Reflectometry (TDR)	Permittivity, conductivity	Determining soil water content and soil density Detecting leaks
Seismic Refraction	Elastic moduli, density	Determining depth to bedrock and depth to water table Locating sinkholes
Seismic Surface Wave	Rayleigh wave	Determining depth to bedrock Determining soil stiffness and verifying ground improvement
Microgravity	Gravity	Locating buried structures and cavities Determining density Conducting mineral exploration

The use of geophysical techniques in geoscience is very promising, and advances have been made to correlate geotechnical parameters with geophysical tests.

At low frequencies (below 10 MHz), measured with resistivity or vector-impedance sensors, the polarisation mechanisms significantly affect the readings. The dielectric spectrum of a saturated, clayey soil measured at low frequencies is affected by salt concentration, temperature, flocculation, anisotropy, water content, type and

percentage of clay (Liu, 2007). Therefore, low frequency measurements have been used to study items such as:

- i. porosity, void ratio and anisotropy (Archie, 1942; McCarter and Desmazes, 1997; Lech and Garbulewski, 2009);
- ii. the water content of soil (Kalinski et al., 1993);
- iii. the mechanical compaction of soil (Abu-Hassanein et al., 1996);
- iv. effective porosity (Sénéchal et al., 2005);
- v. the liquefaction of granular material (Arulanandan and Yogachandran, 2000);
- vi. the microstructure and double-layer processes in clays (Fukue et al., 1999); and
- vii. salt content (Fukue et al., 2001).

At high frequencies (between 10 MHz and 1 GHz) measured, for example, with TDR, polarisation mechanisms have a lower effect on the measurements. The dielectric dispersion of a saturated, clayey soil measured at high frequencies is controlled by the water content, type and percentage of clay (Liu, 2007). Therefore, these interdependencies help one to study areas such as:

- i. the stress–strain behaviour of fine-grained soils (Arulanandan et al., 1983);
- ii. the porosity of the soil (Fam and Santamarina, 1995);
- iii. the GWC and d_d (Jung et al., 2013a);
- iv. the soil water-retention curve (Ekblad and Isacsson, 2007).

A brief summary is presented in Table 2.2. (It should be noted that only a few selected examples have been chosen to provide an overview of the findings.)

Table 2.2. General summary of the correlations between geotechnical and geophysical parameters (Liu, 2007)

Geophysical Parameter	Engineering Parameter	Frequency	Reference
<i>Electrical Conductivity</i>	Void Ratio	<1 MHz	McCarter et al. (2005)
	Anisotropy (in the direction of the current)		
	Stiffness	<1 MHz	Arulanandan (2003)
	Liquefaction		
	Hydraulic Conductivity		
<i>Real Permittivity</i>	Void Ratio	About 1 GHz	Dong and Wang (2005)
<i>Dielectric Permittivity</i>	Hydraulic Conductivity	1-150 MHz	Arulanandan (2003)
	Residual Strength		
	Compressibility		
	VWC	~200-500 MHz	Topp et al. (1980)
<i>Dielectric Dispersion ($\Delta\epsilon_0$)</i>	Mineralogy	1-150 MHz	Arulanandan (1973)
	Total SSA		Meegoda (1985)
	Swelling Potential		Basu and Arulanandan (1973)

Due to the heterogeneous nature of soil, there are a large number of potential combinations between soil components and the specific responses to electromagnetic methods operating at certain frequencies; hence, establishing correlations between the geotechnical parameters of soil and geophysical responses is very challenging.

Van Dam et al. (2005) list 22 dielectric mixing models that aim to relate geotechnical parameters to the geophysical properties of soil. The choice of an appropriate model depends on the input data available, expected output parameters and desired level of accuracy. In certain cases, a soil-type-specific calibration may be the preferable approach (Curioni, 2013; Jacobsen and Schjønning, 1993).

Creating a database of the electromagnetic properties of soil related to the geotechnical parameters is suggested by Thomas et al. (2010b). It is pointed out that geophysical soil tests have been carried out worldwide, predominately on a small number of soils, in accordance with procedures specific to a given country, and the data provided often lacks a full quantitative description. Given that 'the response of a material submitted to an electromagnetic impulse is a characteristic of this material' (Ledieu et al., 1986), developing 'data inter-compatibility methods', as suggested by Thomas et al. (2010b), is of particular importance to further the understanding of the soil's geophysical responses.

2.3.2 SELECTED GEOPHYSICAL TECHNIQUES (ER AND TDR), AND THEIR APPLICATION IN FINE-GRAINED-SOIL VOLUME MONITORING

Although several studies on combining selected geophysical methods have been undertaken (Sénéchal et al., 2005; Cosenza et al., 2006; Schwartz et al., 2008; Cataldo et al., 2014), which reveal that a synergetic approach can provide a more-detailed picture of the ground conditions, such research is still ongoing and could be explored further. Sénéchal et al. (2005) indicate that the porosity measurements carried out with ER are comparable with those for ground-penetrating radar (GPR) for soil samples with a low clay content. Similarly, both instruments were able to detect lithological boundaries. The ER method – which is sensitive predominately to salinity, water content and porosity changes – was found to be very useful for ground monitoring in field conditions, due to its spatial and temporal capabilities. The ER enables the

monitoring of large areas through the set grid of an electrode array, which can be further visualised through electrical-resistivity tomography (ERT) in two dimensions (2D) or three dimensions (3D) (Loke et al., 2013). Therefore, ER is suggested as a potential tool for warning about ground changes (Gunn et al., 2015). Long-term monitoring, combining GPR and the ER technique (Pringle et al., 2016) suggests that, whilst GPR is optimal for target detection, ER proves more reliable in conductive environments, where GPR signals are lost.

In laboratory studies, a positive correlation between the void ratio and electrical conductivity ($EC = 1/ER$) during vertical loading was found in sands (Comina et al., 2008), and inactive (Fukue et al., 1999; McCarter, 2005; Kibria, 2014) and expansive clays (McCarter and Desmazes, 1997; Fukue et al., 1999; Kibria, 2014), with a low measurement frequency (0.01 Hz–100 kHz). Soils containing bentonite exhibit the opposite trend at loading stages above 78 kPa, which is assumed to be the result of a DDL deformation (Fukue et al., 1999).

Meanwhile, TDR has become a popular method of analysis in soil physics, mainly due to its adaptability and the continuous development of novel applications (Robinson et al., 2003). It is noted as being promising for geotechnical soil characterisation (Mojid et al., 2003), and amongst the valued benefits are a lack of permanent residual effects and the possibility of remote control (Mitchell and Liu, 2006). It is one of the few instruments that can be used in the field to estimate both AP and BEC (Robinson et al., 1999). The correlation between AP and VWC, expressed as a third-order polynomial

equation (Topp et al., 1980), makes it a suitable water-content-measurement tool for a wide spectrum of soils; TDR is included in the ASTM-D6780/D6780M standard (ASTM, 2012) as a method for measuring the density and GWC of compacted soils (Jung et al. 2013). Nonetheless, TDR is still not widely used in geotechnical-engineering practice. Specialist data analysis and data interpretation are amongst the most frequently mentioned downfalls (in personal communication with Dr Curioni). Furthermore, TDR measurement accuracy is reduced in the case of poor contact between the probe head and probe rods, as well as in the presence of air gaps between the soil and the rods (Yu and Drnevich, 2004). The TDR signal's travel-time interpretation is also strongly affected by attenuation in highly conductive (>300 mS/m) soils (Mojid et al., 2003); TDR measurements are taken within a frequency bandwidth, and therefore AP readings cannot be correlated with a specific frequency (Thomas et al., 2010).

Despite these imperfections, TDR can be useful in geotechnical applications if its limitations are well understood. The accuracy of TDR with respect to VWC estimation has been found to be within 1–2% (Jones et al., 2002), when calibrated to specific soil conditions. For this reason, it has been extensively applied as a monitoring tool for the seasonal changes in anthropogenic soils (Curioni et al., 2017); groundwater levels (Thomsen et al., 2000); liquefaction (Scheuermann et al., 2010) and earth-dam settlement (Janik et al., 2017). In the laboratory, during the oedometer consolidation of fine-grained soils, TDR has also been used at the end of each loading stage, and this showed a positive correlation between the AP and void ratio (Liu, 2007).

It can be concluded that the application of TDR in soil monitoring has been researched predominately in unsaturated conditions, whilst the research on its application in a saturated soil environment remains limited. Early warning ground-monitoring systems incorporating ER and TDR have been proposed by Gunn et al. (2015) and Curioni et al. (2018), respectively. However, the correlations between TDR/ER measured parameters and geotechnical changes in the properties of saturated fine-grained soils that are subject to vertical loading have not been addressed. Based on the AP correlation with VWC and void ratio, as well as the link between the BEC measured with TDR and the EC measured with the ER method, it is concluded that combining these two techniques could be explored to investigate the changes in fine-grained soil due to vertical load application. Research on the correlations between AP, BEC and EC with the geotechnical parameters of concern is reviewed further in Section 2.5.

2.4 ELECTROMAGNETIC PROPERTIES OF SOIL

Although soils are often perceived as dielectrics, they contain weakly bonded charges that are set in motion to form an electric current when an external field is applied (Parkhomenko, 1967). Their response to the application of electric current is a combination of the contribution of the phases from which they are made (solid, liquid and gas) and interfacial effects.

Due to the wide range of electrical responses, soils should not be perceived as dielectrics but rather as 'lossy dielectrics' (Cassidy, 2009) or even conductors, whose

properties can be described in terms of their complex electrical permittivity (ϵ^*), complex conductivity (σ^*) and complex magnetic permeability (μ^*).

Magnetic properties are considered important only if their effects constitute a significant proportion of the electrical response; hence, they are often neglected unless the analysed materials contain magnetite-rich igneous rocks, haematitic sands or man-made smelting wastes (Cassidy, 2009).

The electromagnetic properties of soil are also referred to as geophysical or geoelectrical (Loke et al., 2013).

2.4.1 DIELECTRIC PERMITTIVITY

Dielectric permittivity (ϵ) describes the ability of a material to restrict the flow of free charges; in other words, it is the degree of polarisation of a material to which an electric field is applied (Cassidy, 2009).

The application of an external electric field leads to the displacement of electric charges within a material. Once the charges reorient with the direction of the electric current, they become polarised, resulting in the storage of the energy. However, as the charges interact, some of the energy turns into heat, resulting in some energy loss. Therefore, permittivity is considered to be a complex dielectric permittivity (ϵ^*),

reflecting both the polarisation and conduction properties of a material, as described by Eq. 2.4:

$$\epsilon^* = \epsilon' - j\epsilon'' \quad \text{Eq. 2.4}$$

Where ϵ' refers to the real permittivity, ϵ'' is the imaginary permittivity, and j (imaginary number) equals $\sqrt{-1}$.

Complex permittivity is usually normalised by the permittivity of a vacuum (ϵ_0) equalling 8.8542×10^{-12} [F/m], and is consequently further referred to as complex relative permittivity. For ease of reference, this term will be simplified to permittivity throughout this thesis.

The real part of permittivity describes the storage of energy, and in older texts is referred to as a dielectric constant (κ); however, as a frequency-dependant value, it should not be perceived as a constant (Figure 2.2). The real permittivity may change over a certain frequency range, and this process is described as dielectric dispersion ($\Delta\epsilon_0$) (Liu, 2007).

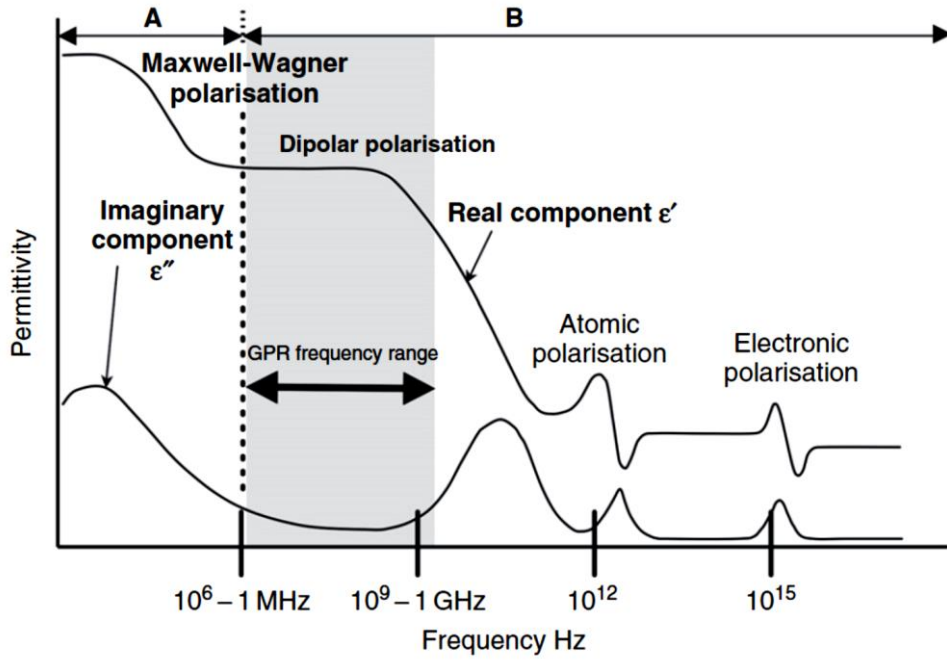


Figure 2.2. Variation of the complex permittivity components (Cassidy, 2009)

The imaginary part of permittivity describes the magnitude of the processes responsible for the loss of energy, which are identified predominately as polarisation and conduction loss. Polarisation loss reflects molecular relaxation ($\epsilon''_{\text{relax}}$) taking place when the molecules are no longer able to keep up with the speed of alteration, and electrical conductivity (EC_{dc}) produces a significant loss of energy as heat to the surrounding matrix.

Therefore, complex permittivity is described further by Eq. 2.5:

$$\epsilon^* = \epsilon' - j(\epsilon''_{\text{relax}} + EC_{dc}/2\pi f \epsilon_0) \quad \text{Eq. 2.5}$$

Where $2\pi f$ refers to the angular frequency (ω) of a sinusoidal wave at a single frequency (f) (Robinson et al., 2003).

The relaxation mechanisms can be related either to bound-charge effects or to free-charge effects. Bound-charge effects relate to the relaxation response of individual atoms or molecules, and include electronic, atomic and dipolar polarisation. Free-charge effects relate to the relaxation phenomenon of 'trapped' free ionic charges in water and on grain surfaces (Cassidy, 2009).

In soils, AP is predominately dependent on the asymmetry of the charge in the water molecules, which leads to a small displacement of the positive and negative charge centres creating a permanent dipole moment. Given that water can be present in soil in different forms, including free and bound water, the influence of a specific polarisation differs depending on the soil type and frequency. For instance, measurements on wet clay may be affected by all the types of polarisation described above, whilst wet sand, which does not contain bound water, will exhibit only free-water relaxation (Zambrano et al., 2006), as presented in Figure 2.3. The relaxation of free water is found to take place within a frequency range from 17–19 GHz (Thomas, 2010), and, as a result, does not affect the TDR bandwidth. However, bound water can relax at much lower frequencies.

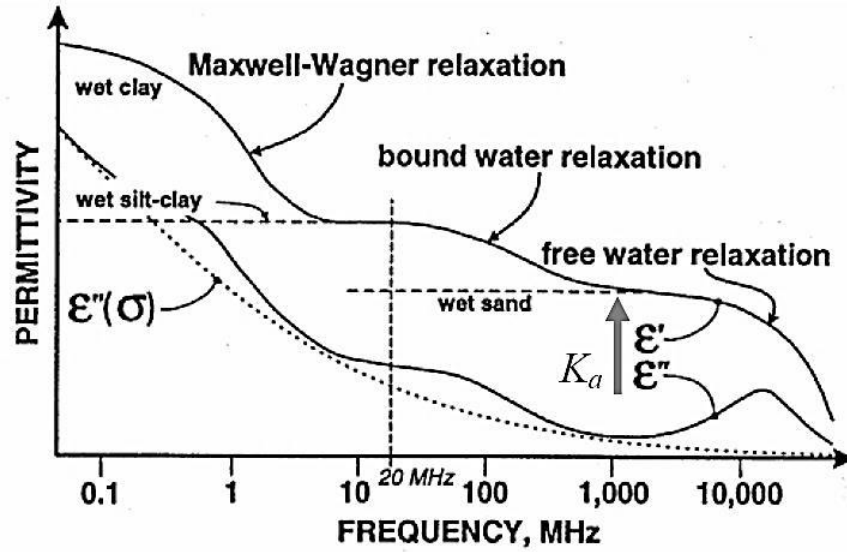


Figure 2.3. Relaxation types with regards to soil type (Zambrano et al., 2006)

Electrical permittivity determines the velocity and reflection coefficient by using high-frequency electromagnetic tools, such as TDR (Tabbagh et al., 2000), and is a function of the proportion between the three soil phases (Ledieu et al., 1986). Thus, it is a function of soil water content, porosity and density, and also mineralogy, the shape and size of particles, temperature, frequency, and salinity.

TDR-measured permittivity is a proxy of the propagation velocity (v) of an electromagnetic wave in a transmission line of a known length, where v is described as in Eq. 2.6:

$$v = \frac{c}{\sqrt{\left(\epsilon' \frac{1 + \{1 + \tan^2 \delta\}^{1/2}}{2}\right)}} \quad \text{Eq. 2.6}$$

Where c is the speed of light in free space ($2.988 \times 10^8 \text{m/s}$), and the denominator of Eq. 2.6 describes the AP, in which $\tan\delta$ (loss tangent) is described by Eq. 2.7 as follows:

$$\tan\delta = \frac{\varepsilon'' + EC_{dc}/\omega\varepsilon_0}{\varepsilon'} \quad \text{Eq. 2.7}$$

For a $\tan\delta$ significantly lower than 1, the velocity is approximated as Eq. 2.8:

$$v = \frac{c}{\sqrt{AP}} \quad \text{Eq. 2.8}$$

For low-loss materials, AP is assumed to equal the real permittivity (Topp et al., 1980). Variations in the AP of fine-grained soils are largely due to the loss tangent and the decrease in the effective signal frequency (Thomas, 2010).

Since the signal travels down and back, a TDR probe with a length (L) has a time (t) for the signal's travel, which is given as Eq. 2.9:

$$t = \frac{2L}{v} [\text{s}] \quad \text{Eq. 2.9}$$

By substituting equations Eq. 2.9 with Eq. 2.8, AP measured with TDR can be defined by Eq. 2.10:

$$AP = \left(\frac{ct}{2L} \right)^2 \quad \text{Eq. 2.10}$$

And by introducing an apparent length ($l_a = \frac{ct}{2}$) it can be simplified to Eq. 2.11:

$$AP = \left(\frac{l_a}{L} \right)^2 \quad \text{Eq. 2.11}$$

As shown in Eq. 2.7, the level of electrical permittivity is affected by the conductive properties of the soil, which are discussed as follows.

2.4.2 ELECTRICAL CONDUCTIVITY

Electrical conductivity (EC [S/m]) describes the ability of a material to transmit electric charges under the influence of an applied electric field (Cassidy, 2009).

A current directed through a soil can be conducted in one of three ways:

- i. electrolytic conduction, which involves the slow movement of ions, and depends on their type, concentration and mobility;
- ii. electronic (ohmic) conduction reflects the rapid movement of the electrons that carry the charge; and
- iii. dielectric conduction, which occurs in very weak conductors when an alternating field is applied; it involves the separation of charges at an atomic level (Reynolds, 1997).

Furthermore, the current is considered to flow through three pathways in soil, via:

- i. the pore fluid and conducting soil particles in series;
- ii. soil particles in contact with each other; and
- iii. the pore fluid itself (Arulanandan et al., 1983).

The electrical conductivity in soils is considered to combine the contributions of particle conduction, surface conduction and pore-fluid conduction, as well as the effects of particle shape and fabric. Surface conduction plays a particularly important

role in soils with a high specific surface, where it increases with decreasing porosities in low-ionic concentration pore fluids, whilst an increase in conductivity of the electrolyte in the pore fluid is associated with higher porosities. Therefore, the conductivity of a soil with a high specific surface may be greater than the conductivity of the low-conductive fluid on its own.

The contribution of the electrolyte is restricted by the porosity of the medium (Klein and Santamarina, 1997); hence, in soil, EC is a function of porosity, degree of saturation, pore-water composition, mineralogy, soil structure and surface conductance (Yu and Drnevich, 2004). The EC is also affected by the connectivity of the pores and the distribution of resistive bodies (Friedman, 2005).

Electrical conductivity measured with TDR is computed from the attenuation of the TDR pulse (Yanuka et al., 1988) and reflects the conductive loss (EC') that coexists with polarisation loss (Heimovaara, 1994); $EC'' = \varepsilon'' \omega$ represents a complex value and is referred to as the real effective conductivity (EC^e) (Cassidy, 2009), and is calculated as in Eq. 2.12:

$$EC^e = EC' + EC'' \quad \text{Eq. 2.12}$$

The literature refers to the electrical conductivity read with TDR as effective (apparent) EC_a (or σ_a) (Friedman, 2005) or bulk (EC_b in Jung et al. [2013]; BEC in Thring et al. [2014]; σ_{soil} in Bechtold et al. [2010]). Here, the BEC abbreviation is adopted to distinguish TDR-measured electrical conductivity from the low-frequency

measurements (EC). The EC'' is often not considered in the BEC interpretation: firstly, because the common TDR measurements do not provide information about the real and imaginary conductivity components (Campbell Scientific Inc., 2010), and, secondly, due to the prevailing effect of EC' on the effective conductivity (Turner and Siggins, 1994). Nonetheless, the variation in the inertial properties of the soil components, and thus the difference in the speed of the charges' responses to the applied current, may need to be considered in saturated clay soils, where free charges present in the electrolyte coexist with bound charges (Cassidy, 2009).

2.4.3 ELECTRICAL RESISTIVITY

Electrical resistivity measured with a resistivity meter is considered to be a bulk apparent resistivity, as it is a product of a measured resistance (R) and a geometric factor (k), reflecting the spread of the electrodes ($\rho = k \cdot R$) (Reynolds, 1997). However, for simplicity it will be referred to as electrical resistivity (ρ) (Ohm.m), a reciprocal of EC ($\rho = 1/EC$).

The magnitude of resistance indicates how soil opposes the flow of electrons, and is calculated from the Ohm's law, as shown in Eq. 2.13Eq. 2.12:

$$R = \frac{\Delta V}{I} \quad \text{Eq. 2.13}$$

Where ΔV is the potential difference between two points and the current (I) (amps).

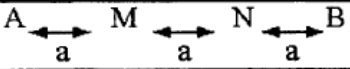
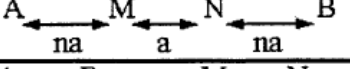
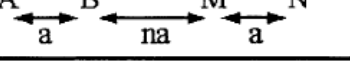
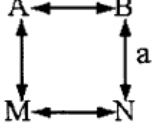
Since resistance is directly proportional to the length (L) and inversely proportional to the area (A) of a conductor, resistivity is described as follows in Eq. 2.14:

$$\rho = \frac{\Delta V A}{I L} \quad \text{Eq. 2.14}$$

Where $A/L=k$.

Soil resistivity measurements are commonly obtained in the field with an arrangement of four metal electrodes, by injecting a current between two electrodes (C1 and C2) and measuring the potential difference between the other two electrodes (P1 and P2). The most commonly applied arrays include Wenner, Schlumberger, dipole-dipole (and square dipole-dipole); their electrode configurations are presented in Table 2.3. The separation of the electrodes determines the depth to which the current penetrates, whilst the configuration of the electrodes is selected based on the target of the investigation (Reynolds, 1997). For example, the Wenner array is found to be sensitive to horizontal structure, whilst the dipole-dipole array is sensitive to vertical structures (Samouëlian et al., 2005).

Table 2.3. Examples of common electrical-resistivity arrays (Samouëlian et al., 2005)

Electrodes array	K
	$2\pi a$
	$\pi n(n+1)a$
	$\pi n(n+1)(n+2)a$
	$\frac{2\pi a}{2 - \sqrt{2}}$

A and B current electrodes, M and N potential electrodes
A: spacing between electrodes used in a particular measurement
n: spacing factor (integer values 1-6)

The sensitivity of an array is described as the degree to which a change in ρ influences the potential measured by the array (Loke, 1999). The depth of the investigation, reflected in the ER measurement, is considered to be the median depth of the investigation, in which the sections of the earth above and below contribute to the ER reading in the same way (Loke, 1999). Due to the heterogeneity of the soil, this depth can only be approximated, and for the Wenner array is assumed to be approximately 0.5, whilst for the dipole-dipole array it is 0.9 of the C1-C2 electrode spacing (Loke, 1999).

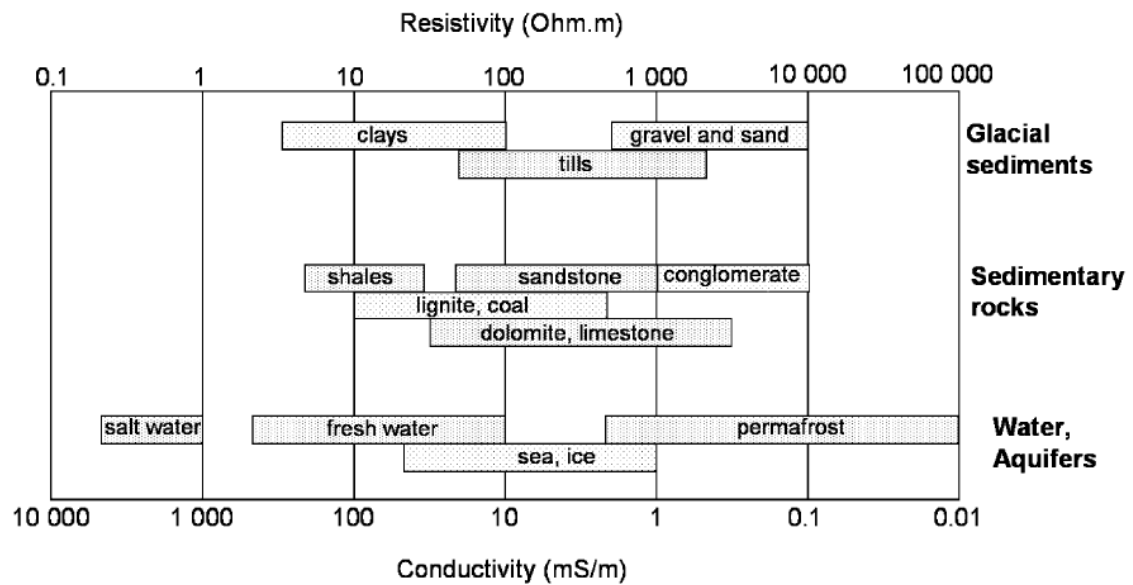
The ER is frequency dependent, and decreases as the frequency increases (Olhoeft, 1985). Each frequency can potentially reflect different pore spaces, based on the difference in the particle acceleration at a given frequency (Revil, 2012). High-frequency measurements are suggested (Shankland and Waff, 1974) to indicate

volume, whilst direct current (DC) measurements connected volume of the conductive fluid.

Examples of the ‘typical’ resistivity range in common earth materials are presented in

Table 2.4:

Table 2.4. Typical range of electrical resistivity/conductivity of common earth materials (Samouëlian et al., 2005)



2.5 FINE-GRAINED-SOIL VOLUME-CHANGE CORRELATIONS WITH AP, BEC AND ρ

Fine-grained-soil volume changes in saturated and near-saturated conditions are reviewed in the context of the AP, BEC and EC's relationships with the VWC, GWC and void ratio.

2.5.1 AP-SOIL WATER CONTENT

2.5.1.1 AP-VWC

The measurement of water content with TDR has been made possible on the basis of the significant variance between the dielectric permittivity of water (78 at 25 °C) (Cassidy, 2009) and other soil constituents (e.g. sand AP 3-6 and clay 2-20) (Annan, 2009).

Topp, Davis and Annan (1980) established an empirical relationship between AP and VWC at a TDR frequency range (approximately 200MHz to 500 MHz) by fitting a third-order polynomial to the observed relationships, as in Eq. 2.15:

$$\text{VWC} = -5.3 \times 10^{-2} + 2.92 \times 10^{-2} \text{ AP} - 5.5 \times 10^{-4} \text{ AP}^2 + 4.3 \times 10^{-6} \text{ AP}^3 \quad \text{Eq. 2.15}$$

As the formula (referred to as Topp's equation) was fitted to results that included variations in soil type, density, temperature and soluble salts, and were not normally

distributed; hence, further use of the model could not be applied to 'every' soil. Furthermore, it is maintained by Topp et al. (1980) that the data obtained at low and high moisture contents (in this case with a minimum water content of 1.6% and a maximum of 55%), did not present a good fit to the equation. Later research reveals that the aforementioned formula failed to represent the relationship adequately for organic soils, mineral soils high in organic matter or clay content (Jones et al., 2002), or even for soils with a GWC above their plastic limit (Thomas, 2010). Notwithstanding the advances of the findings of Topp (1980), which includes a low-error estimate of VWC (+/-1.3%), a further study of the AP and VWC relationship was needed to confirm the AP's independency of the soil type, density, temperature and soluble salt content.

The dry-density (d_d) effect, which has been investigated on a range of mineral and organic soils (Malicki et al., 1996), implies that the VWC prediction could be improved by the inclusion of d_d information. However, the effect of density may not be prominent for soils with a small range of bulk densities.

Mironov et al. (2009) propose a model incorporating sand and clay percentages. Although accounting for the amount of clay improved the accuracy of the permittivity measurements, adding information regarding the sand percentages did not seem to affect the results. Inclusion of either the clay percentage or the d_d is also demonstrated to improve the VWC prediction based on a linear correlation with the refractive index (the square root of AP) (Skierucha, 2000).

$$\text{VWC} = 0.13\sqrt{\text{AP}} - 0.18 \quad \text{Eq. 2.16}$$

The presence of bound water exhibiting an AP that is much lower (~4) than a liquid phase (~80) is suggested to underestimate the VWC estimate based on TDR readings (Jones and Or, 2003); however, the bound water's effect on the AP readings is suggested to be outweighed by the pore connectivity (Blonquist et al., 2006).

The release of bound water with an increase in temperature is mentioned as one of the factors affecting the accuracy of the VWC estimation based on AP readings (Jones and Or, 2003). Given that free water exhibits a decrease in AP, from 87 to 77, when the temperature increases from 0–30 °C (Jones and Or, 2003), if soil follows the same trend, then a 0.3 AP change would be expected per 1 °C. Tests carried out on a range of soils and at a range of VWCs from 0–60 °C (Skierucha, 2009) indicate that only at very high water contents was an AP temperature dependency observed; however, this did not occur in all the samples. The AP temperature dependence in unsaturated soils has been found to be negligible at the temperature range from 0–20 °C (Thring et al., 2014).

In highly conductive soils (BEC above 0.25 S/m), the contribution of imaginary loss is suggested to result in higher AP values, leading to an overestimation of water content (Bittelli et al., 2008).

Discrepancies amongst the VWC estimations based on the AP are suggested to result from the assumption that AP measured with TDR is equal to real permittivity (Thomas

et al., 2010a). Given that TDR measurements are taken within a frequency bandwidth, it is not known which frequency corresponds to a given AP measurement, and hence the real and imaginary parts cannot be determined by using a simple commercial TDR. The AP varies with frequency, and this effect is even more pronounced in clay-containing soil (Thomas et al., 2010a).

2.5.1.2 AP-VWC TDR-PROBE ORIENTATION

Probe orientation is shown to be an important factor in VWC estimation with TDR probes. In a material of uniform porosity, grain size and shape, such as glass beads, the TDR is expected to be nearly the same in any direction, apart from minor discrepancies that can arise from the water distribution along the rods (Jones and Friedman, 2000). According to the layered system described by Robinson et al. (2005), in the porous aggregated media the water level changes perpendicular to the vertically orientated probe. This was investigated further by Pastuszka et al. (2014), who conclude that a vertically inserted probe represents the arithmetic mean of soil moisture for the investigated depth, whilst horizontally inserted probes reflect the water content of a single layer at a specific depth. It is suggested that the insertion of a probe at 45° (Skierucha et al., 2004) may give the most reliable representation of the soil moisture in a field. Jones and Friedman (2000) report that a vertically measured AP could be twice as high as a horizontally measured AP in soils containing platy particles (however, this result could have been affected by the particular experimental arrangement used in the study).

No research has been identified that links the TDR-probe orientation to AP-VWC in fine-grained soils under a vertical loading.

2.5.1.3 AP-GWC

The GWC is more commonly used in geotechnical practice than the VWC; however, its correlation with AP is more difficult to obtain under field conditions, since information on d_d is needed. A relationship between AP, normalised by d_d , and GWC is proposed by Thomas (2010), which suggests a linear correlation.

Thring et al. (2014) conducted a laboratory analysis including a range of d_d s, which proposes that GWC can be estimated within a 5% accuracy based on a soil-specific third-order polynomial equation fitted to the GWC and AP/ d_d relationship. The fit of the estimate to the measured data is presented in Figure 2.4.

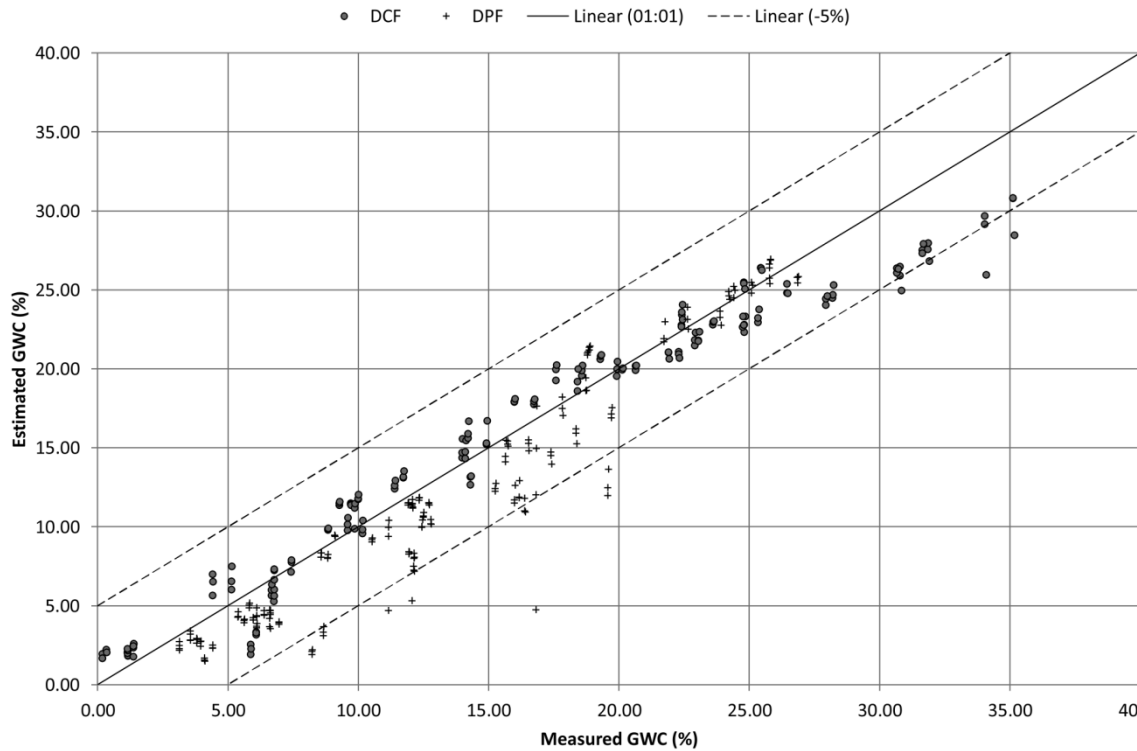


Figure 2.4. GWC prediction based on a soil's specific AP/ d_d relationship in sandy clay (DCF) and silty sand (DPF) (Thring et al., 2014)

It is concluded that VWC estimation based on AP readings can be affected by a number of factors; nonetheless, the accuracy of the prediction is encouraging (5% at a low AP and 10–12% at a high AP of over 30 [Thring et al., 2014]). Furthermore, GWC prediction is also possible with a 5% accuracy (Thring et al., 2014); however, obtaining information about d_d may make it more challenging.

Although research on TDR-probe positioning has been carried out in the context of VWC monitoring (e.g. Pastuszka et al., 2014), no research was identified that links TDR-probe orientation to AP-VWC in fine-grained soils under a vertical loading.

2.5.2 AP-VOID RATIO

The void ratio (e) is a parameter commonly used in geotechnical assessments; for example, it is used to predict the compression index (C_c) from the void ratio-log effective stress correlation (Barnes, 2000). Therefore, a correlation between AP and e could potentially enable the further estimation of C_c . Research on e -AP correlation is limited; however, given the successful correlation between AP and VWC, and the relationship between VWC and e , the correlation e -AP can be also expected.

This assumption has been confirmed by the testing conducted with a three-rod TDR probe inserted, at the end of the consolidation stages, into the soil samples tested in an oedometer (Liu, 2007).

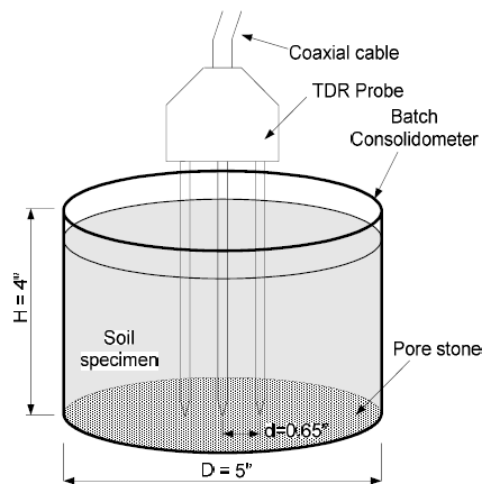


Figure 2.5. TDR test in an oedometer soil sample (Liu, 2007)

Furthermore, earth-dam-settlement monitoring was carried out with TDR in the field, which reveals a 19% accuracy in settlement prediction based on the AP measurements (Janik et al., 2017).

2.5.3 BEC AND EC-VOID RATIO

Given that electrical conduction in soils takes place primarily through the electrolytes (Reynolds, 1997) and the contribution of the electrolyte is restricted by the porosity of the medium (Klein and Santamarina, 1997), it can be expected that the expulsion of fluid during the consolidation results in decreased conductivity values.

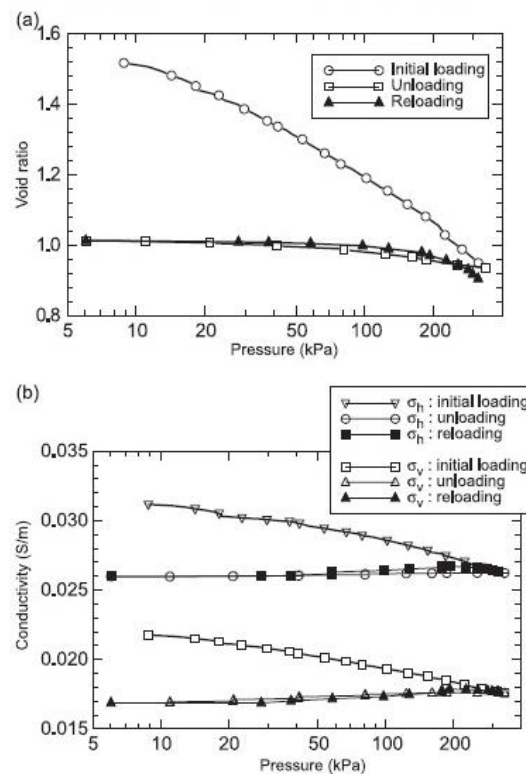


Figure 2.6. Kaolinite's consolidation-void ratio relationship with pressure: (a) vertical conductivity response to loading; and (b) horizontal conductivity response to loading (McCarter et al., 2005)

On this basis, a positive correlation between the void ratio and conductivity during 1D consolidation was found in sands (Comina et al., 2008), inactive clays (Fukue et al., 1999; McCarter et al., 2005; Kibria, 2014) (Figure 2.6 and Figure 2.7), and expansive

clays (McCarter and Desmazes, 1997; Fukue et al., 1999; Kibria, 2014) (Figure 2.8) with a low measurement frequency (0.01 Hz–100 kHz).

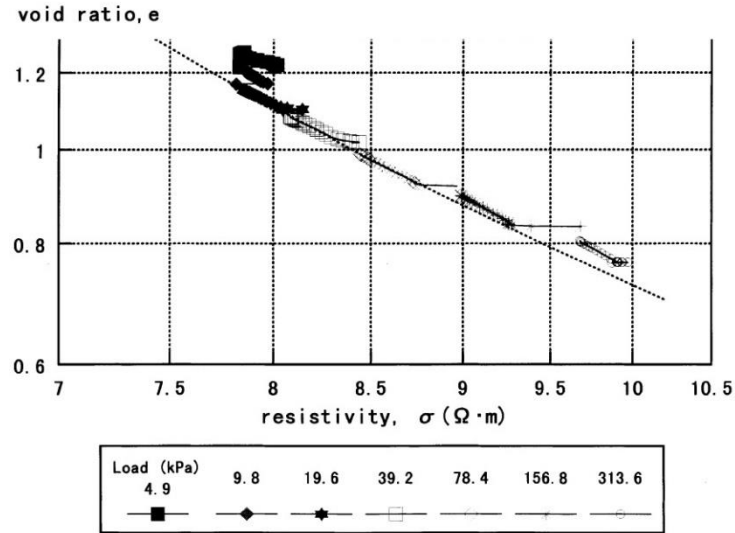


Figure 2.7. The consolidation-void ratio relationship with resistivity for inactive clay (Fukue et al., 1999)

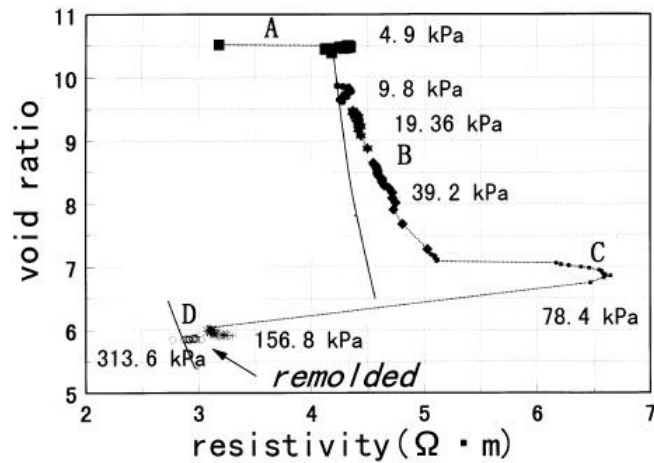


Figure 2.8. The consolidation-void ratio relationship with resistivity for bentonite (Fukue et al., 1999)

Work carried out by Comina et al. (2008) on EC measurements during the consolidation of sand implies that under an initial load the EC of the sample increased, as illustrated in Figure 2.9. This is most likely a result of the experimental arrangement, as the bottom drainage was closed, limiting the outflow of the pore fluid; nonetheless, it implies that a change in e was not the main factor controlling the EC response (it can be observed that the settlement curve decreased at the point of the elevated EC reading).

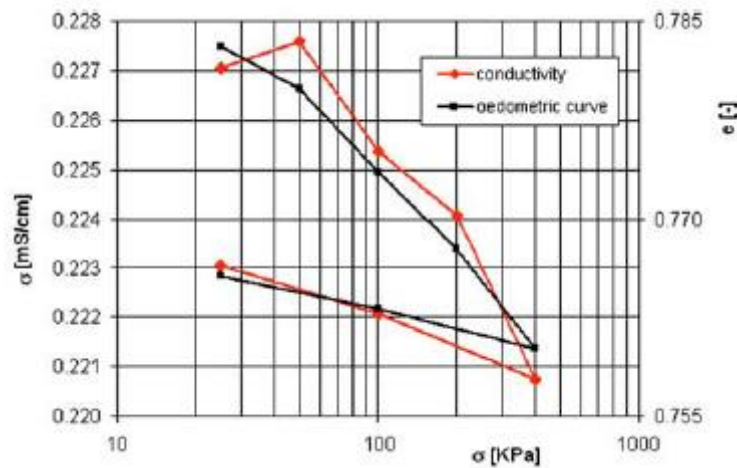


Figure 2.9. Void ratio-EC relationship during consolidation of sands (Comina et al., 2008)

Boadu and Owusu-Nimo (2010) point out that the DC-resistivity method cannot provide sufficient information about changes in fine-grained clay soils, as it does not provide information about the movement of the surface charges at the interface between the solid particles and pore fluid. It is noted that the geotechnical parameters correlate better with surface conductance as presented by Bryson and Bathe (2009). The surface conduction and the diffusion of ions are noted as the main reasons that volumetric mixing models, used to determine the electrical conductivity of composite

material, do not work for fine-grained soils (Ngoc, 2012). However, surface conductance is considered to have a negligible effect on bulk conductivity, if the electrolyte is more conductive than the surface conductivity (Klein and Santamarina, 1997; Brovelli and Cassiani, 2011). This prevailing effect of pore-fluid conductivity on the BEC should be observed in saturated expansive soils, whose pore-fluid conductivity is typically above 100 mS/m. Work carried out by Liu (2007) with TDR reveals that, whilst for some clays the BEC decreased with fluid expulsion, measured at the end of subsequent consolidation stages, others exhibited a negligible change.

During the process of vertical loading and consequent consolidation, the free movement of the liquid within the pores is gradually reduced. Once the pores are getting smaller under the application of a load, the DDL becomes a barrier for ion movement (Boadu, 2011). Pressure forcing the fluid out of the soil sample during the consolidation process may lead to the crystallisation of salts in the smaller pores, and thus the decreasing fluid solubility is reflected in increased resistivity (or decreased EC) readings (Ghorbani et al., 2012), although this may be more likely in arid soils with a high salt content. This suggests that EC responds to changes in the void ratio in sand and inactive clays; however, uncertainties surround its changes with respect to the loading of expansive soils (Fukue et al., 1999). Also, the initial loading may or may not result in the expected decrease in EC, despite the void-ratio reduction (Comina et al., 2008). Research on the BEC response to a void-ratio change is very limited.

2.5.4 BEC-VWC

The laboratory study conducted by Thring et al. (2014) suggests that there is a relationship between BEC and VWC; however, BEC appears to level off at a certain VWC, as shown in Figure 2.10. This identifies the predominant effect of connectivity of the pores on EC (Friedman, 2005).

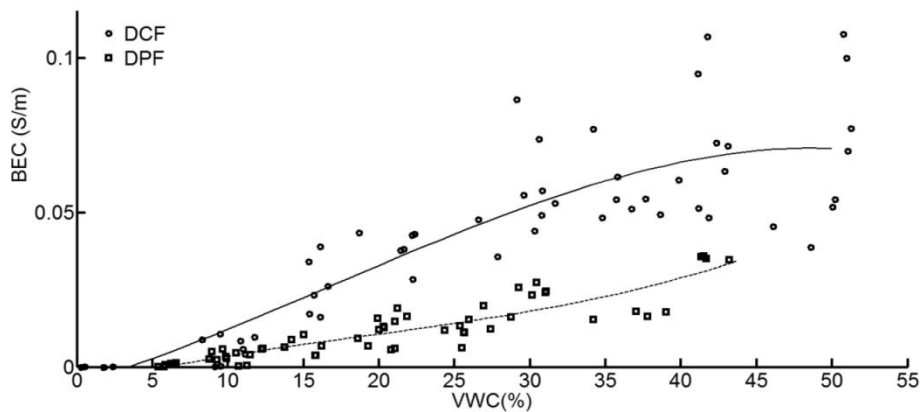


Figure 2.10. BEC-VWC relationship in sandy clay (DCF) and silty sand (DPF) (Thring et al., 2014)

The BEC and AP respond differently to changes in VWC and void ratio; BEC (and EC) appear to be responding more to pore connectivity (Friedman, 2005) than AP, which potentially reflects the structural changes more. This potentially indicates a very interesting TDR application, where AP readings could be used to monitor structural changes, whilst the BEC response to pore connectivity could provide further information regarding fluid transport (Blonquist et al., 2006). Combining TDR point measurements with spatially distributed ER arrays could provide useful information about geotechnical changes in the ground's behaviour.

2.6 SUMMARY AND IDENTIFICATION OF KNOWLEDGE GAPS

Following on from the examination of the literature in this chapter, it is apparent that the application of geophysical techniques presents an interesting and sustainable option for geotechnical ground investigation/monitoring. The application of the geophysical methods is constrained by the cost of the equipment; ambiguous data interpretation, which needs to cope with the heterogeneous nature of soil; and consequent lack of a universal model that could be applied to any soil conditions. Therefore, improvements in data processing and interpretation, as well as the further applications of the geophysical methods to investigate the ground are still an active field of research.

The incorporation of ER (Gunn et al., 2015) and TDR (Curioni et al., 2018) measurements into an early warning ground-monitoring system could be beneficial to long-term geotechnical asset management. However, TDR and ER research in this context is very limited. Understanding the correlations between the AP, BEC and p responses in relation to changes in the properties of saturated and near-saturated fine-grained soils that are subject to vertical loading is crucial to facilitate this application. Therefore, several knowledge gaps, as identified in this research, are brought into consideration:

- i. Although TDR is sensitive to volumetric changes in soil (Topp et al., 1980), information on TDR responses in fine-grained soil subjected to vertical loading

in a nearly or saturated state (at the liquid limit [LL] or above) is very limited (Thomas, 2010).

- ii. TDR has previously been applied at the end of consolidation-induced settlements (Liu, 2007); however, to the author's knowledge, no controlled laboratory research has been carried out with TDR inserted into the soil throughout the duration of the consolidation / vertical-loading process; this would allow further insights on soil behaviour to be found.
- iii. The effect of the TDR-probe orientation is not fully understood, and has not been researched, to the author's knowledge, in the context of soil loading.
- iv. Based on the successful correlation between ER and the void ratio – which was investigated using an oedometer (McCarter et al., 2005; Bryson and Bathe, 2009; Kibria, 2014) – and the link between EC (ER) and BEC (TDR), the simultaneous application of ER and TDR offers the possibility of monitoring the responses of fine-grained soils to vertical loading on a larger scale, due to the spatial coverage provided by the ER arrays, yet obtaining detailed point monitoring from the TDR. However, these two techniques have not been tested concurrently.
- v. ER was tested during consolidation using an oedometer (McCarter et al., 2005; Comina et al., 2008); however, information about changes within the soil layers during consolidation remains limited.
- vi. Finally, the ER technique can be operated at a range of frequencies, which provides the opportunity to investigate changes in the soil at a range of pore

scales, and thus provides further insight into the micro changes in soil during vertical loading.

A trial to address these gaps has been undertaken within the present research. Its details are described in Chapter 3, Chapter 4 and Chapter 5, and the results are presented and discussed in Chapter 6.

CHAPTER 3: OVERARCHING RESEARCH PHILOSOPHY AND METHODS

This chapter describes the experimental laboratory programme developed as a result of the knowledge gaps identified in Chapter 2. In particular, the research aims to investigate the relationships between changes in the geotechnical properties of the soil and the electrical responses of the volumetric soil changes under external loading and unloading, specifically utilising TDR and ER.

This chapter includes the details of the background philosophy for the research approach, and the justification for the decisions made, including the choice of soil used and its characterisation, the loading apparatus, the testing programme and the validation of the methodology.

The research programme specifically focused on using TDR and ER within a saturated and near-saturated environment. The bespoke laboratory arrangements were developed that were based on 1D oedometer testing to investigate AP and BEC in a bespoke TDR chamber, and to investigate EC in a bespoke ER chamber during the vertical loading of fine-grained soils; these are described in detail in separate chapters, which are Chapter 4 and Chapter 5, respectively.

For ease of reference, a flow chart presenting the development stages of the methodology and the corresponding chapters is shown in Figure 3.1.

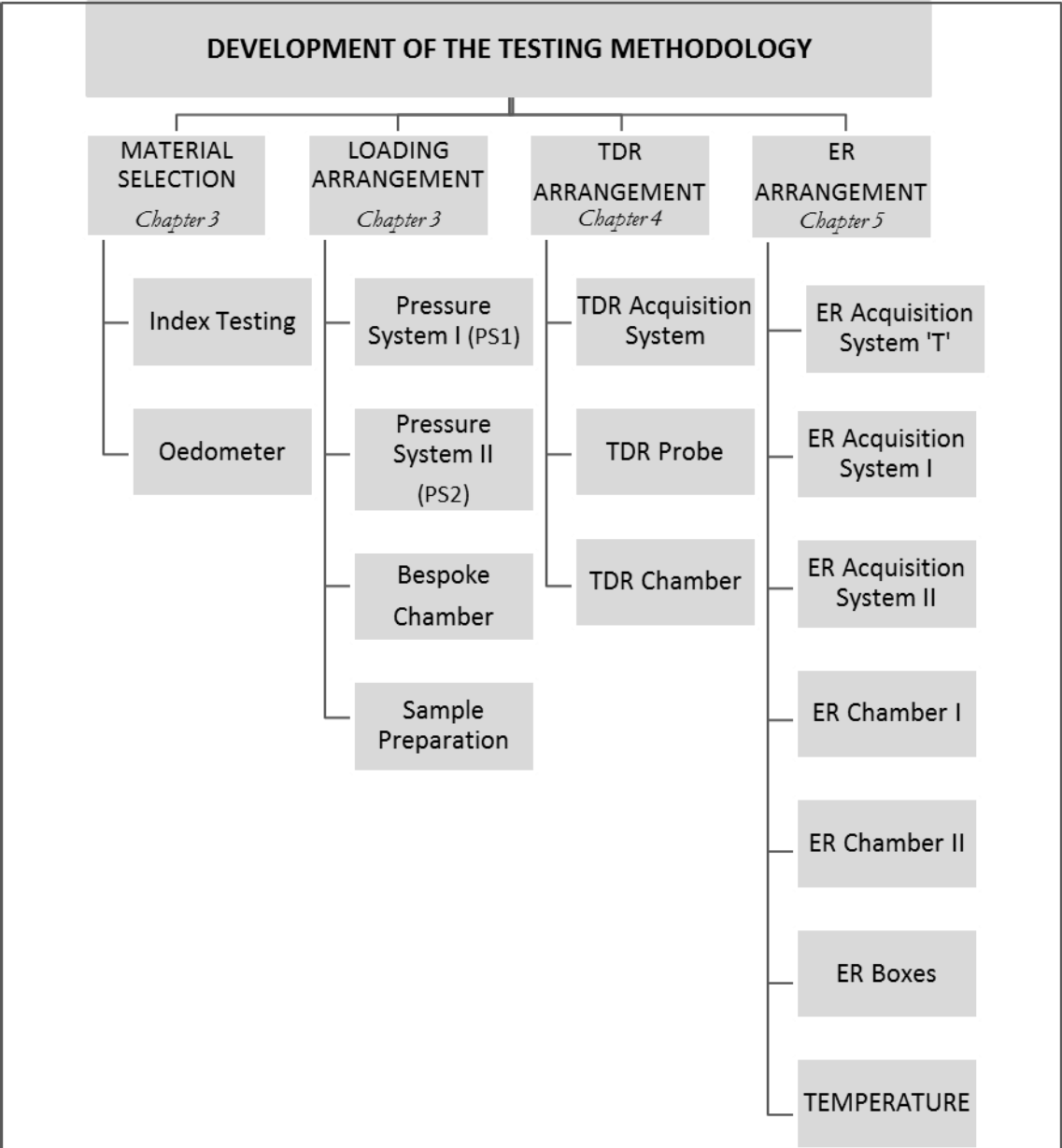


Figure 3.1. Schematic showing the methodology adopted for the research

3.1 TESTING PROGRAMME OVERVIEW

This section provides an overview of the experimental development process, leading to the design of TDR and ER instrumented chambers; subsequent loading testing combined with AP, BEC and ER measurements; and the validation of the results. Figure 3.2 shows diagrammatically the testing programme:

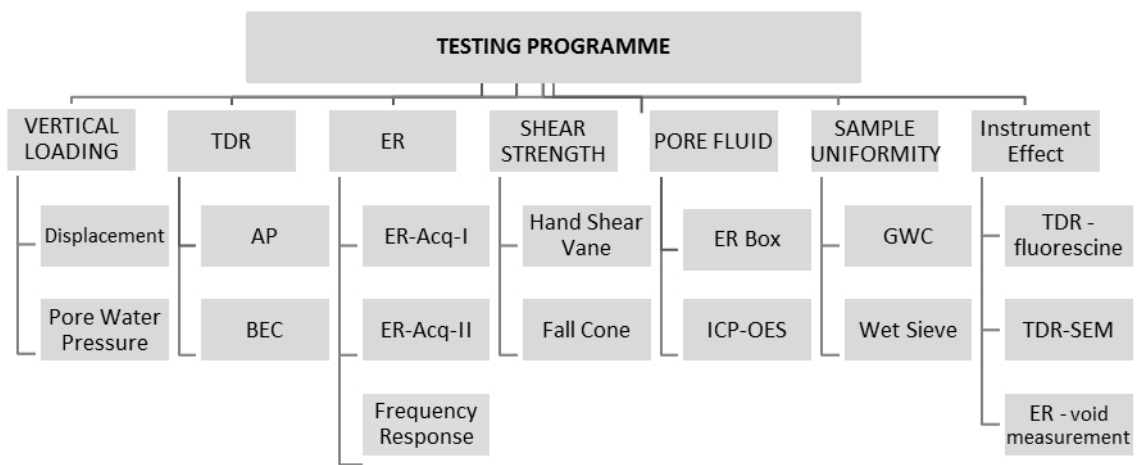


Figure 3.2. Testing programme schematic overview

The testing development process was begun with the selection and characterisation of the soils (Section 3.2). Once the bespoke chambers (Section 3.3.1.3) were designed, soil slurries were prepared (Section 3.3.1.4) to be consolidated under pressure system PS1 (Section 3.3.1.1) and modified further to PS2 (Section 3.3.1.2). Pore-water pressure monitoring was conducted on the selected samples (Section 4.2).

During the preliminary tests using the PS1 system, one sample was set in the TDR chamber and one in the ER chamber to enable the measurement of the electrical

parameters at the same consolidation stage. The readings were obtained at the end of the loading stage.

Following a number of initial trials, it was concluded that PS1 was not sufficiently reliable and efficient, since it allowed only two samples to be tested at the same time. Therefore, the pressure system was redeveloped to improve testing quality and efficiency. PS2 allowed six samples to be tested in parallel. However, the upgrade of the apparatus took a significant amount of time (approximately seven months), and during this time tests were conducted using only three TDR chambers.

Once the ER equipment was ready, the testing regime involved the following steps:

- Soil mixtures were tested with both TDR and ER in parallel, and the measurements were taken at the same time intervals.
- During loading, the pore fluid was collected and stored to be subject to chemical analyses (inductively coupled plasma optical emission spectrometry [ICP-OES]). Whenever sufficient volume was collected, the pore fluid was also tested in soil resistivity boxes and with TDR (Section 3.4).
- In order to investigate the load-transfer distribution within the samples, indicative undrained shear-strength measurements were taken with a shear vane and correlated with GWC.

Due to the significant presence of the instrumentation in the bespoke chambers, an investigation of the instrumentation's effects on the AP, BEC and ER measurements

was carried out. This included fluorescein testing and scanning electron microscopy (SEM) in a TDR chamber (Chapter 4); the measurement of the gaps developing underneath the electrodes in the ER chamber (Chapter 5); and the settlement of soil samples without any instrumentation.

The results obtained from the testing are described in Chapter 6.

3.2 SOIL CHARACTERISATION

Given that fine-grained soils are dominant in the UK (Rogers et al., 2009), these soils can experience volumetric changes with loading over long periods of time (and larger overall movements than associated with coarse-grained soil); thus, understanding the changes in their properties is crucial, and, in particular, their effect on the hydraulic conductivity of a soil and, in turn, settlement.

Soil mixtures were prepared to be representative of mineral soils with a range of plasticity, corresponding to a range of compressibility. This included commercially available components using different proportions of English china clay (ECC) (Puraflo supplied by Sibelco), sodium-activated bentonite (B) (Berkbent 163, supplied by Tolsa) and kiln-dried fine sand (S) with a grain size smaller than 425 μm . The proportion of bentonite is known to affect both the geotechnical and geoelectrical properties (Kibria, 2014). Due to the attenuative influence of bentonite on the TDR waveform (Mojid et al., 2003), its content had to be determined experimentally. It was found that 5%

bentonite resulted in BEC at approximately 130 mS/m, which did not interfere with the interpretation of the TDR waveform.

Three types of soil mixtures were prepared to reflect high-plasticity clay (CH), intermediate-plasticity clay (CI) and low-plasticity clay (CL). The plasticity classification has been chosen as the name for the investigated soil mixtures, which are referred to in the text as CH, CI and CL. The proportions of the S, ECC and B fractions are presented in Table 3.1.

The sample size was planned to be of 110 mm diameter by 300 mm height (Section 3.3.1.3); therefore, due to the time required to complete the consolidation for the proposed sample size, only three mixtures were considered in this study.

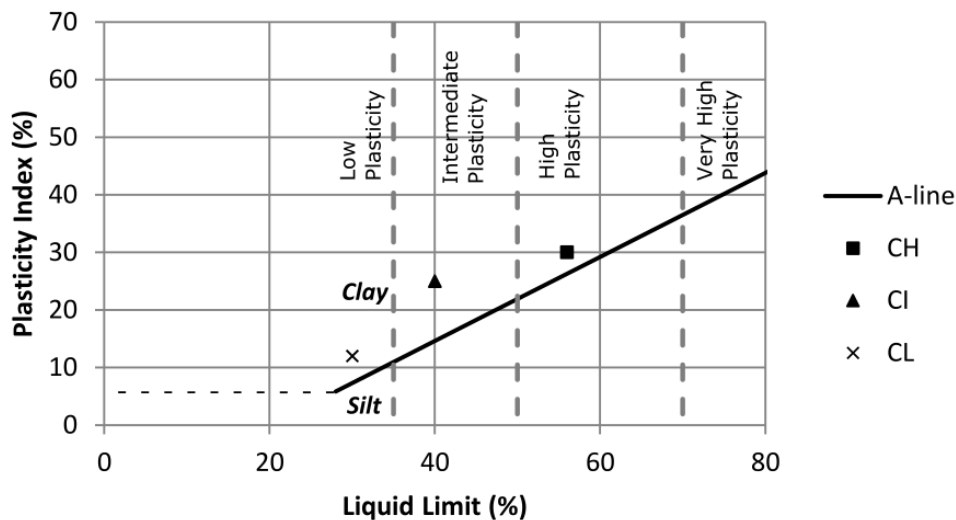
3.2.1 INDEX TESTING

In order to assess the plasticity of the soil mixtures, correlated with soil compressibility (Tiwari and Ajmera, 2012), Atterberg-limits (index) testing was carried out in accordance with BS 1377-2 (BSI, 1990a). Based on the LL and plastic limit (PL) results, the plasticity index (PI) was calculated as $PI = LL - PL$. The results are presented in Table 3.1.

Table 3.1. Index test results of the soil mixtures

Soil Mixture	Composition			Index Tests		
	ECC	B	S	LL	PL	PI
	%			%		
CH	85	5	10	56	26	30
CI	45	5	50	40	15	25
CL	50	0	50	30	18	12

Based on the index test results, the soil mixtures were classified as clays of high (CH), intermediate (CI) and low (CL) plasticity, in accordance with the plasticity chart (BSI, 2015). The LL values were used to make a decision on the start conditions of the main tests described later in Section 3.3.1.4.

**Figure 3.3. Soil classification in accordance with the plasticity chart (BSI, 2015)**

It is noted that presence of bentonite has a significant effect on the soil properties. This can be expected, given that the LL of montmorillonite is within 100–900% and kaolinite of 30–110% (Mitchell and Soga, 2005). The addition of bentonite also

increases uncertainty in the plasticity-index estimation (Barnes, 2000), which is considered to be a subjective test.

In order to enable index testing, the size of the sand grains had to be below 425 μm . Therefore, the kiln sand was sieved, and a particle-size analysis was carried out in accordance with BS1377-2 (BSI, 1990a). The fraction used in the soil mixtures consisted of 10% grains with an effective diameter (D_{10}) of 0.20 mm and 60% of grains with an effective diameter (D_{60}) of 0.28 mm. This resulted in a uniformity coefficient ($C_u = D_{60}/D_{10}$) of 1.4, indicating that the sand was uniformly graded (Barnes, 2000), which helped with the preparation of mixtures with similar initial porosity.

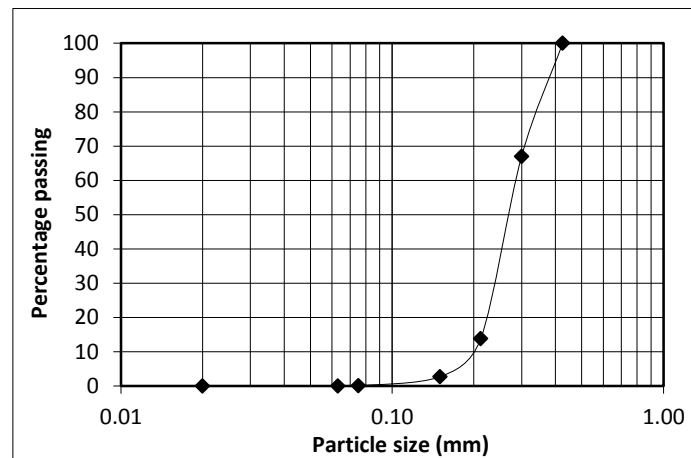


Figure 3.4. Fine-sand particle-size distribution (PSD)

3.2.2 PARTICLE DENSITY

Information about the particle density is necessary to calculate the initial porosity and initial void ratio of a soil sample (Eq. 3.2). Therefore, particle-density measurements

were carried out with the small pycnometer method according to BS1377:2 (BSI, 1990), and with the gas pycnometer method described in ASTM D5550-06 (ASTM, 2000).

The first method resulted in a measurement error exceeding the BS1377:2 guideline of 0.03 g/cm^3 as the maximum measurement difference between two repetitions. Therefore, the gas pycnometer, which was found to be more reliable and enabled a higher number of repetitions to be obtained in a shorter time (Pring, 2016), was selected. The testing was carried out with the helium pycnometer AccuPyc 1340 II. The sample preparation involved drying the soil at 105°C for a minimum 24 hours prior to the test. The dry soil was then stored in an airtight container.

In order to carry out the test in the AccuPyc II 1340, dry sand, ECC and bentonite were mixed in the testing vessel (1 cm^3) in adequate proportions to obtain CL, CI and CH. Due to the small sample size, the preparation of a representative soil mixture was problematic and resulted in a measurement variability exceeding the 0.03 g/cm^3 threshold (BSI, 1990). Therefore, separate samples of sand, kaolinite and bentonite were tested in three repetitions each, which provided results within the guidelines (Table 3.2).

The AccuPyc 1340 II's operational procedure suggests that the mass of the prepared sample should be 10% higher than the mass of the container; hence, the clay samples had to be slightly compacted in the container, by tapping, to increase the mass of the sample.

Table 3.2. Particle density of selected soils measured in a helium pycnometer

Soil	Measured Particle Density (Mg/m ³)		
	R1	R2	R3
Sand	2.64	2.67	2.65
ECC	2.65	2.68	2.65
Na-bentonite	2.71	2.71	2.71

Based on the sand, ECC and Na-bentonite results, the particle density was calculated for each soil mixture, based on the proportion of each constituent. The calculated particle density of CH, CI and CL was at 2.66 Mg/m³, corresponding to the commonly adopted 2.65 Mg/m³ for mineral particles.

3.2.3 OEDOMETER

The compressibility of the soil mixtures were investigated initially in the standard 1D consolidation oedometer, in order to understand the response of the chosen soils to loading and unloading. The compressibility parameters, provided as follows, were used to estimate the time needed to reach 90% of the primary consolidation in the bespoke samples. The analysis of the void-ratio changes, as well as the primary and secondary consolidation of the samples tested in the bespoke arrangement, was based on the standard oedometer consolidation analysis. Given that the void-ratio change forms the core of further correlations with the TDR and ER responses, this section also includes the formulas that were used in the analysis of the consolidation results.

The oedometer tests were carried out with a front-loading hanging-weight oedometer in accordance with BS1377-6 (BSI, 1990b). The samples were prepared at the LL of each soil to fit a stainless-steel ring of 75 mm diameter and 20 mm height. Due to the very soft consistency of the sample, the soil was placed into the chamber with a spatula (filter paper and porous stone were fitted to the ring to provide support). Top and bottom drainage was enabled via porous stones covered with filter paper. No lubricant was applied to the inner wall (this was to correspond to the bespoke chambers [see 3.3.1.3], where the application of grease was not possible).

Four CI and CL, and two CH samples were tested under four-step loading (25 kPa, 50 kPa, 100 kPa, 200 kPa) and gradual unloading in the same intervals. Each pressure step was applied until 90–100% of the primary consolidation was reached, as confirmed by the Taylor’s square-root-of-time method (Figure 3.6).

The initial and final GWC were measured by oven drying the soil samples for a minimum of 24 hours at 105 °C. Based on the initial GWC, an initial dry mass (m_d) (Mg) was calculated. Subsequently, the soil sample’s d_d (Mg/m³) was obtained from the dry mass and container volume (V) relationship in accordance with Eq. 3.1:

$$d_d = \frac{m_d}{V} \quad \text{Eq. 3.1}$$

Given that the soil samples were prepared at the LL, the saturation ratio (S_r) for fully saturated soils was assumed to be 1, and the initial void ratio (e_0) was calculated as shown in Eq. 3.2:

$$e_0 = GWC * G_s \quad \text{Eq. 3.2}$$

Where G_s is the ratio (unit-less) of the unit weight of the solid particles to the unit weight of distilled water, which is equal to the particle density.

In 1D consolidation, the volumetric changes (ΔV) are assumed to take place in a vertical direction only, and hence are expressed as a change in height ($\Delta h = \Delta V$). Following this, the void ratio is estimated for each loading step. For each pressure increment, the final equilibrium void ratio (e_f) was calculated using Eq. 3.3:

$$e_f = e_0 - \frac{\Delta h}{h_0} (1 + e_0) \quad \text{Eq. 3.3}$$

Where h_0 is the initial height (mm).

Consequently, the coefficient of volume compressibility (m_v) (m^2/kN) was calculated using Eq. 3.4:

$$m_v = \frac{\Delta h}{h_0} \frac{1}{\Delta \sigma'} \quad \text{Eq. 3.4}$$

Where $\Delta \sigma'$ is the effective stress increment ($\sigma'_1 - \sigma'_2$) (kPa) and $\frac{\Delta h}{h_0} = \frac{e_1 - e_2}{1 + e_0}$

Consequently, the compression index (C_c) and the swelling index (C_s) were estimated using Eq. 3.5 and Eq. 3.6:

$$C_c = (e_1 - e_2) \log_{10} \frac{\sigma'_1}{\sigma'_2} \quad \text{Eq. 3.5}$$

$$C_s = (e_1 - e_2) \log_{10} \frac{\sigma'_1}{\sigma'_2} \quad \text{Eq. 3.6}$$

Where e_1 and e_2 are the final void ratios at the end of the consecutive-consolidation stage at given effective stresses of σ'_1 and σ'_2 , respectively. The C_c and C_s results are presented in Table 3.3 and in Figure 3.5.

Table 3.3. Oedometer test C_c and C_s results

Soil	C_c	C_s
	[-]	
CH	0.38	0.08
CI	0.32	0.05
CL	0.13	0.03

The proportion of C_s relative to C_c was approximately 0.2, which corresponds to the values given in Barnes (2000) for similar soils.

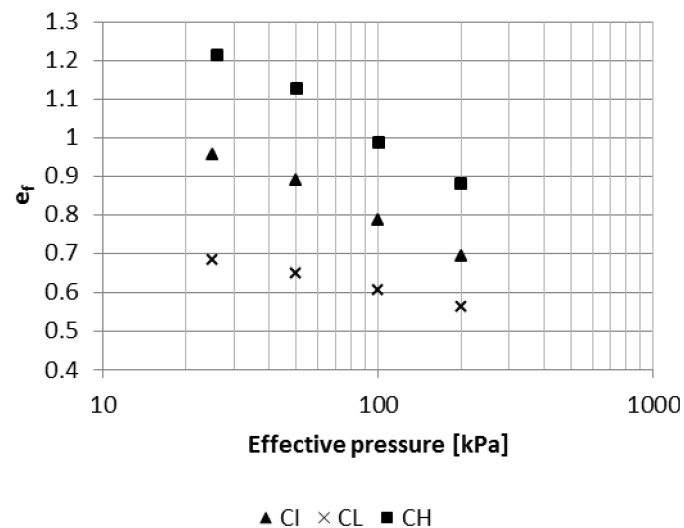


Figure 3.5. Compression index results (standard oedometer)

The reference soils, with similar LL and PL values corresponding to those investigated (CH, CI and CL), were included for comparison (Table 3.4). Most of the selected

reference soils lie on top of the A-line, apart from the *Ton IV* and *Residual clay*, which are classed as high-plasticity silt (MH). The mineral composition of the *Brown soil 1* – which included montmorillonite, kaolinite, muscovite and quartz – is considered to be closely related to the CH mix; however, the *red earth* – composed of kaolinite, montmorillonite, muscovite and quartz – relates to CI. The CL mix correlates with the properties of the *silty clay*.

Table 3.4. Reference soil properties

Soil Name	Index Tests (%)			Classi- fication	C _c	Source
	LL	PL	PI			
Brown soil 1	59	32	26	CH	0.43	Sridharan and Nagaraj, (2000)
Red earth 2	48	23	27	CI	0.40	
Silty soil	39	30	9.5	CI	0.20	
Ton IV	58	26	32	MH	0.32	Skempton (1944)*
Residual clay	58	27	31	MH	0.34	Ramiah (1959)*
Weald clay	39	19	20	CI	0.24	Skempton (1944)*
Ton V	36	18	18	CI	0.25	Skempton (1944)*
Silty clay	28	20	8	CL	0.14	Ramiah (1959)*
Boulder clay	28	14	14	CL	0.12	Skempton (1944)*
CH	56	26	30	CH	0.38	This research
CI	40	15	25	CI	0.32	This research
CL	30	18	12	CL	0.13	This research
* Data from Burland, (1990)						

In order to measure the rate at which the consolidation proceeded, the coefficient of consolidation (c_v) (m^2/yr) was calculated based on the square-root-of-time method, as shown in Eq. 3.7:

$$c_v = \frac{T_{v90} h_d^2}{t_{90}} \quad \text{Eq. 3.7}$$

Where T_{v90} equals 0.848, h_d is the drainage path (given that top and bottom drainage was provided, this reflects half of the drainage path at t_{90} for a given load increment), and t_{90} is the time required to achieve 90% consolidation.

According Taylor's method, t_{90} is determined from the gauge readings versus the square root of the time plot (consolidation curve) by fitting a line through the straight portion of the graph, as illustrated in Figure 3.6. The point at which the line crosses the gauge readings' axis is taken as the initial height (h_0), thus eliminating the changes caused by the initial compression. At a gradient 1.15 times the gradient of the straight line, a second line is drawn, which crosses the h_0 point. The point at which the second line crosses the consolidation line is considered to be t_{90} .

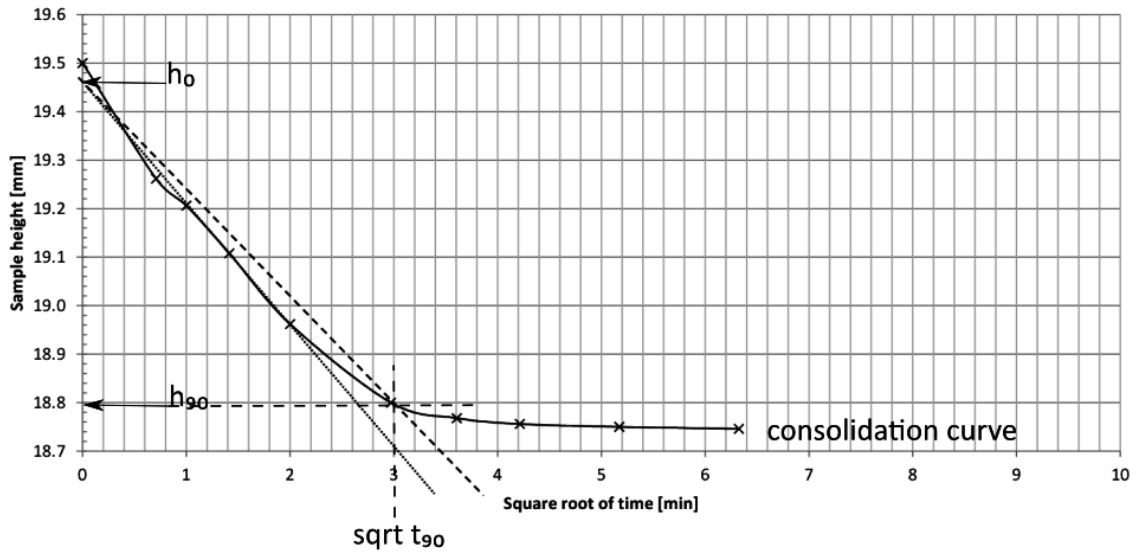


Figure 3.6. Example square-root-of-time method for determining t_{90} based on a sample of CL

The oedometer results were also analysed with the Casagrande log-time method, in which a 50% consolidation time (t_{50}) forms the base of the c_v calculations. The results were found to be comparable with the previous approach, and, for the ease of reference only, the results based on Taylor's method are reported herein.

Based on the c_v and m_v results, the coefficient of hydraulic conductivity (k) (m/s) was estimated using Eq. 8:

$$c_v = \frac{k}{m_v \gamma_w} \quad \text{Eq. 3.8}$$

The average calculated from the samples of CH, CI and CL (Tables 3.5–3.7) indicates c_v values in the order of 10.42, 0.15 and 0.23 m^2/yr , respectively, and k values in the order of $8\text{E-}11$, $4\text{E-}11$, and $1\text{E-}09$ m/s, respectively. Whilst CL exhibited a much faster consolidation time, which resulted from a higher hydraulic permeability than CI and CH, the behaviour of the latter two was very similar. It was expected that 50% of the

sand in CI, as opposed to 10% in CH, would be reflected in a significantly different permeability range; however, the presence of bentonite at equal proportions (5%) appeared to have a dominant effect on the consolidation parameters of these two clays.

The hydraulic conductivity of the CL mixture corresponds to that of stratified silt / clay deposits with poor permeability, whilst the CI and CH soils fall within the practically impervious soil range, which can be observed in unweathered clays (Barnes, 2000). The CH and CI results also correspond with the hydraulic conductivity of 95% silt and 5% bentonite, which was found to be between around $10\text{E-}09$ m/s (Sivapullaiah et al., 2000).

Table 3.5. Oedometer test results – CL

Soil sample	Load Step	σ'	e_f	m_v	c_v	k
		kPa	[-]	[m ² /MN]	[m ² /yr]	[m/s]
CL.R1	1	25	0.71	0.75	3.14	7.E-10
	2	50	0.68	0.46	7.59	1.E-09
	3	100	0.63	0.25	18.54	1.E-09
	4	200	0.59	-	-	-
	3	100	0.59	0.09	-	-
	2	50	0.60	0.21	-	-
	1	25	0.61	1.21	-	-
		1	0.66	-	-	-
CL.R2	1	25	0.66	0.78	11.04	3.E-09
	2	50	0.63	0.47	19.75	3.E-09
	3	100	0.59	0.25	11.94	9.E-10
	4	200	0.54	-	-	-
	3	100	0.55	0.09	-	-
	2	50	0.56	0.21	-	-
	1	25	0.57	1.14	-	-
		1	0.61	-	-	-
CL.R3	1	25	0.60	0.82	2.84	7.E-10
	2	50	0.57	0.44	9.80	1.E-09
	3	100	0.53	0.24	13.14	1.E-09
	4	200	0.49	-	-	-
	3	100	0.49	0.09	-	-
	2	50	0.50	0.21	-	-
	1	25	0.51	1.15	-	-
		1	0.56	-	-	-
CL.R4	1	25	0.65	0.80	3.14	8.E-10
	2	50	0.61	0.46	7.59	1.E-09
	3	100	0.57	0.25	18.54	1.E-09
	4	200	0.53	-	-	-
	3	100	0.53	0.09	-	-
	2	50	0.54	0.21	-	-
	1	25	0.55	1.08	-	-
		1	0.59	-	-	-
CL (average)					9.17	1.E-09

Table 3.6. Oedometer test results – CI

Soil sample	Load Step	σ'	e_f	m_v	c_v	k
		kPa	[-]	[m ² /MN]	[m ² /yr]	[m/s]
CI.R1	1	50	0.73	0.92	0.12	3.E-11
	2	100	0.64	0.45	0.12	2.E-11
	3	200	0.55	-	-	-
CI.R2	1	50	0.79	0.89	0.14	4.E-11
	2	100	0.70	0.46	0.10	1.E-11
	3	200	0.60	-	-	-
CI.R3	1	25	1.00	1.17	0.10	4.E-11
	2	50	0.93	0.96	0.23	7.E-11
	3	100	0.83	0.10	0.24	8.E-12
	4	200	0.80	-	-	-
	3	100	compression gauge fault			
	2	50	0.81	0.23	-	-
	1	25	0.82	0.71	-	-
		1	0.86	-	-	-
CI.R4	1	25	0.96	1.25	0.16	6.E-11
	2	50	0.89	0.93	0.18	5.E-11
	3	100	0.79	0.42	0.21	3.E-11
	4	200	0.69	-	-	-
	3	100	0.70	0.12	-	-
	2	50	0.71	0.27	-	-
	1	25	0.73	1.19	-	-
CI (average)					0.16	4.E-11

Table 3.7. Oedometer test results – CH

Soil sample	Load Step	σ'	e_f	m_v	c_v	k
		kPa	[-]	[m ² /MN]	[m ² /yr]	[m/s]
CH.R1	1	25	1.13	1.78	0.36	2.E-10
	2	50	1.02	1.06	0.22	7.E-11
	3	100	0.90	0.43	0.13	2.E-11
	4	200	0.79	1.63	0.23	1.E-10
	1	100	0.80	0.18	0.36	2.E-11
	2	50	0.82	0.40	0.22	3.E-11
	3	25	0.85	-	0.13	-
CH.R2	1	25	1.21	1.40	0.44	2.E-10
	2	50	1.12	1.11	0.22	8.E-11
	3	100	0.99	0.43	0.23	3.E-11
	4	200	0.88	1.74	0.21	1.E-10
	1	100	0.89	0.18	0.44	3.E-11
	2	50	0.92	0.41	0.22	3.E-11
	3	25	0.94	-	0.23	-
CH (average)					0.26	8.E-11

3.3 DEVELOPMENT OF THE TESTING EQUIPMENT

The testing equipment was designed to combine the vertical loading of fine-grained soil with ER and TDR measurements. To avoid interference between the ER and TDR sensors, these two techniques were tested on separate samples. Therefore, two types of bespoke chamber were designed (a TDR chamber and an ER chamber).

This section provides the details of the process involved in the development of the testing methodology, including the design, construction and modification of the

loading arrangement. It also introduces the development of the TDR and ER arrangements, which are discussed further in Chapter 4 and Chapter 5, respectively.

3.3.1 LOADING ARRANGEMENT

A vertical soil-loading arrangement was built for the purpose of this research, and it consisted of the customised chambers and a pressure system. Two types of pressure system were used; these were initial-lever loading – which is described in the following sections as Pressure System 1 (PS1) – and direct-frame loading – which is referred to as Pressure System 2 (PS2).

3.3.1.1 PRESSURE SYSTEM 1 (PS1)

The choice of the pressure system was based on its reliability and its effect on the electrical instrumentation. Initially, the incorporation of a hydraulic pressure system was considered; however, based on the previous experience of other researchers (e.g. Al-Obaidy, 2017), the application of low pressure (which was essential in this study) was difficult to maintain at a constant rate. Therefore, a dead-weight system was considered to be a better solution, as it allowed the application of low pressure in small increments and did not include any electrical noise that could interfere with the electrical sensors.

The PS1 approach involved the adaptation of the consolidation rig previously used by (Moghareh Abed, 2016). The rig comprised two loading arms, each equipped with a splitter enabling the loading of two samples per arm. Although having four samples under investigation at the same time would have saved time, using the splitter was considered to be unreliable due to the possibility of unequal load transfer. Therefore, a hole was drilled in the centre of the splitter to allow the loading of one sample per arm at a time (Figure 3.7). The load was transferred to the sample via a brass rod, which was joined to the top drainage plate.

Each beam was balanced with a dead weight positioned at one end and was subsequently loaded on the other end. The applied pressure was calculated from the moment relationship.



Figure 3.7. Initial loading arrangement for PS1, including lever arms for load transfer to a soil sample

In order to reduce the friction between the top drainage plate and the chamber wall, a polytetrafluoroethylene (PTFE) tape was used around the edge of the plate.

The initial testing revealed that, even when only one sample was loaded per arm, the presence of the splitter made the loading rod tilt, and therefore affected the loading transfer. In addition, given that the existing rig could accommodate only two samples at a time, it was decided to modify it to make it more reliable and efficient.

3.3.1.2 PRESSURE SYSTEM 2 (PS2)

The modifications of the PS1 loading arrangement focused on increasing the magnitude of pressure acting on the sample, increasing the number of samples monitored at the same time and providing support to the loading rod to avoid tilting.

In order to increase the magnitude of pressure acting on the sample, it was decided that the dead weights should be applied directly to the sample rather than via the swivel arms. The arms were removed and replaced by two metal shelves. This new arrangement allowed up to six samples to be placed on the shelves at the same time. The maximum load that could be applied to the sample was limited to 130 kg (including 125 kg dead weights and the 5 kg loading frame; this corresponded to a loading pressure of approximately 134 kPa) due to the strength of the plastic chamber, which was already weakened by the presence of the opening for the electrodes and the size of the loading rig. Lateral expansion of the chamber was monitored, and the compression gauges were positioned normally to the chamber wall. No expansion was observed.

In order to enable direct loading with the dead weights, a loading frame was designed. It was to be hung directly on the loading bar, thus taking into consideration the size of the bespoke chamber, and accommodating the electrodes and cabling, as well as the separation of the slots present in the support shelf.

Six identical frames (Figure 3.8) were made out of threaded steel rods with a 10-mm diameter. They were 280 mm wide, and their height was 1260 mm to allow for the hanging of the weights below the support shelf, given that the frame would travel a maximum of 90 mm during the settlement process. The position of the weight shelf was adjustable. At the same time, the size of the chamber was modified slightly (Section 4.1) and the length of the loading rod was set to 200 mm to allow movement from 295 mm to 200 mm.

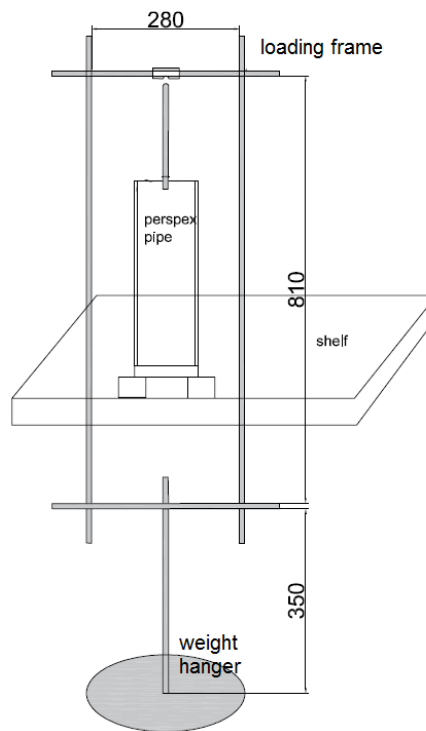


Figure 3.8. Loading frame design (units in mm)

The initial trial with the new arrangement was not successful, as the loading bar tilted (Figure 3.9).

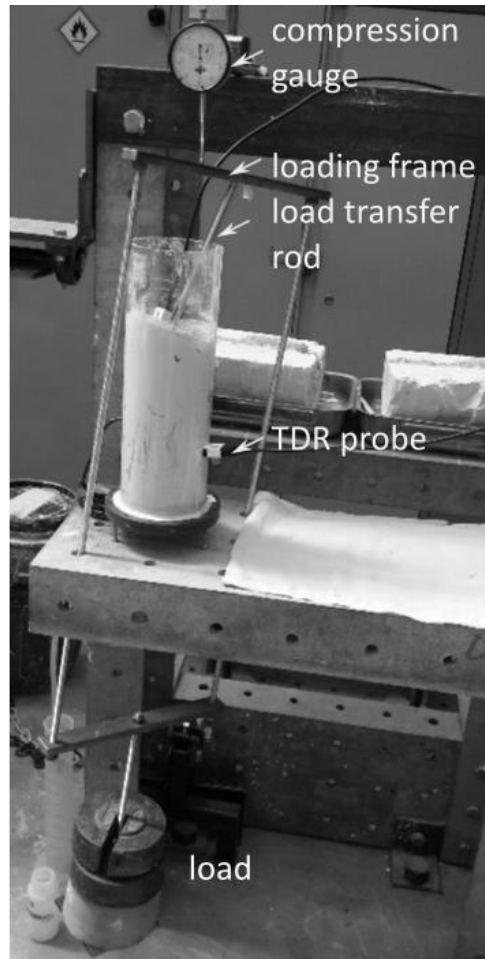


Figure 3.9. Initial (unsuccessful) trials of the PS2 arrangement

However, incorporating a centring ring at the top of the chamber solved the problem (Figure 3.10). This also worked as a cap, which reduced evaporation, and therefore provided additional control in the testing environment. An additional metal shelf was also mounted on the top of the rig to accommodate the compression gauges.

Compression clock gauges with 0.01 mm accuracy were used during the tests. Their readings were compared, on a daily basis, against the measuring tape placed on the chamber wall. The PS2 arrangement was redeveloped further by the addition of side shelves to accommodate more samples (Figure 3.10b).

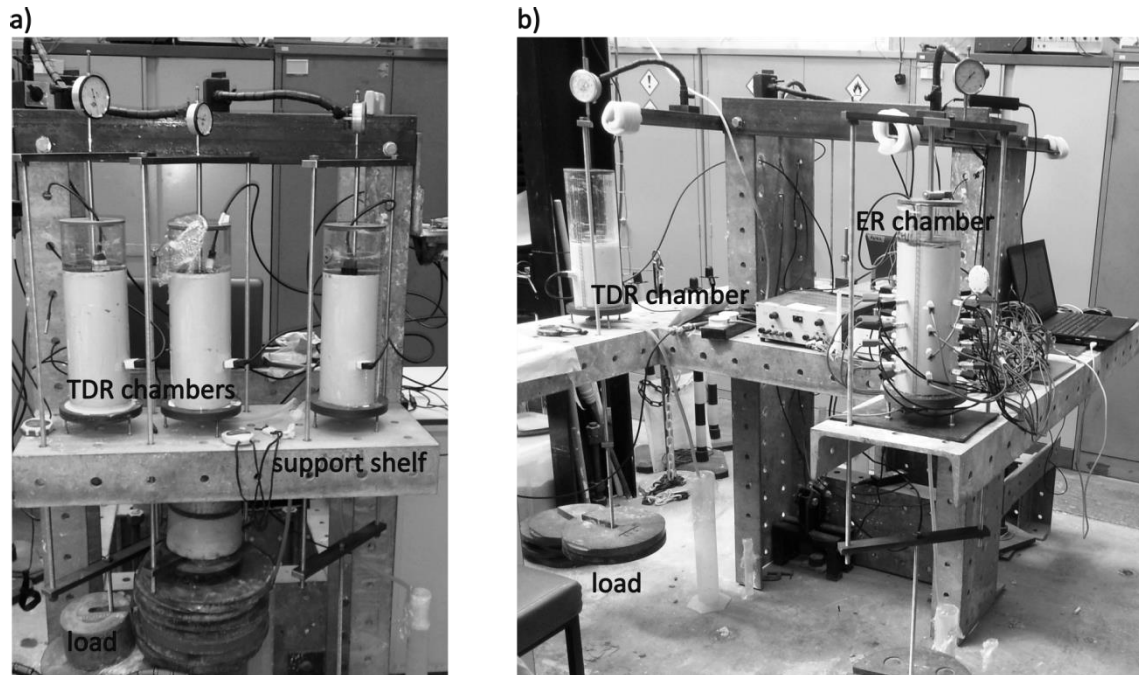


Figure 3.10. Loading rig PS2: (a) initial stages of development; and (b) final PS2 arrangement

3.3.1.3 BESPOKE CHAMBER-SAMPLE SIZE

The design of the bespoke chamber took into consideration the standard guidelines on 1D consolidation (BS1377-6), whilst incorporating the ER and TDR instrumentation.

Given that the ER and TDR instrumentation could not be placed in one chamber at the same time, since they could interfere with each other, two separate chambers were designed and constructed to enable TDR and ER testing during the loading of soil. Further details on the TDR and ER arrangements and the corresponding measurements are described in Chapters 4 and 5, respectively.

In traditional oedometer tests, the sample diameter is recommended to be larger than the height to ensure uniform consolidation (BS1377-6). In this work, incorporating two TDR probes dictated the sample height, which was set to a minimum of 300 mm to enable the observation of the settlement and free movement of the vertical probe (TDR_v) without interfering with the horizontal probe (TDR_h). The diameter of the sample was set at 110 mm, as a minimum, thus allowing the operation of TDR_v and TDR_h in one chamber, and ER in the other, without excessive influence from the side friction.

The bespoke samples included a 'full size' diameter to height (D/H) ratio of ~ 0.4 with TDR_v and TDR_h or ER instrumentation; and 'half size' D/H ratio of ~ 0.6 with TDR_h and a sample without any electrical instrumentation (N). It was expected that, in this arrangement, the sample was unlikely to consolidate uniformly, as demonstrated in the consolidation study on samples with a D/H ratio of 1:4 (Valls-Marquez, 2009); nonetheless, this did not preclude establishing a correlation between the geotechnical and geophysical parameters. On the contrary, it presented an opportunity to apply electrical readings to monitor non-uniform moisture distribution, and identify further links with the changes taking place in the field.

The initial loading tests (PS1) were performed in 340 mm tall chambers. Following the trials, it was concluded that the chamber height could be reduced slightly to 300 mm (PS2) in order to increase the rate of settlement. The subsequent incorporation of a plastic centring ring (supporting the loading rod) had to take into account the space

needed to accommodate the TDR-probe head, and therefore the final sample height was from 278–294 mm in both the TDR and ER chambers.

Additionally, a few selected tests were performed on the samples with TDR_h, which was only to investigate whether the distance of the probe from the loading plate influenced its response. The initial height of these samples was therefore reduced to 160–170 mm.

Finally, an additional chamber was built to investigate the relationship between the parameters measured using TDR and pore-water pressure (further details are reported in Section 4.2).

3.3.1.4 SAMPLE PREPARATION AND VALIDATION OF SAMPLE UNIFORMITY

In order to prepare a sample suitable for settlement testing in the bespoke chambers, soil mixtures were prepared at 1–1.5 LL following Burland's (1990) research, who linked intrinsic compressibility (inherent to the soil and independent of its natural state) to the type and amount of clay of a soil in a reconstituted state (i.e. soil mixed with water to 1–1.5 times LL). It was found that this water content was too low for the pore-water-pressure investigation in a bespoke arrangement (Section 4.6); therefore, one sample was prepared at 1.8 LL.

In order to ensure uniform mixing, the dry sand, kaolinite and bentonite were mixed by hand, in the proportions presented in Table 3.1, to obtain CL, CI and CH. In the case of CH, with 90% clay, sand was added once the clay powders were mixed. For CL and CI, with a 50/50 sand to clay content ratio, the clays were added to the sand. Once the powders were mixed thoroughly, distilled water was poured in gradually to achieve the required GWC. Following the hand mixing, the slurry was placed in a mechanical mixer for at least 30 minutes, and then transferred to a plastic bag for a minimum of 48 hours to allow curing and ensure uniform moisture distribution.

Given the size of the bespoke chamber and the consistency of the soil at its LL being similar to thick toothpaste, transferring the slurry to the chamber was challenging. Initially, the soil paste was squeezed out from the plastic bag into the chamber in layers and then stirred with a plastic stick. However, this approach led to the presence of large air voids. Using a vibrating poker was considered; nevertheless, to avoid the risk of agitating the natural balance between the clay particles and pore water, developed during the curing, this option was eliminated. Therefore, in order to minimise the presence of the voids, the soil paste was placed in the chamber in small amounts (approximately 6–8 cm³) with a scoop. Complete elimination of air was not possible, and the potential effect of the resultant partial saturation is discussed in Section 3.3.2.3.

To verify whether the preparation method delivered a uniform sample, the sand content and d_d were measured. The sand content was investigated at the end of the

loading process by taking three soil samples at four different depths, which were then subject to a wet-sieve analysis. The soil samples were initially dried at 105 °C to determine the GWC, and were later crushed and soaked in water for a minimum of 2 hours. Subsequently, they were wet sieved through both a 75 µm and a 63 µm sieve to wash away the clay fraction, and dried for 24 hours at 105 °C. The results (Table 3.8) indicated that the maximum difference in sand content within the layers was within 0.8%. The samples from the CH soil imply that the sand content was 13% rather than the expected 10%; however, its distribution was uniform. It should be noted that no deflocculant was used during the wet sieving, hence it is likely that the percentage weight content of the sand was increased by bentonite particles adhered to its surface.

The d_q was also investigated in selected samples at the end of loading by taking subsamples, at three points and at two depths, with copper cylinders (30 mm diameter and 50 mm high) sharpened at the end and lubricated to facilitate insertion. However, due to the final soft-to-very-soft consistency of the sample, this method was deemed unreliable. Fall-cone-testing trials (Section 3.3.3.2) were also carried out; however due to faulty equipment, the results could not be used.

Table 3.8. Post-loading sample-uniformity verification (sand content) in four samples (CH.S4.TDR, CI.S6.ER, CH.S5.ER and CI.S10.N)

Depth (mm)	Sand Content	Depth (mm)	Sand Content
CH.S4.ER		CI.S6.ER	
200–140	13.3%	219–200	49.8%
130–110	13.3%	200–170	50.0%
80–50	13.4%	135–110	50.3%
40–20	13.5%	100–70	50.2%
20–0	13.6%	75–45	50.0%
		55–35	50.1%
		35–0	50.3%
CH.S5.TDR		CI.S10.N	
215–185	12.9%	154–140	50.3%
185–165	13.3%	140–120	50.3%
130–100	13.1%	120–80	50.2%
100–80	13.2%	80–40	50.8%
80–90	12.9%	40–0	50.0%
60–0	13.2%		

3.3.2 BESPOKE LOADING-ARRANGEMENT CONSTRAINTS

3.3.2.1 PRESSURE-HEAD DIFFERENCE

In the standard oedometer tests, an equal pressure head is maintained at the top and bottom of the sample as it is immersed in water, and the upper and lower porous stones are in hydraulic connection with the surrounding fluid. In the design of the bespoke ER and TDR chambers, it was not possible to place the sample in a water bath, due to the presence of the measuring electrodes. In order to equalise the pressure

head, filling the bottom drainage pipe with water to the level of the top drainage plate was considered. However, adding water to the drainage pipe would have diluted the pore fluid, and as a result preclude the chemical and electrical investigation of its properties. Therefore, whilst the upper and lower drains were used in the bespoke cells, the water in each was not at the same pressure head; the bottom drain allowed the fluid to drip out of the chamber (via an air-filled pipe) and was collected in a container approximately 1 m below the bottom of the cell. Pore fluid seeping out of the upper face of the sample accumulated on top of the perforated loading plate (Figure 3.11).

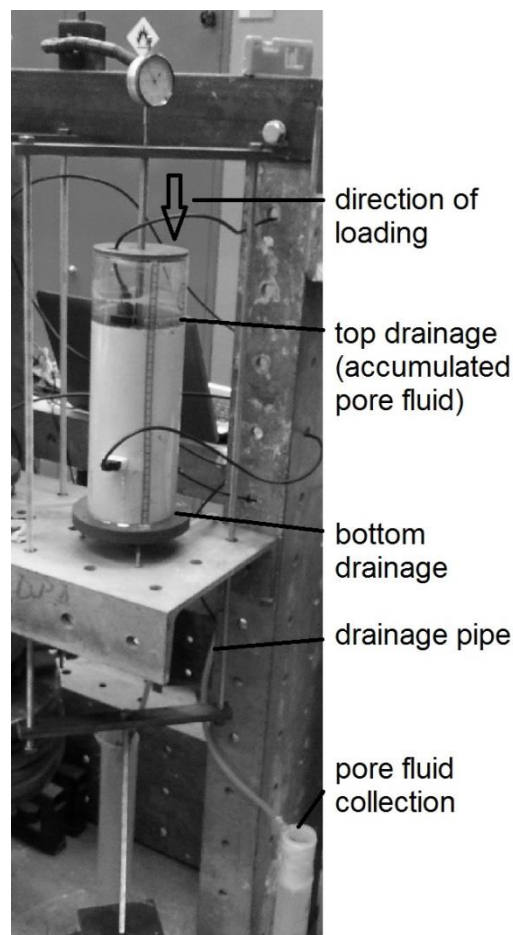


Figure 3.11. Bespoke chamber – loading and drainage locations

The settlement of the sample resulted in a transient difference in the pressure-head difference, as water seeped out of the two drains; hence, the hydraulic gradients acting on the samples were also transient in nature. This is discussed further in Chapter 6.

3.3.2.2 LOAD TRANSFER AND FRICTION

The load transfer in the bespoke chambers was expected to be affected by the friction between the soils and the walls of the chamber, due to the low D/H ratio and the lack of a lubricated slip lining. Friction increases with load and sample depth (Rosine and Sabbagh, 2015), and results in a decrease in the effective stress with the depth of the sample during loading, when compared with the applied external load (Olson, 1986). The exact extent of the friction effect could not be measured directly in this research. Since the density measurements and fall-cone tests were not reliable, the GWC readings, taken at the end of loading, were considered to be the main indicator of the load transfer within the investigated soils, with pore-water volume and shear-vane measurements also being considered. As indicated in the preceding section, in the CI and CH soils, the volume of the water collected on the top of the chamber was higher than at the bottom, indicating that the level of compression was higher in the top layer. This was also supported by the shear-vane measurements, indicating a difference in undrained peak shear strength (c_u) between the top and bottom of the sample; i.e. in the range 3–13 kPa in the CH soil, and 1 kPa in the CI soil. This suggested that the stress within the soil caused by the applied load decreased with depth.

During the final GWC sampling, samples were taken along the chamber walls to compare them with the soil samples taken away from the boundary; however, no consistent trend was noted (Figure 3.12). Samples CI.S8 and CI.S9 appeared to have been partially consolidated, based on the GWC results.

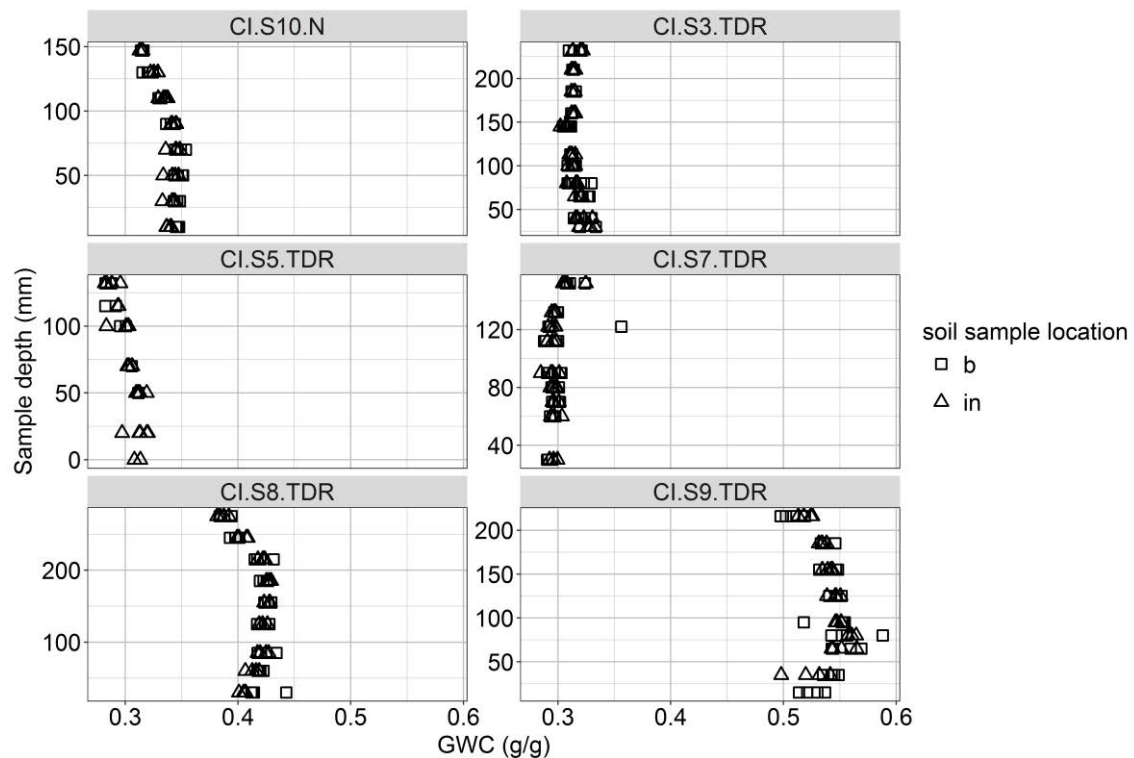


Figure 3.12. GWC variation within the horizontal layers at the end of the loading of the CI samples (b = GWC sample collected at the boundary, and in = sample collected away from the boundary)

It was observed that the GWC variability within the sample, at the end of the consolidation, depended on the number of load stages and the magnitude of the pressure applied (Figure 3.13). In the samples loaded in three or more loading stages to a maximum value of effective stress at approximately 100 kPa, the GWC variation with the depth was between 3% and 5%, whilst in samples where only one load stage

was applied (resulting in effective stress at 15 kPa and 5 kPa), the final GWC values within the vertical plane were 6% and 9%, respectively.

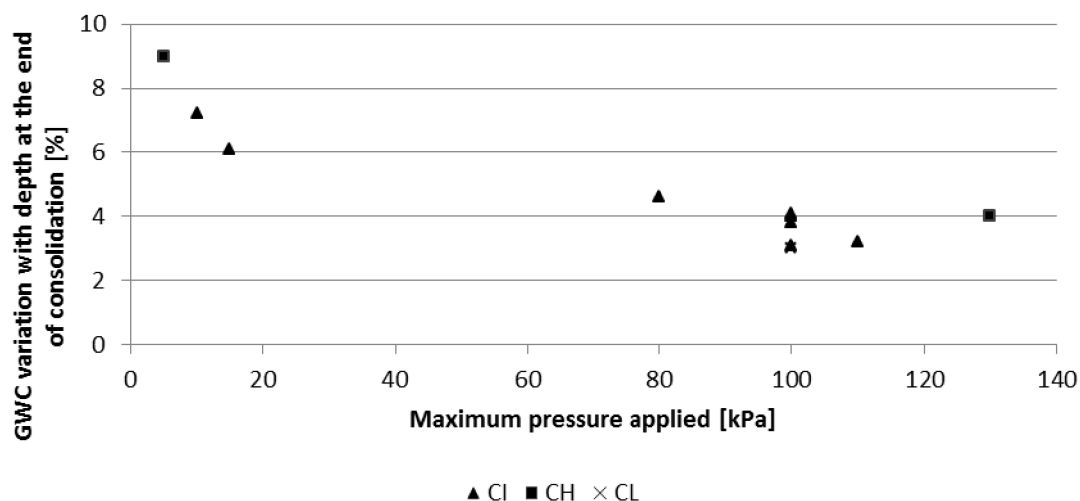


Figure 3.13. GWC variation (in the vertical plane) within the CL, CI and CH samples at the end of the loading

3.3.2.3 PARTIAL SATURATION

Although the samples were prepared at 1.0–1.5 LL (and one sample at 1.8 LL), partial saturation (calculated from the initial bulk density) was encountered in several samples (Table 3.9). The lowest saturation degree was found in the CH.S002.TDR sample at 89%. This was one of the first trials, where large voids were present in the sample due to the difficulties in sample preparation. During the PS2 stage, the soil paste was placed in layers and mixed thoroughly; however, the partial saturation was determined to be between 94% and 97% in six samples.

Table 3.9. Samples with a saturation degree below 100%

Sample Reference	Initial GWC	Saturation Degree
CI.S2.TDR	0.45	0.97
CI.S5.TDR	0.45	0.94
CI.S7.TDR	0.39	0.97
CI.S10.TDR	0.45	0.97
CH.S002.TDR	0.58	0.89
CH.S5.TDR	0.82	0.96
CL.S2.TDR	0.31	0.95

Unsaturated soils with a degree of saturation of over 90–99% are considered to be unsaturated with occluded air bubbles, in which the dissipation of the excess air pressure can either take place instantly upon load placement (Fredlund and Rahardjo, 1993) or dissipate simultaneously with the pore-water pressure (Zhou and Zhao, 2014). Unsaturated soil exhibits a higher initial-volume change when subject to a total-stress increase, but exhibits a lower change over time in comparison with saturated soils (Fredlund and Rahardjo, 1993).

The settlement of the soils was also compared against the volume of the collected fluid, indicating that the change in the sample settlement was approximately 2% higher than the volume of water seeping out (Figure 3.14); this is potentially due to the voids closing and air seeping out of the samples.

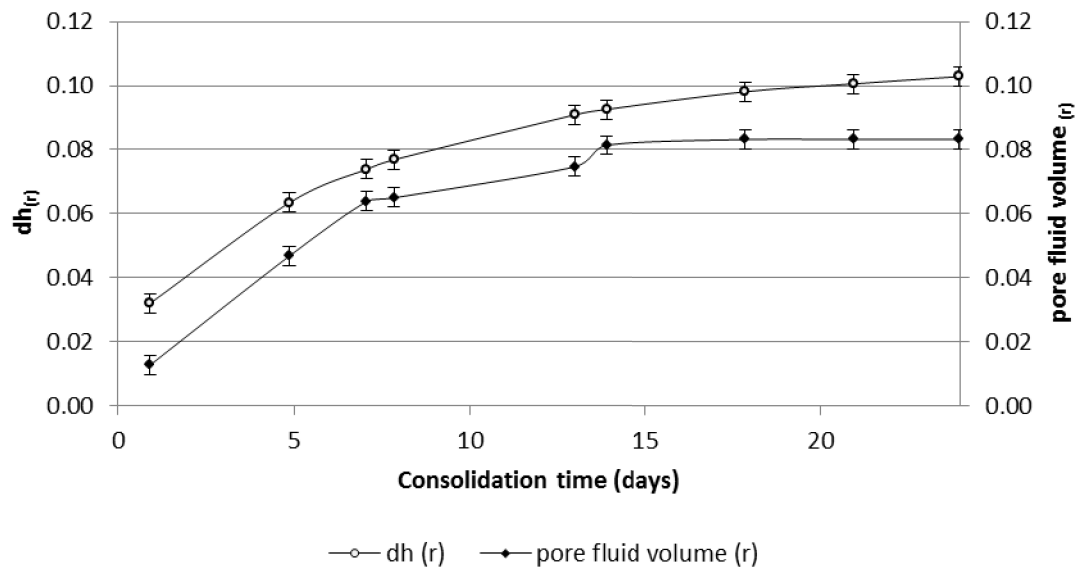


Figure 3.14. Example (CI.N sample) of changes in settlement (dh) and the pore-fluid volume collected from the top and bottom drainage points normalised (r) by the initial reading. The error bars are indicative representations of the approximately 0.5mm error associated with reading the pore-fluid level from a measuring tape.

The ratio of the initial compression to the final height of the sample at a given load for two partially saturated samples (CI.S5.TDR and CI.S7.TDR) was compared to a fully saturated sample (CI.S3.TDR). The results illustrate that during the initial loading the unsaturated samples exhibited a higher initial-compression-to-final-height ratio; however, as loading progresses, the difference in the ratio reduces. Although a limited number of comparable data points are available, this suggests that there is an evident discrepancy between the partially and fully saturated soils during the initial loading. Given that the initial compression is not included in the estimation of c_v , this does not, therefore, affect the estimation of k . However, the $e - \log \sigma'$ relationship may differ when saturated samples are compared with unsaturated samples.

3.3.3 SHEAR STRENGTH

Given that the post-loading consistency of the soils was from soft to very soft (BSI, 2015), two methods commonly used to determine the c_u within this strength range were investigated, i.e. the hand shear vane and the fall-cone method (Lu and Bryant, 1997). Both tests were conducted for all the soils investigated, and the results are described in the following sections.

3.3.3.1 HAND-SHEAR-VANE SOIL-SHEAR-STRENGTH MEASUREMENTS

The hand-shear-vane measurements were carried out on selected soil samples; samples that were subject to the dry-density verification with the use of cylinders could not be tested with the shear vane, as the soil was already disturbed during sampling. Depending on the expected strength of the sample, a 19 mm or 33 mm vane was gently inserted into the sample in three points at each of three depths. Due to the size of the chamber, an extension rod was required to reach the lower depths. An average of three repetitions was then linked with the GWC results to obtain an approximation of the GWC- c_u relationship for a given soil (Figure 3.15).

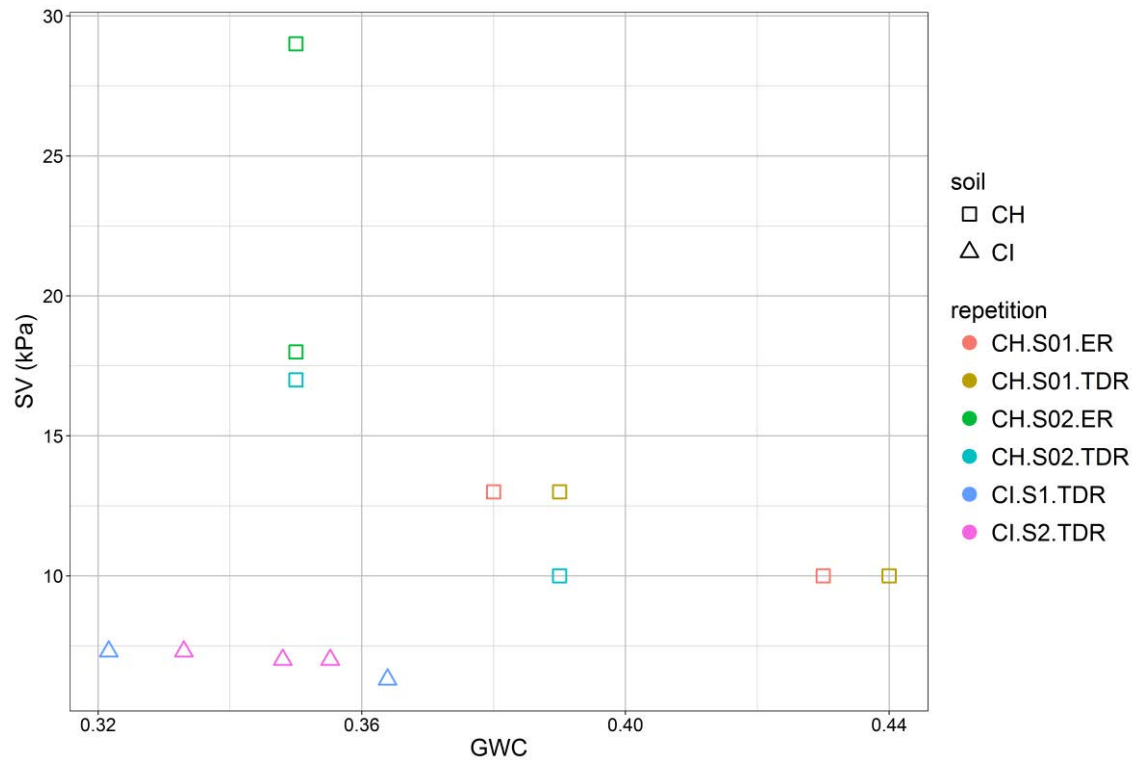


Figure 3.15. GWC- c_u relationship in selected CH and CI samples, measured at the end of the consolidation test

Although the hand shear vane is not considered very reliable due to difficulties in maintaining a constant rate of stress and verticality (Valls-Marquez et al., 2008), in this research it was the only approach that was considered reliable enough to provide an approximation of the c_u readings at the selected sample depths. Due to the low reliability of this method, the obtained shear-strength measurements are considered indicative only and are used only to investigate post-loading variability within the sample.

3.3.3.2 FALL-CONE SOIL-SHEAR-STRENGTH MEASUREMENTS

Fall-cone shear-strength measurements were considered as an alternative method to obtain an approximation of c_u , as this method has been tested successfully in other slurries of similar properties those examined in this study, e.g. (Lu and Bryant, 1997).

A standard LL fall cone was modified to be used in the bespoke chambers. The length of the rod was extended to reach to lower depths of the sample (Figure 3.16); however, the new length resulted in instability when the cone was dropped, and significant variations in the measurements were repeated at the same depth. Support for the rod was added to the system, but it did not solve the problem. Further enhancements of the equipment arrangement were not attempted due to time constraints. Therefore, the fall-cone method was not used in the determination of c_u .

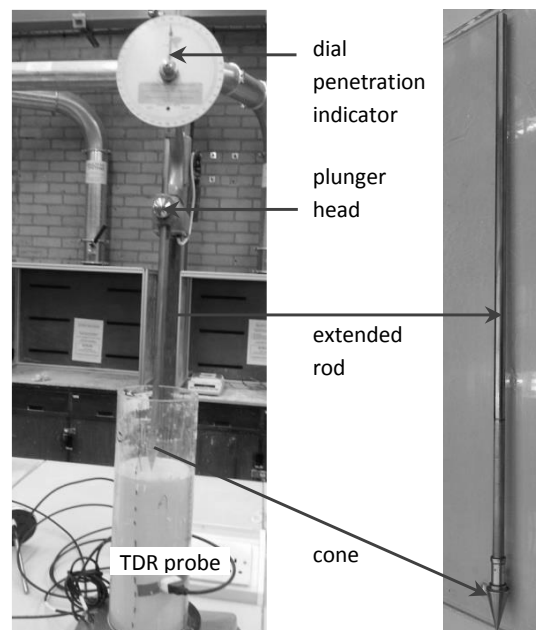


Figure 3.16. Shear-strength measurements in a TDR chamber with a fall-cone method

3.3.4 TEMPERATURE

Temperature measurements are crucial during electrical-conductivity investigations as a 1 °C temperature variation can result in a 2% change in its value (Campbell et al., 1948). Therefore, temperature readings were collected during this investigation at regular intervals.

During the primary testing, a mercury thermometer was used, which had an accuracy of ± 1 °C. Subsequently, a digital Brannan England RTD thermometer with a PT100 probe was used, which had an accuracy of ± 0.5 °C. Furthermore, automatic temperature-data collection was incorporated into the ER and TDR chambers during the PS2 stage. Temperature measurements were collected every 15 minutes in ambient air and inside each chamber by an automated node (Sadeghioon et al., 2014) and a waterproof DS18B20 probe, which had an accuracy of 0.5 °C (Figure 3.17). The temperature sensor used inside the chamber was 26 mm long and had a diameter of 7 mm. This was placed 110 mm above the base of the chamber, i.e. far enough away from the base to reliably measure the temperature within the soil, but positioned so it did not influence the TDR and ER measurements.

The node enabled the connection of four temperature sensors at a time; therefore, two nodes were used during this research. The measurements were obtained with Termite software operated from a laptop.

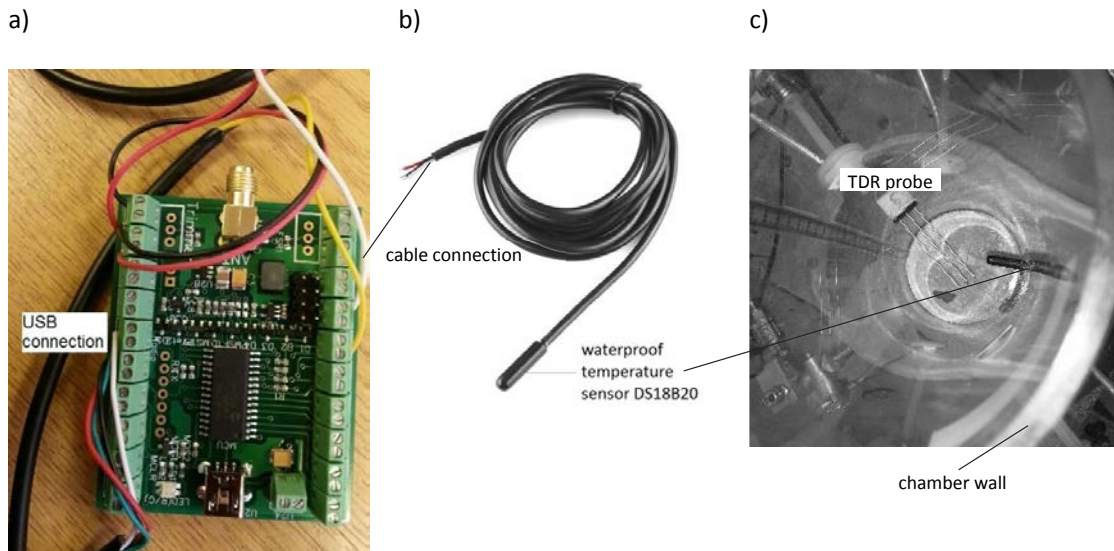


Figure 3.17. (a) Automatic temperature-acquisition node; (b) the waterproof temperature sensor DS18B20; and (c) its position in the TDR chamber

3.4 PORE-FLUID TESTING

It was planned to monitor the EC, BEC and AP of the pore fluid that seeped out from the sample after the completion of each loading stage of consolidation; however, there was not enough fluid to carry out this testing with the available equipment. Therefore, the pore fluid was stored, and the ER, BEC and AP values were obtained for the total fluid collected from a given sample at the end of the loading process using the ER boxes (described in Section 5.1.1) and with a TDR probe.

In addition, chemical analyses were conducted with ICP-OES to investigate the composition of the fluid and identify any traces of metal that could indicate the potential corrosion of the electrodes. The ICP-OES testing (Figure 3.18c) was carried

out using the Perkin Elmer Optima 8000, based on the ENS 10-safe operating procedure (Orgill, 2015). The instrument measured the concentration of the selected elements by comparing the intensity of the light emitted by the elements with the intensity of a standard of known concentration. The most sensitive wavelengths for a given element were selected prior to the testing. The results from these tests are presented in Chapter 6, Table 6.3.

The preparation of the samples included filtration through a 0.2 μ m filter (Figure 3.18a), the dilution of the pore fluid to 10% in a 2% solution of nitric acid, and the preparation of reference solutions for 15 metals (Ca, Na, Mg, K, P, S, Al, Fe, Zn, Co, Cr, Mn, Cu, Ni and Si) at six concentrations (0.05, 0.1, 1, 5, 10 and 20 ppm). The range of the dilutions was based on the anticipated concentrations. The diluted samples were stored in airtight containers (Figure 3.18b).

a)



b)



c)



Figure 3.18. ICP-OES testing: (a) sample filtration; (b) storage of the samples; and (c) sample testing using the Perkin Elmer Optima 8000

CHAPTER 4: DEVELOPMENT OF THE BESPOKE TDR ARRANGEMENT

This chapter provides the details of the design and development of a bespoke TDR arrangement, including a TDR chamber and associated acquisition system (commercial). It also includes the details of the development of the experimental laboratory-testing programme, calibration and preliminary results of the soil-loading tests conducted in the bespoke TDR chambers.

4.1 BESPOKE TDR CHAMBER

Following the design principles described in Section 3.3.1.3, the primary constraint dictating the size of the bespoke chamber was the sampling volume of the TDR probes, which were 75 mm long and 25 mm wide. Given that two TDR probes were planned to be placed inside the chamber – one in the vertical direction and one in the horizontal direction – and the TDR probes' sampling volume extends to approximately 30 mm from the rods (Suwansawat and Benson, 1999), the diameter of the chamber had to be set to a minimum of 105 mm and the sample height to a minimum of 115 mm. In order to enable observation in the vertical direction over a range of sample heights, the initial chamber height was set to 340 mm (PS1, Section 3.3.1.1). Following the initial testing with the PS1 arrangement, it was concluded that a 300 mm height would be sufficient to conduct the settlement observation for the selected soil mixtures (PS2, Section 3.3.1.2) and shorter drainage would improve the time efficiency by shortening the settlement time.

The final bespoke chamber was made from a Perspex pipe, with a 110 mm diameter and 300 mm height, to enable the observation of the visual changes. The Perspex chamber was equipped with top and bottom drainage through using plastic plates perforated with 8 x 6 mm and 6 x 3 mm holes. The top plate was mounted on a metal bar to transfer the load (Section 3.4.1.2) (Figure 4.1). Each TDR chamber was also equipped with a temperature sensor, which was placed approximately 100 mm from the bottom (discussed in Section 3.3.3).

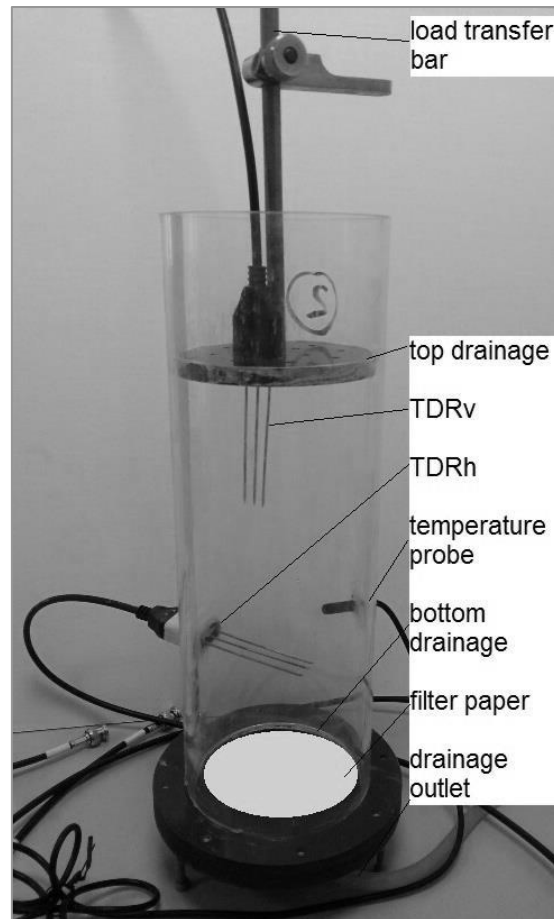


Figure 4.1. TDR chamber

4.2 PORE-WATER-PRESSURE MEASUREMENTS IN THE BESPOKE TDR CHAMBER

One of the TDR chambers was modified to include the collection of pore-water-pressure measurements. Six external pore-water-pressure sensors were mounted radially on the walls of the chamber at three depths from the base (Figure 4.2a):

- i. 210 mm, corresponding to the height of TDR_v (PS-t);
- ii. 147mm, in the middle of the sample (PS-m); and
- iii. 84 mm, corresponding to the depth of TDR_h (PS5-b).

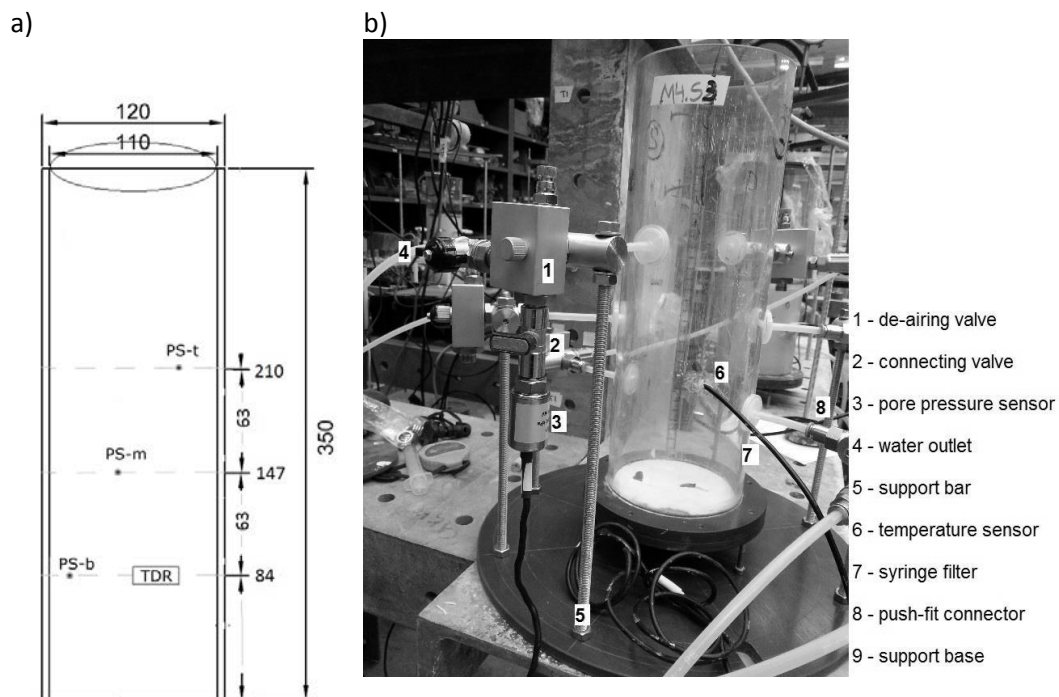


Figure 4.2. (a) Pore-water-pressure TDR chamber design; and (b) prototype

In order to reduce the outflow of clay particles with the pore fluid, through the holes made in the wall to connect the sensors, these were covered with a syringe filter of 0.2 μm pore size. However, as it was observed that pore fluid was not flowing out of

the sample under the application of external pressure, it was concluded that the capacity of the filter was too low to enable the free movement of water. As a result, the paper part of the syringe filter was punctured and a fresh piece of filter paper (the same as that used on the top and bottom of the sample) was glued over the opening, ensuring that the glue did not block the hole. The plastic part of the syringe filter remained in the wall as it provided a good link with the connecting pipes. The plastic outlet of the syringe filter was glued to a plastic pipe connected to the de-airing valve ('1' on Figure 4.2b), through a push-fit connector ('8'). The de-airing valve was connected to the pore-pressure sensor ('3') via a valve ('2'), equipped with a closing handle. The weight of the sensors and de-airing valve was higher than the weight of the chamber; therefore, a support frame ('5' and '9') was needed to ensure the stability of the arrangement.

Due to the number of connections, sustaining a waterproof system was challenging. The chamber was filled with water in order to check if any leaks were present. The leaks' locations were marked, the chamber was dried and the faulty locations were sealed with silicone sealant. Overnight, the sealant dried and the water test was repeated. It took approximately a week until a watertight arrangement was obtained. Once no leaks were noted, the pressure was monitored in a water-filled chamber for a minimum period of 24 hours.

4.3 TDR ACQUISITION SYSTEM

The TDR acquisition system (Figure 4.3) comprised the following:

- i. a TDR100 Campbell Scientific operated via PCTDR software provided by the manufacturer;
- ii. stainless-steel probes made of three rods (with diameter 1 mm, length 75 mm and separation 5 mm);
- iii. coaxial cable; and
- iv. a laptop.

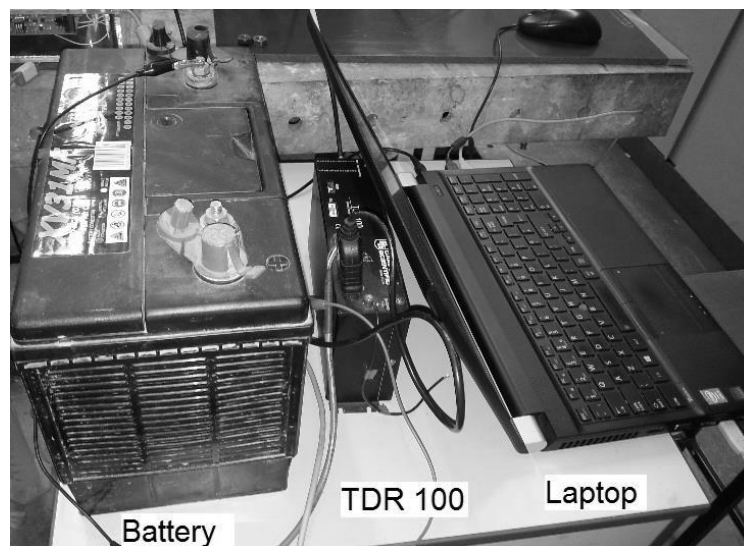


Figure 4.3. TDR acquisition system

The choice of the probe size was a compromise between the accuracy of the testing, minimum sample disturbance and practicality. Short probes were found to be more suitable in conductive soils (Robinson, 2003); therefore, commercially available and easy-to-handle short probes with thin rods were found to be suitable for this study.

The measurements were collected via the TDR100 Campbell Scientific PCTDR software (installed on a laptop) based on the following parameters:

- i. The velocity propagation factor (V_p), describing the ratio between the actual signal velocity v (m/s) and the speed of light in free space c (m/s), was set to 1; this was based on the assumption that the actual signal velocity was equal to the speed of light in a vacuum. This enabled the calculation of an apparent distance (apparent length [L_a]) rather than a real distance (the true velocity of the TDR signal is not known).
- ii. The number of averages (between 1 and 128 for the TDR100 unit). Given that 16 waveforms are required in order to obtain accurate BEC measurements (Bechtold et al., 2010), 20 averages were collected to obtain a smooth waveform without too much noise.
- iii. The number of data points in each waveform was set to the maximum permitted by the TDR100 unit, i.e. 2048, as this enables high-resolution waveforms to be collected.
- iv. The start and length of the waveform plot for the BEC measurements were set to 0 m and 500 m, respectively, based on Curioni (2013); whereas, for the AP measurements, these parameters were set to 4.0 m and 1.3 m, based on empirical testing in air and water calibration. The start was set to include the reflection from the probe head, and the length was based on the tests in water, which exhibits longer waveforms than soil, hence providing a physical upper boundary.

All measurements were taken manually, one probe at a time, at a given consolidation time. The automatization of the TDR measurements via multiplexers was considered; however, in order to avoid further signal attenuation and noise caused by the addition of multiplexers (Curioni, 2017), these were not used in this study.

4.3.1 TDR-PROBE CALIBRATION

Calibration of the TDR probes and cables was required to enable collection of reliable readings (Lin et al., 2008). Therefore, the TDR probes were calibrated in air, water and saline solutions, following the procedure adopted by Curioni (2013), following Heimovara (1993) and Huisman et al. (2008).

4.3.1.1 TDR CALIBRATION – AP

In order to obtain reliable measurements of the soil's AP, the TDR probes needed to be calibrated with materials of known AP. Given that the AP of soil is considered to be a bulk AP, reflecting the influence of air, solids and water with individual APs of approximately 1, 5 (Robinson and Friedman, 2001) and 80 at 20 °C (Malmberg and Maryott, 1956) respectively, it is expected that soil's bulk permittivity falls between these extremes. For this reason, the probe calibration was carried out in the easily accessible reference materials exhibiting extreme AP values, i.e. air and distilled water (Robinson et al., 2003).

The six probes used in this study were calibrated in air and distilled water, in a temperature-controlled room at approximately 20 °C (the exact temperature was recorded with a digital probe during each reading). The distilled-water measurements were taken in an 18-litre, large, plastic container, ensuring that the distance between each probe and container walls was above 100 mm.

Short-circuit measurements in air were carried out with the probes shorted using aluminium foil (Figure 4.4). Open-air measurements were also taken with the probes suspended in the air. Each measurement was repeated six times to reduce uncertainty.

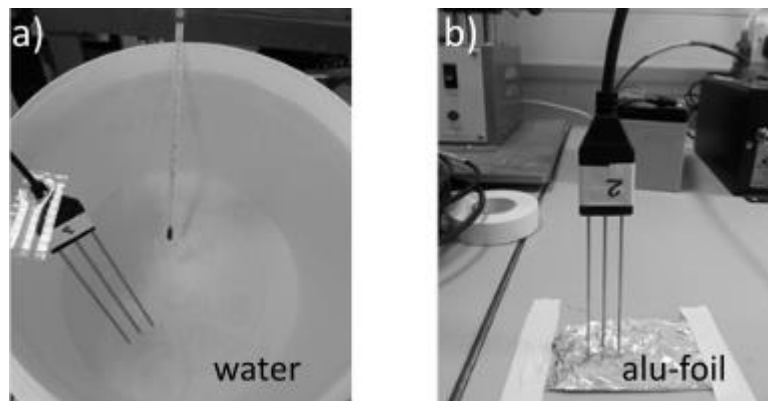


Figure 4.4. TDR-probe calibration in (a) water and (b) short-circuit on aluminium foil (in air)

The waveforms were analysed with script prepared by Curioni et al. (2012) using the R-software, based on the following principles:

- i. A reference point was chosen at the interface between the probe head and the coaxial cable as a constant that would not have differing measurements. It was determined by crossing two tangents corresponding to the first reflection in the probe head (Figure 4.5).

- ii. The end reflection was identified using crossing tangents, as shown in Figure 4.5.

Based on the shorted measurements in air and the water measurements, the apparent distance (L_t) between the reference point and the end reflection point was calculated as an average of the six repetitions. Given that the AP of air is 1 and AP of water is 80.10 at 20 °C (Malmberg and Maryott, 1956), the offset distance within the probe head was calculated from the reference point, the start of the rods, L_0 and the calibrated length of the rods (L_{cal}) (corresponding to the physical length of the rods), following Eq. 4.1:

$$L_t = L_0 + L_{cal}\sqrt{AP} \quad \text{Eq. 4.1}$$

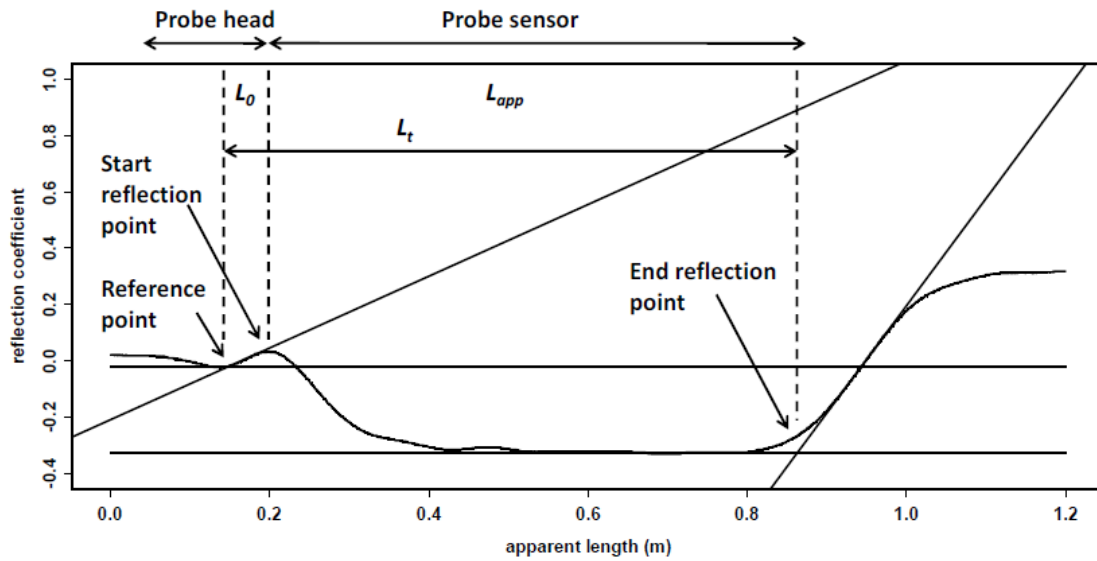


Figure 4.5. TDR waveforms in air and water (Curioni, 2013)

The accuracy and precision of the calibrated probes is discussed in Section 4.3.2.

4.3.1.2 TDR CALIBRATION-BEC

The calibration of TDR for accurate BEC measurements was based on the methodology adopted by Curioni (2013), following Huisman et al. (2008).

In this method, based on long distance measurements taken in a range of saline solutions, the probe constant (K_p) (1/m), and the resistance parameters R_c and R_0 (Ω) – corresponding to the transmission-line elements other than the probe (i.e. the TDR unit, cable and connectors) – were determined in accordance with Eq. 4.2:

$$BEC = \frac{K_p}{R_l - (DR_c + R_0)} \quad \text{Eq. 4.2}$$

Where D , which is the cable length (m), and R_l , which is the load resistance (Ω), were determined using Eq. 4.3:

$$R_l = Z_{out} \frac{1 + \rho_{\infty}}{1 - \rho_{\infty}} \quad \text{Eq. 4.3}$$

Where Z_{out} is the output impedance of the TDR device (i.e. 50 Ω) and ρ_{∞} is the reflection coefficient taken at long distances, when all the multiple reflections have attenuated and the signal has reached a steady-state level.

The saline solutions used for the calibration consisted of eight aqueous potassium-chloride solutions with molarities between 0.000469 M and 0.15 M, corresponding to electrical-conductivity values of 0.0063 S/m and 1.7963 S/m, respectively (Table 4.1).

Table 4.1. TDR conductivity of calibration solutions

Calibration Solution	KCl	BEC
	[M]	[S/m]
SOL 1	0.1500	1.7960
SOL 2	0.1000	1.1910
SOL 3	0.0800	0.8830
SOL 4	0.0300	0.3670
SOL 5	0.0040	0.0248
SOL 6	0.0020	0.0124
SOL 7	0.0010	0.0078
SOL 8	0.0005	0.0063

A reference conductivity (EC_{ref}) measurement was obtained in each solution, prior to the TDR measurement, with a standard conductivity meter (a Hanna HI8733). The conductivity meter was calibrated separately for high (0.3667–1.7963 S/m) and low (0.0063–0.0248 S/m) conductivities with reference solutions on a daily basis. The accuracy of the conductivity meter is stated by the producer to be within 1% for the full measurement scale. The response of the conductivity meters is also noted to drift with time due to absorption of the atmospheric carbon dioxide (Emerson, 2010). As per the Hanna HI8733's operational manual, the conductivity readings within 0.02 S/m per minute are considered to be stable. In order to investigate the magnitude of change in the conductivity meter readings over time, two saline solutions were tested during the calibration. The measurements in the low-conductivity solution (0.00007 S/m) reveal a 0.3% conductivity change per minute, whilst in the medium-conductivity solution (with an initial conductivity of 0.010 S/m) it was 0.1%. The temperature readings, taken regularly with a digital temperature probe, confirm that

the drift in the conductivity meter readings was not a result of temperature changes (Figure 4.6).

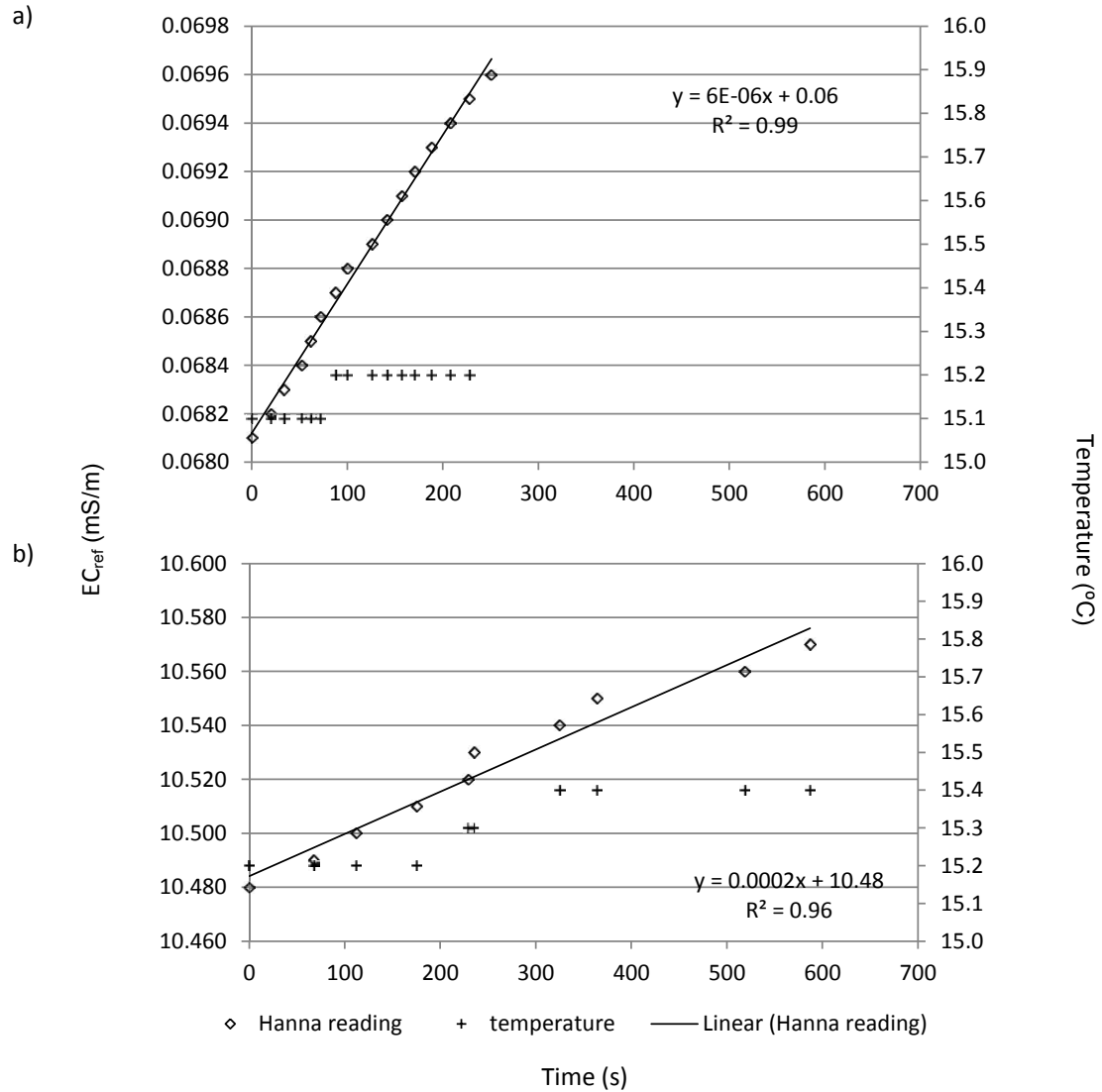


Figure 4.6. Hanna HI8733's conductivity reading drift with time in (a) low- and (b) medium-conductivity solutions, respectively

The BEC calibration calculations were conducted in two steps. Firstly, based on the measurements taken in the low-conductivity solutions, K_p was calculated with Eq. 4.2, assuming that both R_c and R_0 were equal to zero. Given that the reflection coefficient (r_c) for these measurements ranged between 0.5 and 1.0, the cable resistance could be

neglected as per Huisman et al. (2008). The inverse of the TDR load resistance ($1/R_L$) (i.e. the conductance) was then plotted against the reference conductivity measured with the Hanna HI8733 meter to obtain the inverse probe constant ($1/K_p$) (Figure 4.7).

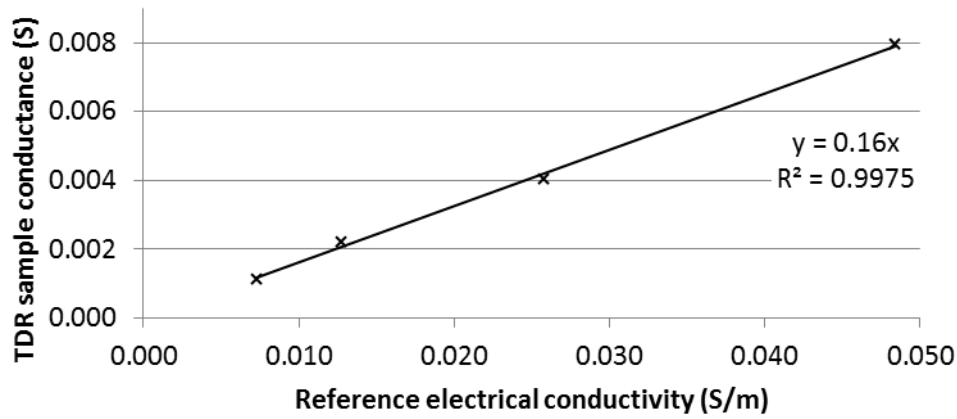


Figure 4.7. BEC calibration (step 1) – inverse K_p , represented by the slope of the line reflecting the relationship between the TDR read conductance $1/R_L$ and the reference conductivity

In the second stage of the BEC calibration calculations, R_c and R_0 were estimated based on the readings taken in all eight saline solutions. This was achieved by minimising the sum of the squared residuals between the measured and modelled EC, using a simplex optimisation algorithm (Curioni, 2012), following Huisman et al. (2008).

The summary of the probe calibration parameters is presented in Table 4.2.

Table 4.2. TDR-probe calibration parameters (TDR57600)

TDR unit	Probe ID	L_{cal}	L_0	R_{open}	K_p	R_c	R_0	L
		[m]	[m]	[Ω]	[1/m]	[Ω]	[Ω]	[m]
TDR100-57600	plab75.2	0.0745	0.0369	0.9586	5.5675	0.1847	0.1986	0.0765
	plab75.3	0.0749	0.0343	0.9600	5.6977	0.1654	0.4337	0.0769
	plab75.5	0.0750	0.0369	0.9602	5.8483	0.4935	0.3668	0.0770
	plab75.6	0.0746	0.0327	0.9608	5.6880	0.1309	0.3610	0.0766
	plab75.7	0.0748	0.0331	0.9596	5.6564	0.2179	0.2463	0.0768
	plab75.8	0.0749	0.0345	0.9598	5.5526	0.2337	0.1784	0.0769

4.3.1.3 CONTAINER-SIZE EFFECT ON TDR MEASUREMENTS

The TDR sampling volume is reported to correspond to the cylindrical volume of the sample of approximately 1.4 times the spacing of the rods (Mojid et al., 2003). Even though the bespoke chamber's design incorporated a sufficient distance between the probes and the chamber walls/base, the effect of the container's size was investigated through AP and BEC readings obtained in distilled water, both within the chamber at seven different heights (Figure 4.8) and within a plastic bucket (diameter 300 mm and height 260 mm).

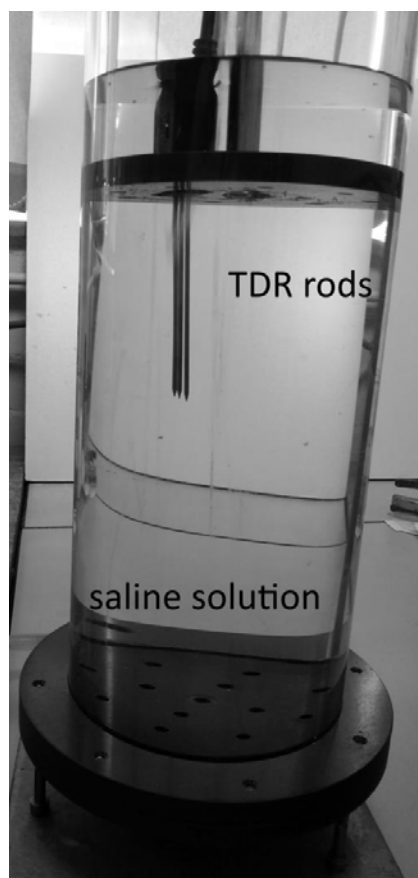


Figure 4.8. Investigation of the effect of the TDR chamber container

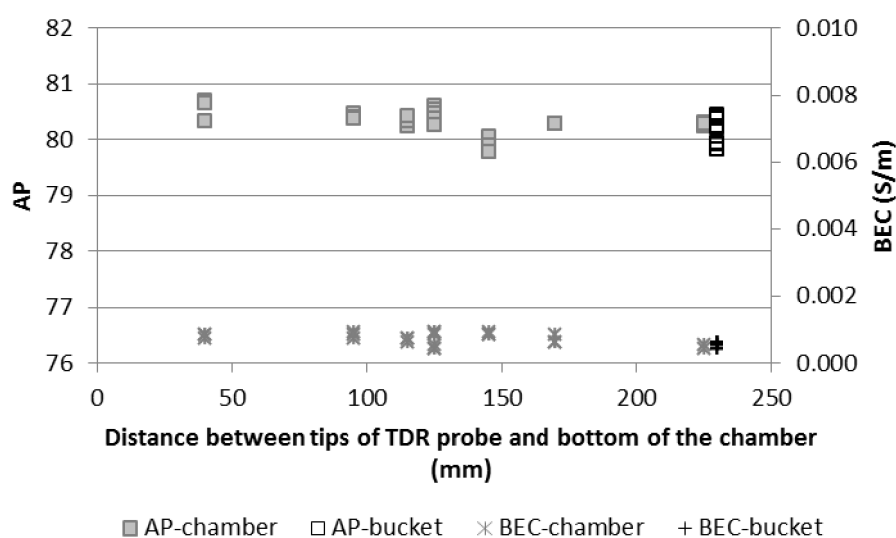


Figure 4.9. Bespoke chamber's effect on TDR-probe readings

The AP and BEC results (Figure 4.9) indicate that the selected container size does not affect the TDR readings. Variations within the measurements at a given depth are likely to be related to slight temperature variations within the containers.

4.3.2 TDR DATA QUALITY

The accuracy of the AP and BEC readings can be affected by the TDR system's intrinsic errors, waveform analysis and calibration-procedure imperfections (Curioni, 2013).

The TDR system's errors were minimised by taking 20 averages during a single measurement, whilst the waveform-analysis errors were minimised by repeating the measurement between three and six times, and taking the average of these measurements.

An average of six repetitions of AP readings taken in distilled water were compared with the real permittivity values presented in the literature (Malmberg and Maryott, 1956) (Figure 4.10).

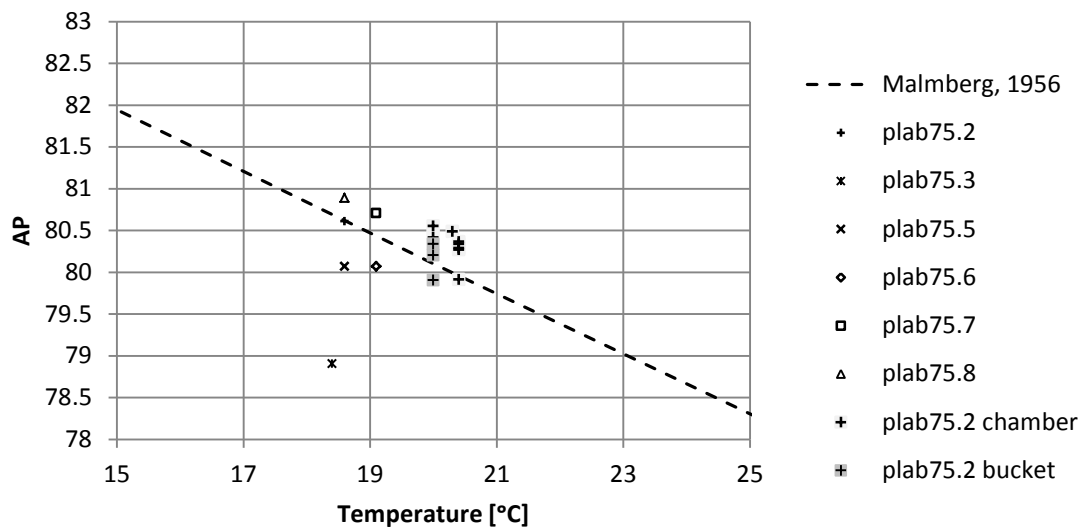


Figure 4.10. Accuracy of the AP readings with reference to the real permittivity of water values presented in Malmberg and Maryott (1956)

The accuracy of the AP measurements was on average within 0.4 (0.5%) of the real permittivity values, with the minimum matching the reference value to one decimal place and the maximum discrepancy reaching 1.8 (2.2%). The latter was most likely a mismatch related to the accuracy of the temperature probe (0.5 °C).

The precision of the AP readings was assessed by calculating the standard deviation of the six repetitions in water and soil, which fell within 0.1 units (0.1%) with a minimum below 0.1 and a maximum of 0.2 (0.3%) in water. The average standard deviation in the soil was within 0.1 (0.2%) and had a maximum of 0.2 (0.4 %). Based on the very close results of the AP readings, the number of repetitions was reduced from six to four to save time.

Table 4.3. The precision of AP and BEC measurements in soil (for the bespoke TDR chamber prior to the load application)

Soil	Probe ID	O	R	AP	ST.DEV _{AP}	ST.DEV _{AP%}	BEC	ST.DEV _{BEC}	ST.DEV _{BEC%}
				[-]	[-]	[%]	[mS/m]	[mS/m]	[%]
CH.S1	plab75.2	V	4	38.6	0.0	0.1	110	0.1	0.1
	plab75.2	V	6	38.7	0.0	0.1	110	0.1	0.1
	plab75.3	H	4	36.8	0.1	0.3	104	0.1	0.1
	plab75.3	H	6	36.8	0.1	0.4	104	0.1	0.1
CH.S2	plab75.5	V	4	38.1	0.0	0.1	108	0.1	0.1
	plab75.5	V	6	38.0	0.1	0.2	108	0.2	0.2
	plab75.6	H	4	37.5	0.0	0.1	109	0.1	0.1
	plab75.6	H	6	37.5	0.0	0.1	109	0.1	0.1
CI.S1	plab75.7	V	4	31.6	0.1	0.1	104	0.2	0.2
	plab75.7	V	6	31.6	0.0	0.1	104	0.2	0.2
	plab75.8	H	4	32.2	0.1	0.4	105	0.1	0.1
	plab75.8	H	6	32.2	0.1	0.3	105	0.1	0.1
CI.S3	plab75.2	V	4	32.4	0.1	0.3	102	0.1	0.1
	plab75.2	V	6	32.3	0.1	0.3	102	0.1	0.1
	plab75.3	H	4	32.6	0.1	0.3	108	0.1	0.1
	plab75.3	H	6	32.6	0.1	0.2	108	0.1	0.1
Average					0.1	0.2		0.1	0.1
MIN					0.0	0.1		0.1	0.1
MAX					0.2	0.4		0.2	0.2
O - probe orientation (V - vertical, H - horizontal)									
R - number of repetitions									
ST.DEV _{AP(BEC)} - standard deviation calculated from 6 or 4 repetitions of AP(BEC) measurements									

The accuracy of the TDR probes' BEC readings was investigated in four saline solutions, representing the range of conductivities likely to be encountered during the investigation (0.012–0.181 S/m). The reference conductivity reading (EC_{ref}) was obtained with the conductivity meter.

The results, presented in Table 4.4, were normalised to the same temperature (20 °C), using Eq. 5.1. The measurements demonstrate that the precision of the BEC measurements is within 0.1–0.7%, whilst the median accuracy of all the measurements, when compared to the Hanna HI8733 conductivity meter, was around 2%. There were occasional cases for which the accuracy dropped to 6%. It is noted that conductivity meters are also affected by a measurement error ($\pm 1\%$) and the conductivity measurements are very sensitive to small temperature variations.

Table 4.4. Accuracy and precision of BEC measurements in a saline solution

Probe ID	EC _{ref}	BEC	ST.DEV _{BEC}	ST.DEV _{BEC%}	ACC _{BEC%}
	S/m		%		%
plab75.2	0.012	0.012	0.082	0.7	0.5
	0.021	0.021	0.089	0.4	-2.2
	0.078	0.077	0.055	0.1	-2.0
	0.181	0.177	0.197	0.1	-2.5
plab75.3	0.012	0.012	0.082	0.7	1.9
	0.021	0.021	0.052	0.2	-0.4
	0.078	0.078	0.071	0.1	-0.6
	0.181	0.180	0.147	0.1	-0.8
plab75.5	0.012	0.013	0.063	0.5	5.7
	0.021	0.022	0.052	0.2	2.3
	0.078	Equipment malfunction			
	0.181				
plab75.6	0.012	0.013	0.075	0.6	6.1
	0.021	0.022	0.084	0.4	3.1
	0.078	0.080	0.045	0.1	2.1
	0.181	0.184	0.137	0.1	1.3
plab75.7	0.012	0.013	0.052	0.4	6.3
	0.021	0.022	0.103	0.4	2.5
	0.078	0.081	0.045	0.1	2.9
	0.181	0.186	0.216	0.1	2.5
plab75.8	0.012	0.012	0.089	0.7	-0.2
	0.021	0.020	0.098	0.5	-4.4
	0.078	0.075	0.055	0.1	-4.5
	0.181	0.172	0.190	0.1	-4.9
EC _{ref} - reference conductivity read with Hanna meter ST.DEV _{BEC} - standard deviation calculated from 6 repetitions of BEC measurements ST.DEV _{BEC%} = ST.DEV _{BEC} /MEAN (precision) ACC _{BEC%} = 100*(EC _{ref} - BEC)/ EC _{ref}					

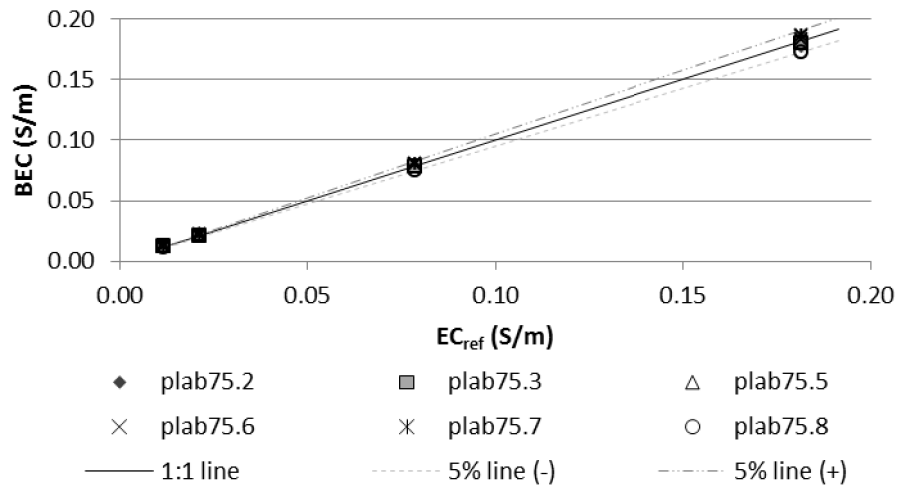


Figure 4.11. Investigation of the TDR probes' BEC accuracy

4.4 INITIAL SOIL-LOADING TESTING IN THE BESPOKE TDR CHAMBER

(PS1)

The initial TDR testing during loading in the bespoke chamber was carried out in the arrangement described in Section 3.4.1.1. Three CH samples – CH.S01.TDR, CH.S02.TDR and CH.S03.TDR were tested, where CH.S03.TDR was a control sample without any load applied.

Sample CH.S01.TDR was subject to a gradual load increase in the following sequence: loading at 40, 80 and 160 kPa, then unloading at 80 kPa. Initially, two-way drainage was created; however, it was later observed that the bottom drainage was not working properly. This was assumed to be a result of the filter paper moving; therefore, during the subsequent sample preparation, the filter paper was glued to the bottom drainage plate.

Sample CH.S02.TDR was subject to the application of only two load steps of 40 kPa and 80 kPa, because the loading rod failed when the subsequent load was applied.

During this initial approach, only the vertical TDR probe was present in the CH.S01.TDR sample (Figure 3.7), whilst samples CH.S02.TDR and CH.S03.TDR were equipped with both vertical and horizontal probes. The TDR measurements were taken at the end of the loading stage.

The initial results reveal that the vertical AP_v measured in CH.S01.TDR and CH.S02.TDR was decreasing with a decrease in the sample height (Figure 4.12). However, the AP_h measured in CH.S02.TDR appeared to follow a similar trend towards the end of the test, but exhibited a sharp jump at the beginning, when AP_h was found to be significantly higher than the initial value (by approximately 10 AP units). It is concluded that the measurement frequency was too sparse to understand this anomaly.

The initial results were also compared to the ER values obtained in ER chamber I (Chapter 5), indicating that the BEC values (converted to $ER = 1/BEC$) followed the same trend as the ER readings (Figure 4.12).

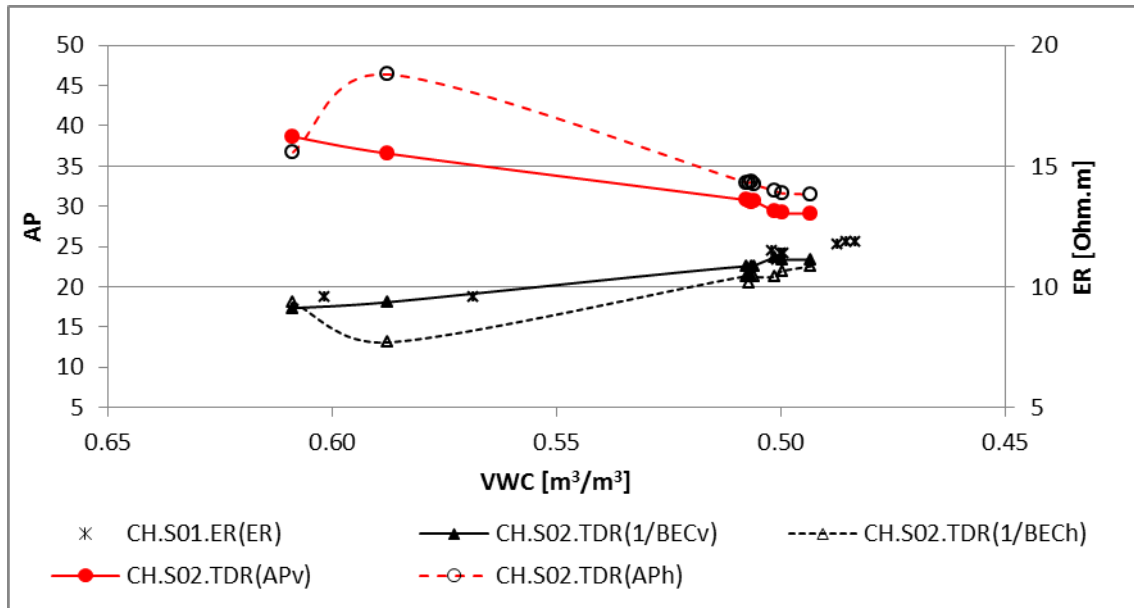


Figure 4.12. Initial TDR arrangement (PS1) – AP and correlation with VWC

Based on the initial results, it is hypothesised that AP_h and BEC_h could be sensitive to changes in the pore-water pressure, whilst the vertical readings reflect changes in the VWC/void ratio. Nonetheless, the measurement frequency had to be increased in order to make further conclusions.

4.5 INITIAL SOIL-LOADING TESTING IN THE BESPOKE TDR CHAMBER (PS2)

Following the initial experiments, the pressure system was adjusted, as discussed in Section 3.4.1.2. Three samples were monitored at the same time with respect to TDR_v and TDR_h (Figure 4.13). The TDR measurement frequency was increased to include measurements immediately upon the load placement. First, the measurements were taken every five minutes in four repetitions after the load placement. However, as the water was flowing out and the structure of the soil was changing rapidly within the

initial stages, it was observed that the average of four measurements resulted in a higher standard deviation than implied by the precision analysis (Section 4.3.2). The average was not a true representation of the rapid change in the soil; therefore, a series of 10 single TDR measurements taken every 2 minutes was carried out approximately 10 minutes after load placement, and repeated at 30 minute-intervals for approximately 5 hours, and repeated every hour thereafter. Following 24 hours of loading time, four repeated measurements were taken twice a day. No measurements were taken overnight.

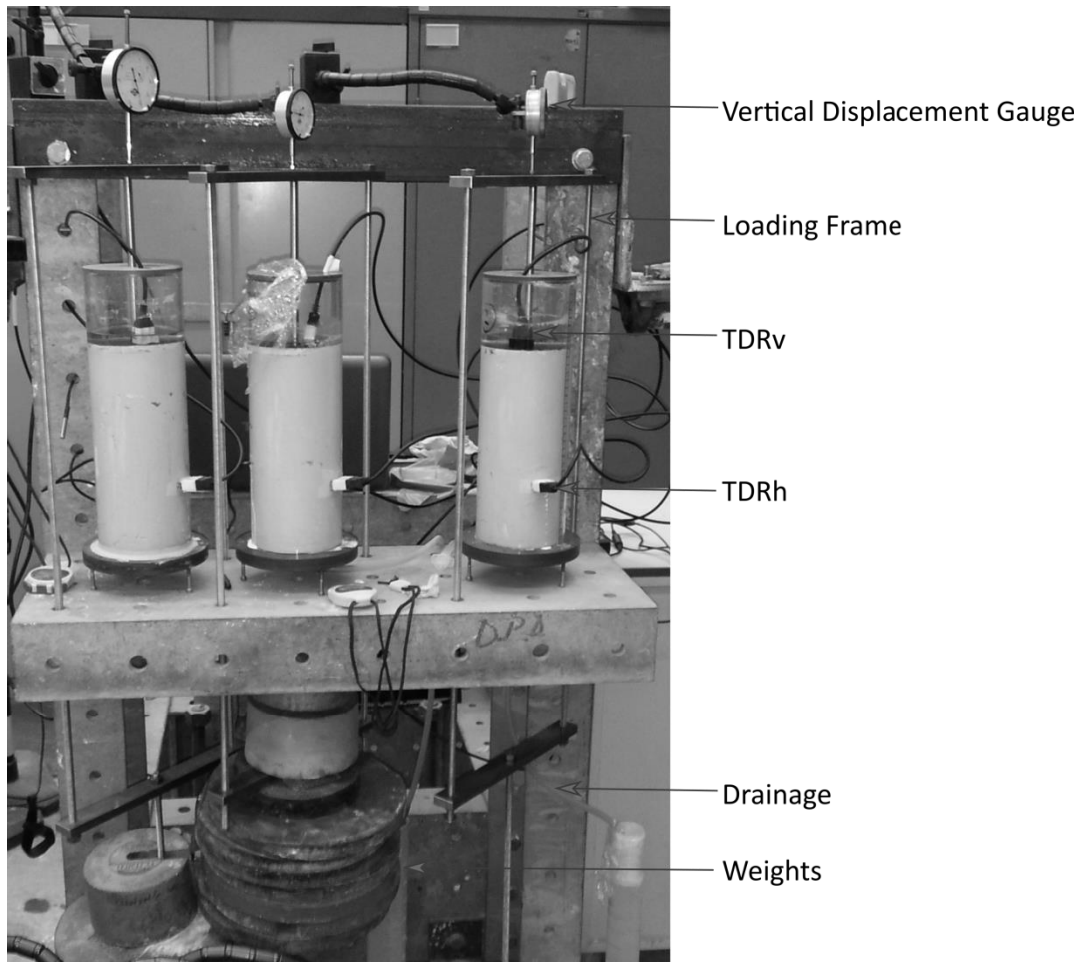


Figure 4.13. Bespoke TDR chamber and soil-loading arrangement (PS2)

This modified approach created the core for the rest of the research programme. The summary of the testing carried out with the modified approach is presented in Table 4.5.

Table 4.5. Testing carried out with TDR (PS2) approach (P - pore-water pressure)

TEST NO	SOIL MIX	REPETITION	SENSOR	Loading sequence (kPa)						
				L1	L2	L3	L4	L5	L6	L7
1	CL	S1	TDR	15	25	50	85	100	5	-
2	CL	S2	TDR	15	25	50	85	5	-	-
9	CH	S5	TDR	5	10	20	40	-	-	-
10	CI	S1	TDR	15	25	35	62	83	5	-
11	CI	S2	TDR	20	36	60	35	5	107	5
12	CI	S3	TDR	25	50	100	5	-	-	-
14	CI	S5	TDR	20	50	100	-	-	-	-
16	CI	S7	TDR	25	50	100	50	25	5	
17	CI	S8	TDR-P	5	15	-	-	-	-	-
18	CI	S9	TDR-P	5	0	-	-	-	-	-

4.6 PORE-WATER-PRESSURE MEASUREMENTS IN A BESPOKE TDR

CHAMBER

In order to investigate the TDR responses in relation to a pore-water-pressure increase, measurements were carried out in a customised chamber (Section 4.2). Pressure sensors with associated de-airing valves and a data logger were purchased from Controls Testing Equipment Ltd. Several pore-pressure-sensor suppliers were considered; however, the selected company was found to provide the most suitable sensor, with an associated de-airing system and data-acquisition system, enabling the automatic logging of the required number of sensors.

Measurements were obtained with a GEODATALOG 16 data logger (Figure 4.14b), equipped with 16 channels, connected to a laptop and operated via the DATACOMM software.

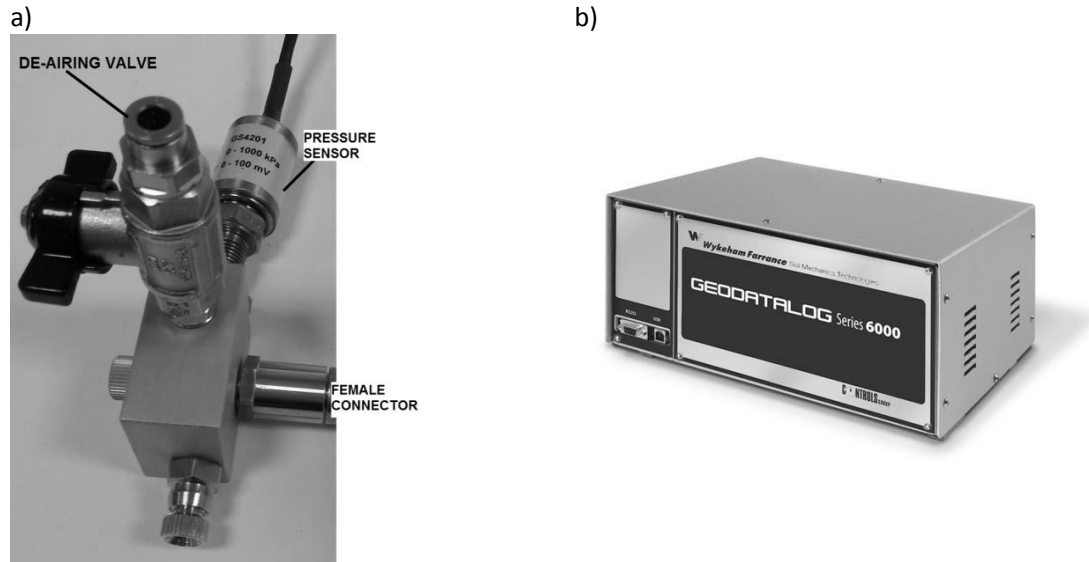


Figure 4.14. (a) Pressure sensor with a de-airing valve; and (b) a data logger

Each pressure transducer (Figure 4.14a) was operated in the 0–1000 kPa pressure range, and its specifications are presented in Table 4.6.

Table 4.6. Pressure-sensor specification

Code	28-WF6300
Input voltage	10
Output voltage	100 mV
Resolution	infinite
Accuracy	±0.25 FSO
Temperature [°C]	-40 to +85
Temperature effect*[FS/°C]	±0.015%
Removable cable	No
Dimensions** [length x dia.]	5.8 x 2.55
Weight [g]	100
* Typical thermal zero and span coefficients	
** nipple included	

The pore-water pressure was recorded at a sampling rate of three readings per second per channel. The pore-water-pressure arrangement was created at a late stage of the research, when it was concluded that AP_h may be responsive to pore-water-pressure-induced changes. Therefore, only two TDR-pore water pressure experiments were carried out.

The first trial (Cl.S8.TDR) (Figure 4.15a) demonstrated that the arrangement was not airtight. Although the fluid was topped up with de-aired water to remove any air bubbles present within the tubes (Figure 4.15b), when the sample was examined the following day, the problem persisted.

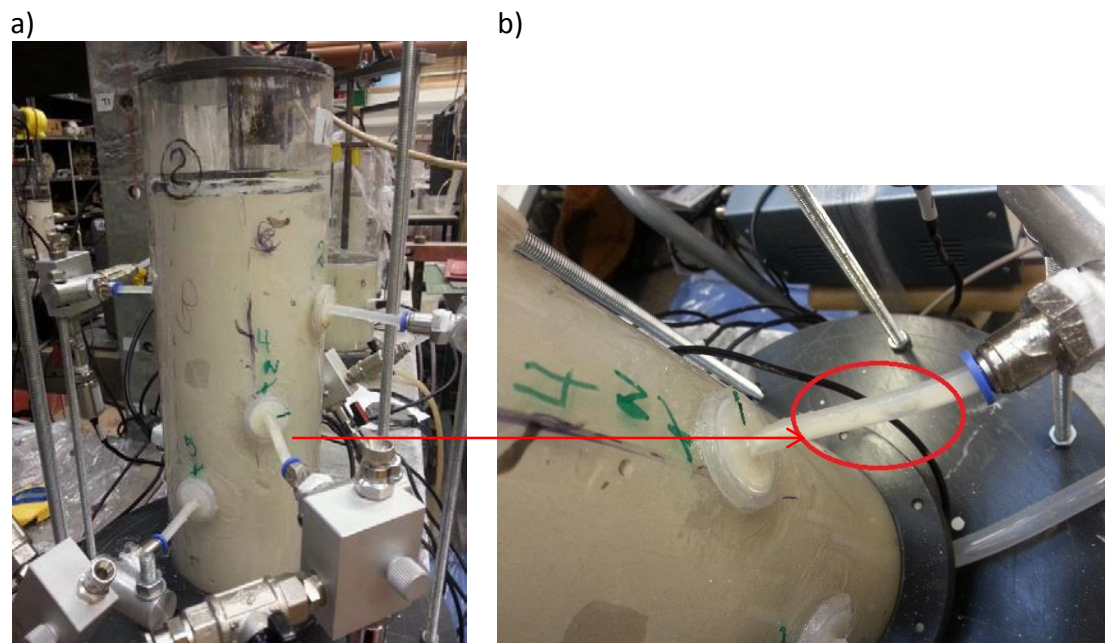


Figure 4.15. (a) TDR-pore-pressure bespoke arrangement; and (b) air bubble in the connecting pipe

The glued connections were subsequently resealed, and a metal wire was fitted around the push-fit connectors (it was possible that, due to the very low pressure in

the pipes, the push-fit connector was not tight enough). The adjustments were tested in a water-filled chamber and observed overnight; the pressure level did not change, indicating that the improvements were successful.

The second trial was prepared on the same soil type; however, the initial GWC was increased to 1.8 times LL to ensure that the soil was fully saturated. Occasional air bubbles were still noted within the pipe; however, their size was much smaller than previously. The pressure was again observed overnight, and it remained unchanged.

The results from these tests are presented in Chapter 6.

4.7 TDR INSTRUMENTATION'S EFFECT ON THE PROGRESS OF SETTLEMENT

The presence of six rigid metal rods in the consolidating soil was likely to affect the progress of settlement by providing a preferential drainage path, as well as creating a potential barrier (the horizontal probe), which could lead to the development of arching around the probe. These potentially negative effects were investigated by injecting a fluorescein solution to monitor the water flow during the loading process, and SEM testing to observe the alignment of the clay particles adjacent to the probes. These tests are described in the following sections.

4.7.1 TDR – FLUORESCEIN TESTING

In order to investigate further the flow of water around the rods, a 5% fluorescein sodium-salt solution was injected into the holes created by the TDR rods (Figure 4.16c). The concentration of the dye tracer was chosen as the minimum that could be seen with the naked eye and meanwhile would not affect the TDR readings. The solution was prepared by mixing 50 mg of fluorescein sodium salt (Figure 4.16a) with 1 l of tap water.

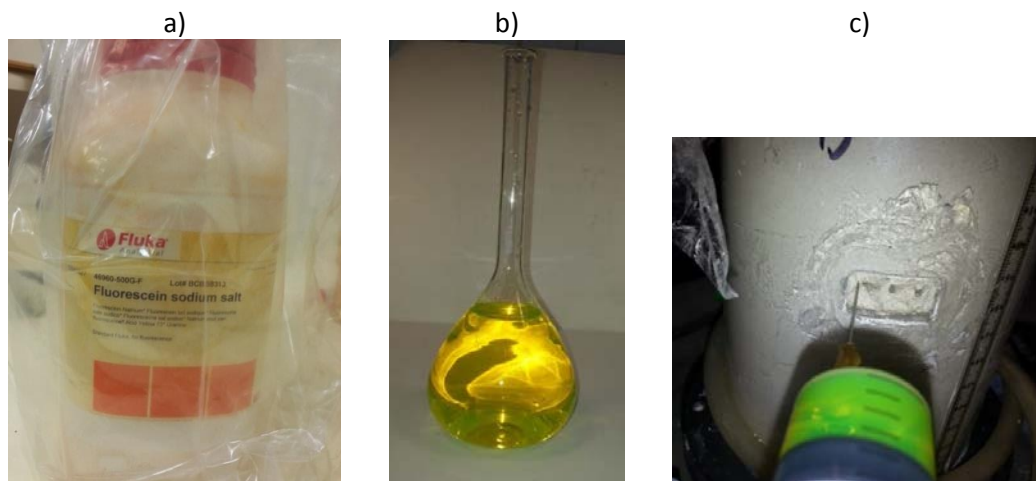


Figure 4.16. Fluorescein (a) powder, (b) solution and (c) injection into the CI.S7.TDR soil sample

A sample of water was tested using TDR before and after the addition of the fluorescein, to investigate its effect on the fluid's properties. It was found that the addition of fluorescein had a negligible effect on the AP and BEC of the fluid (Table 4.6).

Similarly, the investigated soil mixture (CI.S7.TDR) was tested using TDR before and after the injection of the fluorescein solution, which indicated there were negligible changes; therefore, the AP and BEC readings could be compared to the other samples.

Table 4.7. TDR measurements for CI.S7.TDR with fluorescein

Medium	Calibration Solution	AP _h	BEC _h
		-	[mS/m]
CI.S7.TDR	Prior to the fluorescein injection	30	105.4
		30	105.5
		30	104.5
		30	103.8
		30	105.5
	After the injection	30	99.4
		29	98.9
TAP WATER		79	12.0
5% FLUORESC EIN SOLUTION		80	14.1

4.7.2 SEM-TDR

Following the loading of the CI.S5.TDR sample, SEM images were taken with a Philips XL-30 (LaB6) with Link Isis EDS electron microscope to investigate the effect of the TDR-probe rods on the clay particles' alignment.

The Cryo-SEM method, performed on samples frozen in liquid nitrogen, was selected as the most suitable for the electron imaging of specimens with high moisture content (JEOL, 2011).

Three samples were subject to testing. The first sample (S1) was obtained from the top centimetre of CI.S5.TDR to provide information on the particle arrangement and pore connectivity after loading. Samples S2 and S3 were obtained from the area affected by the insertion of the TDR probe. In order to obtain these samples, the probe was gently removed from the chamber and a soil specimen was cut out through the rectangular TDR hole on the side of the cylinder. S2 was obtained from the left side of the probe and S3 from the right (Figure 4.17), approximately 1 cm from the chamber wall.

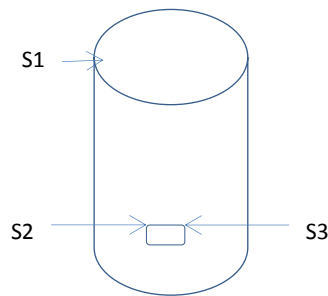


Figure 4.17. Location of the SEM samples within the consolidation chamber

As approximately a 1 cm^3 soil specimen was needed to perform the Cryo-SEM scanning, the top loading plate was removed, and a soil cube was cut out with a sharp scalpel. The specimen was then glued to a sample holder and rapidly frozen in a nitrogen slush. Subsequently, it was loaded into a cryo-chamber, where it was subject to etching for 15 minutes (the temperature in the chamber was increased from $-132\text{ }^{\circ}\text{C}$ to $-90\text{ }^{\circ}\text{C}$ and maintained at $-90\text{ }^{\circ}\text{C}$ for 15 minutes) to remove the ice crystals. Following this procedure, the sample was broken to unveil an area not affected by the cutting/sheering. The soil was then covered in platinum to provide a conductive surface and to avoid electron accumulation on the top of the clay surfaces (Bohor and Hughes, 1971) . The electron scanning was performed at 5 mV.

Samples S2 and S3 were not fractured, as it was very difficult to obtain a representative undisturbed sample due to the consistency of the soil and limited space.

4.8 PRESSURE EFFECT ON THE TDR MEASUREMENTS IN FLUIDS

In order to investigate whether the change in pressure inside a loading chamber affects the TDR measurements, a TDR probe was tested in a modified triaxial cell. One of the TDR probes used in the soil investigation was inserted into a triaxial cell through the loading-piston outlet and then sealed.

Three sets of tests were carried out. In the first test, the cell was filled with distilled water, and in the second and third trials it was filled with a KCl solution with initial electrical conductivity of 0.04 S/m. During each test, the pressure inside the cell was gradually increased between 0 and 300 kPa, and then decreased. The upper threshold was a conservative approach, since the maximum pressure during the testing was not expected to exceed 200 kPa. The results identify that the changes in AP values compared to the initial reading were below 0.6%. The BEC values in the KCl solution (Figure 4.18 b and c) were found to vary within 1%. There was a 2.6% change in the BEC recorded in distilled water (Figure 4.18 a); however, this is assumed to be a result of contamination with clay particles (the chamber was typically used for testing the shear strength of clay samples). From this, it is concluded that pressure changes

encountered within the range during this investigation do not significantly affect the TDR measurements.

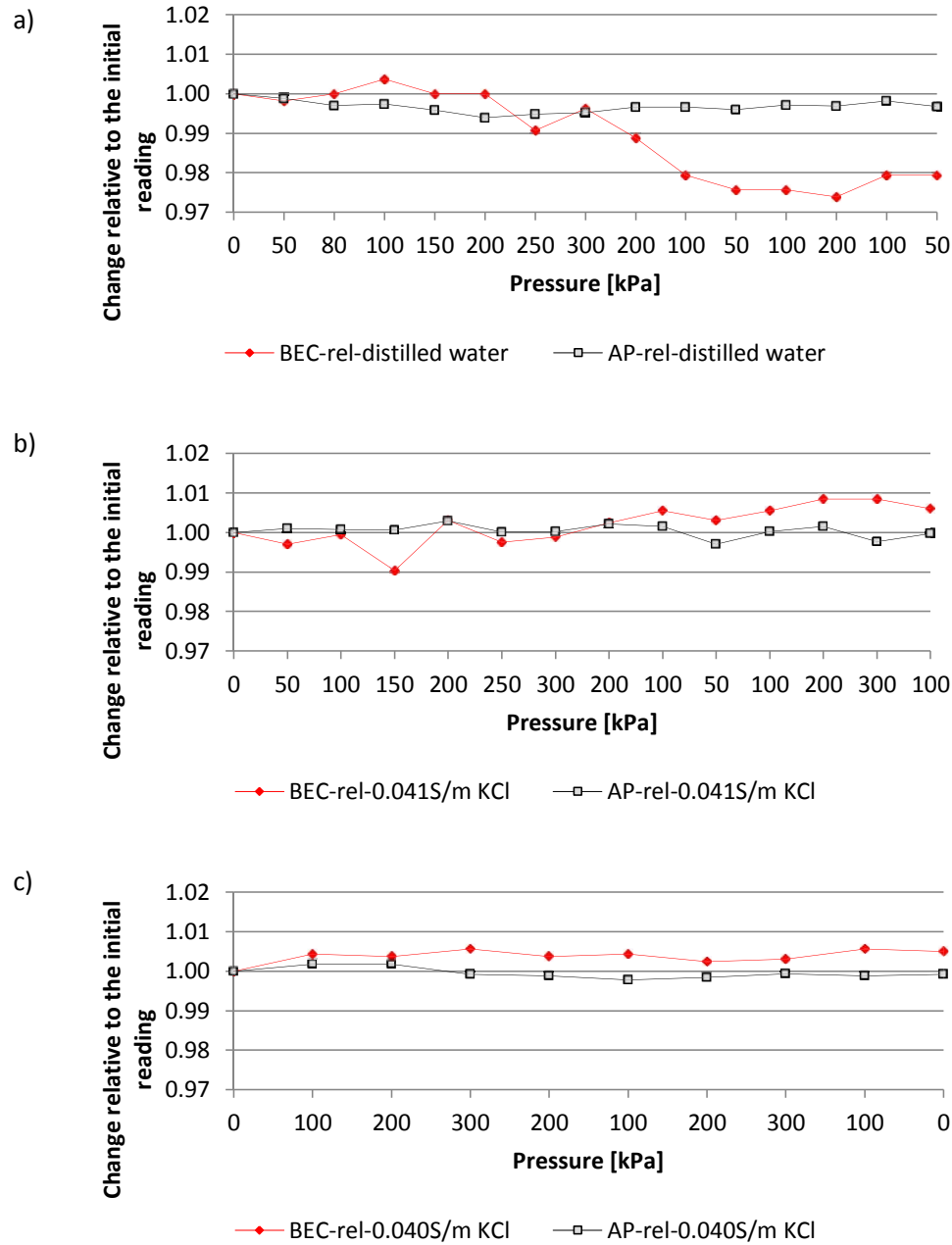


Figure 4.18. TDR response to pore-water pressure variations measured in a customised triaxial cell; in (a) distilled water, (b) KCl solution trial 1 and (c) KCl solution trial 3

CHAPTER 5: DEVELOPMENT OF THE BESPOKE ER ARRANGEMENT

This chapter provides details of the design, development and modification of a bespoke ER arrangement, including an ER chamber and bespoke ER-acquisition system. It also includes details of the development of the experimental laboratory-testing programme, calibration, validation and preliminary results.

The development of the ER arrangement involved a few experimental stages. Initial tests were conducted in order to investigate the benefits and shortcomings of the ER method, through simple soil testing in resistivity boxes connected to a current generator and an oscilloscope (acquisition system 'T') (Section 5.1.2). Based on the initial observations and the literature review, an acquisition system (ER-Acq-I) was designed and built to enable the measurement of soil electrical resistivity (ρ) at a range of frequencies. This equipment was then tested on the ER boxes (Section 5.1.1) and subsequently connected to a bespoke consolidation chamber (ER Chamber I) (Section 5.2.1) used during loading with PS1. In order to provide further information about the changes in the soil layers, the chamber was then modified to include an increased number of point electrodes (ER Chamber II). Simultaneously, the acquisition system was also modified to enable automatic data collection (ER-Acq-II) (Section 5.3.2) and the pressure system was improved (PS2), as described in Section 3.3.1.2.

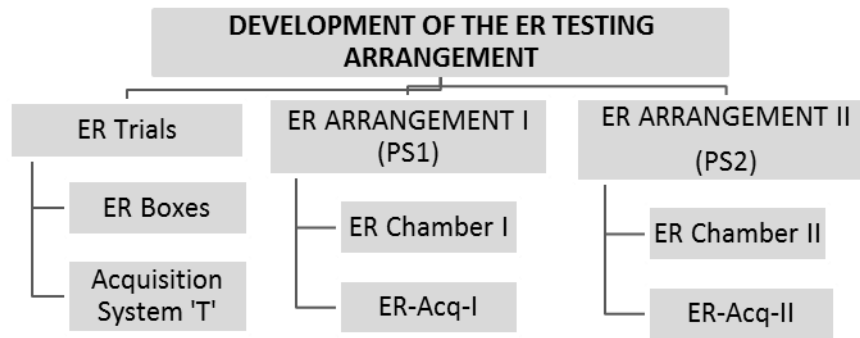


Figure 5.1. Schematic representation of the ER-arrangement development process

5.1 PRELIMINARY ER TESTING

Preliminary ER testing was performed using boxes with a current plate and potential rod electrodes at a single frequency (acquisition system 'T') and multiple frequencies (ER-Acq-I). The tests were performed in saline fluids and selected soils to understand the benefits and limitations of the method.

5.1.1 ER BOXES

The initial ER measurements were carried out on unsaturated soil samples compacted into the resistivity boxes, as shown in Figure 5.2. The first set of boxes was hired from the British Geological Survey (BGS) and the subsequent boxes were purchased from McMiller (designed in accordance with ASTM [2006]). The BGS boxes were made of a soft plastic (3D printed); were 72 mm long, 25 mm wide and 25 mm high; and perforated along the sides to enable the wetting and drying of the samples. Square steel-plate electrodes were fitted on the 25 x 25 mm walls to inject the current, and

the potential was measured on the pin copper electrodes (1 mm diameter) inserted into the soil at the mid-point of the 72-mm long wall. The current plates were connected to the metal handles, which were fastened with a rubber band at both ends to improve the contact between them and the soil.

The geometric factor of the boxes ($K = A/L$) was calculated as 0.024 m, given that the cross-sectional area of the current-plate electrode (A) was equal to 0.00061 m^2 and the spacing between the potential-point electrodes (L) was equal to 0.025 m.

The boxes were used to investigate the GWC- ρ relationship and the effect of the electrode-soil contact on the ρ readings (the results are not reported herein).

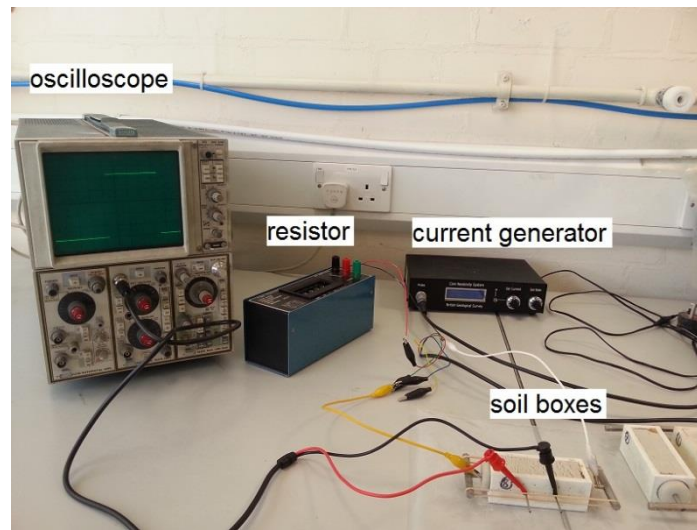


Figure 5.2. Preliminary ER arrangement: BGS box, current generator and oscilloscope

The BGS equipment was hired only temporarily; therefore, a set of new boxes was purchased from McMiller. These boxes were made of Perspex, and, similarly to the BGS boxes, the current was injected through the steel plates, whilst the potential was

measured on the brass rods located at the mid-point on the length of the sample. The length of the rods, which was nearly the same as the sample width, was considered to be too extensive, and thus the rods were shortened (to extend 10 mm into the sample) and sharpened to provide point measurements. The geometric factor of the boxes was calculated at 0.009 m, given that the cross-sectional area of the current-plate electrode was equal to 0.00064 m^2 and the spacing between the potential-point electrodes was equal to 0.069 m. These boxes were subsequently used to measure the ρ of selected soil mixtures at their LL, the ρ -temperature dependence in selected soils (Section 5.1.4) and the pore-fluid conductivity (Section 3.4).

5.1.2 ER-ACQUISITION SYSTEM 'T'

The preliminary ER measurements were taken with the BGS current generator and a 20Ω resistor, operating at a 10 Hz frequency. The output was read from an oscilloscope (Tektronix 5103N). Based on this arrangement, a custom-built acquisition system was developed and is described in the following section.

5.1.3 ER-ACQUISITION SYSTEM I (ER-ACQ-I)

ER-acquisition system I (ER-Acq-I) was developed by the Department of Electrical Engineering at the University of Birmingham to enable multiple frequency ρ measurements.

Alternating current (AC), as opposed to direct current (DC), was chosen as it is expected to almost eliminate the contact-resistance effect between the soil specimen and the electrode (Abu-Hassanein et al., 1996), and is superior in investigating clay soils (Boadu and Owusu-Nimo, 2010).

Low-frequency (below 1 kHz) sensing techniques respond to chemical reactions, such as oxidation-reduction and ion exchange (Olhoeft, 1985), and each frequency can potentially reflect different pore spaces, as particle acceleration differs depending on the frequency (Revil, 2012). Therefore, ER-Acq-I was designed to sweep through a range of frequencies from 0.01 Hz to 1000 Hz to investigate the changes taking place in fine-grained soils. Following the initial measurements, it was concluded that this wide frequency range was not time efficient; therefore, it was reduced to 1 Hz to 100 Hz.

The ER-Acq-I, as shown in Figure 5.3, was equipped with National Instruments module NI 9178, and populated with a signal source, generating a sinusoidal pulse. Two channels were used: channel 1 to inject the current (C1 and C2) at a constant 1 mA (its stability was monitored during the measurements), and channel 2 was used to measure the voltage (P1 and P2) across the 1 k Ω resistor.

The system was operated via a MATLAB interface script, enabling the modification of the frequency range and the number of automatic repetitions (within the selected configuration; automatic switching was not enabled).

a)

b)

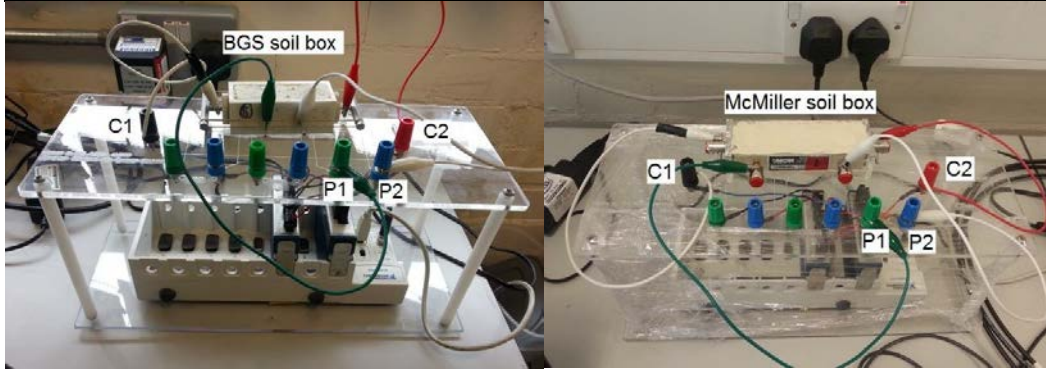


Figure 5.3. ER-Acq-I: a) with the BGS box; and b) with the McMiller soil box, with annotated current injection (C1 and C2) and potential measurement channels (P1 and P2)

Soil resistivity readings were taken for the soil samples with acquisition system 'T' and ER-Acq-I, revealing that the difference between the two devices was within 0 to 1 Ohm.m (0 to 0.1% of the resistivity value).

5.1.4 TEMPERATURE EFFECT ON ρ

Given that the electrical current in soils is conducted predominately through the electrolytes present in the pore fluid, and the mobility of the ions is dependent upon the temperature, the soil's ρ is also affected by the temperature. In the temperature range 15–35 °C, an increase in temperature per degree Celsius decreases the electrical resistivity of an electrolyte by approximately 2.02% (Campbell et al., 1948). In order to account for the temperature changes, Eq. 5.1 (Keller and Frischknecht, 1966) is commonly applied (e.g. Abu-Hassanein et al., 1996; Kibria, 2014).

Eq. 5.1

$$\rho_T = \frac{\rho_0}{1 + \alpha (T - T_0)}$$

Where ρ_T refers to ρ at ambient temperature (T), ρ_0 is the ER measured at the reference temperature T_0 , and α is a temperature coefficient for resistivity.

The temperature coefficient (correction factor) is commonly taken as 0.025, even though it corresponds to the ρ -temperature relationship for electrolytes. Although this approach may not be suitable for unsaturated soils (where α depends on the water content and soil type), it tends to approximate well the soil resistivity at a reference temperature for soils near saturation (Besson et al., 2008).

In order to investigate the relationship between ρ (at 10 Hz) and temperature, CI and CH at their LL were placed in the McMiller boxes, and were subject to cooling from 28 °C to 5 °C (CH) and from 25 °C to 20 °C (CI) in a temperature-controlled incubator. Four boxes were available, three of which (MC2, MC3 and MC4) were used to test the reproducibility of the testing, and the remaining box (MC1) was a control sample, into which a digital probe was inserted to check whether the sample's temperature reached the required level. The boxes were sealed with cling film; however, a 3–5% GWC loss was observed in CH and a 1–2% GWC loss in CI (soil from the boxes was oven dried upon completion of the ρ -temperature testing).

Based on the results provided in Table 5.1, which show changes in the ρ readings taken within the temperature range 5–28 °C, the ER percentage change per 1 °C was

calculated for each box (Table 5.2). This demonstrates that ρ changed between 0.9% and 2.9% per 1 °C in CH, and between 1.3% and 2.6% per 1 °C in CI. Although a certain level of variability was observed between the repetitions of each sample, this was considered to be negligible as it was within 0.2% in both soils, corresponding to approximately 0.02 Ohm.m.

Table 5.1. ρ variations in CH and CI, with temperature measured at the LL in the McMiller boxes

Temperature (°C)		28	27	25	20	19	15	10	5
ρ (Ohm.m)	CH-MC2	5.59	5.73	5.88	6.78	6.96	7.74	8.92	10.07
	CH-MC3	6.07	6.12	6.40	7.40	7.57	8.45	9.71	11.07
	CH-MC4	5.96	6.13	6.27	7.19	7.37	8.21	9.48	11.03
Temperature (°C)		25	24	23	22	21	20		
ρ (Ohm.m)	CI-MC2	7.45	7.61	7.72	7.92	8.08	8.19		
	CI-MC3	7.56	7.71	7.86	8.04	8.21	8.36		
	CI-MC4	7.26	7.39	7.54	7.74	7.92	8.05		

Table 5.2. ER percentage change per 1 °C measured in CH and CI at their LL in the McMiller Boxes

Soil-Box Reference No	ρ change per 1 °C (%)		
	Min	Max	Average
CH-MC2	1.23	2.66	2.36
CH-MC3	0.87	2.72	2.23
CH-MC4	1.04	2.88	2.42
CI-MC2	1.30	2.59	1.91
CI-MC3	1.75	2.33	2.04
CI-MC4	1.56	2.64	2.08

Following the preliminary ρ -temperature correlations, it was concluded that the temperature-correction factor differs slightly depending on the soil type and temperature range. The soils' ρ change per 1 °C was on average 2%; however, this average value can drift by to up to $\pm 1\%$, and hence a 1–3% ρ change per 1 °C can be expected in the investigated soils.

It was not feasible to determine a correction factor for each bulk sample used during the loading tests (due to the time required to equilibrate to a given temperature). Moreover, even if an average temperature correction factor is specified for a given sample, it may differ slightly at different stages due to changes in pore connectivity having an effect on the ion mobility. As it was not possible to determine the temperature correction factor for each loading stage, it was decided to adopt the commonly used Eq. 5.1.

5.1.5 ER DATA QUALITY

The ER data quality can be affected by a number of factors, including poor electrode contact with the soil, electrode polarisation and the effect of temperature. These can be reduced by adopting appropriate measurement sequences and performing reciprocal error analysis (Loke et al., 2013).

The ρ data accuracy and precision can be verified using the following (Hassan, 2014):

- i. known-reference resistors;
- ii. repetition; and
- iii. reciprocity.

A known-reference resistor was used to test the quality of the ER-acquisition system (Section 5.3.2) and saline solutions of known electrical conductivity were prepared to calibrate the ER chambers (Section 5.2.3). The repeatability of the resistivity measurements can be determined, for example, via the calculation of the standard deviation (ASTM, 2005, 2006).

In a noise-free system, the forward (ρ_f) (current injected from C1 to C2) and reciprocal (ρ_r) (current injected from C2 to C1) ρ measurements should be the same; however, in soils a 5% reciprocal error (RE) is accepted (Chambers et al., 2008). RE is suggested as a measure of data quality, following Eq. 5.2 (Wilkinson et al., 2010):

$$RE = 100 * |\rho_f - \rho_r| / |\rho_f + \rho_r| (\%) \quad \text{Eq. 5.2}$$

The results of the RE calculations are included in Sections 5.2.3 and 5.3.4.

5.1.6 PRELIMINARY ER-TESTING SUMMARY

Based on the preliminary ER testing with the equipment hired from BGS, the ER-acquisition system (ER-Acq-I) was designed and built. Initial measurements were carried out with ER-Acq-I and ER boxes to investigate the temperature- ρ dependence of the CH and CI soils. This indicates that ρ changes between 1% and 3% per 1 °C; therefore, a 2% correction factor was adopted in accordance with Eq. 5.1. The ER-Acq-I was subsequently used in the bespoke ER chamber I, as described in the following section.

5.2 ER ARRANGEMENT I (PS1)

This section provides details on the development of the bespoke ER chamber used during the initial soil-loading trials performed with arrangement PS1 (Section 3.3.1.1).

5.2.1 ER CHAMBER I

The design of ER Chamber I was inspired by the successful correlation between changes in the void ratio and ρ during loading in the modified oedometer chambers containing natural clays (McCarter and Desmazes, 1997; Fukue et al., 1999; Kibria, 2014), kaolinite (McCarter et al., 2005) and sand (Comina et al., 2008). Given that 1D settlement monitoring is based on the average change in the void ratio, calculated from the total change in sample height, the aforementioned tests focused on relating

the average ρ readings from across the sample. Some two-point measurements with electrodes embedded in the top and bottom drainage plates were considered satisfactory to provide this information, and were adopted, for example, by McCarter and Desmazes (1997), Ghorbani et al., (2012) and Kibria (2014). However, the disadvantage with two-point measurements is the risk of electrode polarisation (Podoba and Štubňa, 2014). Therefore, four-point measurements that reflect the measurement of the voltage drop in the middle part of a sample (Parkhomenko, 1967) are preferable, as this can help to avoid polarisation. Furthermore, four-point measurements allow measurements to be taken in both the vertical and horizontal directions, and therefore can provide additional information (Anandarajah, 2000; McCarter et al., 2005; Comina et al., 2008).

As described in Section 3.3.1.3, the chamber size was constrained by the size of the TDR probes. The arrangement of the ER electrodes was then designed to correspond to the TDR measurement zone.

The literature review identified that a similar size and shape of ER chamber was adopted by Abu-Hassanein et al. (1996), who applied a four-point ER via two current plates on the top and bottom of the sample, and two potential electrodes inserted in the middle of the sample to investigate the properties of compacted clays. Borsic et al., (2005) also used a cylindrical chamber, but with 16-point electrodes around the sample to investigate heterogeneity in the moisture and density distribution in variously graded sands.

Based on the aforementioned research, a bespoke ER chamber was designed to enable four-point measurements to be taken with ER-Acq-I at a range of frequencies, including 0.1 Hz, 1 Hz, 50 Hz, 100 Hz, 500 Hz and 1000 Hz. A schematic drawing of ER Chamber I is presented in Figure 5.4.

ER Chamber I was initially 390 mm high, and comprised current-injection plates at the top and bottom (following a similar design to the perforated steel plates used in Kibria [2014]), and 8-pin electrodes positioned within the chamber wall. The plate electrodes were made of 3-mm thick marine-steel plates perforated with 12 x 3 mm holes to allow drainage. The top plate electrode (EA) was attached to a 300-mm-long brass rod (diameter approximately 10 mm), which was used as a current conductor and to transfer the load. The bottom plate electrode (EB) was attached to a 20-mm long rod, which was used to inject current.

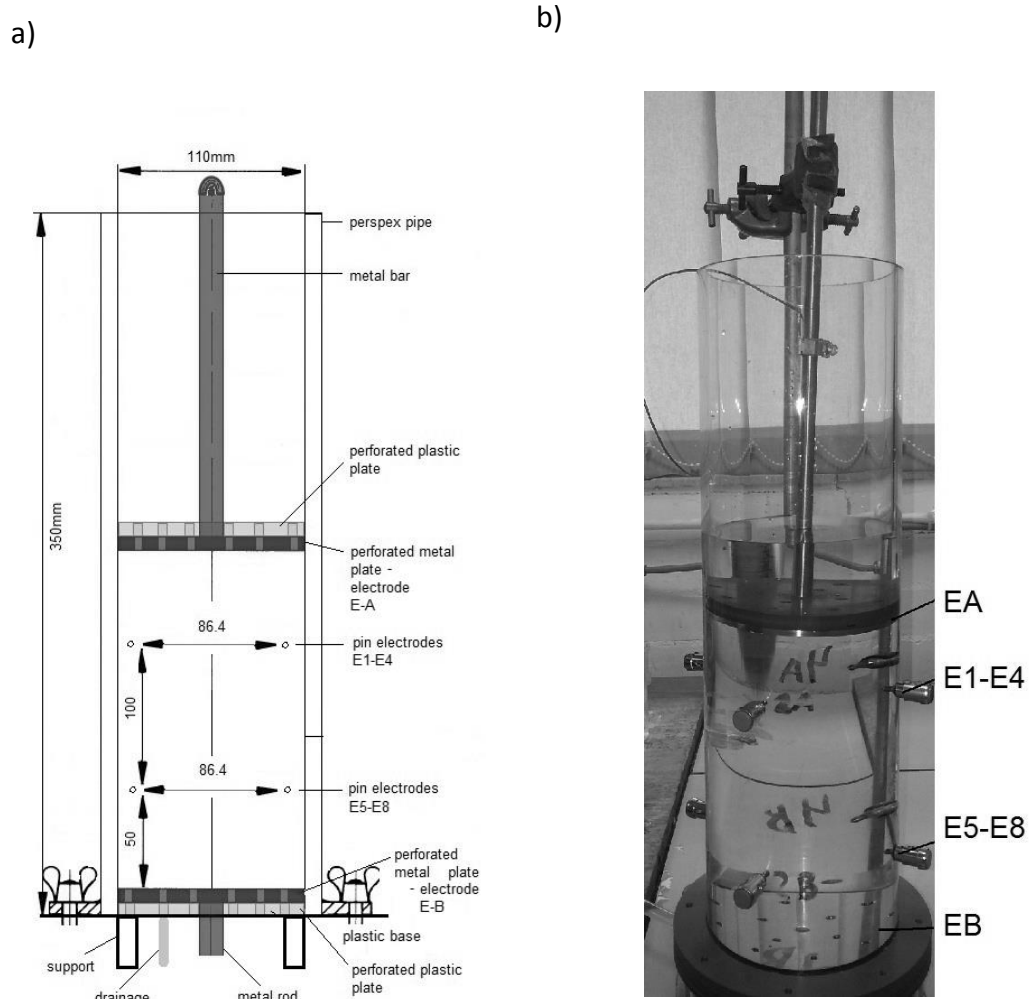


Figure 5.4. ER Chamber I: a) schematic design; and b) prototype

The pin electrodes were 3-mm-thick brass rods purchased from McMiller (the same type of electrodes was used in the soil boxes); however, they were shortened and sharpened at the end to enable insertion into the soil sample up to 10 mm and for point measurement, respectively. Pin electrodes were placed in two rows: four electrodes, E5–E8, were located at 50 mm from the bottom plate electrode; and four electrodes, E1–E4, at 150 mm from the bottom plate electrode, separated laterally by 86.4 mm. The pin electrodes were used both to inject current and measure potential, depending on the configuration, which is described further in the following sections.

5.2.2 ER ARRANGEMENT I – CONFIGURATIONS

The configurations selected for ER Arrangement I included vertical Wenner switches, which were to investigate bulk changes in soil corresponding to TDR_v measurements, and horizontal dipole-dipole switches, which would be focused on the changes within a soil layer.

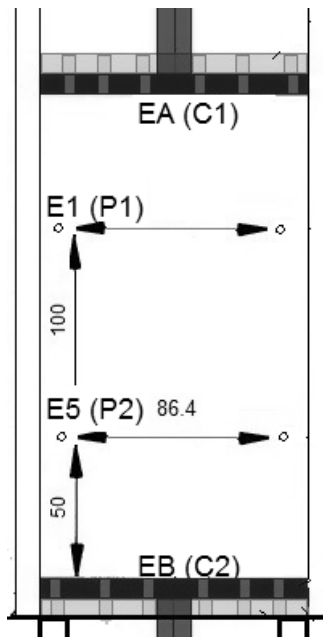
The Wenner configurations were applied through a current injection from the top (EA) to the bottom (EB) plate electrodes, whilst the potential was read on the pin electrodes located in the same column (these configurations are referred to as vertical_1-4). Additionally, the diagonal measurement was obtained by measuring the potential between columns 2 and 4 (diagonal_24). Dipole-dipole measurements were carried out by current injection through the neighbouring electrodes and measuring the potential on the opposite electrodes within the same plane. A list of configurations is included in Table 5.3, and an example of the vertical and horizontal configuration is presented in Figure 5.5.

Initially, the measurements were repeated nine times per sample; however, the results identified that the variability was below 0.03%; therefore, the number of repetitions was reduced to six and subsequently to three. This not only helped to speed the process of data collection but also reduced the time gaps between the readings, making the data more comparable.

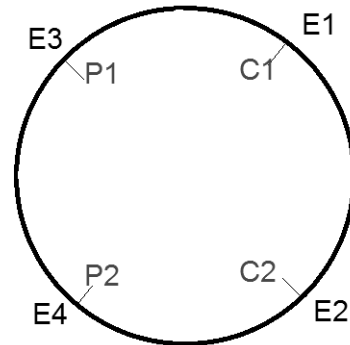
Table 5.3. ER Chamber I electrode configurations

Configuration type	Configuration reference				
		C1	C2	P1	P2
Wenner	vertical_1	E-A	E-B	I-E1	I-E5
	vertical_2	E-A	E-B	II-E2	II-E6
	vertical_3	E-A	E-B	III-E3	III-E7
	vertical_4	E-A	E-B	IV-E4	IV-E8
	diagonal_24	E-A	E-B	II-E2	IV-E8
Dipole-dipole	horizontal_1A	I-E1	II-E2	III-E3	IV-E4
	horizontal_2A	I-E5	II-E6	III-E7	IV-E8
	horizontal_1B	III-E3	IV-E4	I-E1	II-E2
	horizontal_2B	III-E7	IV-E8	I-E5	II-E6

a)



b)

**Figure 5.5. ER Arrangement I: a) vertical; and b) horizontal configurations**

5.2.3 ER ARRANGEMENT I – CALIBRATION

Due to the position of the electrodes within the circular chamber, there was a possibility of the 3D geometry having an effect on the ρ measurements; therefore, the geometric factor (k) had to be determined, either numerically or empirically (Beck et al., n.d.; Hassan, A. and Toll, 2013; Al-Obaidy, 2017). Given that the TDR probes were calibrated through experimental testing in saline solutions, an analogue, empirical approach was followed for the ER arrangement, according to ASTM G57 (ASTM, 2006). Six saline solutions were prepared by mixing KCl and distilled water, resulting in a range of electrical conductivities ($EC=1/\rho$), as presented in Table 5.4.

Table 5.4. ER Chamber I calibration solutions

Saline solutions	ρ (Ohm.m)	EC ($= 1/\rho$) (S/m)	Molarity
1	4	0.25	0.0194
2	8	0.125	0.0097
3	16	0.0625	0.0048
4	32	0.0313	0.0024
5	64	0.0156	0.0012
6	128	0.0078	0.0006

Electrical resistance (R) was read for each configuration in solution SOL1-6 in a temperature-controlled room. The chamber was filled with the solution to a height of approximately 300 mm. The top metal bar was fastened in a sample holder insulated with a plastic material (Figure 5.4b). A digital temperature probe was inserted into the fluid before and after the R measurement was taken to monitor the temperature variations.

The resistance readings for each configuration were compared with the EC measured with the standard conductivity meter (EC_{ref}), which was calibrated as described in Section 4.3.1.2. The geometric factor was then derived as the slope of the ρ_{ref} (reference resistivity) and R line (Figure 5.6), given that $\rho_{ref} = k \cdot R$, where $\rho_{ref} = 1/EC_{ref}$. A summary of the results obtained in the vertical Wenner configurations is presented in Table 5.5, whilst the horizontal dipole-dipole results are included in Table 5.6.

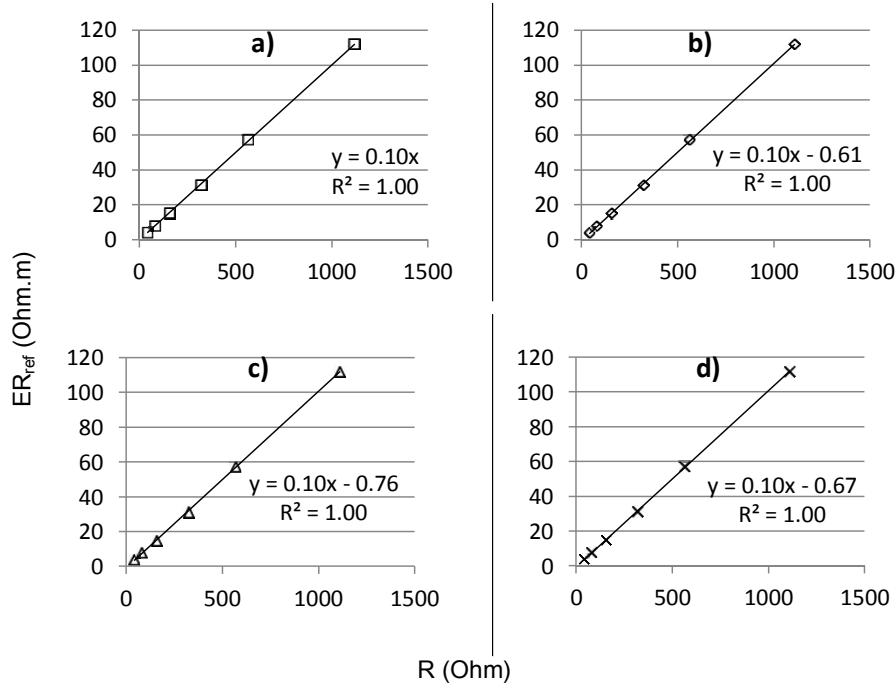


Figure 5.6. ER Chamber I geometric-factor calibration obtained from the ρ_{ref} -R relationship (a, b, c and d correspond to vertical Wenner configurations, vertical_1–4, respectively)

Table 5.5. ER Chamber I geometric-factor calibration results (vertical Wenner configurations)

	SOL6	SOL5	SOL4	SOL3	SOL2	SOL1	Geometric factor (m)
ρ_{ref} (Ohm.m)	112	57	31	15	8	4	
Configuration	R (Ohm)						
vertical_1	1117	566	322	158	82	42	0.10
vertical_2	1109	563	321	157	81	42	0.10
vertical_3	1110	568	325	159	82	42	0.10
vertical_4	1110	566	323	158	82	42	0.10

Table 5.6. ER Chamber I geometric-factor (K) calibration results (horizontal dipole-dipole configurations)

Saline solution:	SOL6	SOL5	SOL4	SOL3	SOL2	SOL1	Geometric factor (m)
ρ_{ref} (Ohm.m):	118	58	34	16	8	4	
Configuration	R (Ohm)						
horizontal_1A	213	101	58	28	15	8	0.58
horizontal_1B	174	101	58	28	15	8	0.58
RE (%)	10.1	0.0	0.0	0.0	0.0	0.0	
horizontal_2A	174	87	50	25	14	7	0.68
horizontal_2B	212	87	50	25	14	7	0.68
RE (%)	9.8	0.0	0.0	0.0	0.0	0.0	
Geometric factor calculated based on SOL1-5 due to high RE in SOL6.							

The horizontal configurations include forward ('a') and reciprocal ('b') measurements. Based on the results presented in Table 5.6, the RE was calculated in accordance with Eq. 5.2, and apart from a 10% RE in high ρ SOL6, SOL1–5 showed an RE below 0.1%. This confirmed that the constructed ER-Acq-I provided high-precision ρ data in fluids.

The accuracy of the ER-Acq-I measurements was investigated by comparing ρ_{ref} with the ρ calculated, based on adopted geometric factors of 0.10 m for the vertical configurations and 0.60 m for the horizontal configurations, as shown in Table 5.7. This resulted in an average accuracy within 3% (when compared to the conductivity meter) and a maximum measurement discrepancy of 6% in vertical configurations; however, the horizontal configurations indicated an average accuracy within 19% (which was particularly poor in the higher-conductivity solutions: SOL1, SOL2 and SOL3).

Table 5.7. Accuracy of vertical and horizontal ρ measurements in ER Chamber I based on the adopted geometric factors

Configuration	Accuracy (ρ) = $100 * (\rho - \rho_{ref}) / \rho_{ref}$ (%)							
	SOL6	SOL5	SOL4	SOL3	SOL2	SOL1	AV	MAX
vertical_1	0	-1	3	5	4	5	3	5
vertical_2	-1	-2	3	5	4	4	3	5
vertical_3	-1	-1	4	6	4	4	3	6
vertical_4	-1	-1	3	5	4	4	3	5
horizontal_1A	-1	1	-1	-9	-16	6	16	20
horizontal_2A	-2	0	-6	-19	-19	9	19	12
$\rho = K * R$, where vertical configurations $K = 0.10\text{m}$ horizontal configurations (1a) $K = 0.58\text{m}$ horizontal configurations (2a) $K = 0.68\text{m}$								

RE analysis was also conducted in the soil samples, as described in the following section.

5.2.4 BESPOKE ER ARRANGEMENT I – SOIL TESTING

The ρ measurements were taken in soil samples placed in the bespoke ER chamber with the electrode configurations described in Section 5.2.2, prior to the load placement and at the end of the loading stage. Two soil samples (CH.S01.ER and CH.S02.ER) were tested with ER Arrangement I under the PS1 loading arrangement, in parallel with the tests (CH.S01.TDR and CH.S02.TDR) conducted in the TDR chamber (PS1), described in Section 4.4. Photographic evidence of the test is presented in Figure 5.7.

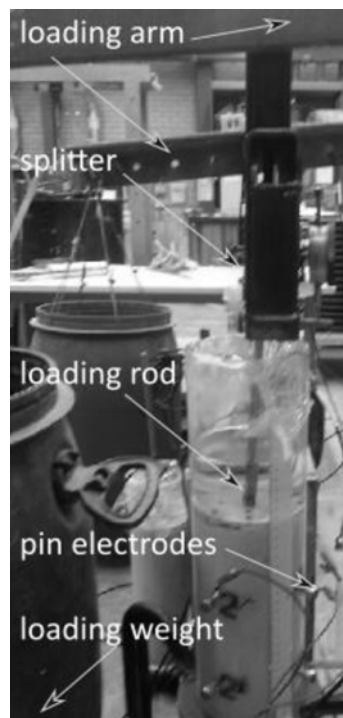


Figure 5.7. Loading bespoke ER Arrangement I

Analogous to the RE calculation in saline solutions (Table 5.6), the RE was calculated for the soil during loading (Table 5.8), which revealed that ER-Acq-I provided high-quality data with an RE below 1%.

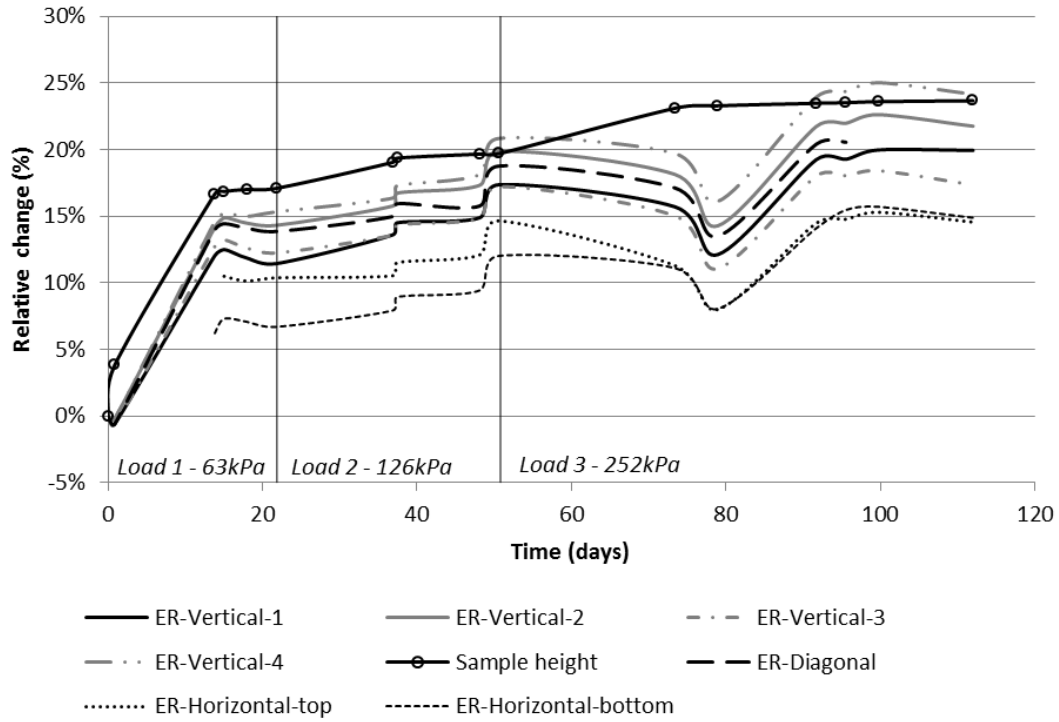
Table 5.8. RE estimation based on the ρ measurement in the CH.S02.ER sample during loading in the bespoke ER chamber I

Configuration	ρ (Ohm.m)								
	L0	L1-T3	L1-T4	L1-T5	L2-T1	L2-T2	L2-T3	L2-T4	L3-T1
horizontal_1A	9.91	11.28	11.60	11.66	11.83	11.93	11.93	12.20	11.91
horizontal_1B	9.91	11.28	11.58	11.62	11.81	11.91	11.89	12.15	11.87
RE (%)	0.0	0.1	0.1	0.3	0.2	0.1	0.3	0.4	0.3
horizontal_2A	9.28	10.27	10.57	10.56	10.82	10.92	10.91	11.17	11.14
horizontal_2B	9.21	10.23	10.54	10.52	10.78	10.89	10.88	11.13	11.12
RE (%)	0.8	0.3	0.3	0.3	0.4	0.3	0.4	0.4	0.2
L0-prior to load application L1-L3-loading stage T1-T4-trial number									

5.2.5 BESPOKE ER ARRANGEMENT I – INITIAL SOIL TEST RESULTS

The ρ results were analysed in terms of the ρ change relative to the initial reading (prior to the load application), referred to as relative ρ ($\rho_{(r)}$). This approach was adopted, for example, by Ghorbani et al. (2013), and is particularly useful in analysing low-resistivity values, as it allows clearer observation of small changes. The $\rho_{(r)}$ results, presented in Figure 5.8, were corrected for temperature using Eq.5.1.

a)



b)

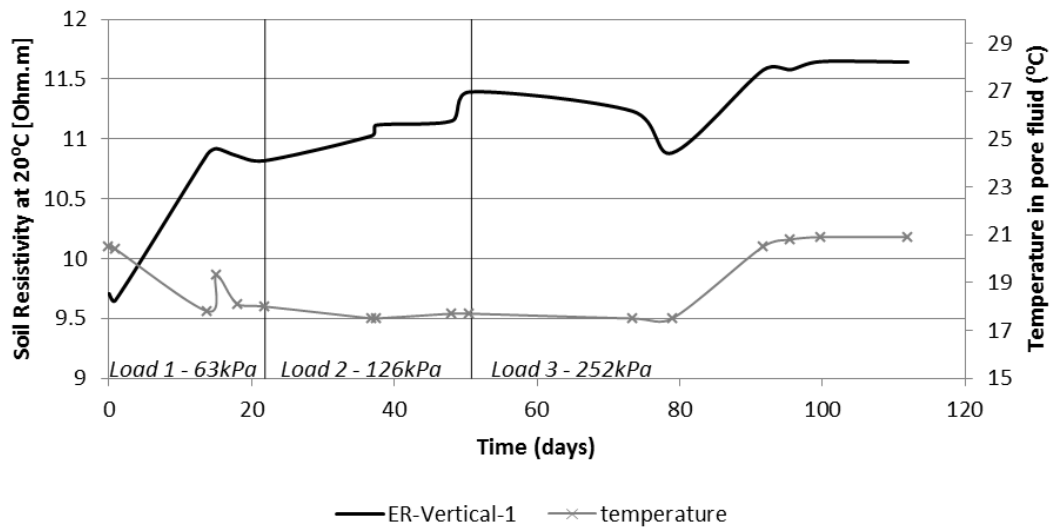


Figure 5.8. Preliminary results for 1D loading of ER Arrangement I (CH.S02.ER): a) vertical, horizontal and diagonal ER configurations (open circles on the settlement line show the times the measurements were taken); b) temperature readings in relation to ER-vertical-1

The purpose of this analysis was to investigate the change in ρ with settlement and also the effect of the temperature variation. It can be observed that a significant change in the temperature is reflected in a certain deviation in the $\rho_{(r)}$ values, from the expected trend around the 80th consolidation day. This can be related to the temperature-correction-factor limitations or the temperature-measurement method. At the time of these preliminary tests, an internal temperature sensor was not available, and the temperature was only measured on the fluid accumulated on the top of the drainage plate; therefore, the soil temperature could have been different from the fluid. Nonetheless, the $\rho_{(r)}$ correlation with the settlement was very encouraging. The magnitude of $\rho_{(r)}$ measured with vertical configurations ($\rho_{v(r)}$) corresponded to the magnitude of the settlement increase. During the second loading stage, it was observed that $\rho_{v(r)}$ increased abruptly once the settlement was negligible (most likely following the primary consolidation stage). The trend was followed by the relative horizontal-ER readings ($\rho_{h(r)}$), which also showed that the magnitude of the $\rho_{h(r)}$ change was lower than $\rho_{v(r)}$. Furthermore, the magnitude of $\rho_{h(r)}$ measured at 150 mm was higher than the readings obtained at 50 mm (measured from the bottom of the sample); this implies that the bottom of the sample experienced less change than the top, and that the bulk $\rho_{v(r)}$ change corresponded better with the void ratio, which was also a bulk measurement based on the total sample-height change. The results are discussed further in Section 6.2.5.

These results were found to offer the possibility of monitoring separate layers of the sample if further point electrodes were provided. This prompted the modification of

the ER arrangement to accommodate the monitoring of the sample's stratification. The modified ER arrangement, referred to as ER Arrangement II is described in the following section.

5.3 ER ARRANGEMENT II (PS2)

5.3.1 ER CHAMBER II AND ELECTRODE DESIGN

The size of the modified ER chamber was the same as ER Chamber I, apart from the height, which was set to 300 mm to fit the new frame design (3.3.1.2) and speed up the settlement process.

ER Arrangement II was designed to accommodate 32 pin (point) electrodes, as shown in Figure 5.9a. Given that the sample height was expected to reduce from 295 mm to 200 mm, the first row of eight point electrodes was positioned 43 mm below the minimum sample height, and the three subsequent rows were separated equally. The electrodes were fastened to the chamber wall via a threaded outlet, and insulated with a plastic threaded washer and a rubber O-ring. The chamber was filled with water to ensure it was not leaking. The top and bottom plate electrodes remained unchanged; however, the top loading rod, which was also used as the current conductor, was changed from brass to marine steel, and its length was shortened to 200 mm to fit the new frame design. The rod was rounded at the top to fit into the loading frame.

The pin electrodes were changed from brass to marine steel in order to avoid any risk of galvanisation. The new electrode design included a 3-mm diameter threaded rod, which was sharpened at the end (Figure 5.9b). The rod was imbedded in a hexagonal-shaped marine-steel bar with an opening to allow the accommodation of a banana plug connection. The same type of connection was made within the new switching-board system. A waterproof, automated temperature sensor (Section 3.3.3), was inserted through the top drainage plate at approximately 100 mm into the sample.

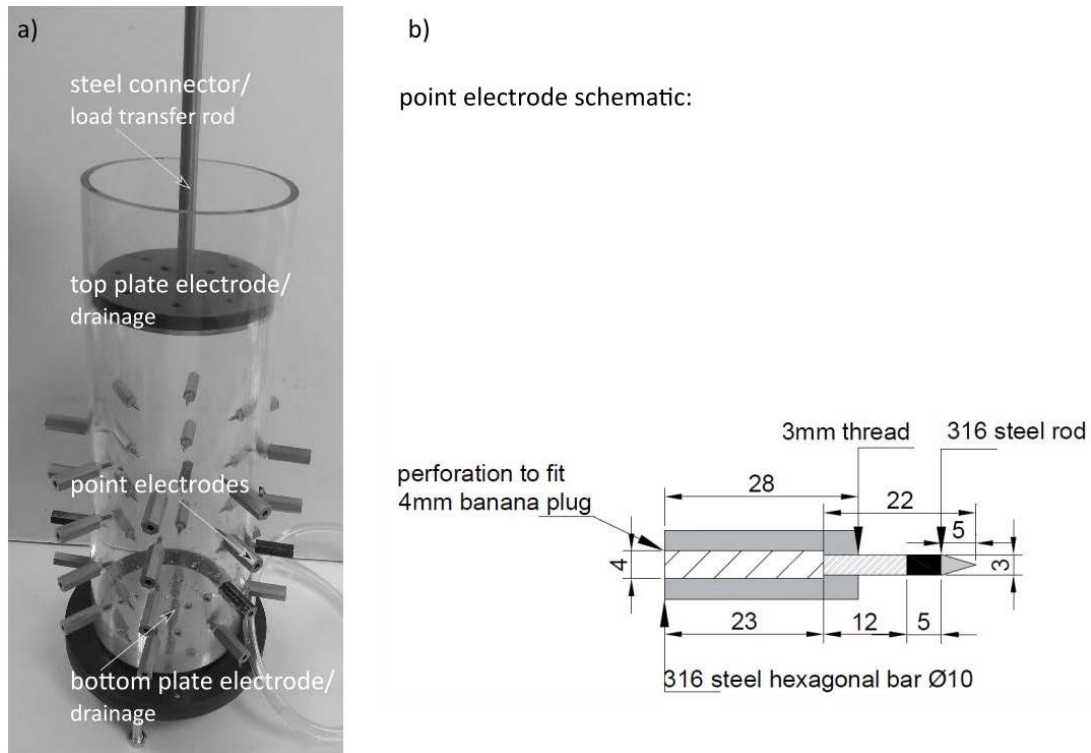


Figure 5.9. a) ER Chamber II and b) point electrode design

In order to operate the ER Arrangement II electrodes, the acquisition system had to be modified, as is described in the following section.

5.3.2 ER-ACQUISITION SYSTEM II

The ER-Acq-II (Figure 5.10) was upgraded based on the ER-Acq-I measurement principles (courtesy of Mr P.A. Atkins).

National Instruments modules NI9239 and NI9263, and a switching board were incorporated to enable automatic switching amongst the 32 electrodes; however, due to the cost of the switching board, it was only possible to incorporate a maximum of 16 channels. A MATLAB script was prepared (courtesy of Mr P.A. Atkins) to collect voltage and current readings from a switched array of electrodes. Each measurement was performed on two pairs of electrodes (C1-C2 and P1-P2) and the time between the measurements was set to 5 seconds.

Analogous to ER-Acq-I, a 1 k Ω resistor was used to measure and limit the current to 1 mA.

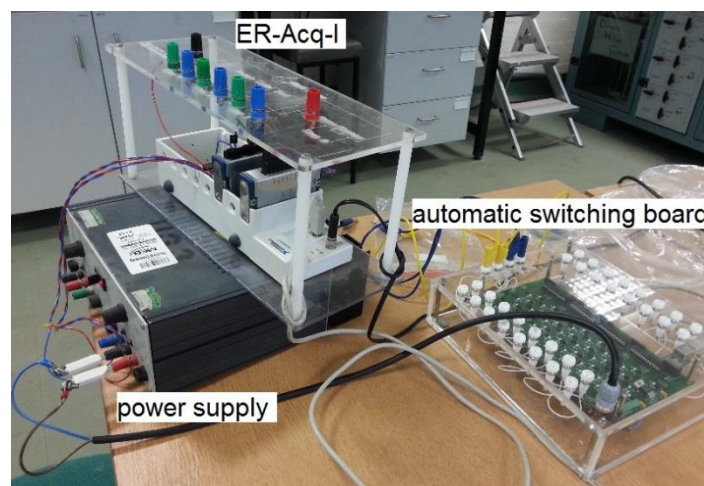


Figure 5.10. ER-Acq-II, including the power supply, automatic switching board the electrical chassis used in ER-Acq-I

The new system enabled a selection of frequencies to be used. Initial trials were performed at 0.1, 1, 10, 50, 100, 200 and 500 Hz; however, in order to minimise the risk of mains frequency interference, this sequence was then modified to 0.1, 1, 11, 51, 101, 201 and 501 Hz.

The system calibration was performed with a known 1 k Ω resistor, by measuring the resistance on eleven vertical and four horizontal configurations at 0.1, 1, 10, 50, 100, 200 and 500 Hz frequency. The resistance results were in the range of 999.95–1000.12 Ohm (Table 5.9). Hence, the accuracy of the resistance readings would be expected to fall within (-) 0.005% and (+) 0.01%, but the manufacturer stated that the tolerance of the resistor was within $\pm 0.01\%$. Based on the results, it was concluded that ER-Acq-II was able to provide high-accuracy and high-precision readings.

Table 5.9. ER-Acq-II reference-resistor (1 k Ω) calibration results

Frequency (Hz)	R (Ohm)			
	Vertical configurations		Horizontal configurations	
	MIN	MAX	MIN	MAX
0.1	1000.01	1000.03	1000.03	1000.03
1	1000.01	1000.02	1000.02	1000.02
10	1000.01	1000.02	1000.02	1000.02
50	999.96	1000.12	999.96	1000.12
100	999.95	1000.04	999.95	1000.03
200	1000.02	1000.04	1000.02	1000.04
500	1000.02	1000.06	1000.02	1000.06

5.3.3 ER ARRANGEMENT II – CONFIGURATIONS

The new switching system allowed automatic data acquisition at selected frequencies from 16 channels. This was a significant upgrade from the previous system, where all the measurements were taken manually.

The design of the configurations is a compromise between the resolution and speed of acquisition (Comina et al., 2008). Given that 34 electrodes (2 plate and 32 point) were incorporated into the new design, and five frequencies were selected, the choice of the configurations enabling the collection of meaningful data in a manageable timeframe and with limited physical switching between sequences was challenging and was adjusted in a few stages.

Initial tests were carried out at 0.1, 1, 11, 51, 101, 201 and 501 Hz; however, it was noted that 51 Hz and 201 Hz provided results very similar to 101 Hz, and therefore were excluded from further testing to reduce the data-collection time. Hence, five frequencies were selected: 0.1, 1, 11, 101 and 501 Hz.

5.3.3.1 ER-ACQ-II CONFIGURATION APPROACH 1

Approach 1 included four steps, between which the electrode cables were switched manually (limiting the amount of switching was taken into consideration in order not to disturb the sample and/or the electrodes). Each step consisted of intermixed horizontal and vertical configurations to avoid the electrode-polarisation effect (by

changing the current-potential electrodes). The point electrodes were divided into four rows (to correspond to soil layers) – labelled from Row 1 (top) to Row 4 (bottom), as in Figure 5.11a – and eight columns (1–8), as in Figure 5.9 and Figure 5.11b. Measurement was performed on selected configurations at a given frequency, and automatically progressed to the subsequent frequency once a set of configurations was completed.

During the first step, columns 1, 3 and 5, and the two top electrodes from column 7 were addressed. Vertical Wenner (W) type measurements followed the principle set in the ER Arrangement I design. Current was injected between the top (C1) and bottom (C2) plates (Figure 5.11a), whilst the potential was measured on the point electrodes, separated by 43 mm (Row 1–2, Row 2–3 and Row 3–4), 86 mm (Row 1–3 and Row 2–4), and 129 mm (Row 1–4). These three types of configuration are represented in Figure 5.11a by shaded areas A, AB and AC, respectively. In order to minimise the risk of electrode polarisation, the current injection was inversed between the top and bottom plates, and, where possible, vertical switches were intermixed with horizontal dipole-dipole (square) measurements. This sequence included 20 configurations. In order to take the measurements at the selected frequencies, each measurement took approximately 5 minutes for each configuration; a full set of measurements with all the 20 configurations took approximately 1.7 hrs.

The second step was performed analogously to the first, within column 5 and 7, and the two bottom rows (3 and 4).

The third step required the physical reconnection of eight cables to incorporate four electrodes that were not included in previous measurements. It was performed on the bottom rows (3 and 4), focusing on the horizontal measurements (Wenner, dipole-dipole and square). There were 40 configurations included in this step, which took approximately 3.4 hrs per full set of measurements.

The fourth step was analogous to the third, but was performed on the top rows (1 and 2).

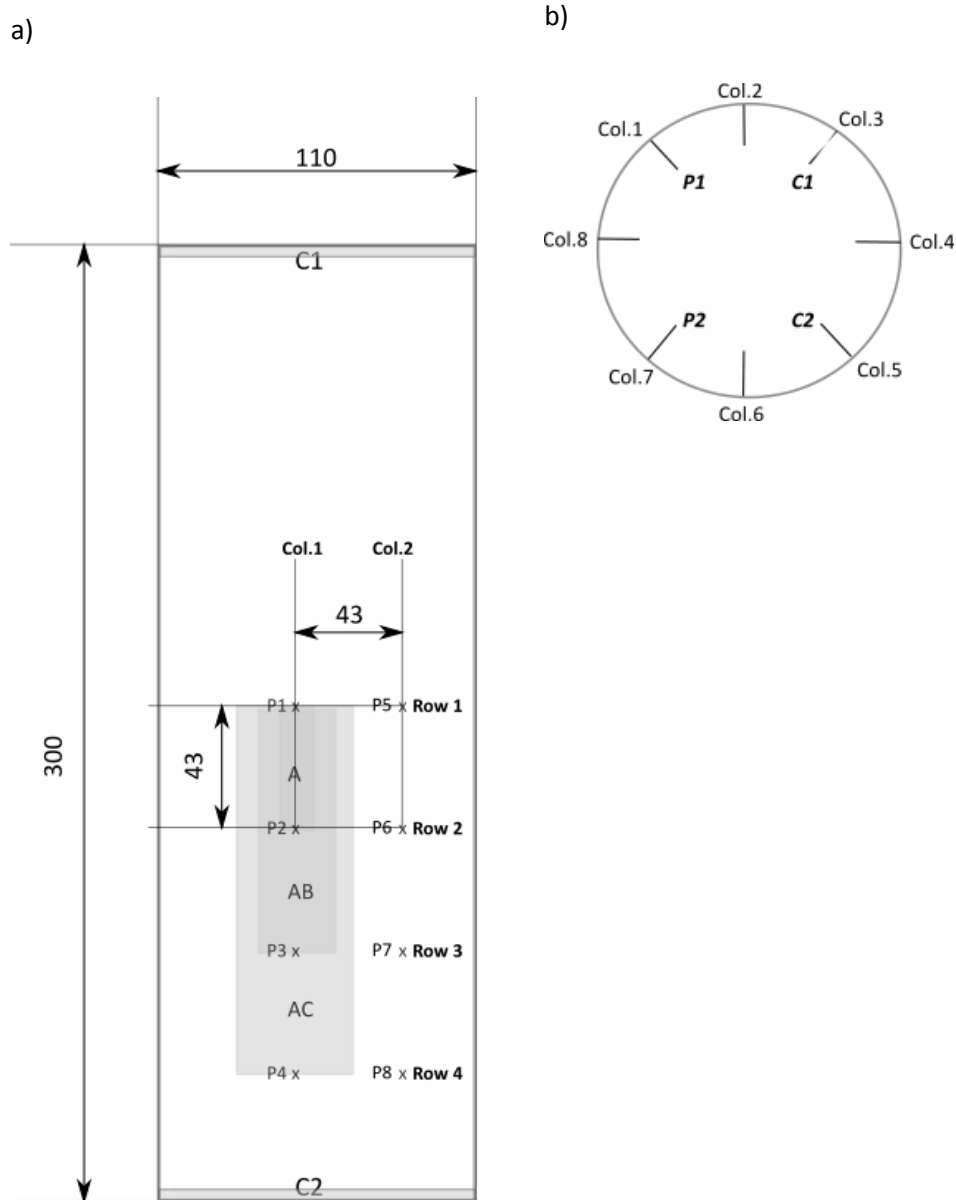


Figure 5.11. ER Chamber II configurations: a) vertical (view from the side); and b) horizontal (view from the top), with measurements in mm

5.3.3.2 ER-ACQ-II CONFIGURATION APPROACH 2

Following the work of Hassan (2014) and Al-Obaidy (2017), additional horizontal configurations were included to enable digital imaging; however, due to significant

measurement variations and the RE exceeding 5%, the results were not found to be reliable. Due to the time constraints, the imperfections in the measurements within the horizontal layers were not investigated further. The focus was given to the vertical configurations within the AD layer, which were found to correspond to the readings obtained with ER-Acq-I. The calibration results for this configuration are included in the following section.

5.3.4 ER ARRANGEMENT II – CALIBRATION

Following the determination of the geometric factor in six saline solutions (Section 5.2.3) in ER Chamber I, it was concluded that, to increase time efficiency, the geometric factor can be estimated, based on a comparison between the conductivity meter readings and resistance measured in one saline solution. Therefore, the geometric factor in ER Chamber II was based on the measurements taken in the KCl solution corresponding to the ρ of CH and CI soil at approximately 8 Ohm.m. Due to several modifications of the configurations and probe-insertion depth, the calibration results presented as follows include only the final arrangement, for which the soil test results are discussed in Section 6.2.5.2.

The estimated geometric-factor results of the AD configurations are plotted in the order of switches conducted with ER-Acq-II (Figure 5.12), presenting a slight variability between frequencies. The results of the calibration reveal that the measurements taken at 1 Hz were most likely affected by polarisation, since the R readings obtained

at this frequency were lower than the 11 Hz, 101 Hz and 501 Hz readings. Also, every first reading at the 11Hz, 101 Hz and 501 Hz frequencies produced a slightly lower R, which was reflected in the higher geometric factor (0.075 m) compared to the subsequent readings (0.074 m).

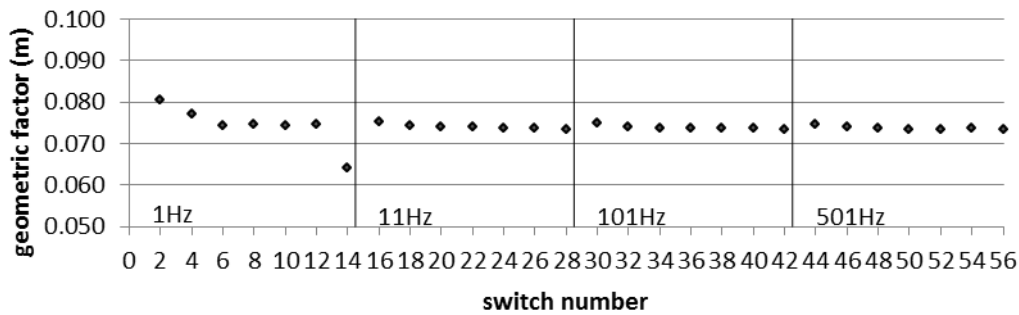


Figure 5.12. ER Arrangement II geometric-factor calibration in the vertical configuration corresponding to the AD soil layer; measurements were carried out in 8 Ohm.m KCl solution

The adopted geometric factor for vertical configurations in the AD layer was 0.074 m, indicating agreement with ER_{ref} within 1%.

Table 5.10. Accuracy of vertical ρ measurements in ER Chamber II based on the adopted geometric factor

Configuration	Accuracy (ρ) = $100 * (\rho - \rho_{ref}) / \rho_{ref}$ (%)					
	1 Hz	11 Hz	101 Hz	501 Hz	ABS.AVG (11-501 Hz)	ABS.MAX (11-501 Hz)
vertical_1	-8	-2	-1	-1	1	2
vertical_2	-4	-1	0	0	0	1
vertical_3	-1	0	0	0	0	0
vertical_4	-1	0	0	1	0	1
vertical_5	0	0	1	1	0	1
vertical_6	-1	0	0	1	0	1
vertical_7	16	1	1	1	1	1
$\rho = K * R$; $K = 0.074$ m						

5.3.5 ER ARRANGEMENT I AND II – SOIL TESTING

Due to the number of changes implemented during the development of the ER arrangement, and the time required to build, calibrate and test the equipment, as well as designing and testing the configurations, the number of soil samples tested during the 1D loading with ER was limited to five. This included two soil samples (CH.S01.ER and CH.S02.ER) tested with ER-Acq-I, ER Chamber I, and three samples tested with ER-Acq-II, ER Chamber II. Table 5.111 provides a summary of the soil-loading ER testing, including the frequencies and configurations used.

Table 5.11. Soil-loading ER-testing summary

Soil mixture	Acquisition system	Frequency (Hz)	Configurations
CH.M1.S01.ER	ER-Acq-I	0.1-500 (10 Hz selected for the analysis)	V: electrodes separated by 100 mm; H: 86.4-mm separation
CH.M1.S02.ER			
CI.M4.S4.ER	ER-Acq-II	0.1; 1; 11; 51; 101; 201; 501	V: separation 43 mm, 86 mm, and 129 mm; H: 86.4 mm
CI.M4.S6.1.ER		0.1; 1; 11; 51; 101; 201; 501	
CI.M4.S6.2.ER		1; 11; 101; 501	V only focused on 129-mm separation
CH.M1.S4.ER		1; 11; 101; 501	

5.3.6 ER ARRANGEMENT II SUMMARY

The ER-Acq-II was found to provide high precision and accurate ρ readings when calibrated with a standard 1 k Ω resistor. However, the calibration tests conducted in the KCl solution demonstrated that the new acquisition system exhibited certain limitations. The first measurement frequency (whether set at 0.1 Hz or 1 Hz) resulted in a lower resistance (R) than those measured at subsequent frequencies. Also, the first reading at any given measurement frequency was observed to display a lower R in comparison with subsequent readings.

Although ER Arrangement II was designed and built to provide further information about changes in the soil layers, the experimental testing carried out with new configurations indicated the poor reliability of the horizontal configurations, with the RE exceeding 5%.

Furthermore, the insertion of additional electrodes appeared to induce a further problem, as voids beneath the electrodes were observed to increase in length with the progress of loading. This resulted in reduced ρ readings due to accumulated fluid around the electrodes, and led to a limited number of readings that could be compared with the primary ER arrangement. Nonetheless, the bulk changes measured with vertical configurations within the AD layer, corresponding to TDR_v measurements, were found to be successful and are discussed further in Chapter 6.

CHAPTER 6: RESULTS**6.1 INTRODUCTION**

In this chapter, the results of the electromagnetic AP, BEC and EC ($1/\rho$) readings are presented and discussed in connection with their correlation with the loading and unloading of the CH, CI and CL samples in the bespoke ER and TDR chambers. It should be noted that changes in the geotechnical parameters are measured in terms of the bulk parameters derived from the initial and final GWC and sample-height measurements during loading and unloading. This is due to the difficulty faced in monitoring changes in parameters (for example, the density and void ratio), without disturbing the soft samples, and hence invalidating the values derived for the parameters investigated. In addition, due to the bespoke character of the consolidation arrangement, which was not hydrostatic, the possibility of determining the effects of hydraulic-gradient induced changes within the sample was also investigated.

Particular focus was given to the TDR-measured AP's and BEC's correlation with the void ratio and pore-water-pressure-induced behaviour, as the observations made during the present investigation were not found to be covered in the past literature. The BEC was investigated in view of its relation to the low-frequency EC (measured in parallel samples using the ER method) and the pore-fluid contribution. The changes in the geophysical properties were examined in the vertical and horizontal planes in

order to establish whether the positioning of the TDR and ER instrumentation affects their readings. Positioning the horizontal probe a sufficient distance away from the vertical probe (so that they did not interfere with one another) also appears to have the advantage, which was not realised at the time, that the horizontal probe was not significantly affected by the load applied during consolidation. The frictional losses along the cell wall resulted in a significantly reduced load being transmitted through the soil with depth (Olson, 1986), but the soil experienced changes due to the change in the hydraulic gradient acting on the sample. Hence, it might be possible to detect the compressing effect of a vertically downward seepage of water with TDR (in addition to the compression due to consolidation). The electromagnetic response to unloading, although based on limited testing, is also studied in order to determine whether TDR and ER could be used in this application.

It is hoped that the correlations between AP, BEC and ER, and geotechnical changes (density, water content, void ratio, etc.) demonstrated herein could justify the potential incorporation of simple geophysical sensors into a geotechnical-monitoring regime for ground conditions subject to loading and unloading. Such an approach may prove a useful early warning system against the loss of ground performance.

For ease of reference, it is considered necessary to present a summary of the tests carried out in the bespoke TDR and ER chambers, as shown in Table 6.1.

Table 6.1. Summary of the tests carried out in the bespoke ER and TDR chambers

TEST NO	SOIL MIX	REPETITION	SENSOR	Applied pressure (kPa)						
				L1	L2	L3	L4	L5	L6	L7
1	CL	S1	TDR	15	25	50	85	100	5	-
2	CL	S2	TDR	15	25	50	85	5	-	-
3	CH	S01*	ER	40	80	160	80	-	-	-
4	CH	S02*	ER	40	80	160	-	-	-	-
5	CH	S01*	TDR	40	80	160	80	-	-	-
6	CH	S02*	TDR	40	80	-	-	-	-	-
7	CH	S03	TDR	No load						
8	CH	S4	ER	5	10	20	-	-	-	-
9	CH	S5	TDR	5	10	20	40	-	-	-
10	CI	S1	TDR	15	25	35	62	83	5	-
11	CI	S2	TDR	20	36	60	35	5	107	5
12	CI	S3	TDR	25	50	100	5	-	-	-
13	CI	S4	ER	25	-	-	-	-	-	-
14	CI	S5	TDR	20	50	100	-	-	-	-
15	CI	S6	ER	5	25	50	100	5	-	-
16	CI	S7	TDR	25	50	100	50	25	5	
17	CI	S8	TDR-P	5	15	-	-	-	-	-
18	CI	S9	TDR-P	5	0	-	-	-	-	-
19	CI	S10	N	25	50	-	-	-	-	-
* Pressure System 1 (PS1) L1-L7 - loading stage TDR-P - pore pressure experiment N - no instrumentation										

Based on Table 6.1, the soil sample's code name of CH.S1.TDR (soil type.repetition.sensor) was adopted.

6.2 ELECTROMAGNETIC RESPONSE TO LOADING AND THE SUBSEQUENT CONSOLIDATION OF THE SOIL SAMPLES

6.2.1 INITIAL TDR RESPONSE PRIOR TO THE APPLICATION OF THE LOAD

The initial TDR readings were taken prior to the application of loading for all the samples. Examples of selected waveforms measured in the soils at their LL or slightly above (1.1 times LL), with reference to the waveform for deionised water, as well as the waveform in the pore fluid collected during the consolidation of the CI soil, are presented in Figure 6.1.

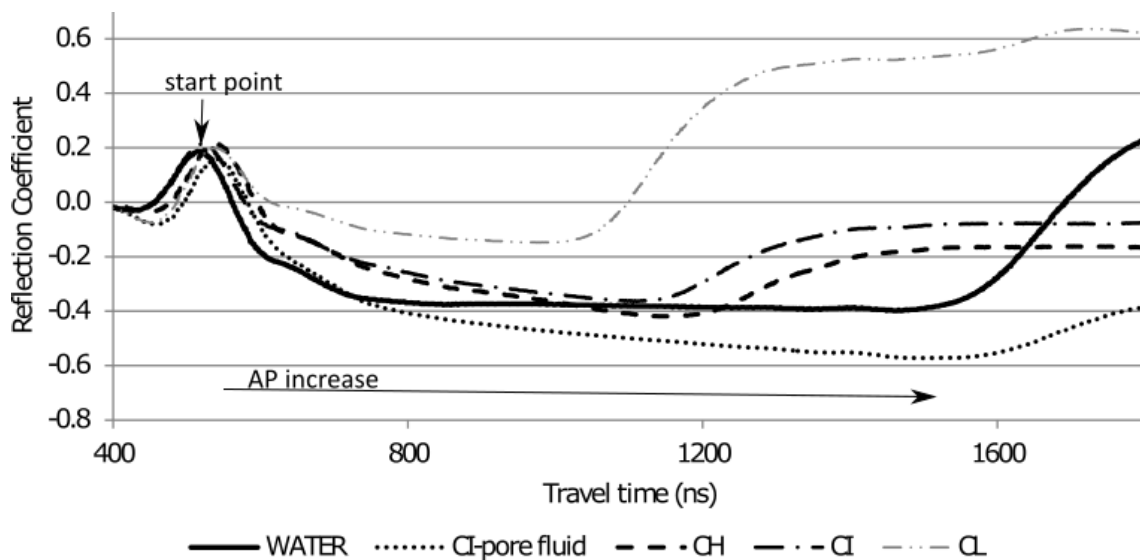


Figure 6.1. TDR waveforms: in water; in the pore fluid from CI; and in the three soil mixtures prior to loading

The initial VWC of the soil mixtures, which was determined based on the oven drying at 105 °C of the selected subsamples, is found to increase with the increase in the plasticity of the soil: for CL it is 44%, for CI it is 55% and CH is 61%. The waveforms

shown in Figure 6.1 indicate that the AP follows the same trend, and confirms its relationship with the VWC and LL in accordance with the published literature (Topp et al., 1980; Thomas et al., 2010a). Furthermore, a higher signal attenuation, implied by the smaller magnitudes of the reflections due to the increasing BEC, is noted in those soil mixtures containing bentonite. Despite a significant difference in the sand content between CH (10% sand) and CI (50% sand), their respective initial APs and BECs were relatively close, with AP values of 36 in CH and 32 in CI, and BEC values of 0.138 S/m in CH and 0.098 S/m in CI. This is as opposed to CL, whose initial AP was 26 and its BEC 0.015 S/m. This suggests the bentonite has a dominant influence on the TDR response, and is investigated further in Section 6.2.4.

6.2.2 AP_V AND AP_H RESPONSES TO THE APPLICATION OF A LOAD AND THE SUBSEQUENT CONSOLIDATION

The reduction in the sample height over time with the application of a load forms the basis of the compressibility estimation for each soil, and is the result of fluid expulsion and the consequential particle rearrangement (Barbour and Fredlund, 1989), ignoring the secondary compression mechanics – these were not considered to be in effect in this study, due to the timescales involved. Given that electrical conduction in soils takes place primarily through electrolytes (Reynolds, 1997), it can be expected that the expulsion of fluid containing solutes takes place during consolidation, along with the reduction in pore volume. For example, a correlation between the void ratio and EC during vertical loading has been found in sands (Comina et al., 2008), and in clays with

low (Fukue et al., 1999; McCarter et al., 2005; Kibria, 2014), medium and high plasticities (McCarter and Desmazes, 1997; Fukue et al., 1999; Kibria, 2014), using low-frequency ER measurements (0.01 Hz–100 kHz). Simultaneously, the decrease in the volume of water during consolidation is expected to change the AP measured by TDR (Liu, 2007). This has been confirmed by the readings taken with TDR_v positioned in the top drainage plate in the direction of the application of the load, which shows that the AP decreased with the expulsion of water following the application of the vertical load. Figure 6.2 shows an example of TDR_v waveforms obtained in a sample of CI prior to the loading (L0) and under the application of 10 kPa at three consecutive times (L1-T1, L1-T2, L1-T3), corresponding to the consolidation stages. Note that, whilst the start point does not change significantly with the application of the load, the travel time, which is directly related to the AP, clearly reduces. If the soil is settling, then TDR can potentially detect this; equally (as illustrated later in this chapter, in Sections 6.2.3 and 6.4.5), perhaps it could detect swelling, which TDR seems able to do in certain circumstances encountered herein.

In contrast, the TDR_h readings for the same soil sample (Figure 6.3) did not follow the same trend during the initial loading stages, but shows an increase in travel time with drainage during the first loading stage (L1-T1). Nonetheless, during the later stages of consolidation (L1-T2 and L1-T3), the travel time decreased and followed the response of TDR_v . Interestingly, during the progress of consolidation, AP_h decreased more than AP_v , as can be seen in the example of a CI sample in Figure 6.4.

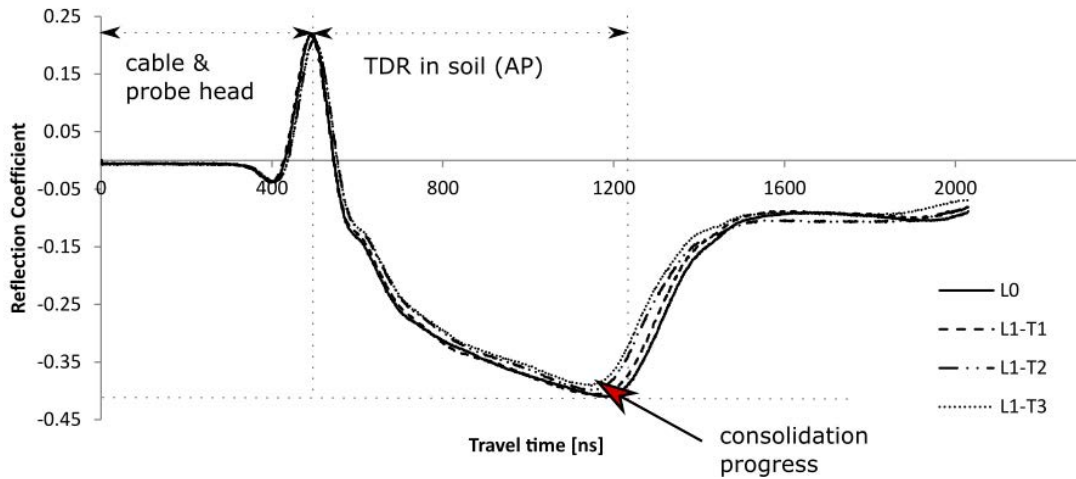


Figure 6.2. TDR waveform collected in CI from TDR_v prior to the load application (L0) and at three consecutive points in time (T1-T3), following the application of a 10 kPa load (L1)

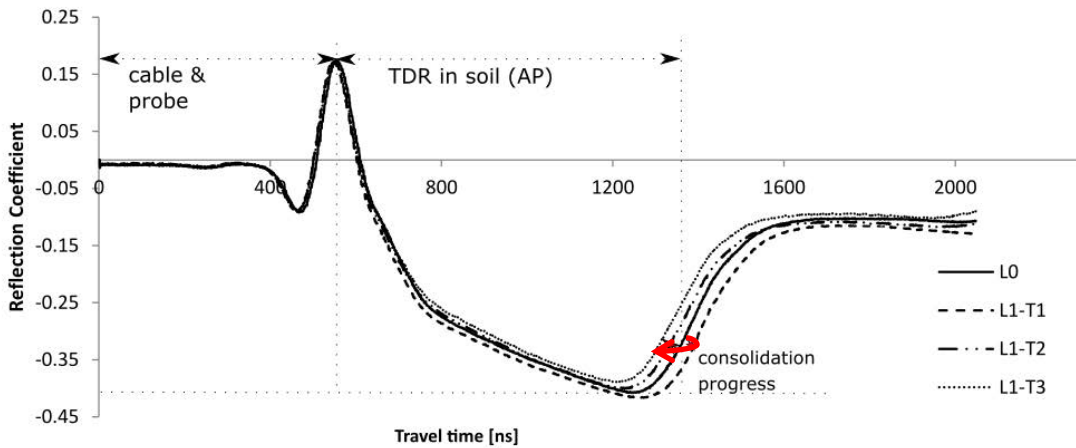


Figure 6.3. TDR waveform collected in CI from TDR_h prior to the load application (L0) and at three consecutive points in time (T1-T3), following the application of a 10 kPa load (L1)

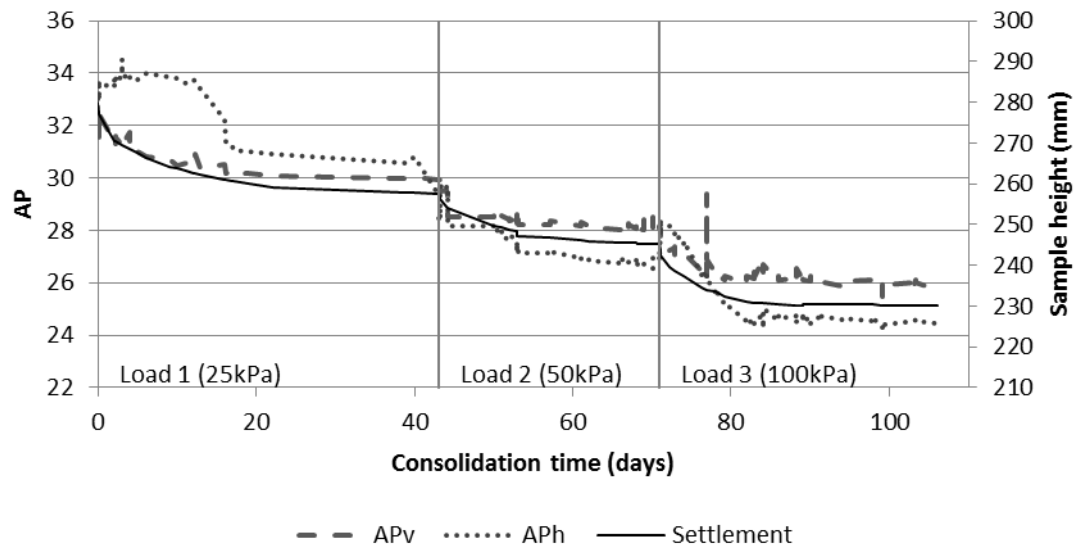


Figure 6.4. AP_v and AP_h responses to changes in settlement in the CI.S3.TDR sample

It is apparent that the GWC varied with depth once the primary consolidation was effectively complete (the GWC was measured at the end of the test, once the settlements had reached an apparent asymptote) (Figure 6.4). This reveals that the average GWC was higher within the part of the sample measured by TDR_h (Figure 6.5), (i.e. the lower layers of the soil sample), which suggests that the d_d could be expected to be lower than within the upper layers of the sample (which are monitored using the TDR_v) (for more information on the testing methodology, please refer to Section 3.3.2.2).

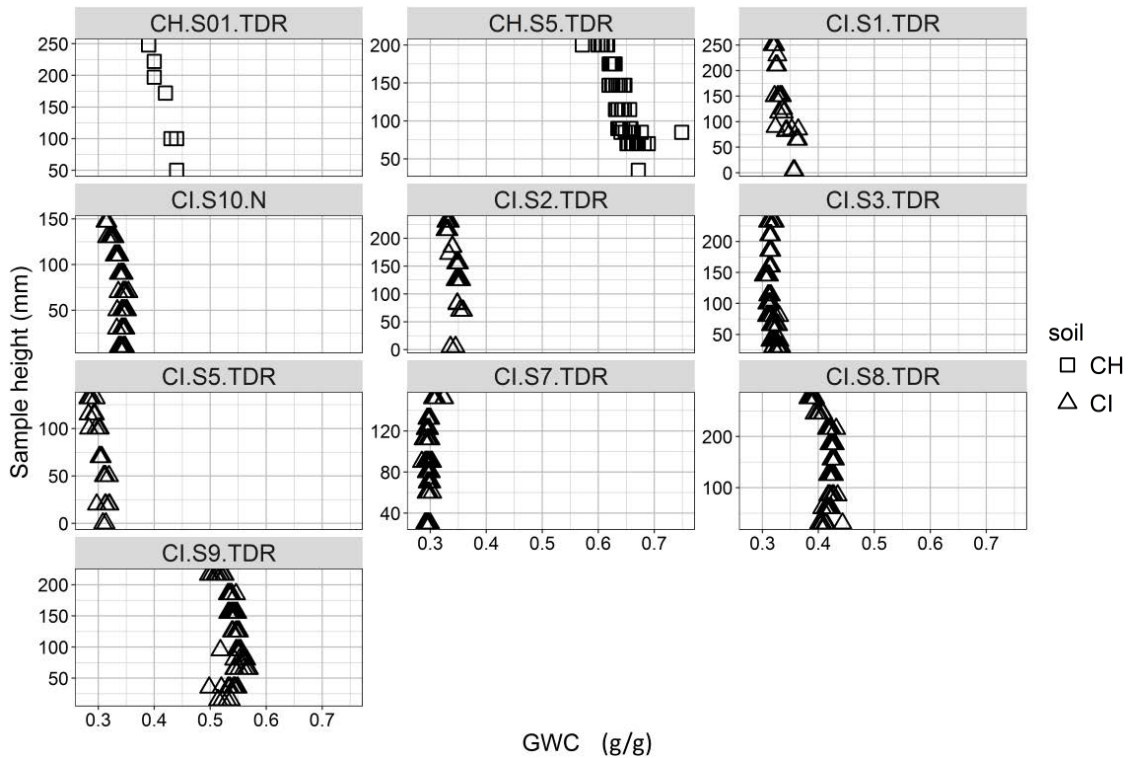


Figure 6.5. GWC variation with depth in the TDR chambers in CH and CI soil (CH.S01.TDR–CH.S9.TDR correspond to sample numbers; CI.S10.N is a control sample with no instrumentation)

A facet of the experiment's set-up used was the lack of a slip lining between the cell wall and the soil; hence, the soil located near the base of the cell was not expected to experience a significant proportion of the load applied, as the frictional forces between the cell and sample were expected to dominate with depth (Olson, 1986). If this were the only mechanism (consolidation with the application of an increasing load) impacting upon the soil samples, then the change in geophysical parameters from the horizontal TDR probe would not be expected to be so pronounced (remembering that the three-rod TDR probes provide a mean value for the AP encountered along the rods (Knight et al., 1997; Nissen et al., 2003; Pastuszka et al., 2014)). Yet, it is apparent that the raw TDR waveform and the associated AP do exhibit changes, implying that the

GWC is changing at this location. Two factors were considered to find an explanation for this response: (i) increased localised density on the top of the TDR_h (a result of consolidation, even at the reduced load experienced at this depth); and (ii) the densifying forces associated with vertically downward seepage due to a hydraulic-gradient increase, which are discussed further in Sections 6.2.2.1 and 6.2.2.2.

6.2.2.1 AP_h RESPONSE – CONSOLIDATION MECHANISM

Due to the presence of the electrodes in the horizontal plane, a localised increase in density around the probes was possible, although this could not be verified due to the very soft consistency of the samples at the end of the tests. However, if ground movements were occurring, then an alignment of the clay particles parallel to the TDR_h probe was expected; this was evidenced by the SEM images, which show an edge-to-edge alignment next to one of the TDR_h probe rods (Figure 6.6) and a flocculated structure can be observed within the top centimetre of the sample (Figure 6.7). The SEM images cannot be regarded as definite proof of the particle alignment around TDR_h , and additional research is required to validate this; however, the images seem to indicate that the probe had a localised impact on the soil surrounding it.

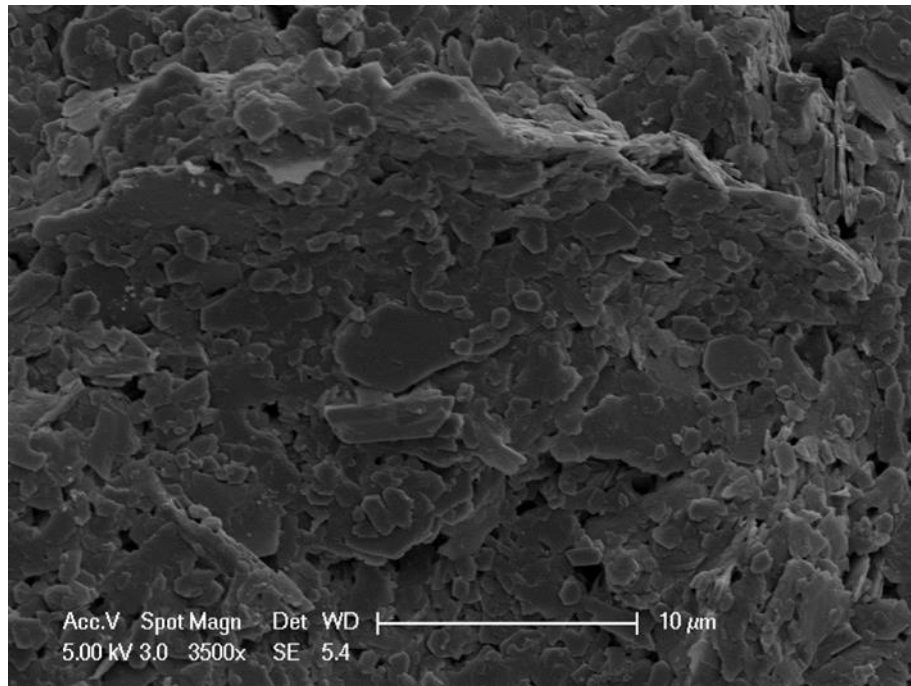


Figure 6.6. Post-consolidation SEM image of the clay particles next to one of the TDR_h probe rods

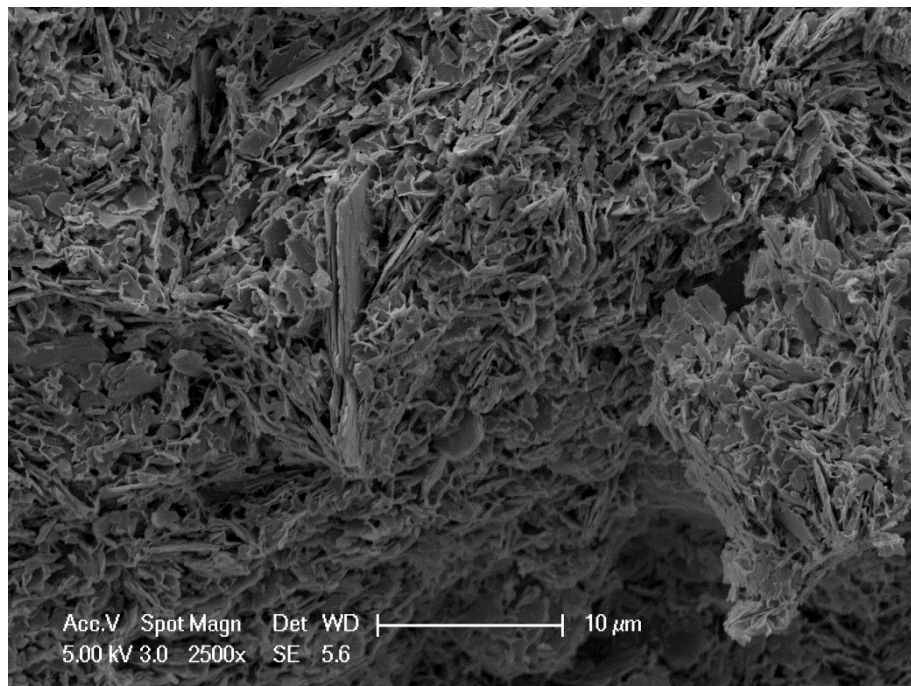


Figure 6.7. Post-consolidation SEM image of the clay particles within the top centimetre of the CI sample

6.2.2.2 AP_H RESPONSE: SEEPAGE FORCES

It is believed (from the SEM images and visual observations of the soil below the TDR probe) that the soil arched around the horizontal probes, resulting in the formation of a lower density 'pipe', which exhibited a higher water content compared to the soil not affected by the presence of the probe. This 'pipe' is thought to have formed a preferential pathway towards the side of the chamber (where the hydraulic conductivity may be higher than in the middle of the sample), and hence acted as a drain. This assumption is supported by the final GWC results, which reveal a higher water content around the TDR_h in two out of the ten samples (CH.S5.TDR and CI.S1.TDR), as shown in Figure 6.5. Therefore, it is also possible that initially increased TDR_h readings reflect increased contact between the probe and the soil, due to elevated pore-water pressure (developed with the consolidation of the upper layers of soil).

In the standard oedometer tests, an equal pressure head is maintained at the top and bottom of the sample (as it is immersed in water, and the upper and lower porous stones are in hydraulic connection with the surrounding fluid) to maintain hydrostatic conditions. In the design of the bespoke ER and TDR chambers, it was not possible to place the sample in a water bath, due to the presence of the measuring electrodes. In order to equalise the pressure head, filling the bottom drainage pipe with water to the level of the top drainage plate was considered. However, adding water to the drainage pipe would have diluted the pore fluid, and, as a result, preclude the chemical and electrical investigation of its properties (which was deemed more important than the

hydrostatic conditions). Therefore, whilst the upper and lower drains were used in the bespoke cells, the water in each was not at the same head. The bottom drain allowed the fluid to drip out of the chamber (via an air-filled pipe) and was collected in a container approximately 1 m below the bottom of the cell (this implies that the lower head, at the base of the cell, was equivalent to atmospheric pressure and was effectively constant). The pore fluid seeping out of the upper face of the sample accumulated on top of the perforated loading plate (Figure 3.11), increasing the magnitude of the upper head acting upon the sample.

Given that the chambers were 110 mm in internal diameter and no grease was applied along the walls due to the presence of the TDR and ER instrumentation, the load distribution throughout the sample was expected to be nonlinear with depth, as frictional forces between the consolidating sample and chamber wall increased with depth (transferring an increasing proportion of the load through the chamber wall). Hence, the upper layers of the sample were likely to experience a greater driver of consolidation; the flow pathway from these layers would be the shortest vertically upward through the sample or horizontally through the sample, and then up along the chamber/soil interface rather than downwards.

Settlement of the sample resulted in a transient difference in the pressure head as water seeped out of the two drains; hence, the hydraulic gradients acting on the samples were also transient in nature (increasing the upper head, in most cases, and reducing the sample thickness). The hydraulic gradients (Figure 6.8) increased in the

CH and CI mixes, which was expected. However, the CL mix behaved differently; whilst fluid initially accumulated on top of the CL samples, it drained through the soil to the bottom by the end of each consolidation step (to reform once the subsequent load was applied and then once again gradually drain with consolidation). Therefore, the reduction in sample length was matched by a reduction in head difference, combining to result in a lowering of the transient hydraulic gradient with each load step.

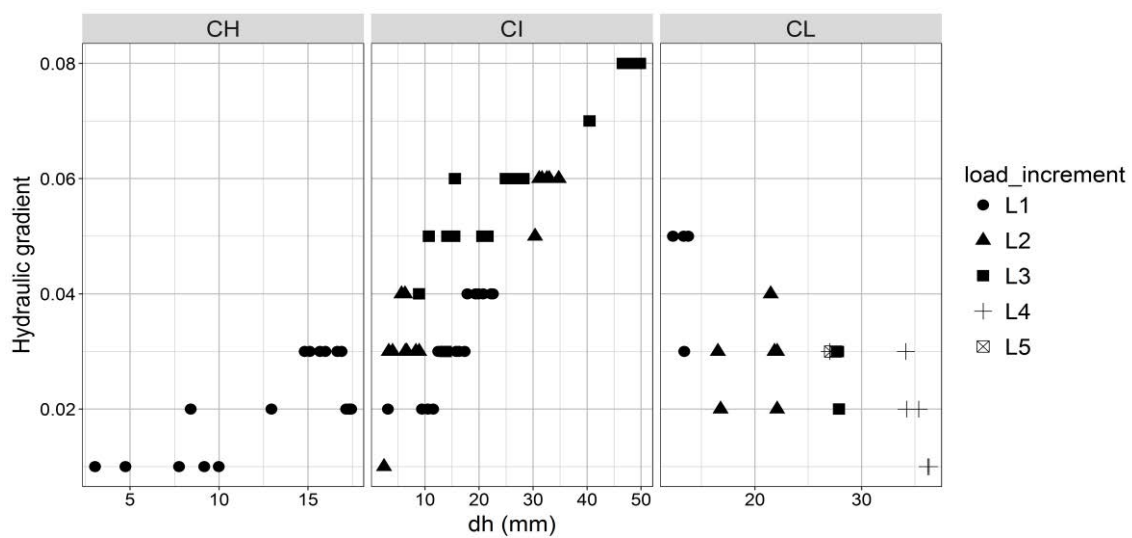


Figure 6.8. Hydraulic-gradient estimation in relation to change in the sample height (dh) in CH, CI and CL samples

However, in the CI samples, the volume of the fluid that gathered on the top of the sample is found to be consistently larger on the top compared to the bottom; an example of which is presented in Figure 6.9.

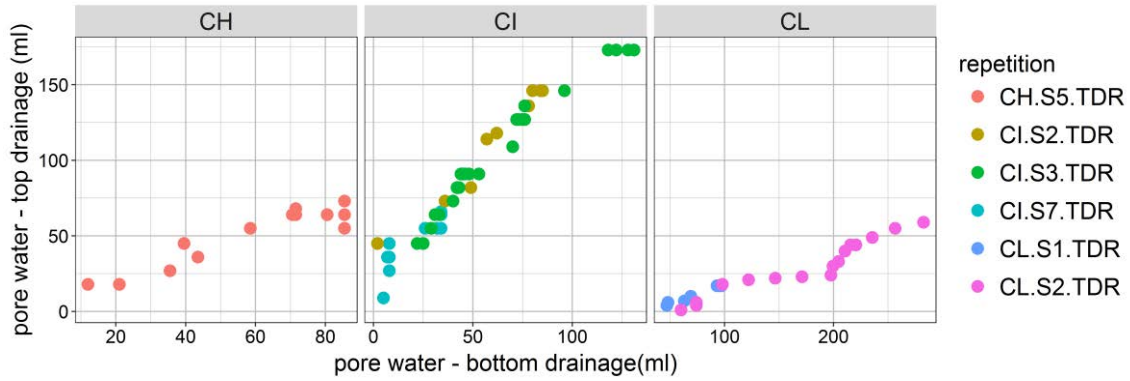


Figure 6.9. Relationship between the volume of water expelled through the top and bottom drainage in the CH, CI and CL samples

Whilst the application of the transitory hydraulic gradient was a consequence of not wanting to dilute the pore fluid emanating from the sample, it does appear to have a potential benefit in that the pore-water pressures generated by the hydrodynamic conditions could mobilise stress changes in the deeper layers of the sample (where the effects of the applied load have dissipated due to side-wall frictional effects). Thus, this would result in potential changes deeper within the soil layer than the consolidating load under hydrostatic loading conditions might achieve (as illustrated by Eq. 6.1).

$$\frac{\partial \sigma_v}{\partial h} = (\gamma_s - \gamma_w) \pm i\gamma_w \quad \text{Eq. 6.1}$$

It should be noted that, when initially loaded, the TDR_h data routinely presents an increase in the AP with the application of the load (Figure 6.10). This increase dissipates with time, resulting in a decrease in the AP with settlement, akin to that observed with the TDR_v . Initially, it was postulated that this 'spike' could be attributed to the increase in pore-water pressure with the application of the increased load. However, this is not a satisfactory explanation, as the 'spike' remains, whilst the

settlements are associated with the draining of pore fluid from the sample. Hence, the apparent increase in pore-water pressures remain at the location of the horizontal TDR probe, whilst the excess pore-water pressures have started to drain, and the soil is consolidating. Perhaps a more convincing explanation is that pore-water pressures increase with the application of the load (and this is detected by the TDR_h probe through the increase in AP). However, this is a function of the load applied, and the development of an increasing hydraulic gradient as the upper layers of soil consolidate (the upper head increases and the sample height reduces), which takes time to develop; hence, the 'spike' in AP becomes apparent after the consolidation has commenced. It is suggested that vertically downwards seepage is affecting the nature of the soil sample in the lower layers (as outlined in Eq. 6.1). It is clear from Figure 6.4 that the AP recorded in the horizontal TDR continues to reduce even after the soil has stopped settling (suggesting that the primary consolidation process in the upper layers has effectively completed).

The magnitude of the seepage mechanism's effect on the stress conditions within the soil samples has not been numerically quantified in the present study (due to the inherent uncertainties of the variation in density profile with depth); hence, the changes in geophysical properties cannot be precisely attributed to the consolidation and seepage mechanisms. Therefore, it is suggested that there is merit in investigating the relative effects on the sample in a future study of the hydraulic gradient changing the stress conditions, and, as a result, changing the geophysical properties of the soil (as would appear to be the case here).

6.2.3 RELATIONSHIP BETWEEN AP AND VOID RATIO

The expulsion of water during the consolidation and seepage processes led to a reduction in the volume of water surrounding the TDR rods, and therefore to a shorter travel time of the TDR signals and a reduction in AP. The void ratio reduces with consolidation, based on the visual observation of the development of gaps underneath the ER pins and the volume of the pore fluid on the top plate exceeding the volume collected from the bottom drainage; it changes most significantly within the upper soil layers surrounding the vertical TDR probe. Hence, there is a clear correlation between the change in void ratio and the change in AP. Furthermore, the correlations between the void ratio and AP with consolidation are not constant across the three soil types considered. There are clear differences in the responses, and this is attributed to the plasticity (the PIs of CI, CL and CH were 12, 25 and 30, respectively) and the initial water content of the samples (Figure 6.10).

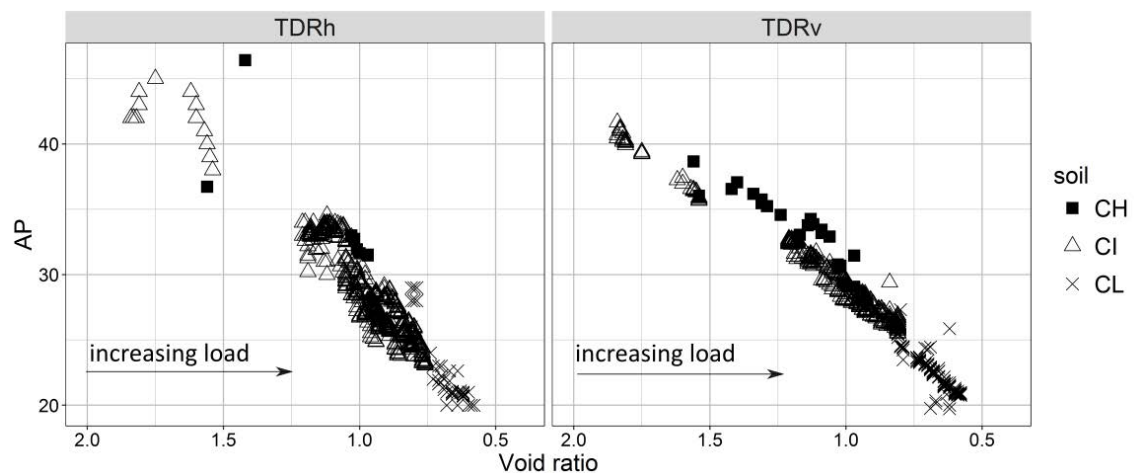


Figure 6.10. AP versus void ratio during the consolidation process, for all load steps; measurements were taken with probes positioned horizontally (TDR_h) and vertically (TDR_v)

It is found that the AP measured vertically (AP_v) exhibits a strong relationship with the void ratio, whilst the relationship between the AP measured horizontally (AP_h) and the void ratio generally followed a similar, but more scattered, trend. This relationship between the void ratio and AP is consistent with the relationships previously reported in the literature (for other materials). For example, Jones and Friedman (2000) confirm that material of uniform porosity (such as glass beads) exhibits nearly the same AP_v and AP_h measured with TDR (apart from minor discrepancies that can arise from the water distribution along the rods). Their measurements of AP_v , taken during the desaturation (by applying suction) of mica flakes, were lower than AP_h . It is noted, however, that the differences could be associated with the variations in VWC at different depths, given that the vertical probe was mounted in the bottom of the cylinder where suction was applied, and the horizontal probe sampled a volume corresponding to the top part of the vertical probe. Furthermore, particle alignment anisotropy, which is expected during vertical loading (Anandarajah, 2000), could be a factor contributing to the discrepancy between AP_v and AP_h ; however, in soils with a high water content this unlikely to affect the AP readings due to the predominant effect of the fluid AP on the bulk AP of the soil (Liu, 2007). Therefore, it is concluded that, in this research, the difference in the TDR_v and TDR_h responses was a result of the experiment's set-up used. The TDR_v was positioned at the location most affected by the application of the load, and therefore was subjected to more significant particle rearrangement compared to TDR_h , as shown in the load-transfer section (Section 3.3.2.2) and as described in the previous section of this chapter. The TDR_h was located normally to the load direction in the bottom part of the sample (at a sufficient depth,

so that the two probes did not interfere with each other), where the applied load was not considered to have a significant impact on the soil properties, and where seepage forces are believed to influence the soil response. Hence, the bulk change in the void ratio calculated for the whole sample did not reflect the void-ratio changes within the TDR_h . This was further confirmed by the final water-content distribution within the samples (Figure 6.5). In most samples, the GWC variation between the top and bottom TDR_v was up to 5%, whereas the TDR_h was within a more homogeneous layer that identifies a maximum water content variation of 2%.

The three soils investigated, with a range of plasticities, appear to follow the same overarching trend: a decreasing AP with a decreasing void ratio. Whilst the positive relationship between AP and void ratio is reported by other authors, based on measurements taken at the end of consolidation experiments (Liu, 2007), this research shows that the relationship can also develop in real time during an active consolidation process. Continuous monitoring during consolidation allowed further insights to be gained into the consolidation process, and the initial response of the soil to the application of a load to be captured. Further discussion is included in Section 6.4.2.

6.2.4 RELATIONSHIP BETWEEN BEC AND VOID RATIO

Considering that the contribution of the electrolytes to the BEC is restricted by the porosity of the medium (Klein and Santamarina, 1997) and the influence of the

conductive particles (Waxman and Smits, 1968), a gradual decrease in the BEC is expected with a decreasing void ratio. This trend is shown in

Figure 6.11; however, it can be seen that several samples do not follow the trend. Apart from the increase in the BEC_h , which is attributed to the initial pore-water-pressure-induced changes (as discussed in the previous section), it is observed that selected CL (CL.S2.TDR) and CH (CH.S5.TDR) samples do not display a change in the BEC_v with a decreasing void ratio. In the low-compressibility CL, this can be attributed to the low magnitude of the settlement; in more compressible CH a change would be expected, as illustrated by the CH.S01.TDR and CH.S02.TDR samples. It is noted that CH.S5.TDR was prepared at 1.5 LL, and hence its initial GWC was much higher than in the two other CH samples, which were prepared at 1.1 LL. Interestingly, at the same consolidation time, the BEC_h was found to be responsive to void-ratio changes.

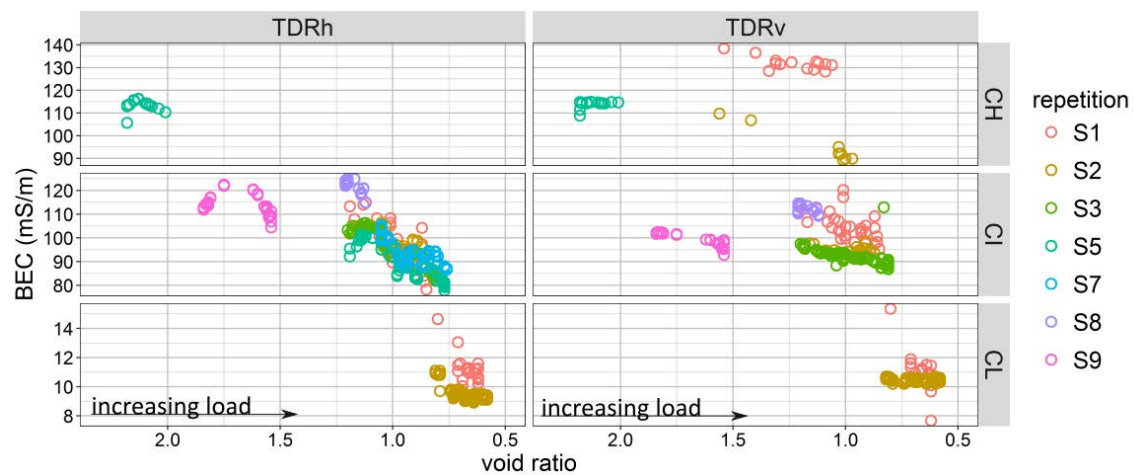


Figure 6.11. BEC versus void ratio for CH, CI and CL during vertical loading, with measurements taken using both TDR_v and TDR_h ; S1–S9 correspond to the sample numbers

The discrepancies in the BEC-void ratio relationship are attributed to differences in structural changes within the soil fabric, which includes cementation (presumably not a major issue in this study) and the packing arrangement (Kibria, 2014). However, if structural changes were the only factor responsible for the BEC response, then its relationship with void ratio would be expected to replicate the trend displayed by the AP.

A number of potentially complementary mechanisms are envisaged as taking place with the expulsion of water from the soil. As the load is applied and the soil consolidates (so water is removed from the soil), an increase in effective stress results in an increase in physical contact and chemical bonds between particles (Terzaghi et al., 1996). When conductive solid surfaces are present in the soil, such as in the presence of clay minerals, electro-chemical interactions between the solid and liquid phases occur in the form of sorbed ions at the charged sites, ion exchange and ion concentration within the pore fluid adjacent to the charged sites, including both cations and anions. A layer of ions forms next to the clay particles due to electrostatic attraction (of the charged sites on the clay particles, or the concentration of oppositely charged ions within a relatively small volume of pore fluid near the surface of the charged soil particles). In order for these ions to remain in solution, the dipolar water molecules must reorientate themselves so that the opposing charge (to that of the ion) within the dipolar moment is adjacent to the charged particle; this results in a change in the viscosity of the fluid, and creates a zone of fluid with a different hydraulic conductivity to that of the 'free' (or not chemically affected) water within the pore.

The formation of a concentrated zone of ions in one part of the void results in the natural diffusion of the ions away from the concentrated zone into parts of the pore space experiencing lower concentrations of ions; equally, the electro-chemical attraction draws these ions back into the concentrated zone. Over time, an equilibrium is reached between the electro-chemical attraction and diffusion and the DDL is established within the pore space (as described by various models such as the Gouy-Chapman surface, the Stern layer, etc. (Mitchell and Soga, 2005)). Under the application of a load, water is displaced from the pore (it is presumed that the water that is initially displaced is from the volume of 'free' water, i.e. the water not affected by the DDL, due to differences in the viscosity of the fluids), resulting in a contraction of the pore space. The reduction in pore volume results in the increasing influence of the DDLs (these surfaces will form adjacent to particle surfaces, and therefore in three dimensions there could be several within a saturated pore space). If the pore space is reduced sufficiently, then these DDLs may overlap, resulting in a pore fluid with comparatively little 'free' water within the pore.

The contribution of the DDL and pore fluid's conductivity was not investigated at the pore scale in this research; however, the contribution of the pore fluid's EC (EC_f) to the BEC of the soil sample was investigated. The TDR waveform, shown in Figure 6.1, was obtained from the measurement of the pore fluid extracted from the CI soil during the consolidation process. For the other soils, since the fluid samples were used for the ICP-OES analyses, it was not possible to extract a sufficient volume of fluid for TDR testing; however, the conductivity was checked using the ER box method (Table 6.2),

which only required 7 ml samples. The TDR and ER (11 Hz) produced comparable results, the BEC of the pore fluid (BEC_f) measured with TDR corresponds to a BEC of 0.288 S/m, and the EC_f measured with the ER method was 0.275 S/m, indicating that the two techniques are comparable.

Table 6.2. Conductivity of the soil mixtures measured with TDR in relation to the pore-fluid conductivity (measured with low frequency [11 Hz] resistivity method)

Soil	EC_f^*	BEC^{**}	BEC/EC_f
	S/m		%
CH	0.247	0.131	53
CI	0.275	0.099	36
CL	0.041	0.010	25
* pore fluid collected during consolidation process (bulk sample average)			
** soil BEC at the end of the consolidation test (average)			

The EC_f results (Table 6.2) indicate that the smectites had a dominant influence on the salt content of the pore fluid, due to the much higher availability of exchangeable ions when compared to kaolinite. This is confirmed by the ICP-OES chemical results, which show sodium was a dominant component in the pore fluid from sodium-activated soil (Table 6.3), and there are close EC_f values for CH and CI, which are values of 0.247 S/m and 0.275 S/m, respectively (Table 6.2). Due to its high mobility, Na is found to have a significant impact on EC_f (e.g. in (Rinaldi and Cuestas, 2002)). In contrast, CL, which contained sand and kaolinite, had an EC_f seven times smaller (approximately 0.041 S/m).

Table 6.3. Cation concentrations observed in pore fluid diluted in HNO₃ (measured using ICP-OES, with detection limits of 0.5 mg/l to 200 mg/l)

Soil Sample	Ca	Na	Mg	K	S	Si	P
	mg/l						
CH.S5.TDR	5.09	>209	3.52	17.88	213.20	1.18	0.42
CI.S2.TDR	7.38	>200	4.95	21.28	307.95	2.33	1.03
CI.S3.TDR	7.37	>200	6.31	12.73	299.09	0.85	1.51
CI.S5.TDR	4.97	>252	4.91	18.96	281.80	0.14	0.99
CI.S7.TDR	5.90	>200	24.18	24.57	317.31	5.87	0.37
CL.S2.TDR	2.95	31.64	<0.5	14.19	18.24	14.14	0.35

Rosenbaum, (1976) finds that the concentration of conductive ions in the pore fluid of soils containing montmorillonite is observed to decrease with the increasing effective stress during consolidation. In the present study, monitoring the AP, BEC and EC of the fluid during consolidation was considered; however, due to the volume required (in excess of what was readily achievable) to undertake the required tests, this approach was rejected. Instead, the pore fluid collected from a few load steps had to be combined. The EC_f and the chemical composition of the combined fluid were found to be very similar in several CI samples (Table 6.3); although this does not provide an answer to whether the concentration of pore fluid inside the sample was the same during consolidation, it appears to demonstrate that the change is most likely negligible given the similarity across the samples. Based on the visual observation, the fluid exiting the samples appeared to be a suspension of partially flocculated and partially dispersed bentonite and kaolinite particles. Its electromagnetic properties were expected to differ from the pore fluid within the soil pores, which were affected by the clay-charge distribution and restricted by the solid grains. Given that the BEC of

soil is dominated by BEC_f (Jung et al., 2012), its response can be perceived in terms of the degree to which the solid particles constrain the electromagnetic response of the 'free' fluid. Based on the pore-fluid analyses (Table 6.2), it is concluded that its BEC_f was governed by the presence of bentonite (5% in both soils), which is reflected in very close BEC_f results for CH and CI. However, the soil BEC appeared to also reflect the resistive (and current-flow-restricting) influence of the sand grains, since the BEC of CH (10% sand) was twice lower than EC_f and three times lower than CI (50% sand). In the CL (50% sand) soil, which contained no bentonite, the sand effect was even more predominant, resulting in the soil BEC being four times lower than its BEC_f .

The response of BEC and EC in soils containing bentonite remains an active area of research. Using low-frequency resistivity measurements, Fukue et al., (1999) find that the electrical conductivity of soils containing bentonite starts increasing at loading stages exceeding 78 kPa, which is hypothesised to result from the DDL deformation. Similarly, an increase in the BEC in a soil containing 60% montmorillonite was observed using TDR when the applied pressure exceeded 110 kPa (Liu, 2007). The latter is attributed to pore-fluid-salinity-dependent DDL suppression, which is hypothesised to increase BEC with a decrease in VWC in sand-bentonite soils with a BEC_f below 0.2 S/m; however, there is no experiment-derived proof supporting this theory. A suppression of DDL is expected with an increase in ion concentration in the pore fluid (Sridharan and Jayadeva, 1982), and, given that the long-range electrical repulsive forces (DDL) resist the compression at a given external applied pressure in smectite-containing soils (Sridharan and Rao, 1973), information about EC_f within the soil pores

could provide further insight into soil's response to loading and unloading. At the current stage of the research, the TDR readings provide only a bulk response, reflecting the closing of the pore spaces during loading and possible changes in the pore fluid. However, whilst it does not focus on pore-scale mechanics, this acknowledgement of limitations in sensitivity is not meant to belittle the findings of this research on the larger scale. It is apparent that changes in a soil sample, which will result in changes in geotechnical properties, can be detected using TDR and ER. This is clearly an important, and potentially far reaching, finding. In addition, the BEC is also found to be sensitive to unloading and this is discussed in Section 6.3.

A few hypotheses were considered to explain the BEC results, as follows:

- i. the change in void around the probe was small, and could not be detected by the TDR (i.e. the soil arched around the probes, and the soft soil within the arch did not experience the effects of the consolidation process to the same extent as the soil outside of the zone of influence of the arch);
- ii. an equipment malfunction;
- iii. contact between the probe and soil;
- iv. the change in the BEC was too small to be detected; or
- v. the soil polarisation affected the BEC measurements using TDR.

The first two assumptions were disregarded, because the AP readings were taken at the same time and followed the change in settlement, and the soil samples were very

soft; thus, arching might not be a significant mechanism (which is, of course, related to the density and stiffness of the soil).

A comparison between the BEC and the volume of fluid expelled from the sample (Figure 6.12) demonstrates that in some samples the BEC_h directly relates to the pore-volume expulsion, whilst, at the same time, the BEC_v was not responding (point iii). It is assumed that this could be a result of a poorer contact between the soil and TDR_v in comparison with TDR_h (where the increased pressure most likely pressed the soil against the probe).

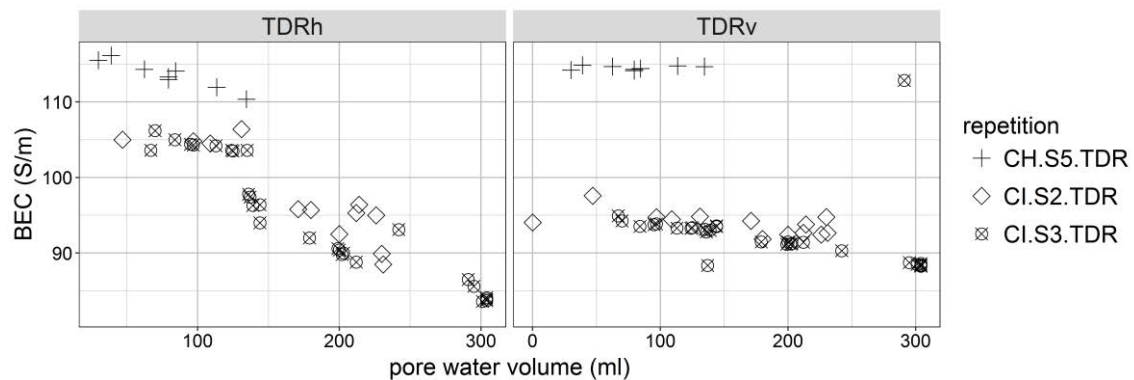


Figure 6.12. BEC relationship with the volume of pore fluid draining out of the sample

The investigation of soil using the low-frequency ER method during loading identifies that low-frequency EC was registering changes in the void ratio, which reflect the observed decreased rate of settlement in the CH.S02.ER sample; however, the TDR-derived BEC, which was measured in parallel in the CH.S02.TDR sample, plateaued after the initial changes (Figure 6.13, point iv). In other cases, however, the ER was also

found not responsive to void ratio changes (Section 6.2.5), which could suggest that pore connectivity, rather than void ratio, affects the responses of BEC and EC (Kibria, 2014).

Olhoeft, (1985) suggests that low-frequency (below 1 kHz) sensing techniques respond to chemical reactions, such as oxidation-reduction and ion exchange, whilst frequencies above 1 kHz are sensitive to physical changes, such as the interfacial Maxwell-Wagner effect (point v). It is noted that the BEC derived from the TDR measurements is computed from the attenuation of the TDR pulse (Yanuka et al., 1988), and in the present research was computed from (comparatively) long-term measurements (Giese and Tiemann, 1975), resulting in a value related to the DC conductivity (EC_{dc}) measured in the kHz frequency range (Bechtold et al., 2010). Hence, the effect of the Maxwell-Wagner polarisation cannot be dismissed.

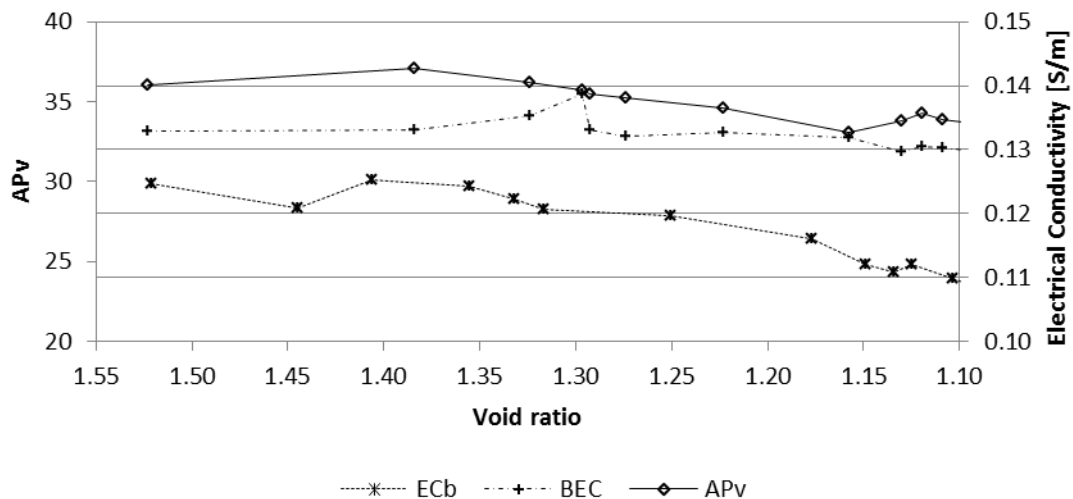


Figure 6.13. BEC_{TDR} (CH.S02.TDR) and EC_b (CH.S02.ER) in relation to void ratio and AP_v

The BEC is a complex value that includes EC' , which corresponds to conduction, and EC'' , which contributes to the storage of energy as a result of the inertial variations (Cassidy, 2009) at a given frequency (ω), as in Eq. 6.2:

$$BEC = EC' + EC''\omega \quad \text{Eq. 6.2}$$

EC' is generally assumed to be equal to the DC conductivity (EC_{dc}) and EC'' is assumed to be zero (Bradford, 2007). However, in saturated fine-grained soils containing clay minerals – where free electrolyte charges coexist with bound charges, and, as a result, respond to the applied current with different speeds – the effect of the EC'' will be higher (Heimovaara, 1994). This is not quantifiable with the common TDR instruments, which do not provide information about the frequency. In order to investigate further the response of the ohmic conductivity, the low-frequency ER results are discussed in the following section.

6.2.5 RELATIONSHIP BETWEEN ρ_v AND VOID RATIO

A low-frequency (0.1 Hz–500 Hz) ρ investigation was carried out in parallel to the TDR testing. As only the bulk void ratio (based on the sample-height changes) was measured, it was correlated with the ρ readings, reflecting bulk sample changes; i.e. vertical ρ (ρ_v) was measured in the direction of loading with the use of potential electrodes separated by 100 mm (PS1) to 129 mm (PS2).

The ρ_v measurements reflect the outcome of two testing approaches, described in Chapter 5: PS1-ER-Acq-1 (samples CH.S01.ER and CH.S01.ER) and PS2-ER-Acq-2

(samples Cl.S4.ER and Cl.S6.ER). In both arrangements, the measurements were carried out with a Wenner array via the injection of a current between two metal plates located at the top and bottom of the sample, and the potential was measured on pin electrodes inserted into the sample to depths of approximately 10 mm (PS1) and 5 mm (PS2). In the CH samples (PS1), eight potential electrodes were present in the sample; four were located at a depth of 50 mm and the other four were located at 150 mm (measured from the bottom of chamber), creating four vertical configurations. The distance between the electrodes in the vertical plane was 100 mm, and the circumferential separation was 86.4 mm (Figure 5.4).

In the CI samples (PS2), 32 pin electrodes were present in the sample, with eight electrodes at each of four depths. The bottom row of electrodes was located 49 mm from the base of the sample, the subsequent rows were separated by 43 mm in the vertical plane and there was a 43-mm circumferential separation between electrodes (Figure 5.11).

The results of the ρ_v changes in CI and CH during consolidation were plotted in relation to the void ratio (Figure 6.14), where each point represents an average result of three repetitions with a measurement error of 0.03% (Section 5.3.4) from the absolute values. The relative values ($e_{(r)}$ and $\rho_{v(r)}$ for the void ratio and vertical electrical resistivity, respectively) were produced by normalising the measured values with respect to the initial results (e_0 and ρ_{v0} for the initial void ratio and vertical electrical resistivity, respectively). These were selected for ease of comparison, based on a

similar approach adopted in research on low- ρ fine-grained soils (Ghorbani et al., 2012). By definition, the point at which both the relative $\rho_{v(r)}$ and $e_{(r)}$ equal 1 corresponds to the initial conditions; it can be seen that in the CH samples $\rho_{v(r)}$ increases with a decrease of $e_{(r)}$. However, the CI samples appear to exhibit an initial decrease in $\rho_{v(r)}$, but by reducing $e_{(r)}$ it gradually approaches the trend exhibited by CH (an increasing $\rho_{v(r)}$ with a reducing e_r). The graph shows an example of one vertical configuration in each sample; however, in CH.S01.ER and CH.S02.ER the measurements were carried out in four vertical and one diagonal arrangement (Figure 6.16), whilst in CI.S4.ER and CI.S6.1.ER seven vertical arrangements were incorporated (Figure 6.17). These are discussed further in order to identify the potential variability within the sample.

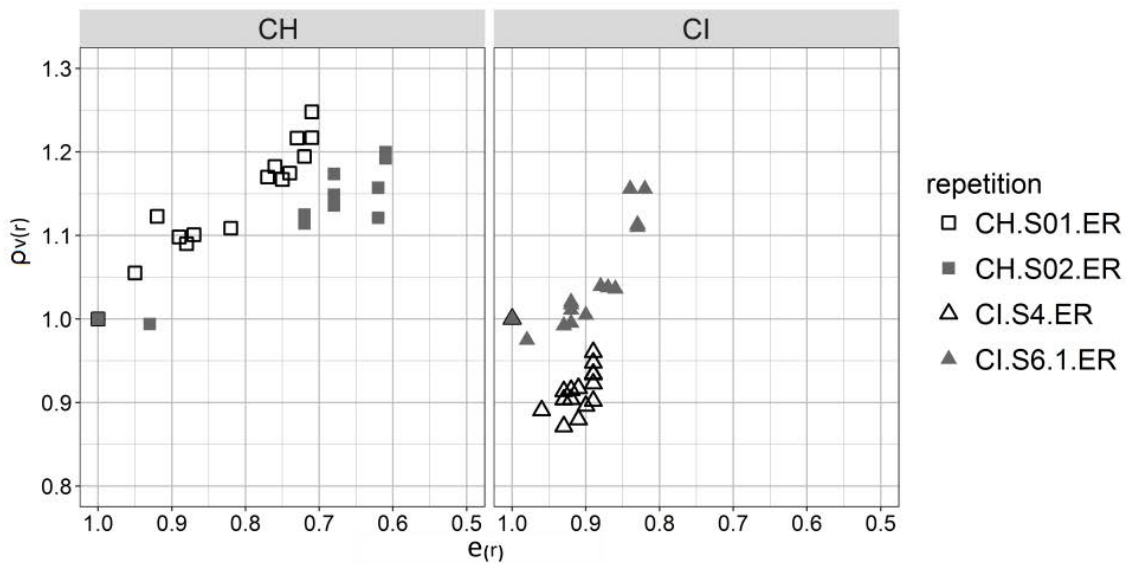


Figure 6.14. Relationship between relative void ratio ($e_{(r)} = e/e_0$) and relative vertical electrical resistivity ($\rho_{v(r)} = \rho_v/\rho_{v0}$) in CH and CI at 10 Hz

6.2.5.1 CH SAMPLES – PS1 ARRANGEMENT

The CH.S01.ER samples (Figure 6.15) reveal that $\rho_{v(r)}$ was increasing with the decrease of relative void ratio; however, at the point of transition from a 0.9 to a 0.8 relative void ratio, a localised decrease in $\rho_{v(r)}$ was noticed, in particular in vertical_4. In order to analyse the significance of this variation, the absolute ρ_v values (i.e. not normalised to the initial value) are presented in relation to settlement (Figure 6.16):

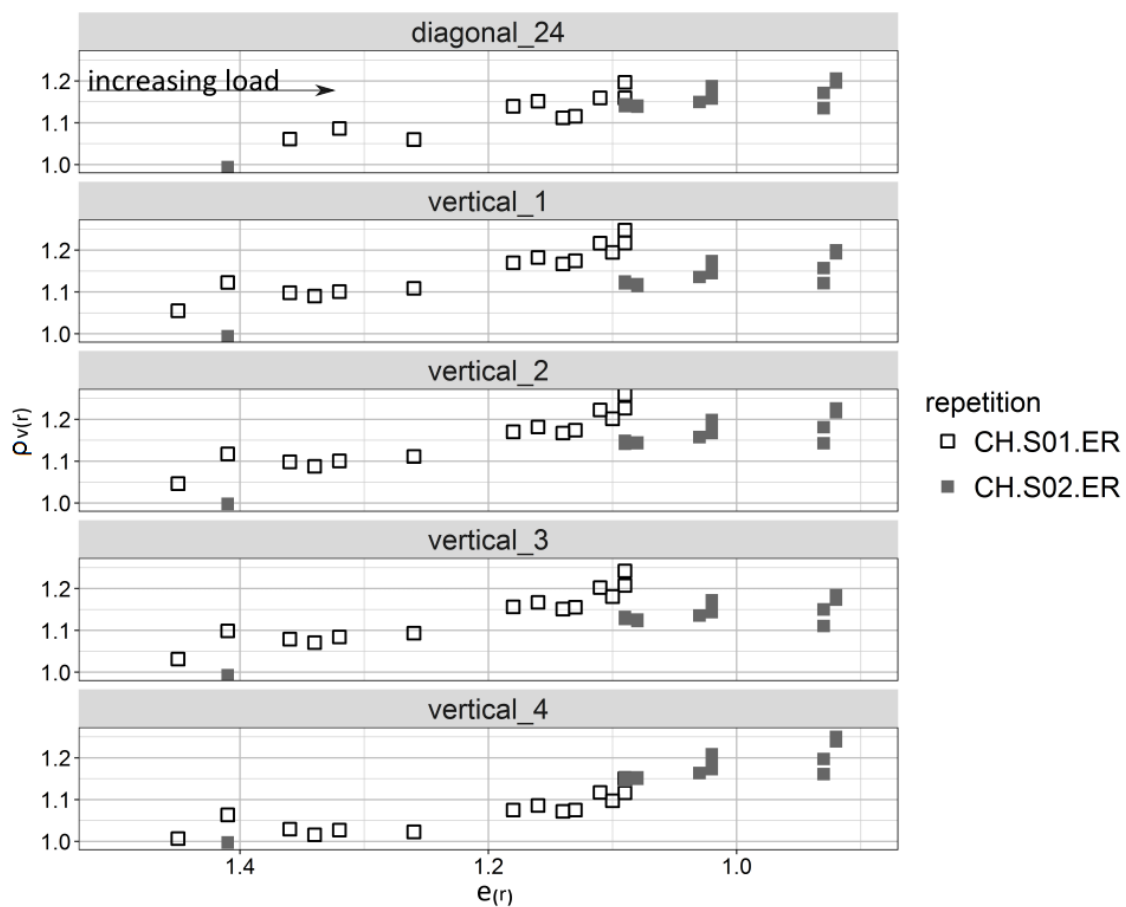


Figure 6.15. Relative (normalised by the initial values) $\rho_{v(r)}$ measured with vertical (1, 2, 3 and 4) and diagonal (24) configurations in relation to the relative void ratio ($e(r)$) in two CH samples (CH.S01.ER and CH.S02.ER)

Based on the results presented in Figure 6.16, it can be seen that the slight decrease in ρ_v may be related to the accuracy of the measurement, which is within 3% when compared to the results from a conductivity meter. Nonetheless, the overall trend of an increasing ρ_v as the consolidation progresses, is observed.

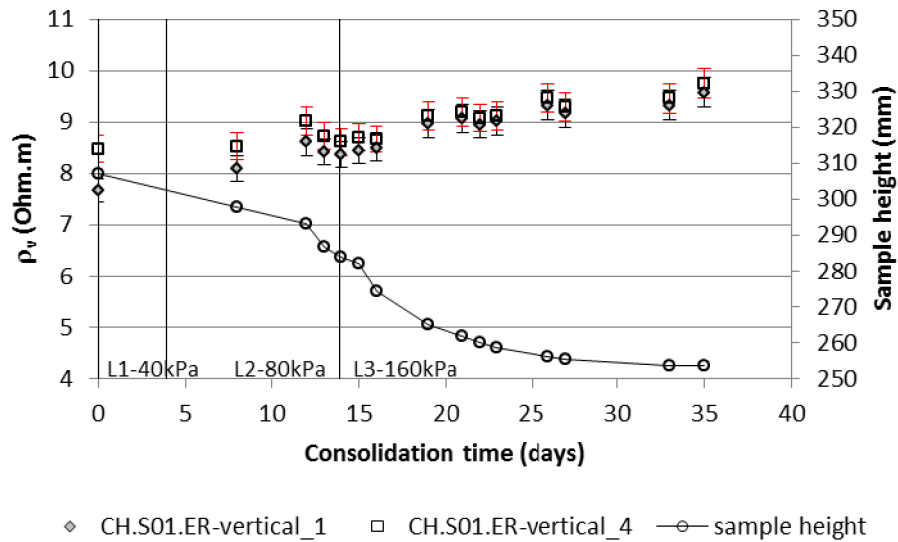


Figure 6.16. Absolute ρ_v (10 Hz) changes in the CH.S01.ER sample (measured with two vertical configurations) during loading in relation to the settlement. The error bars indicate a 3% measurement accuracy.

In the CH.S02.ER sample (Figure 6.17), it can be observed that, after an initial increase in ρ_v (after the application of the first loading step), the ρ_v did not appear to increase significantly (when considering the error associated with measurement) and only started to increase as the void ratio reduced in the third loading stage. In addition, the magnitude of its change was within 2 Ohm.m for a 60 mm settlement (akin to that observed for the first CH sample [Figure 6.16]). The consolidation testing carried out by Kibria (2014) in natural CH soils reveals that the initial loading resulted in various ρ responses, including an increase, a decrease and a lack of noticeable change; however,

as the consolidation progressed, an increase in ρ was noted within approximately 20% of the initial values, corresponding to the CH.S01.ER and CH.S02.ER results.

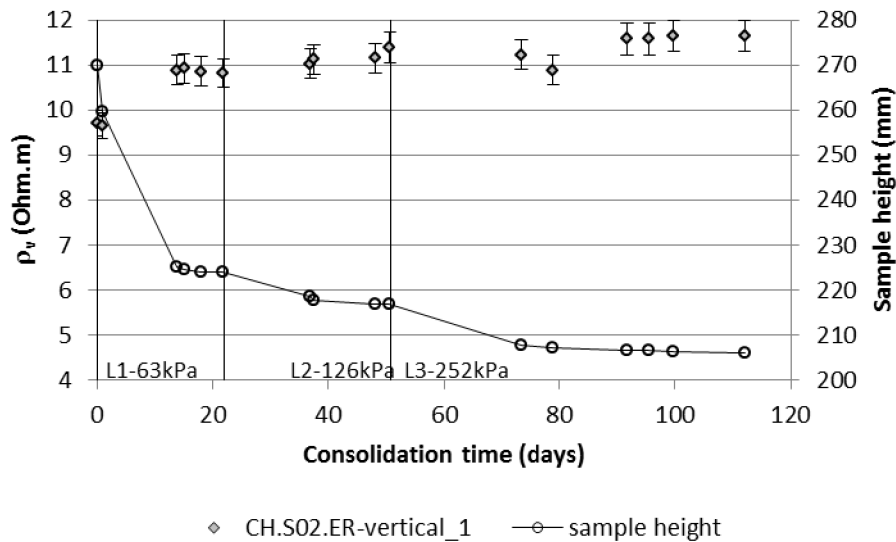


Figure 6.17. ρ_v (10 Hz) changes in the CH.S02.ER sample (measured with two vertical configurations) during loading in relation to the settlement. The error bars indicate a 3% measurement accuracy.

Based on the CH results, it is concluded that, although change in the soil structure takes place (with the compression of the sample), EC_f and its interaction with the clay particles dominates the response of ρ_v . The comparison between the vertical and diagonal measurements in CH revealed a very similar response, indicating that, in the arrangement adopted in the present study, diagonal and vertical configurations could be used interchangeably.

6.2.5.2 CI SAMPLES – PS2 ARRANGEMENT

Due to the change in the experiment's arrangement (the increased number of electrodes and using a modified acquisition system [Section 5.3.2]), the CI results cannot be directly compared with those for CH. However, the $\rho_{v(r)}$ values presented in

Figure 6.14 were selected to demonstrate the outcome of the testing at a similar depth with the same type of Wenner configuration (the potential electrodes were located at depths of 49 mm and 178 mm from the bottom of the chamber in CI, and 50 mm and 150 mm from the bottom of the chamber base in CH).

In order to investigate the response of ρ_v in CI, its relative values (normalised by the initial readings) were plotted in relation to the relative void ratio (Figure 6.18). The corresponding effective stress applied to the sample was determined. The results were divided into the configurations reflecting the soil sample layers.

It can be seen in Figure 6.18 that the initial loading stages of under 5 kPa and 25 kPa resulted in a decrease in $\rho_{v(r)}$, whilst the relative void ratio decreased. As the consolidation progressed under 25 kPa external loading, a gradual increase in $\rho_{v(r)}$ was observed; however, it started falling during the later stages of consolidation under 50 kPa in all layers of CI.S6.1.ER, apart from the DA layer. Based on the visual observation of voids developing underneath the electrodes, the decrease in $\rho_{v(r)}$ is assumed to be a result of the pore fluid infilling these voids, hence gathering around the electrodes and increasing the electrical conductivity locally. This effect was most pronounced in layers AB, BC and CD, with the closest separation being 43 mm, and, as a result, it had the biggest influence on the void volume in respect to the measurement area. The length of the void in the vertical direction increased as the loading progressed (the void size in the horizontal direction could not be measured) and proximity to the top loading plate increased (the longest void was observed underneath the top layer of pin electrodes).

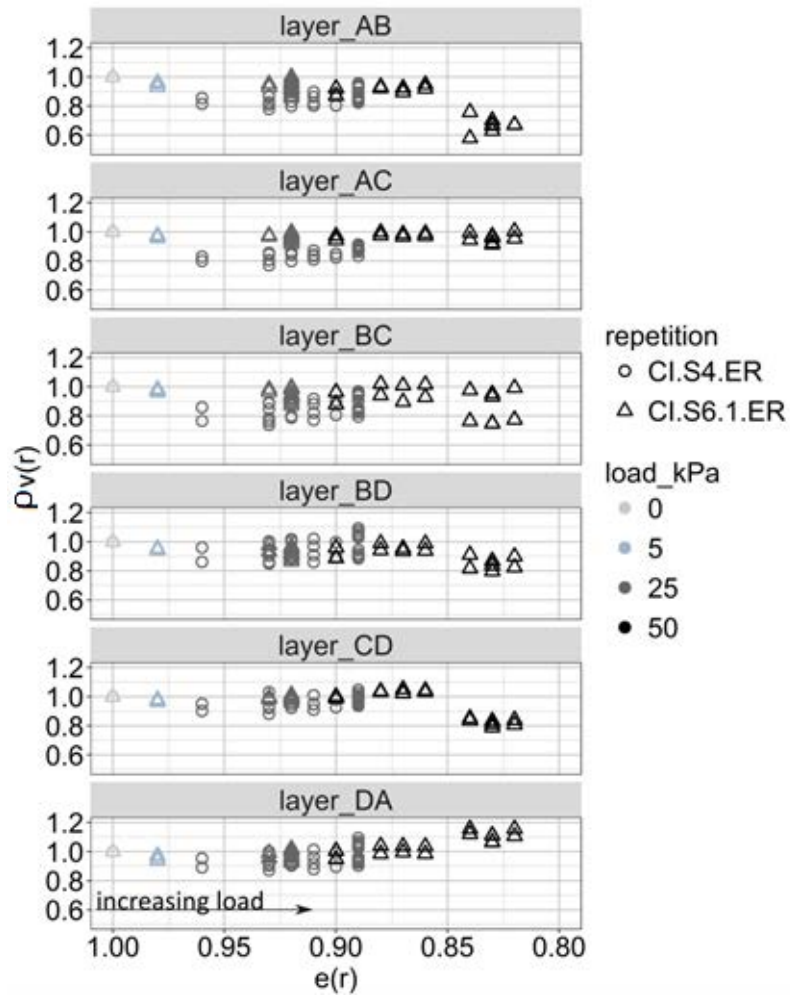


Figure 6.18. Relative (normalised by the initial values) $\rho_{v(r)}$ (11 Hz) measured at different sample heights in two CI samples (CI.S4.ER and CI.S6.1.ER); plotted with respect to the relative void ratio ($e(r)$)

The DA measurements were obtained from pin electrodes separated by 129 mm, and the development of the gap below the pins had a smaller effect in comparison with the measurement volume. The absolute values of ρ_v and its relation to the progress of the settlement are presented in Figure 6.19 and Figure 6.20.

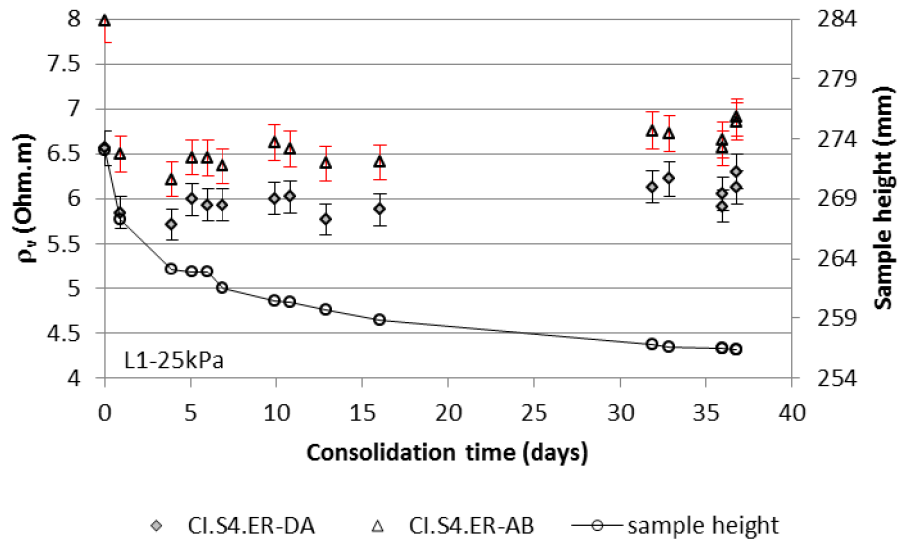


Figure 6.19. Absolute ρ_v (11 Hz) changes during the consolidation of CI.S4.ER

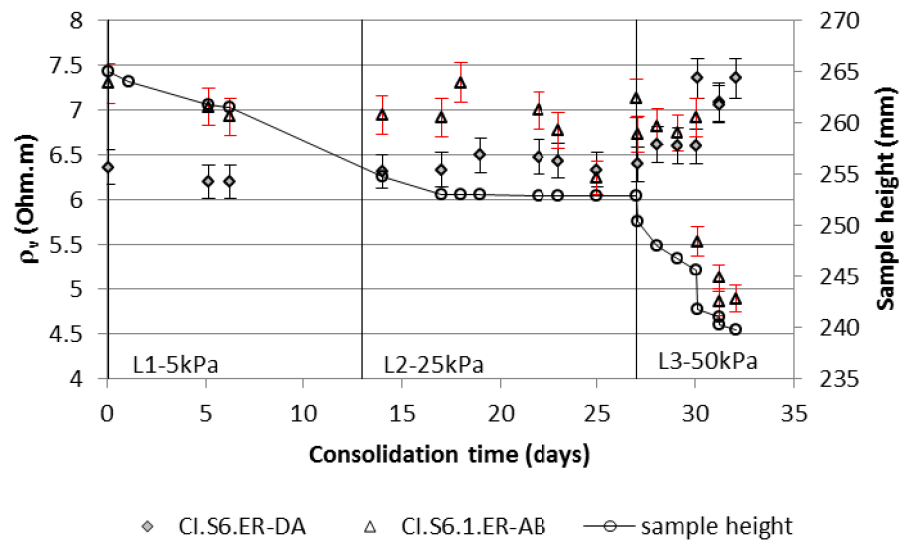


Figure 6.20. Absolute ρ_v (11 Hz) changes during the consolidation of CI.S6.ER

Based on the CI.S6.1.ER results, it was concluded that the electrode-insertion depth should be decreased, and further measurements should focus on the DA layer. Furthermore, it was observed that measurements taken with 0.1 Hz frequency were affected by polarisation, and the 51 Hz and 201 Hz measurements were very close to the 101 Hz readings. In order to reduce the time for testing, the frequencies were

limited to 1 Hz, 11 Hz, 101 Hz and 501 Hz. The measurement sequence was modified to prioritise the switches in the DA layer, and therefore further measurements in the CI.S6.ER sample are referred to as CI.S6.2.

This modified approach revealed that the decrease in the probe-insertion depth was reflected in increased ρ_v values, as shown in Figure 6.21. A further increase in effective pressure to 100 kPa resulted in an initial decrease in ρ_v values during the primary consolidation stage, followed by a gradual increase and subsequent drop.

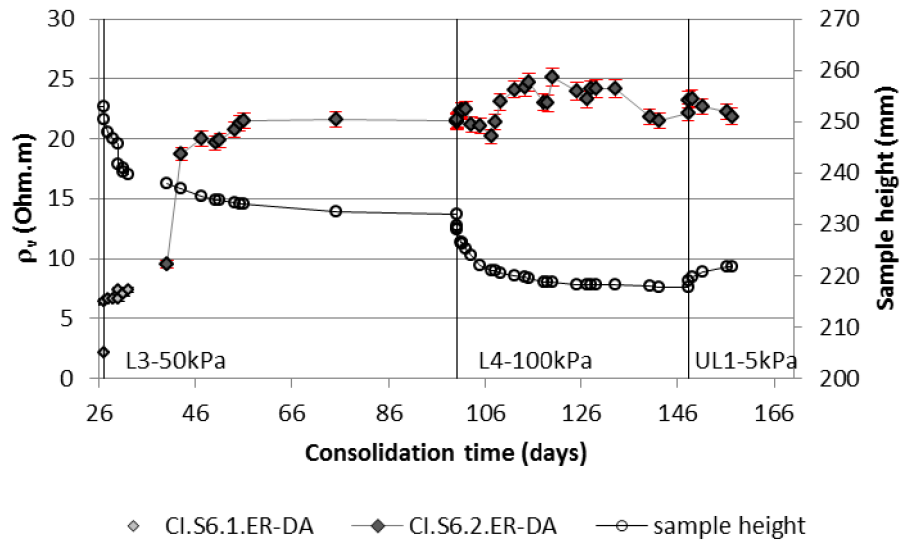


Figure 6.21. ρ_v (11 Hz) changes during the consolidation of CI.S6.ER

When the changes in ρ_v during the consolidation of CI.S6.ER under 100 kPa were analysed in view of the consolidation process (Figure 6.20), it was observed that, during primary consolidation, ρ_v increases in the initial phase, but when a major part of the settlement takes place it drops, and it picks up again when it is approaching the secondary consolidation stage. The decrease in ρ_v corresponds to the stage when the pore-water fluid is seeping from the sample to dissipate the build-up of the excess

pore-water pressure. It is possible, therefore, that the EC of the sample increases due to the increased mobility of the ions within the pore spaces. Once the rate of settlement slows (with the excess pore-water pressure dissipating, and the particles moving closer together), the frictional contacts and the effective stresses both increase, so the soil approaches a new equilibrium (i.e. the soil approaches the drained condition). This illustrates that the excess pore-water pressure has nearly dissipated, and also shows that the ρ_v starts increasing and stabilises during the secondary consolidation stage. This suggests that the ρ_v response is governed by the pore-fluid movement in the initial phases of consolidation, whilst structural changes resulting from the particle rearrangement are reflected in the increase in ρ_v response following the dissipation of the pore-water pressure. The TDR_h provided a very similar response, which is discussed further in Section 6.2.6.

6.2.6 TDR RESPONSE TO PORE-WATER-PRESSURE-INDUCED CHANGES

The AP_h was noted to increase immediately after the load application. When the changes in the AP_h and BEC_h are plotted as relative terms ($AP_{h(r)}$ and $BEC_{h(r)}$, respectively) against consolidation time – with the absolute values normalised to the initial values, in the same manner used for relative void ratio and ρ (as in Figure 6.22) – it is interesting to note that both the $AP_{h(r)}$ and $BEC_{h(r)}$ increase with the application of each additional loading step, and remain high even after the commencement of the consolidation process (where the excess pore-water pressures have started to dissipate and the soil settles). This response is particularly pronounced in CH and CI,

but cannot be seen in CL. There is a time lag between the settlement of the soil samples commencing and the decrease in the AP_h and BEC_h (as reported previously in Section 6.2.2.2). This time lag appears proportional to the plasticity of the sample, and as a result is also proportional to the compressibility of the soil (the soil-specific compression indices (C_c) of CH, CI and CL were in the order of 0.38, 0.32 and 0.13, respectively). This effect was initially thought to be a result of the pore-water-pressure changes in the sample due to the consolidation pressure; therefore, the pressure effect on the TDR was investigated (as considered in Section 4.2 and discussed further in Section 6.2.2.2). However, as the pore-water pressure from the application of the external load did not have a direct effect on the TDR_h , it is most likely influenced by changes resulting from the two mechanical principles controlling the soil's response: the consolidation mechanism (principally affecting the upper layers of the soil due to the nonlinear load distribution within the soil sample) resulting in the seepage of water from the soil to the two drains; and the subsequent development of transient hydraulic gradients acting across the samples, which resulted in the densification of the deeper layers of soil due to the vertical downward seepage of soil.

It is believed that the horizontal insertion of the TDR rods into the soil will result in a 'load-shadow' being developed directly under the rods, and this will create a softer zone of soil around (and especially below) them (akin to the behaviour of soil observed with the ER pins). This results in a preferential pathway for water to seep out of the sample (from the centre of the sample, along the softer zone around the TDR rods and then down the cell-soil interface).

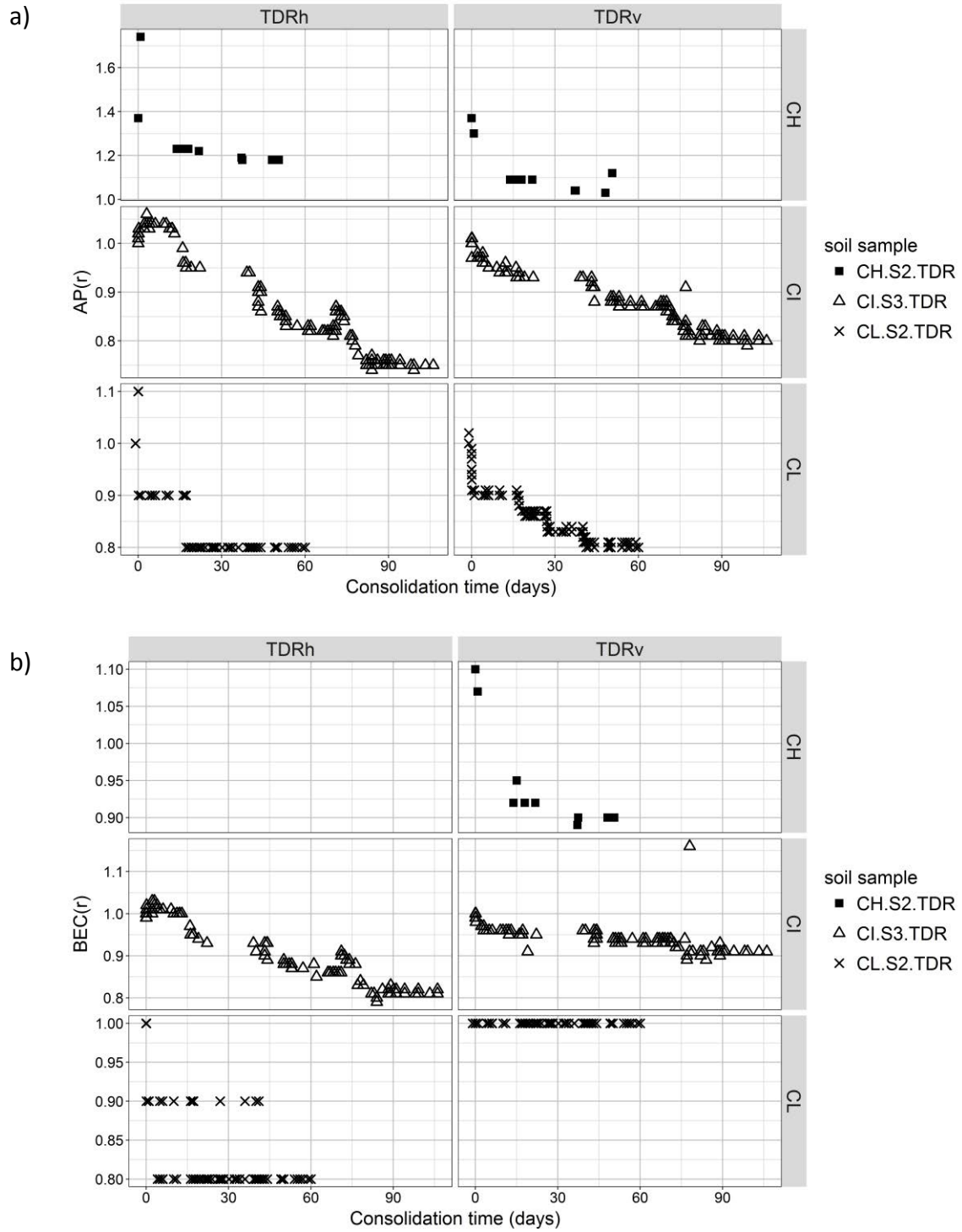


Figure 6.22. Responses for a) $AP(r)$ and b) $BEC(r)$, relative to the initial readings taken during the consolidation process in each of the clayey soils. The results are shown for three loading stages (L1, L2 and L3) for each soil, and there is an unload stage for CI.

Given that the TDR measurements are related to water content, it is believed that the initial increase is an increase in the TDR_h readings seen in CH and CI, and this reflects the changes induced by pore-water pressure with loading (consolidation and seepage mechanisms). This effect was not observed in CL as the pore pressure dissipated very quickly, due to the higher hydraulic conductivity and the reduction in the upper head from the flow through the sample. Initially, this hypothesis was investigated by placing a localised volume of dye (sodium fluorescein) within the centre of the sample at the same height as the horizontal TDR probes, as it was hoped that the fluorescent dye would be detectable when the sample was examined at the end of the test. Despite the samples being white(ish) in colour, and sodium fluorescein being both bright yellow-green in colour (when diluted) and fluorescent under ultraviolet (UV) light, the dye was undetectable at the end of the test.

An alternative attempt to investigate this hypothesis involved instrumenting one of the consolidation cells with external pore-water-pressure sensors; these were positioned at three depths (as reported in Section 4.2), i.e. at the height of TDR_v (PS-t), in the middle of the sample (PS-m) and at the same height as TDR_h (PS5-b).

Figure 6.23 illustrates that AP_h was consistently greater than AP_v , suggesting a region of higher water content near the horizontal probe. In addition, the AP_h trend would appear to approximate that of the lowest pore-water probe positioned at the same level as TDR_h (i.e. PS-b). This would indeed suggest that, whilst the inclusion of the TDR_h may have resulted in the formation of arching and the associated ‘pipe’ around

the probe, this would appear to be reflecting the changes within the soil (the magnitude in AP_h may exceed that of AP_v , but the trends are broadly similar), which was encouraging.

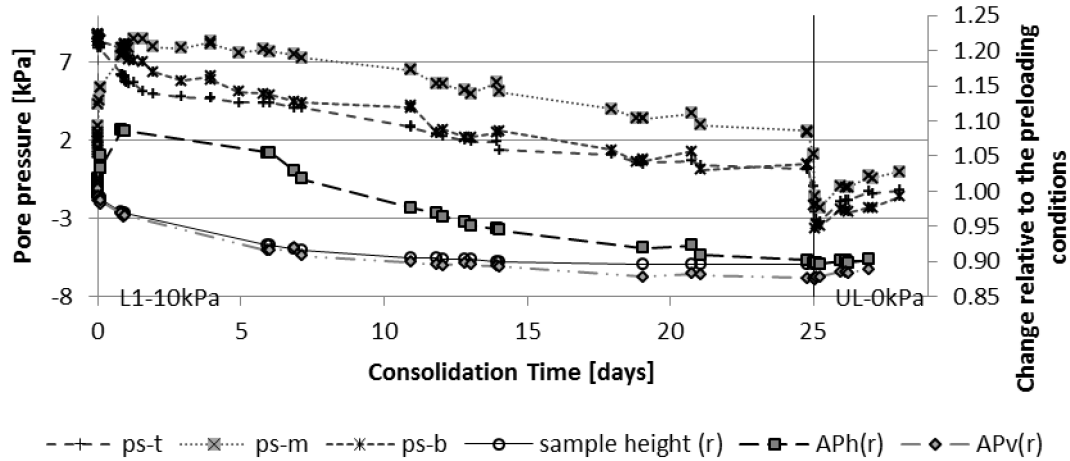


Figure 6.23. AP_h and AP_v changes (normalised by the pre-loading measurement) in relation to the settlement and the pore-water-pressure dissipation recorded at the top (PS-t), in the middle (PS-m) and at the height of the TDR_h (PS-b)

The TDR_h results are found to be comparable with the ρ_v response (Figure 6.21), and, although the ρ_v measurements correspond to the current flow in the vertical plane, the ER electrodes were positioned in the same way as TDR_h (normal to the direction of loading). This suggests that considering the load direction during the instrumentation of a sample/site is of significant importance, as the probes normal to the loading direction (here, TDR_h) appear to be responsive to the pore-water-pressure-induced changes, whilst probes positioned parallel to the loading direction (TDR_v) respond to structural changes.

6.3 ELECTROMAGNETIC RESPONSE OF THE SAMPLES TO UNLOADING

During unloading, the physical and chemical bonds between the particles, which developed during the loading process, break (Terzaghi et al., 1996). The undrained conditions are established and the excess pore-water pressures (which will be reduced when the soil reaches drained conditions, and in certain circumstances could even become negative) result in the soil samples experiencing suction. Hence, the samples heave (but to a lower magnitude than the settlement from the application of load) as water is drawn back into the soil.

In kaolinite soils, the rebound (heave) is controlled only by a hydrostatic-pressure deficiency developed in the undrained phase; whereas, in smectite dominated soils, DDL repulsive forces are also found to control its magnitude (Sridharan and Rao, 1973). In the soils considered herein (where the bentonite content was limited to 5% by the weight of the sample), it is suspected that both mechanisms will be prevalent (in CI and CH samples). The testing of the electrical response to unloading was limited to six samples and a maximum of two unloading steps; nonetheless, it is interesting to note that, when unloaded, both the AP_v (Figure 6.24) and BEC_v (Figure 6.25) rebounded as water was drawn back into the soil fabric. Once again, the trend observed geophysically appears to be similar to that observed geotechnically, i.e. the profile of the settlement curve for the corresponding consolidation profile.

This rebound was observed mostly in the samples where a significant part of the load was removed straight after loading (rather than unloading in steps). Unloading in small graduations (where between 50% and 80% of the load was removed [Figure 6.25]) did not result in observable changes in the AP and BEC when using the experimental apparatus, until the difference between the maximum load applied and load removed became sufficient. Given that the rebound was limited by the swelling properties of the CH, CI and CL soils, as indicated by the respective C_s values of 0.08, 0.05 and 0.03, the volumes of water being drawn into the samples are relatively small. Nonetheless, it was encouraging to observe that even these small changes were reflected in the AP_v and BEC_v readings. It is clear that there is a sensitivity threshold, which is either a function of the experimental apparatus used herein, a function of the change in void space within the soil (and the concentration of ions being drawn back into the soil), or both. It is noted that, although this rebound was observed in a laboratory setting, in field conditions the magnitude of change may lie within the sensitivity limitations of the equipment, which requires further research.

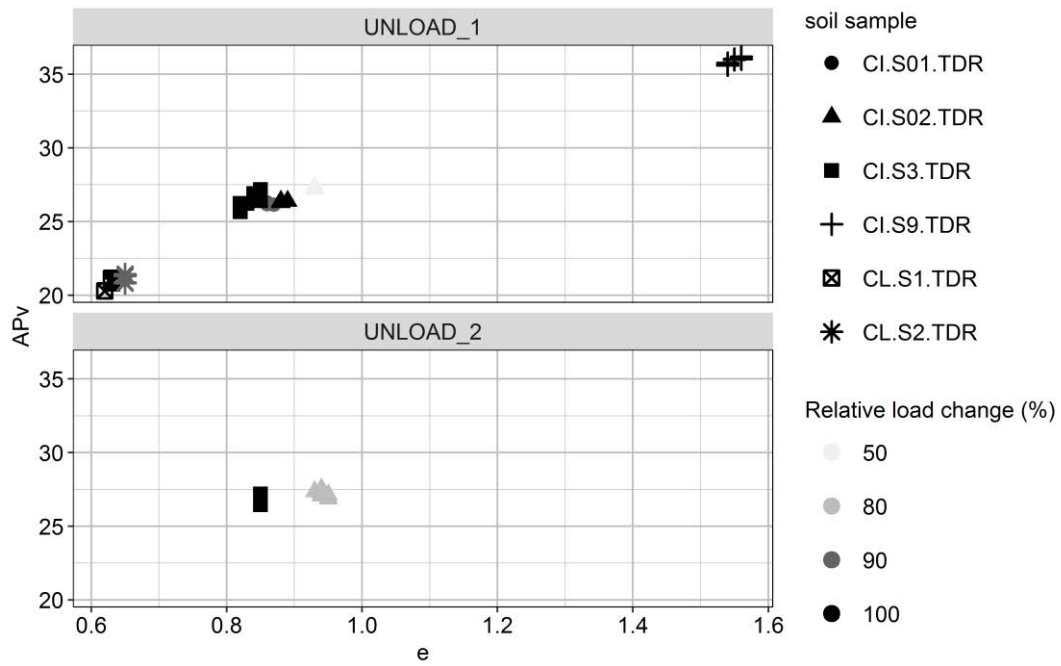


Figure 6.24. AP_v - e relationship during the unloading of the CI and CL samples in two steps (Unload_1 and Unload_2)

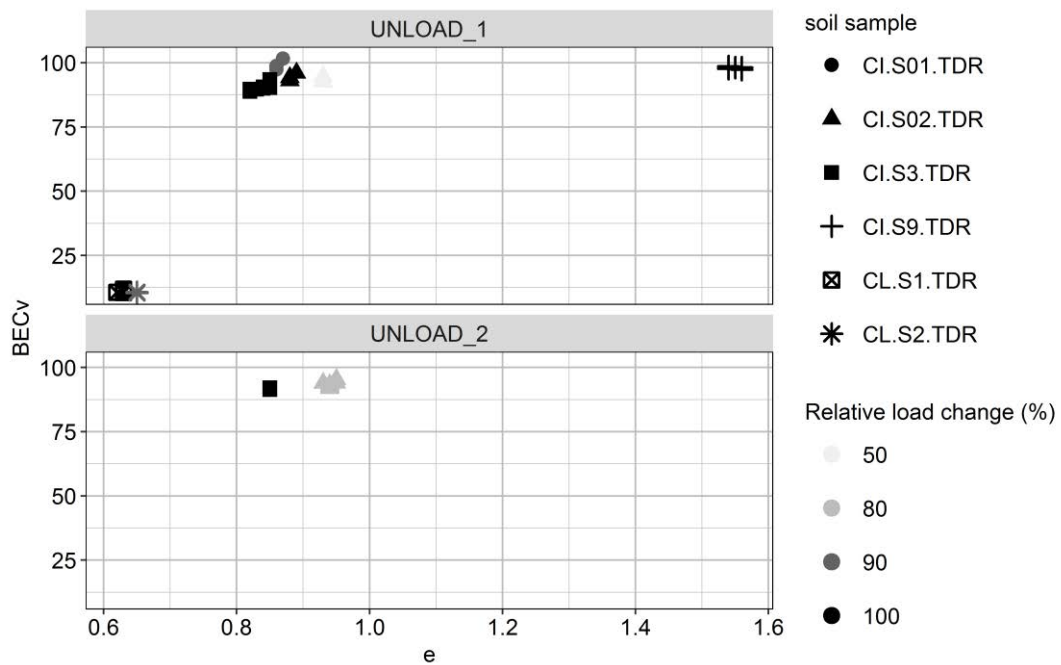


Figure 6.25. BEC_v - e relationship during the unloading of the CI and CL samples in two steps (Unload_1 and Unload_2)

The fact that there appears to be a correlation between the geophysical properties (i.e. AP, BEC and EC) and the geotechnical properties (i.e. e , GWC, and, by extension, C_c , C_s , c_v , m_v and ρ_d), and employing the existing geotechnical correlations – potentially, the effective stresses and shear-strength parameters – in both loading (compression) and, to a lesser extent (as noted previously), unloading (swelling) is extremely encouraging. Installing relatively simple probes into newly installed earth structures, or retrofitted in existing ones, could provide asset owners/operators with real-time information on how the asset is performing. Relative change (rather than absolute) could be used to inform of the relative ‘health’ of the asset, with trigger levels designated when corrective action may be required, based on the correlations between the geotechnical and geophysical parameters; this is discussed further in the following sections.

6.4 CORRELATIONS BETWEEN THE GEOTECHNICAL AND GEOPHYSICAL PARAMETERS

The correlations between the geotechnical parameters and the geophysical responses are an active field of research; this could improve the efficiency of geotechnical monitoring and provide further insight into soil behaviour.

In this chapter, the key findings presented in the previous sections are discussed in view of their applicability in the geotechnical monitoring of saturated fine-grained soil subject to an external load. Although certain overarching trends have been identified between the BEC and EC ($1/\rho$), the ρ data are considered to be too limited to draw

conclusions from and this requires further research. Therefore, the focus is given to the geotechnical parameters' (VWC, GWC and void ratio) correlations with the TDR-measured AP and BEC.

6.4.1 VWC'S RELATIONSHIP WITH AP IN SATURATED SOILS

The relationship between VWC and AP can be described, for example, by using a third-order polynomial equation (Topp et al., 1980) or a linear-refractive-index (square root of AP) correlation (Skierucha, 2000).

The correlations observed in this study are compared to these equations to determine which provides the best VWC prediction (based on the data obtained in the present study).

6.4.1.1 VWC-AP IN RELATION TO TOPP'S MODEL

In unsaturated soils, the third-order polynomial relationship proposed by Topp et al. (1980) (Eq. 2.10) is commonly applied to estimate the VWC from the AP results. Although this model is found to not be accurate for soils with a GWC above their PL (Thomas et al., 2010), it is included herein to provide a comparison of the estimated soil response to the response of the soil measured during vertical loading.

The VWC measured (based on changes in the sample height) in the bespoke TDR chambers (Section 3.2.4) during vertical loading is plotted against AP_v and compared against the estimated VWC based on Topp's equation (Figure 6.26). It is observed that the greater the VWC (and, therefore, the AP), the greater the magnitude of the discrepancy between Topp's equation and the measured data. This confirms the findings of other research; for example, Thomas et al. (2010).

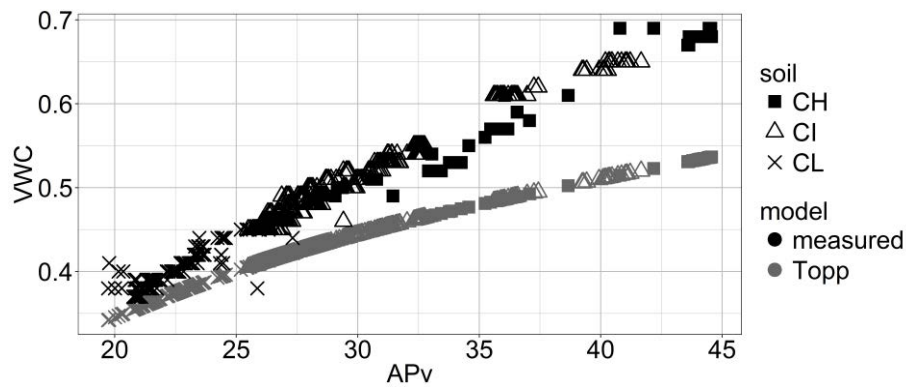


Figure 6.26. AP_v -VWC relationship in relation to Topp's model (for all TDR samples)

Topp's equation assumes that the AP increases much faster with VWC than shown by the measurements (Figure 6.27). This suggests that the influence of the clay particles and associated DDL restricts the ability of the water molecules to rotate to a higher degree than expected by the structural (VWC) correlation. The higher the SSA of soil, the larger the amount of water bound around the clay particles. Given that 'bound water' exhibits an AP close to that of solid particles (Jones and Or, 2003), it is observed that the discrepancy between the predicted and measured AP_v is most significant in the CH soil, in which the amount of bound water is expected to be the largest.

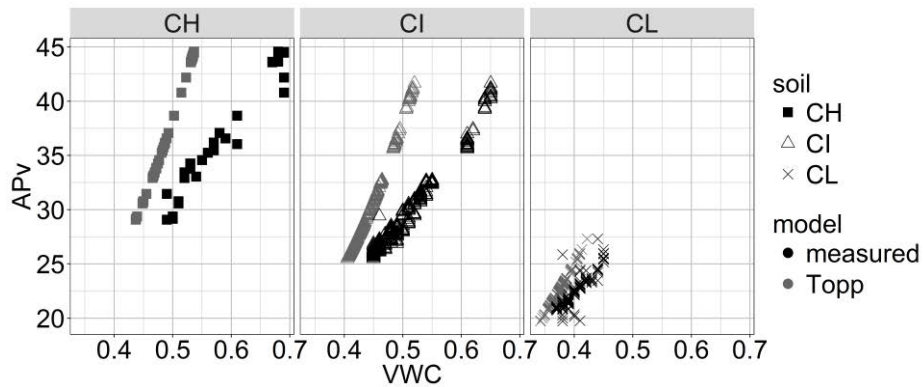


Figure 6.27. VWC- AP_v relationship in relation to Topp's model in the CH, CI and CL samples

Furthermore, the AP read with the TDR is affected by dispersion, and results in an AP higher than the real permittivity, particularly in the presence of clay particles and salts causing a high BEC (Topp et al., 2000). Therefore, the estimated VWC based on AP (TDR) can be erroneous. VWC-estimation models based on the real permittivity are proposed, for example, by Liu (2007) and Thomas et al. (2010) ; however, with the present state of technology, obtaining the real part of the AP from TDR is not easily achievable.

It is noted that the VWC measurements obtained during this study are based on bulk sample changes, as the local changes in d_d could not be measured, and the reference GWC was measured at the beginning and end of consolidation. Therefore, the correlation between AP and VWC obtained in this study is likely to contain intrinsic errors, and it is suggested that it should be used to identify trends rather than for obtaining absolute values.

6.4.1.2 VWC-AP CORRELATION

Thomas (2010) suggests that there is a linear relationship between a soil's AP and its VWC at LL, and the third-order polynomial equation proposed by Topp et al. (1980) is the most commonly used model to represent the AP-VWC relationship. Therefore, a trial was undertaken (Figure 6.28) to fit linear (Eq. 6.3), second-order (Eq. 6.4) and third-order (Eq.6.5) regression equations, using the least squares method, to the data obtained from the TDR_v measurements.

$$VWC = 0.0136AP_v + 0.0976 \quad \text{Eq. 6.3}$$

$$VWC = -0.0001AP_v^2 + 0.0199AP_v + 0.0055 \quad \text{Eq. 6.4}$$

$$VWC = -4E^{-06}AP_v^3 + 0.0003AP_v^2 + 0.008AP_v + 0.1218 \quad \text{Eq. 6.5}$$

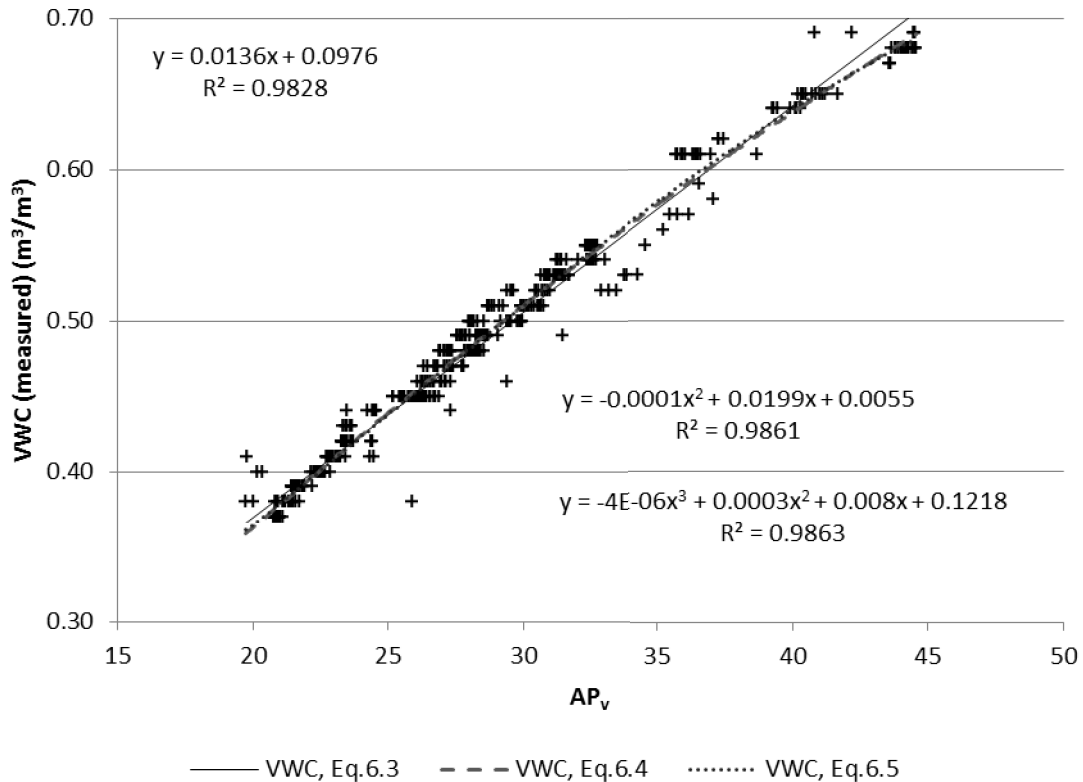


Figure 6.28. Relationship between VWC and AP_v , shown for the CH, CI and CL results

The comparison amongst these three models, presented in Figure 6.29, reveals that all three enable the prediction of VWC to within a 5% estimation error, based on the data collected in the present study. It can be seen in Figure 6.27 that the CH, CI and CL soils display slightly different trends; therefore, the accuracy of the prediction can be improved further by fitting soil-specific regression equations.

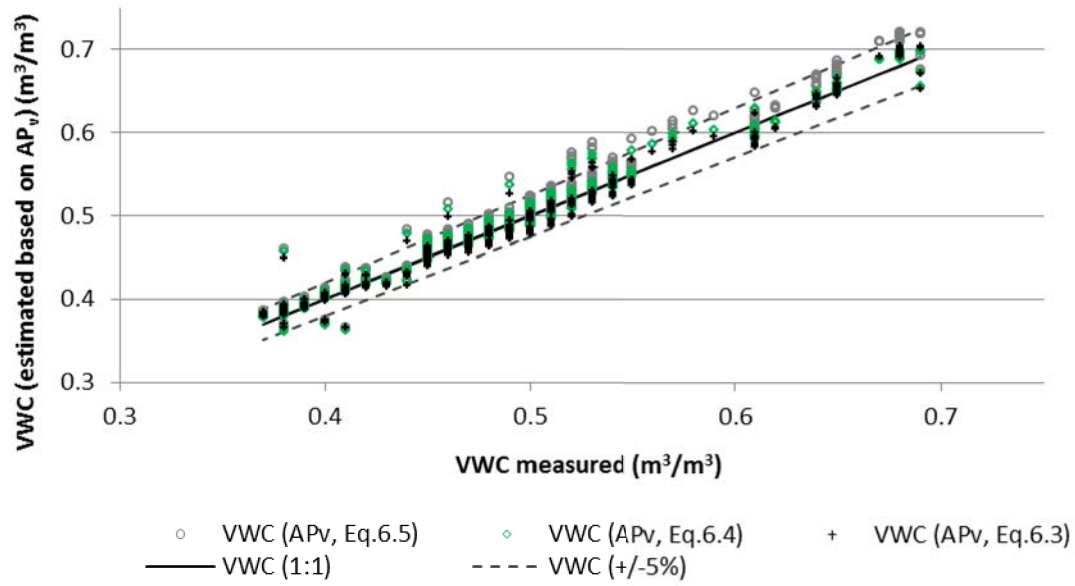


Figure 6.29. Comparison between VWC measured during the vertical loading and the estimated VWC based on the AP_v -VWC correlations (Eq.6.3, Eq. 6.4 and Eq.6.5)

6.4.1.3 VWC-REFRACTIVE INDEX CORRELATION

A linear correlation is shown to describe the VWC relationship with the square root of the AP (refractive index); this is described in Eq. 6.6 (Skierucha, 2000), which is based on 663 samples (395 of which were inorganic):

$$VWC = 0.13\sqrt{AP} - 0.18 \quad \text{Eq. 6.6}$$

Given that the inorganic soil specimens exhibited a porosity range between 0.32 and 0.6, which relate to the porosity of the samples tested in the present study, a comparison with this large soil database was undertaken.

The VWC results measured during the present study were plotted against the refractive index (Figure 6.30) and the linear trend is described by Eq. 6.7:

$$\text{VWC} = 0.15\sqrt{\text{AP}_v} - 0.31 \quad \text{Eq. 6.7}$$

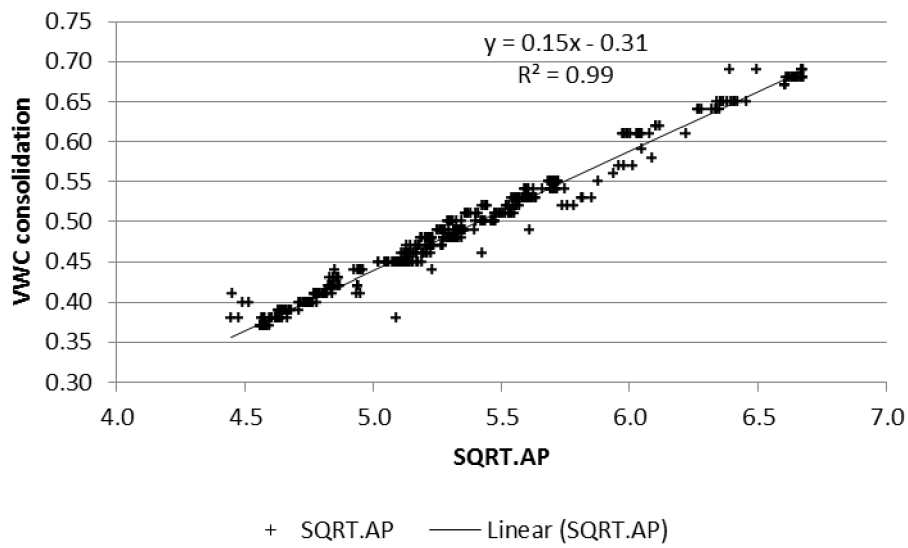


Figure 6.30. Correlation between the VWC measured during the consolidation and the refractive index (square root of AP)

The VWC measured during the loading was then compared with the VWC estimated from the refractive index (Eq. 6.7), based on the results of the present study and Eq. 6.6, which is proposed in Skierucha (2000).

The estimated VWC was plotted in relation to the measured values (Figure 6.31), indicating that the VWC prediction, based on Eq. 6.7 and derived from the present

study dataset, provided an estimation within 5% (with occasional outliers). The estimation based on Eq. 6.6 was found to be within 5% for the VWC range above 50%; however, below this value the estimation error exceeded 5%.

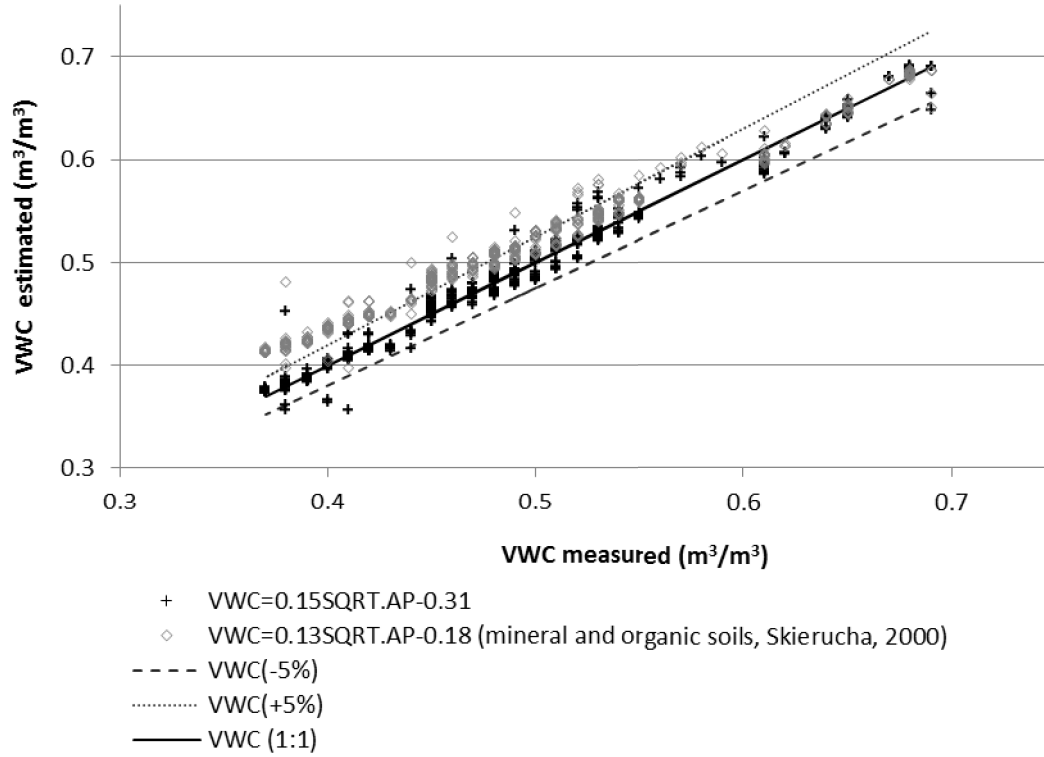


Figure 6.31. VWC estimation based on the refractive index (square root of AP) correlation, Eq. 6.7 and Eq. 6.6, in relation to the measured VWC

It is noted that the VWC prediction, based on the refractive index, can be improved by the inclusion of either clay content or d_d (Skierucha, 2000); nonetheless, the VWC prediction that is within 5% and based on one parameter only can be satisfactory in some applications.

6.4.2 GWC RELATIONSHIP WITH AP

The GWC is more commonly used in geotechnical practice than VWC; therefore, the GWC correlation with AP maybe of more interest during geotechnical assessments. A relationship between AP, which is normalised by d_d , and GWC is proposed by Thomas (2010). The GWC results measured during the present study were plotted against AP_v normalised by d_d (the range of d_d was limited to 0.82–1.71 [Mg/m^3]) (Figure 6.32):

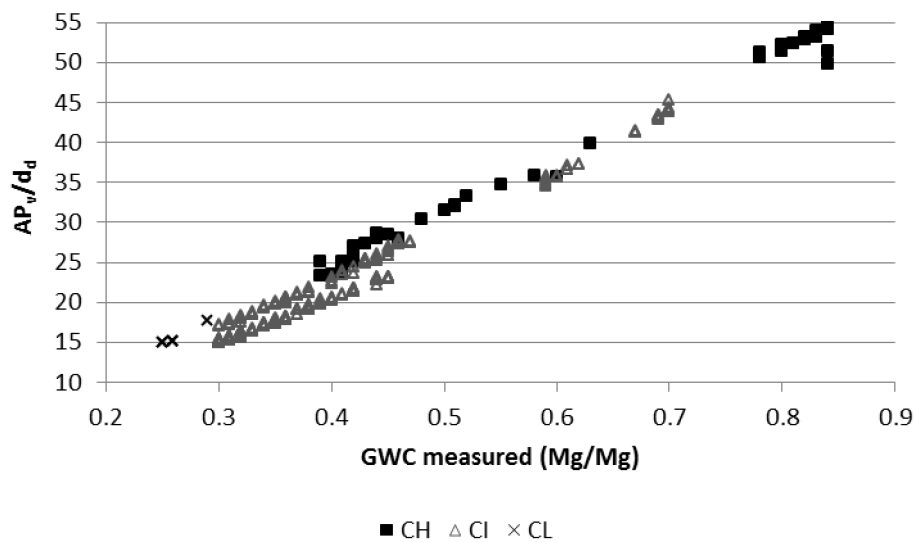


Figure 6.32. GWC relationship with AP_v normalised by d_d

Given that the VWC can be estimated to within 5% accuracy, based on the AP_v correlation (Figure 6.29), the TDR can be very useful for predicting the GWC if the d_d is known, as shown in Figure 6.32.

6.4.3 VOID-RATIO RELATIONSHIP WITH AP IN SATURATED SOILS

Void ratio (e) is a parameter that is commonly used in geotechnical assessment; for example, to predict C_c from the $e - \log \sigma'$ correlation. Therefore, the relationship between the void ratio and AP or refractive index is also discussed below.

6.4.3.1 VOID RATIO-AP CORRELATION

As posited in Section 6.2.3, a clear positive relationship between AP_v and e was observed during the vertical-loading process. The correlation is re-plotted on Figure 6.33.

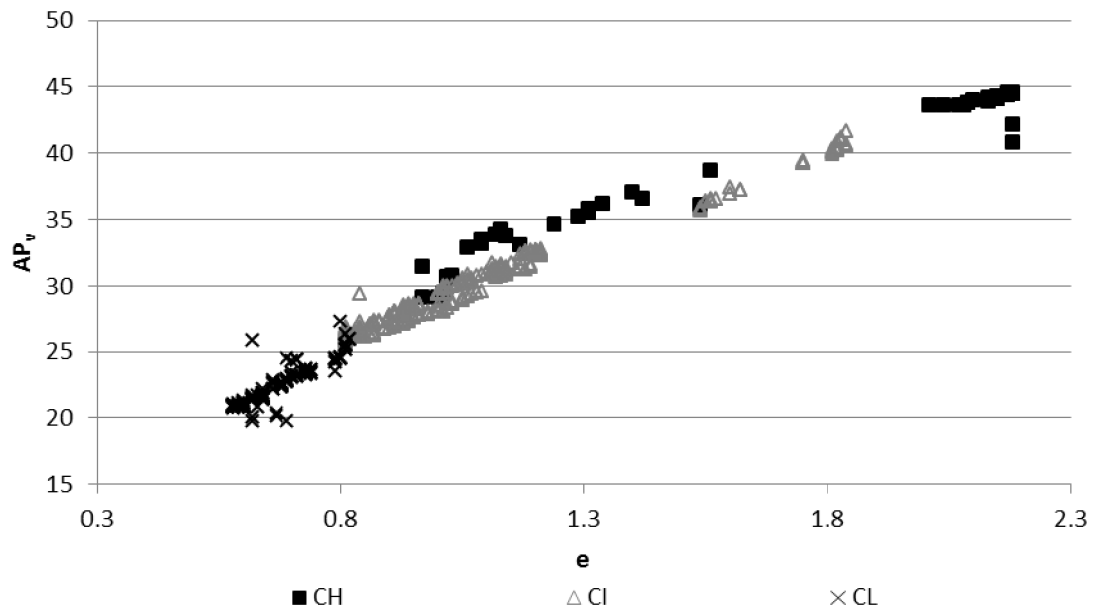


Figure 6.33. AP_v -void ratio relationship in the CH, CI and CL samples

Analogous to the VWC-AP analyses, the values of e were plotted against AP_v with linear, second-order and third-order polynomial equation fitting using the least squares method (Figure 6.34), resulting in Eq.6.8, Eq.6.9 and Eq.6.10, respectively:

$$e = 0.0613AP_v + 0.7483 \quad \text{Eq. 6.8}$$

$$e = 0.0013AP_v^2 + 0.0211AP_v + 0.4677 \quad \text{Eq. 6.9}$$

$$e = -2E^{-06}AP_v^3 + 0.0016AP_v^2 - 0.0275AP_v + 0.5297 \quad \text{Eq. 6.10}$$

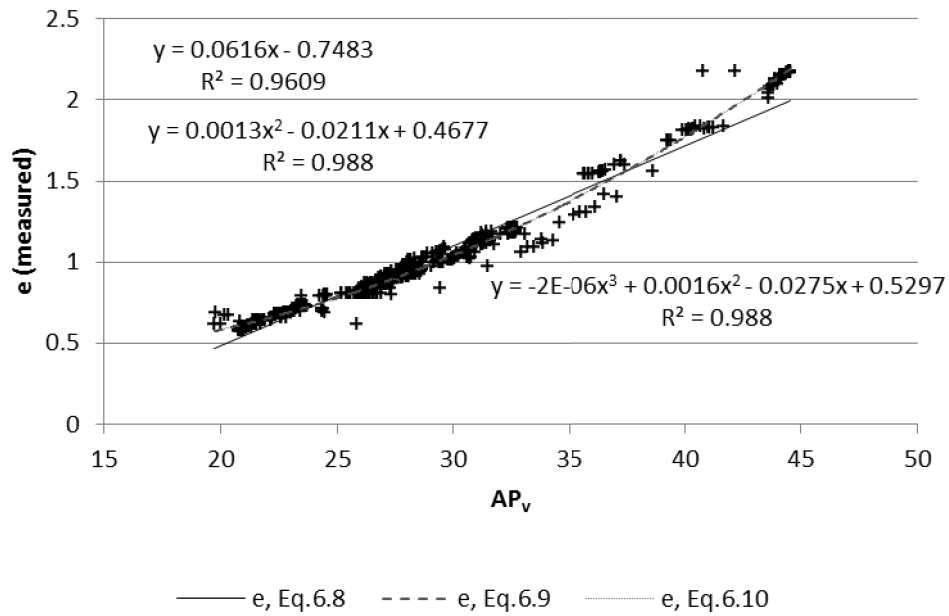


Figure 6.34. The relationship between AP_v and e , shown for the CH, CI and CL samples

Subsequently, e measured during the consolidation was compared against e estimated based on Eq. 6.8, Eq. 6.9 and Eq. 6.10 (Figure 6.35). The comparison reveals that all three equations provide an estimation of e within 5–10% accuracy (with occasional outliers).

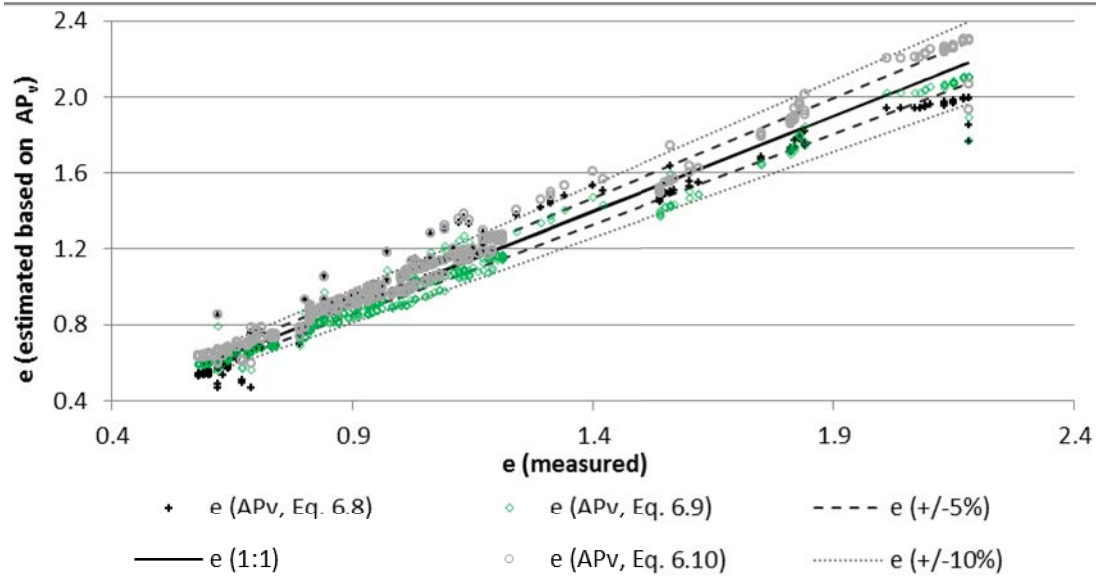


Figure 6.35. Void-ratio estimation based on the AP_v relationship, from Eq. 6.8, Eq. 6.9 and Eq. 6.10

6.4.3.2 VOID RATIO-REFRACTIVE INDEX CORRELATION

The void ratio was plotted against the refractive index using linear and second-order polynomial equations fitted by the least squares method, resulting in Eq. 6.11 and Eq. 6.12:

$$e = 0.67\sqrt{AP} - 2.53 \quad \text{Eq. 6.11}$$

$$e = 0.23AP - 1.81\sqrt{AP} + 4.14 \quad \text{Eq. 6.12}$$

Based on Eq. 6.11 and Eq. 6.12, the estimated e was plotted against the e measured during consolidation (Figure 6.36). The results demonstrate that, in both cases, it is possible to predict e within 5% accuracy, with some data points within 10% accuracy

and with occasional outliers. The second-order polynomial refractive index- e relationship exhibits a tendency to overestimate e . The linear relationship appears to underestimate e within the range corresponding to the CL and CH soils, whilst within the CI range it is overestimating e .

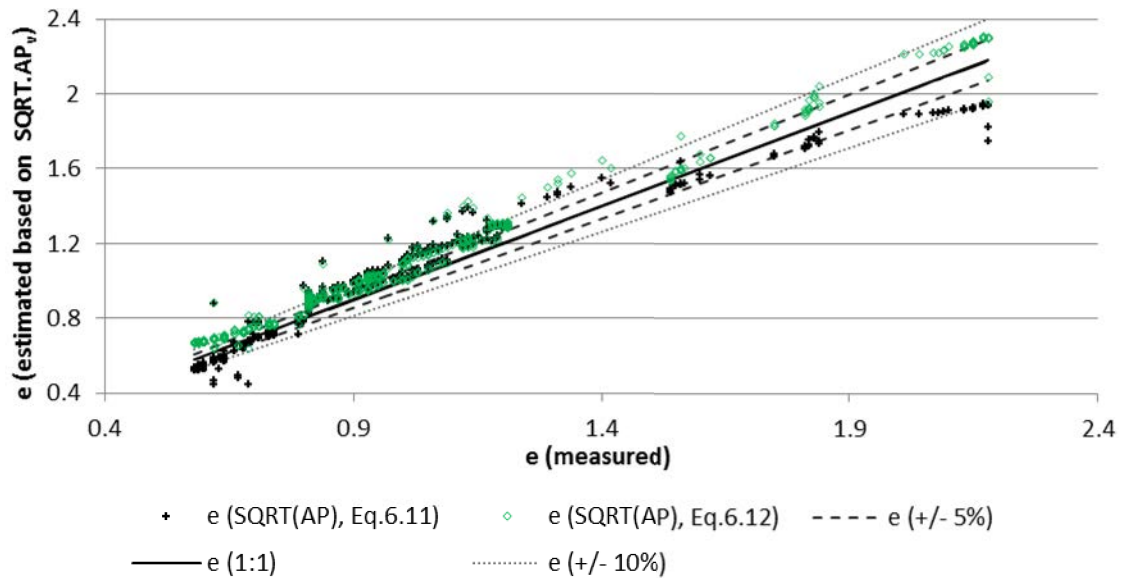


Figure 6.36. Void-ratio estimation based on the SQRT.AP_v relationship, from Eq. 6.11 and Eq. 6.12

Based on Figure 6.35 and Figure 6.36, it is concluded that AP and SQRT.AP_v provide a similar level of accuracy (within 5–10%) when predicting e (based on the equations derived from the present research dataset).

Based on the AP correlation with void ratio, further correlation between C_c and AP may be possible. A trial was undertaken within the present study; however, the number of samples was found too limited to establish an equation. This could be researched further.

6.4.4 BEC CORRELATION WITH VWC AND VOID RATIO

A nonlinear relationship between BEC and VWC is found in sands (Ferre et al., 1998). However, the results of the present study, as shown in Figure 6.37, indicate that in the clay-containing soils this relationship is affected by significant scatter. It can be seen that, for example, the BEC at 0.1 S/m reflects a VWC between 45% and 65% in the CI soil, resulting in a 20% VWC estimation error.

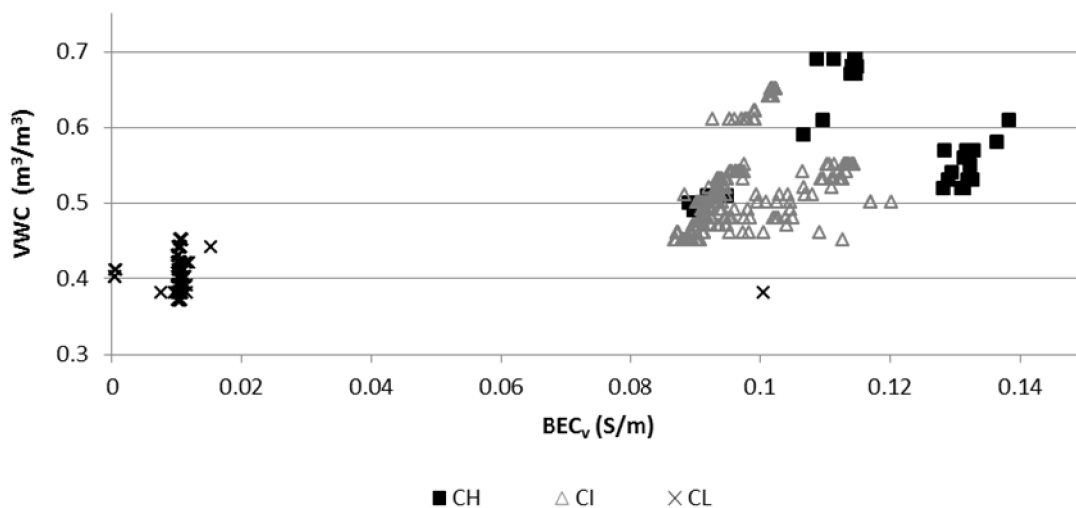


Figure 6.37. BEC relationship with VWC

The BEC_v for a fine-grained soil containing clay minerals is a function of a number of mechanisms, and, whilst it responds to VWC changes in some samples, this was not always the case for the soils investigated (analogous to the void-ratio response [Figure 6.38]). Nonetheless, the BEC is potentially indicative of the soil-plasticity range, as demonstrated by the clustering shown in Figure 6.37 and Figure 6.38:

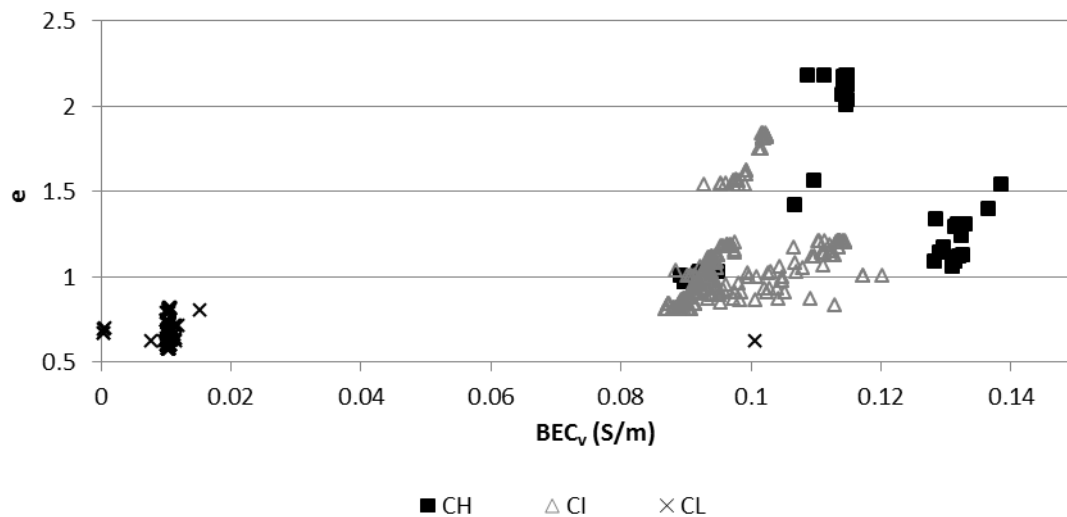


Figure 6.38. BEC_v - e relationship during loading

The BEC_h was found to be related to ρ_v , and this correlation, of potential use in ground monitoring, is discussed further in the following section.

6.4.5 ESTIMATING CONSOLIDATION STAGE BASED ON AP , BEC AND ρ

The results of the TDR and ER investigation imply that AP_v responds very well to structural changes in soil, which is reflected in the positive correlation with the void ratio, as shown in Figure 6.35. However, the AP_h , BEC_h and ρ_v readings were found to respond differently immediately after the load placement, illustrating a response to changes that are assumed to relate to increased pore-water flow and possibly a bigger volume of fluid surrounding the probe. This result indicates that combining instrumentation positioned in the vertical and horizontal plane can provide complementary information, and thus facilitate the monitoring of ground movement.

An example of an analysis of the relative AP and BEC changes (read with TDR_v and TDR_h), in the context of the consolidation phases in the CI soil, is presented in Figure 6.39. Due to the hydraulic head influences, as previously discussed, the primary and secondary consolidations (based on Terzaghi's theory and Taylor's 90% consolidation time estimation) are marked on the graph for information only. Nonetheless, it can be seen that the rapid decrease in the relative sample height is reflected in a rapid $AP_{v(r)}$ decrease. Simultaneously, an elevated $AP_{h(r)}$ and $BEC_{h(r)}$ are observed initially, and their relative values begin to merge with AP_v towards the end of the primary consolidation.

In addition, the ρ measurements identify that, immediately after loading, a decrease in ρ_v can be observed. This is most likely a result of increased ion mobility due to excess pore-fluid migration. As the settlement progresses, $\rho_{v(r)}$ begins to increase gradually (Figure 5.8); however, the scatter in the response is higher than with $AP_{v(r)}$, indicating that $\rho_{v(r)}$ may be more suitable for long- rather than short-term monitoring. Furthermore, the ρ_h measured at two different depths confirms that the $\rho_{h(r)}$ change within a soil layer was lower than that which the bulk change reflected in $\rho_{v(r)}$. The $\rho_{h(r)}$ measured at 150 mm from the bottom of the sample was also found to be higher than that measured at 50 mm, suggesting the possibility of monitoring the changes within soil layers with the ER technique.

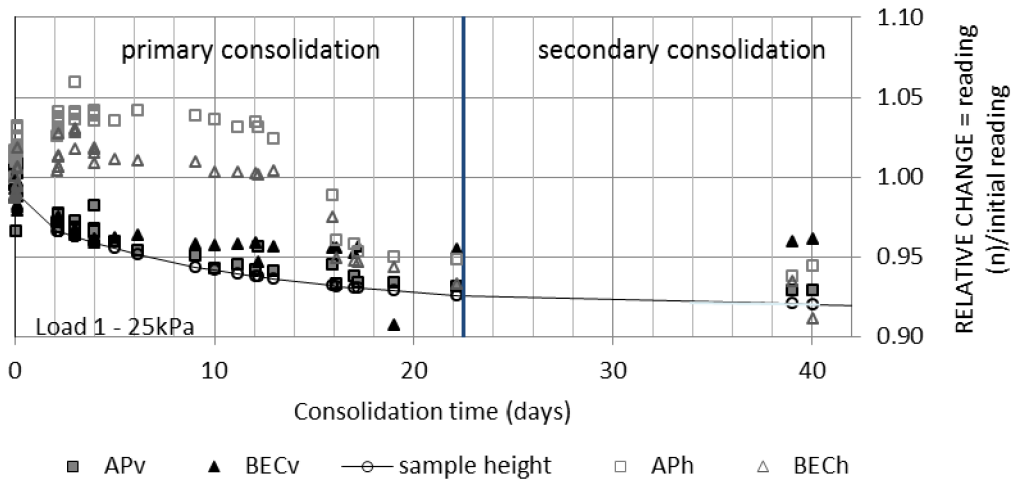


Figure 6.39. Primary and secondary consolidation in relation to TDR readings during first loading stage (25 kPa) of CI.S3.TDR

The trends observed could be used to act as a coarse, but relatively inexpensive, monitoring system, with prescribed trigger values where additional investigation is required. Alternatively, correlations (such as those postulated previously) could be used to help estimate the geotechnical parameters of the soil (for example, for design purposes).

6.5 SUMMARY OF THE RESULTS AND DISCUSSION

The analysis of the AP, BEC and ρ responses to the changes in fine-grained soils under vertical loading reveal a positive and clear relationship between AP, measured in the direction of the load application, and the VWC, GWC and void ratio of soils with a range of plasticities. This is in line with the findings of Liu (2007). Nonetheless, for what is believed to be the first time, TDR measurements were taken continuously and in two

planes, revealing that the AP immediately after loading may change due to the application of the load, and that a two-directional positioning of the probes can provide further insight into the changes in soils during settlement. Whilst vertically measured values increased only immediately after the loading (the magnitude of which was strongly dependent on the clay's plasticity), the horizontally located probes exhibited elevated AP and BEC levels for much longer. This coincided with the consolidation mechanisms and the associated, but time-lagged, development of transitory hydraulic gradients acting across the sample as water was displaced from the soil; this resulted in increased fluid flow through the soil (and the densification of the deeper layers of the sample with the vertically downward flow of the water). The corresponding ρ ($=1/EC$) was recorded with probes positioned perpendicular to the direction of loading, revealing that the initial loading stages caused the EC values to increase.

The BEC and ρ were found to be correlated with the void-ratio decrease in a few samples; however, there were also cases where they plateaued whilst the structural changes continued to take place. This suggests that pore connectivity rather than the void ratio has a predominant effect on the values of BEC and EC (Friedman, 2005; Kibria, 2014).

It was also highlighted that discrepancies between the BEC (TDR) and EC (ER) can be expected, as they represent different mechanisms. Although both are controlled predominately by ion mobility within the pore fluid, the interface between the fluid

and clay particles affects the BEC response, particularly in clay-containing soils. The EC and BEC responses in pore fluid were found to be very similar.

In addition, during the initial testing under PS1, the $\rho_{h(r)}$ implied the possibility of monitoring the volumetric changes within the sample layers; however, it was not possible to continue this observation under PS2, due to the experiment's constraints.

Both BEC and AP were found to be sensitive to unloading. Due to a much lower magnitude of C_s in comparison with C_c , and, as a result, a lower amount of water being drawn into the sample during unloading compared to the loading process, a change in the geophysical response was observed, predominantly when the entire load was removed. This area requires further research.

The present research focused on a change in the geotechnical properties and associated changes in the geophysical properties of the soils (rather than conducting an experimental investigation into the consolidation process). One finding of this study is that the experiment's set-up is not suitable for investigating the consolidation mechanisms, and if it is desired to investigate the consolidation mechanisms in an apparatus larger than triaxial or oedometer samples, then it is suggested that the experimental arrangement used in this study should not be used (at least not without modification before undertaking the tests).

The results imply that combined TDR and ER measurements can provide further insight into changes in soil subject to loading. The AP readings are very sensitive to the changes in soil induced by loading. AP can provide an immediate response, both when the soil is compressed and when it starts expanding. Whilst AP_v can be used to predict VWC or e changes, AP_h responds to the increased water flow resulting from the excess pore-water pressure. The ER method was found to be less sensitive to immediate changes; nonetheless, ρ_v may be more suitable for long- rather than short-term monitoring. Furthermore, the rate of change of ρ_h described as relative ($\rho_{h(r)}$) was found to be indicative of the magnitude of the change within a given soil layer. The concurrent application of ER and TDR measurements in the field can provide spatial coverage through the ER arrays and can provide point verification through the TDR probes.

Finally, the regression equations were derived based on AP_v or square-root AP_v results to indicate the trend (rather than for obtaining absolute values) between the geophysical change and geotechnical parameters (VWC, GWC, and e), in order to assist with incorporating the geophysical responses in geotechnical ground monitoring. The analysis demonstrated that linear, second-order and third-order regression equations provide similar levels of accuracy when predicting VWC (within 5% of the measured values) and e (within 10% of the measured values) based on AP_v readings. The empirical correlations established between AP and VWC/GWC/ e can be incorporated into soil-behaviour-monitoring models. Although the dataset is limited to three soil types, it can aid comparison with other soils. Ground models, based on these bulk

trends, could be used for monitoring ground subject to vertical stress, such as from structures, roads and embankments. The successful implementation of ground monitoring, based on AP measurements at a certain depth, could support a prevention system in which AP-trigger values lead to the identification of geotechnical concerns before damage is observed on the surface.

CHAPTER 7: CONCLUSIONS AND RECOMMENDATIONS FOR FURTHER WORK

7.1 RESEARCH OUTCOMES AND CONCLUSIONS

Based on the literature review, it was found that there has been limited research on the electromagnetic response to changes in the properties of saturated fine-grained soils undergoing volumetric changes under the application of a vertically applied load. AP measured with TDR is known to be sensitive to the VWC fluctuation in soil (Topp et al., 1980); hence, it could provide further insights into soil properties correlated with VWC. Although TDR has previously been applied at the end of consolidation experiments (Liu, 2007), no controlled laboratory research had been conducted with TDR probes inserted within the soil throughout the duration of the consolidation process.

Furthermore, the correlation between ρ and the void ratio was identified in modified oedometer tests (McCarter et al., 2005; Bryson and Bathe, 2009; Kibria, 2014). Given the strong relationship between ρ ($=1/EC$) and BEC measured with TDR, the simultaneous application of low-frequency ρ -measurement techniques (ER and TDR) suggests that these two techniques could complement each other. The spatial coverage provided by the ER arrays and the detailed point monitoring from the TDR could facilitate the monitoring of fine-grained-soil volume changes, yet these two techniques had not been tested concurrently in this application.

Therefore, this study aimed to investigate the changes in AP, BEC and EC measured using the TDR and ER techniques for a range of fine-grained soils subjected to volumetric changes caused by vertical loading. The outcome of the investigation was intended to provide greater clarity as to whether TDR and ER readings taken individually or simultaneously could be used to estimate geotechnical parameters, and therefore provide the basis for monitoring saturated or near-saturated geotechnical structures in the field. To fulfil this aim, bespoke laboratory experiments were designed, in which TDR and ER instrumentation was incorporated into specially constructed chambers (based on a modified 1D consolidation apparatus) that housed the soil, the loading frame and the geophysical sensors. Three soil mixtures exhibiting a range of plasticities (CH, CI and CL) were investigated in this study.

For what is believed to be the first time, TDR measurements were taken continuously and in two planes during vertical loading and unloading. Additionally, TDR and ER investigations of fine-grained-soil volume-change behaviour were run in parallel using the bespoke apparatus. Unlike the flat electrodes used during the previous investigations of soil consolidation with ER (Borsic et al., 2005; McCarter et al., 2005), the present study used ER electrodes embedded in the soil to measure distinct layers within the sample, and corresponded with the TDR-probe-insertion method.

The following points summarise the main outcomes of the investigation:

- It was found that the AP_v , BEC_v and ρ_v responded to the decrease in void ratio and VWC during loading. However, only vertical AP (AP_v) was clearly related to the decrease in the void ratio and VWC. The regression equations fitted to the

relationship between AP_v and void ratio (or VWC) suggested that the VWC can be estimated from AP_v within 5% accuracy, and the void ratio can be estimated within 5-10% accuracy. This indicated a novel TDR application for the continuous monitoring of settlement in real time during an active consolidation process. It also showed, for the first time, that the positioning of the TDR probes affects the AP and BEC responses during the process of vertically loading soil.

- Although BEC_v and ρ_v appeared to follow the trend identified by AP_v , they exhibited large fluctuations that would preclude their use in the continuous monitoring of the void-ratio change in real time. These readings, taken at the end of consolidation, potentially show the progress of the settlement. However, they appeared to be affected more by the connectivity of the pores rather than the void ratio, which corresponded to the approach presented, for example, by Friedman (2005).
- A direct correlation between BEC and ρ was not possible to establish since the TDR and ER sensors were installed in separate samples. However, the electrical conductivity measured with both techniques in the pore fluid extracted from the soil samples was found to be nearly identical. In the soil mixtures containing clay, in which the interface between the fluid and clay particles can affect both the EC and BEC, a potential difference in their responses can be expected. Although both BEC and EC are associated with ion mobility, BEC reflects the conductive loss (corresponding to the kHz frequency range) recorded during

transmission and an electromagnetic pulse; however, ρ (typically below 100 Hz) corresponds to the flow of current injected into a soil sample. Furthermore, high-frequency ρ measurements were suggested to indicate the total-volume of the conductive fluid, whilst DC measurements connected-volume of the conductive fluid (Shankland and Waff, 1974). This requires further investigation to determine if TDR and ER instrumentation can be used interchangeably to measure BEC and EC.

- The unloading process was monitored with TDR for what is believed to be the first time. It was observed to induce both BEC and AP changes, where the change in AP was dependent on the magnitude of the load removed, reflecting the magnitude of the structural rebound. The low magnitude of the swelling index, when compared to the compression index, is such that the volume of water drawn back into the soil is significantly less than the volume displaced; and this may interfere with the geophysical detection of the swelling mechanism under small reductions in loads. This aspect of the soil's response requires additional research.
- The simultaneous measurement of AP_h revealed that its initial response differed from AP_v . Whilst the vertically measured values increased only immediately after the loading (the magnitude of which was strongly dependent on the plasticity of the clay), the horizontally located probes exhibited elevated AP levels for much longer. This corresponded with elevated BEC_h and ρ_v readings, and coincided with the increase in the excess pore-water pressure.

The ρ_v readings reflected that the current flow was predominately in the vertical direction. Therefore, it was concluded that the positioning of the probes, rather than the propagation of current in a direction normal or parallel to the loading direction, had the predominant effect on the TDR_h response in this experiment.

- The previous point suggests that a two-directional positioning of the probes can provide further insight into the changes in soils during settlement. Whilst AP_v can indicate a decreasing void ratio with loading, the initially elevated AP_h response can demonstrate pore-water-pressure dissipation. This is a novel finding, which requires further validation; nonetheless, the results were very encouraging.
- Based on the differences between the AP_v and AP_h readings, it is also hypothesised that TDR_h was detecting a vertically downward seepage of water, in addition to the compression due to the consolidation.

Following the aforementioned findings, it has been concluded that the aim of the research has been achieved. The geotechnical parameters (water content, void ratio and pore-water pressure) measured during the volume change of soil under vertical loading have been correlated with geophysical parameters, including AP , BEC and ρ . The geotechnical-geophysical links, demonstrated within the present research, justify the potential use of simple geophysical sensors for a geotechnical-monitoring regime, where the ground conditions are subject to loading and unloading. Such an approach may prove a useful early warning system against the loss of ground performance or

failure. The geophysical sensors could be installed underneath the foundations of buildings, roads or within embankments. TDR probes, calibrated to a given soil, could provide relative changes in AP/BEC. On the basis of the relationship between, e.g. AP and VWC, trigger values could be set to provide alerts for geotechnical changes that need inspection before damage is visible at the ground's surface. Sensitivity of AP to unloading suggests that TDR could be potentially used in investigation of the effect of an excavation on the adjacent ground.

Given that the TDR-probe measurements represent only a limited volume of soil, and the number of probes that would need to be used to cover large areas in monitoring situations in the field, combining TDR with ER instrumentation provides a sustainable solution. TDR can be imbedded in soil at a given depth and provide localised response, which may not be visible to the ER probes mounted on the surface. Since ER can reflect long-term changes in the void ratio, and TDR is sensitive to both immediate and long-term changes in soil that are induced by loading, the concurrent application of these two methods can be potentially used as a tool to predict and monitor soil settlement. Furthermore high sensitivity of AP to the pore fluid movement could provide information on the variations in the water table.

Although simultaneous application of ER and TDR in investigating load induced changes in soil is promising, their response requires further validation. Suggestions for further works are presented in the following section.

7.2 RECOMMENDATIONS FOR FURTHER WORK

It is apparent that the geophysical-geotechnical correlations observed within the present research suggest that geotechnical asset monitoring could be undertaken using simple geophysical sensing technologies. The trends observed could be used to act as a coarse, but relatively inexpensive, monitoring system, with prescribed trigger values indicating where additional investigation is required. Alternatively, the correlations between AP_v and VWC (or void ratio) could be used to help estimate the geotechnical parameters of the soil; for example, for design purposes. The installation of relatively simple probes into newly constructed earth structures, or retrofitted into existing structures, could provide asset owners/operators with real-time information on how the asset is performing. Relative (rather than absolute) changes could be used to inform about the relative 'health' of the asset, with relative trigger levels designated for when corrective action may be required.

In order to facilitate this monitoring system, it will be beneficial if further investigation is carried out to address the following areas:

- The TDR response to the volume change of a wider range of soils. The research conducted herein indicated the response of idealised, inorganic soil mixtures, representing clays with a range of plasticities (i.e. CH, CI and CL). Investigation of soils in field conditions would be useful to further validate the findings.
- The TDR response to loading, unloading and reloading conditions. The range of loads and resulting effective pressure ranges tested within the present research

was relatively limited, to approximately 100 kPa, due to the pressure-system constraints and the fragility of the TDR probes used. To facilitate field testing, laboratory analysis should include higher effective stresses and, in parallel, more robust TDR probes that are able to withstand them. This could enable the testing of over-consolidated soils as well.

- Based on the results of this investigation, the positioning of the TDR probes in relation to the loading direction has been shown to reflect different processes. It would be interesting to test further the responses of the horizontal probes positioned at different depths and the associated excess pore-fluid pressure. In addition, testing the horizontal and vertical TDR probes positioned close to each other at a similar distance from the applied load could provide further information about their responses to loading.
- TDR and ER instrumentation could be tested on the same sample to provide further insights into the BEC and EC correlation.
- Measurements of pore water's chemical and electromagnetic properties during the process would be beneficial to investigate the effect of the pore-fluid changes on the BEC and EC.
- The ER arrangement developed in this study could potentially be used to test pore-scale changes within the soil at a range of frequencies.
- Field trials, based on the findings of this research, incorporating TDR and ER to monitor AP, BEC and ρ changes during the vertical loading of soil would be required to test the sensitivity of the geophysical response to the load-induced

changes in the field settings. It is noted that both ER and TDR are sensitive to temperature, salinity and clay content, and therefore the primary field trials may need to focus on a known homogeneous soil and controlled volume. In time, it would be interesting to investigate the sensitivity of TDR and ER to the load-induced changes in man-made soils.

The TDR and ER arrangements developed in this study as part of the bespoke laboratory equipment can be used to investigate further the relationships between AP, BEC and ρ , and their responses to soil behaviour.

LIST OF REFERENCES

- Abu-Hassanein, Z.S., Benson, C.H. and Blotz, L.R. (1996) Electrical resistivity of compacted clays. *Journal of Geotechnical Engineering*, 122 (MAY): 397–406.
- Al-Obaidy, N. (2017) *Treatment of collapsible soil using encased stone columns*. PhD thesis, University of Birmingham.
- Anandarajah, A. (2000) On influence of fabric anisotropy on the stress-strain behavior of clays. *Computers and Geotechnics*, 27: 1–17.
- Annan, A.P. (2009) “Electromagnetic Principles of Ground Penetrating Radar.” In *Ground Penetrating Radar: Theory and Applications*. First. Amsterdam: Elsevier. pp. 1–40.
- Archie, G.E. (1942) The Electrical Resistivity Log as an Aid in Determining Some Reservoir Characteristics. *Transactions of the AIME*, 146 (01): 54–62.
- Arulanandan, Dafalias, Herrman, Anandarajah, Meegoda, A. (1983) In Situ Characterization Of Soils For Prediction Of Stress-Strain Relationship. *Final Report to the Air Force Office of Scientific Research*, Grant Numb.
- Arulanandan, K. (1973) Electrical dispersion in relation to soil structure. *Journal of the soil foundations division*, 99: 1113–1131.
- Arulanandan, K. (2003) *Soil Structure: in Situ Properties and Behavior*.
- Arulanandan, K., Dafalias, Y., Herrmann, L.R., et al. (1983) *In Situ Characterization Of Soils For Prediction Of Stress-Strain Relationship. Final Report to the Air Force Office of Scientific Research*.
- Arulanandan, K. and Yogachandran, C. (2000) Dielectric Dispersion Method For Non-Destructive Quantification Of Soil Composition. *Computer Simulation of Earthquake Effects*, pp. 1–34.
- ASTM (2000) *Standard Test Method for Specific Gravity of Soil Solids by Gas Pycnometer*. ASTM D5550-06. Pennsylvania: American Society for Testing and Materials.
- ASTM (2005) *Standard test method for measurement of soil resistivity using the two-electrode soil box method*. ASTM G187. Pennsylvania: American Society for Testing and Materials.
- ASTM (2006) *Standard test method for field measurement of soil resistivity using the Wenner four-electrode method*. ASTM G57. Pennsylvania: American Society for Testing and Materials.
- ASTM (2012) *Standard Test Method for Water Content and Density of Soil In situ by Time Domain Reflectometry (TDR)*. ASTM D6780M – 12. West Conshohocken: ASTM International.
- Barbour, S.L. and Fredlund, D.G. (1989) Mechanisms of osmotic flow and volume change in clay soils. *Canadian Geotechnical Journal*, 26 (4): 551–562.

- Barnes, G.E. (2000) *Soil Mechanics. Principles and Practice*. Palgrave Macmillan.
- Basu, D., Misra, A., Puppala, A.J., et al. (2013) Sustainability in geotechnical engineering – general report. *Proceedings of the 18th ICSMGE, Paris*, 7062 (ii): 3155–3162. Available at: <http://www.cfms-sols.org/sites/default/files/Actes/3155-3162.pdf>.
- Basu, R. and Arulanandan, K. (1973) “A new approach for the identification of swell potential in soils.” *In Proceedings of the 3rd international conference on expansive soils*. Haifa, Israel, 1973.
- Bechtold, M., Huisman, J.A., Weihermüller, L., et al. (2010) Accurate Determination of the Bulk Electrical Conductivity with the TDR100 Cable Tester. *Soil Science Society of America Journal*, 74 (2): 495..
- Beck, Y.-L., Lopes, S.P., Ferber, V., et al. (n.d.) *Microstructural Interpretation of Water Content and Dry Density Influence on the DC-Electrical Resistivity of a Fine-Grained Soil*.
- Bell, F.G. and Culshaw, M.G. (2001) “Problem Soils: a review from a British Perspective.” *In* Jefferson, I., Murray, E.J., Faragher, E., et al. (eds.) *Problematic Soils. Proceedings of the Symposium Held at the Nottingham Trent University on 8 November 2001*. Nottingham: ICE. pp. 1–37.
- Besson, A., Cousin, I., Dorigny, A., et al. (2008) The Temperature Correction For The Electrical Resistivity Measurements In Undisturbed Soil Samples. *Soil Science*, 173 (10): 707–720.
- Bittelli, M., Salvatorelli, F. and Pisa, P.R. (2008) Correction of TDR-based soil water content measurements in conductive soils. *Geoderma*, 143: 133–142.
- Blonquist, M.J., Jones, S.B., Lebron, I., et al. (2006) Microstructural and phase configurational effects determining water content: Dielectric relationships of aggregated porous media. *Water Resources Research*, 42: 1–13.
- Boadu, F.K. (2011) Predicting the engineering and transport properties of soils using fractal equivalent circuit model: Laboratory experiments. *Geophysics*, 76.
- Boadu, F.K. and Owusu-Nimo, F. (2010) Influence of petrophysical and geotechnical engineering properties on the electrical response of unconsolidated earth materials. *Geophysics*, 75 (3): G21.
- Bohor, B.F. and Hughes, R.E. (1971) Scanning electron microscopy of clays and clay minerals. *Clays and Clay Minerals*.
- Borsic, A., Comina, C., Foti, S., et al. (2005) Imaging heterogeneities with electrical impedance tomography: laboratory results. *Géotechnique*, 55 (7): 539–547.
- Bowles, J.E. (1984) *Physical and geotechnical properties of soils*. Second. McGraw-Hill.
- Bradford, J.H. (2007) Frequency-dependent Attenuation Analysis of Ground-Penetrating Radar Data. *Geophysics*, 72 (3): J7–J16.
- Brovelli, A. and Cassiani, G. (2011) Combined estimation of effective electrical conductivity and permittivity for soil monitoring. *Water Resources Research*, 47 (January): 1–14.

Bryson, S.L. and Bathe, A. (2009) Determination of Selected Geotechnical Properties of Soil Using Electrical Conductivity Testing. *Geotechnical Testing Journal*, 32 (3): 101632. doi:10.1520/GTJ101632.

BSI (1990a) "Part 2: Classification tests. BS 1377-2: 1990." *In Methods of test for soils for civil engineering purposes*. London.

BSI (1990b) "Part 6: Consolidation and permeability tests in hydraulic cells and with pore pressure measurement. BS 1377-6: 1990." *In Methods of test for soils for civil engineering purposes*. London: BSI.

BSI (2014) *PAS 128:2014. Specification for underground utility detection, verification and location*. London: BSI.

BSI (2015) *BS5930:2015. Code of practice for ground investigations*. London.

BSI (2017) *BS ISO 6707-1:2017. Buildings and civil engineering works. Vocabulary. General terms*. BSI.

Burland, J.B. (1990) On the compressibility and shear strength of natural clays. *Géotechnique*, 40 (3): 329–378.

Campbell, R.B., Bower, C.A. and Richards, L.A. (1948) Change of electrical conductivity with temperature and the relation of osmotic pressure to electrical conductivity and ion concentration for soil extracts. *Soil Science Society Proceedings*, pp. 66–69.

Campbell Scientific Inc. (2010) *Time Domain Reflectometry*., p. 60.

Cassidy, N.J. (2009) "Electrical and magnetic properties of rocks, soils and fluids." *In* Jol, H.M. (ed.) *Ground Penetrating Radar: Theory and Applications*. First Edit. Amsterdam: Elsevier. pp. 41–72.

Cataldo, a., Persico, R., Leucci, G., et al. (2014) Time domain reflectometry, ground penetrating radar and electrical resistivity tomography: A comparative analysis of alternative approaches for leak detection in underground pipes. *NDT & E International*, 62: 14–28.

Chambers, J.E., Gunn, D. a., Wilkinson, P.B., et al. (2008) *Non-invasive time-lapse imaging of moisture content changes in earth embankments using electrical resistivity tomography (ERT)*., (100017897): 475–480. Available at: <http://nora.nerc.ac.uk/7001/>.

Clarke, B.G., Middleton, C. and Rogers, C. (2016) The Future of Geotechnical and Structural Engineering Research. *Proceedings of the Institution of Civil Engineers - Civil Engineering*, 169 (1).

Comina, C., Foti, S., Musso, G., et al. (2008) EIT oedometer: An advanced cell to monitor spatial and time variability in soil with electrical and seismic measurements. *Geotechnical Testing Journal*, 31 (5): 404–412.

Cosenza, P., Marmet, E., Rejiba, F., et al. (2006) Correlations between geotechnical and electrical data: A case study at Garchy in France. *Journal of Applied Geophysics*, 60 (3–4): 165–178.

Craig, R.F. (2004) *Craig's Soil Mechanics, Seventh Edition*. CRC Press.

- Curioni, G. (2013) *Investigating the seasonal variability of electromagnetic soil properties using field monitoring data from Time-Domain Reflectometry probes*. PhD thesis, University of Birmingham.
- Curioni, G., Chapman, D.N., Metje, N., et al. (2012) Construction and calibration of a field TDR monitoring station. *Near Surface Geophysics*, 10 (3): 249–261.
- Curioni, G., Chapman, D.N. and Metje, N. (2017) Seasonal variations measured by TDR and GPR on an anthropogenic sandy soil and the implications for utility detection. *Journal of Applied Geophysics*. doi:10.1016/j.jappgeo.2017.01.029.
- Curioni, G., Chapman, D.N., Pring, L.J., et al. (2018) Extending TDR capability for measuring soil density and water content for field condition monitoring. *Journal of Geotechnical and Geoenvironmental Engineering*, 144 (2).
- Van Dam, R.L., Borchers, B. and Hendrickx, J.M.H. (2005) Methods for prediction of soil dielectric properties: A review. *Detection and Remediation Technologies for Mines and Minelike Targets X, March 28, 2005 - April 1, 2005*, 5794 (1): 188–197.
- Dong, X.B. and Wang, Y.H. (2005) EM-wave based characterizations of local void ratios in soils. *Geo-frontier*.
- Driscoll, R. and Skinner, H. (2007) *Subsidence damage to domestic buildings*. BRE Trust.
- Drnevich, V.P., Siddiqui, S., Lovell, J., et al. (2001) Water content and density of soil insitu by the purdue TDR method. *Second International Symposium on Time Domain Reflectometry*.
- Ekblad, J. and Isacsson, U. (2007) Time-domain reflectometry measurements and soil-water characteristic curves of coarse granular materials used in road pavements. *Canadian Geotechnical Journal*, 44: 858–872.
- Emerson (2010) *Calibrating contacting conductivity sensors. Application data sheet. ADS 43-024*. (July) pp. 1–4. Available at: <http://www.emerson.com/documents/automation/application-data-calibrating-contacting-conductivity-sensors-en-70580.pdf>.
- Fam, M. and Santamarina, C. (1995) Study of geoprocesses with complementary mechanical and electromagnetic wave measurements in an oedometer. *Geotechnical Testing Journal*, 18: 307–314.
- Ferre, P.A., Redman, J.D., Rudolph, D.L., et al. (1998) The dependence of the electrical conductivity measured by time domain reflectometry on the water content of a sand. *Water Resources Research*, 34 (5): 1207–1213.
- Financial Ombudsman (2018) *Buildings insurance: subsidence*. Available at: http://www.financial-ombudsman.org.uk/publications/technical_notes/building-subsidence.htm# (Accessed: 8 January 2018).
- Fredlund, D.G. and Rahardjo, H. (1993) *Soil mechanics for Unsaturated Soils*. New York: John Wiley and Sons, Inc.
- Friedman, S.P. (2005) Soil properties influencing apparent electrical conductivity: A review. *Computers and Electronics in Agriculture*.

- Fukue, M., Minato, T., Horibe, H., et al. (1999) The micro-structures of clay given by resistivity measurements. *Engineering Geology*, 54 (1–2): 43–53.
- Fukue, M., Minato, T., Matsumoto, M., et al. (2001) Use of a resistivity cone for detecting contaminated soil layers. *Engineering Geology*, 60 (1–4): 361–369.
- Ghorbani, A., Cosenza, P., Badrzadeh, Y., et al. (2012) Changes in the electrical resistivity of arid soils during oedometer testing. *European Journal of Environmental and Civil Engineering*, 17 (February 2015): 84–98.
- Giese, K. and Tiemann, R. (1975) Determination of the complex permittivity from thin-sample time domain reflectometry improved analysis of the step response waveform. *Advances in Molecular Relaxation Processes*, 7 (1): 45–59.
- Gunn, D.A., Chambers, J.E., Uhlemann, S., et al. (2015) Moisture monitoring in clay embankments using electrical resistivity tomography. *Construction and Building Materials*, 92: 82–94.
- Hassan, A. and Toll, D. (2013) (2013) Electrical Resistivity Tomography for Characterizing Cracking of Soils. *Geo-Congress 2013*, pp. 818–827. Available at: <http://ascelibrary.org/doi/abs/10.1061/9780784412787.083>.
- Heimovaara, T.J. (1994) Frequency domain analysis of time domain reflectometry waveforms 1. Measurement of the complex dielectric permittivity of soils. *Water Resources Research*, 30 (2): 189–199.
- Huisman, J. a., Lin, C.P., Weihermüller, L., et al. (2008) Accuracy of Bulk Electrical Conductivity Measurements with Time Domain Reflectometry. *Vadose Zone Journal*, 7 (2): 426–433. doi:10.2136/vzj2007.0139.
- Jacobsen, O.H. and Schjønning, P. (1993) A laboratory calibration of time domain reflectometry for soil water measurement including effects of bulk density and texture. *Journal of Hydrology*, 151 (2–4): 147–157.
- Janik, G., Dawid, M., Walczak, A., et al. (2017) Application of the TDR technique for the detection of changes in the internal structure of an earthen flood levee. *Journal of Geophysics and Engineering*, 14: 292–302.
- JEOL (2011) *Introducing Cryo Scanning Electron Microscopy*. JEOL Application Data Sheet. SM-B-004-00E. (C) pp. 3–5.
- Jones, L.D. and Jefferson, I. (2012) Chapter C5 - Expansive Soils. *Institute of Civil Engineers Manuals series*, pp. 1–46.
- Jones, S.B. and Friedman, S.P. (2000) Particle shape effects on the effective permittivity of anisotropic or isotropic media consisting of aligned or randomly oriented ellipsoidal particles. *Water Resources Research*, 36 (10): 2821–2833.
- Jones, S.B. and Or, D. (2003) *Modeled effects on permittivity measurements of water content in high surface area porous media.*, 338: 284–290.
- Jones, S.B., Wraith, J.M. and Or, D. (2002) Time domain reflectometry measurement principles and applications. *Hydrological Processes*, 16 (1): 141–153.

- Jung, S., Drnevich, V.P., Asce, D.M., et al. (2013a) New Methodology for Density and Water Content by Time Domain Reflectometry. *Journal of Geotechnical and Geoenvironmental Engineering*, 139 (May): 659–670.
- Jung, S., Drnevich, V.P., Asce, D.M., et al. (2013b) Temperature corrections for time domain reflectometry parameters. *Journal of Geotechnical and Geoenvironmental Engineering*, 139 (5): 671–683.
- Kalinski, R.J., Kelly, W.E., Bogardi, I., et al. (1993) Electrical resistivity measurements to estimate travel times through unsaturated ground water protective layers. *Journal of Applied Geophysics*.
- Keller, G. and Frischknecht, F.C. (1966) “Electrical methods in geophysical prospecting.” *In Volume 10 of International series of monographs on electromagnetic waves*. Pergamon Press.
- Kibria, G. (2014) *Evaluation of Physico-Mechanical Properties of Clayey Soils Using Electrical Resistivity Imaging Technique*. PhD thesis, University of Texas at Arlington.
- Kibria, G. and Hossain, M. (2012) Investigation of Geotechnical Parameters Affecting Electrical Resistivity of Compacted Clays. *Journal of Geotechnical and ...*, (December): 1520–1529.
- Klein, K.A. and Santamarina, J.C. (1997) Electrical Conductivity in Soils : Underlying Phenomena. *Journal of Environmental and Engineering Geophysics*, December 2003, Volume 8, Issue 4, pp. 000–000.
- Knight, J.H., Ferré, P.A., Rudolph, D.L., et al. (1997) A numerical analysis of the effects of coatings and gaps upon relative dielectric permittivity measurement with time domain reflectometry. *Water Resources Research*, 33 (6).
- Lambot, S., Grandjean, G., Cousin, I., et al. (2009) *Technical specifications of the system of geophysical sensors.*, (March): 86.
- Lech, M. and Garbulewski, K. (2009) Określanie porowatości gruntów niespoistych na podstawie pomiarów oporności elektrycznej Evaluation of cohesionless soil porosity using electrical resistivity measurements. *Przegląd Naukowy Inżynieria i Kształtowanie Środowiska*, 18.
- Ledieu, J., De Ridder, P., De Clerck, P., et al. (1986) A method of measuring soil moisture by time-domain reflectometry. *Journal of Hydrology*, 88 (3–4): 319–328.
- Lin, C.-P., Chung, C.-C., Huisman, J.A., et al. (2008) Clarification and calibration of reflection coefficient for electrical conductivity measurement by time domain reflectometry. *Soil Science Society of America Journal*, 72 (4): 1033–1040.
- Liu, N. (2007) *Soil and site characterization using electromagnetic waves*. PhD thesis, Virginia Polytechnic Institute and State University.
- Loke, D.M. (1999) Electrical imaging surveys for environmental and engineering studies. *A practical guide to 2-D and 3-D surveys*. (1999) pp. 1–61.
- Loke, M.H., Chambers, J.E., Rucker, D.F., et al. (2013) Recent developments in the direct-current geoelectrical imaging method. *Journal of Applied Geophysics*.

Lu, T. and Bryant, W.R. (1997) Marine Georesources & Geotechnology Comparison of vane shear and fall cone strengths of soft marine clay Comparison of Vane Shear and Fall Cone Strengths of Soft Marine Clay. *Marine Georesources & Geotechnology*, 15 (1): 67–82.

Malicki, M. a, Plagge, R. and Roth, C.H. (1996) Improving the calibration of dielectric TDR soil moisture determination taking into account the solid soil. *European Journal of Soil Science*, 47 (3): 357–366.

Malmberg, C.G. and Maryott, A.A. (1956) Dielectric constant of water from 0 to 100 C. *Journal of Research of the National Bureau of Standards*, 56 (1): 1.

McCarter, W.J., Blewett, J., Chrisp, T.M., et al. (2005) Electrical property measurements using a modified hydraulic oedometer. *Canadian Geotechnical Journal*, 42: 655–662.

McCarter, W.J. and Desmazes, P. (1997) Soil characterization using electrical measurements. *Geotechnique*, 47 (1): 179–183.

McDowell, P., Barker, R., Butcher, A., et al. (2002) Geophysics in engineering investigations. *Geological Society, London, Engineering Geology Special Publications*, p. 260.

Meegoda, N. (1985) *Fundamental characterization of soils for the development of an expression for permeability for application in in-situ testing*. PhD thesis, University of California, Davis.

Mironov, V.L., Kosolapova, L.G. and Fomin, S. V. (2009) Physically and mineralogically based spectroscopic dielectric model for moist soils. *IEEE Transactions on Geoscience and Remote Sensing*, 47 (7): 2059–2070.

Mitchell, J. and Liu, N. (2006) Usefulness of EM waves for site and soil property characterization in geotechnical engineering. *ASCE Geotechnical Special Publication*, (Gsp 149): 136–143.

Mitchell, J. and Soga, K. (2005) *Fundamentals of soil behavior*. Third. Hoboken: John Wiley and Sons, Inc.

Moghareh Abed, T. (2016) *Experimental investigation of cast iron corrosion on clay soil and GPR performance*. PhD thesis, University of Birmingham.

Mojid, M.A., Wyseure, G.C.L. and Rose, D.A. (2003) Electrical conductivity problems associated with time-domain reflectometry (TDR) measurement in geotechnical engineering. *Geotechnical and Geological Engineering*.

Ngoc, P.Q. (2012) *An investigation on petrophysical and geotechnical properties of soils using multivariate statistics*. PhD thesis, Clausthal University of Technology.

Nissen, H.H., Ferré, T.P.A. and Moldrup, P. (2003) Sample area of two- and three-rod time domain reflectometry probes. *Water Resources Research*, 39 (10): 1–11.

Norbury, D. (2010) *Soil and Rock Description in Engineering Practice*. Whittles Publishing.

Olhoeft, G. (1985) Low-frequency electrical properties. *Geophysics*, 50 (12): 2492–

2503.

Olson, R.E. (1986) "State of the art: consolidation testing." In Yong R. N. and C., T.F. (eds.) *Consolidation of soils: testing and evaluation. Special technical publication STP 892*. West Conshohocken, PA: American Society for Testing and Materials. pp. 7–70.

Orgill, E. (2015) *Standard Operating Procedure for the Analysis of Samples by ICP-OES using the Perkin Elmer Optima 8000*.

Parkhomenko, E.I. (1967) Electrical Properties of Rocks. *Physics and Chemistry of Rocks and Minerals*, pp. 262–278.

Pastuszka, T., Krzyszcak, J., Sławiński, C., et al. (2014) Effect of Time-Domain Reflectometry probe location on soil moisture measurement during wetting and drying processes. *Measurement: Journal of the International Measurement Confederation*, 49: 182–186.

Podoba, R. and Štubňa, I. (2014) "Geometric factor for conversion of electrical resistance into resistivity." In *15th International conference of Ph.D students, young scientists and pedagogues*. Nitra, 2014. Faculty of Natural Sciences, Constantine the Philosopher University in Nitra. pp. 386–391.

Pring, L.J. (2016) *Soil-based analysis methods to aid the detection of cropmarks over buried features*. PhD thesis, University of Birmingham.

Pringle, J.K., Jervis, J.R., Roberts, D., et al. (2016) Long-term Geophysical Monitoring of Simulated Clandestine Graves using Electrical and Ground Penetrating Radar Methods: 4-6 Years After Burial. *Journal of Forensic Sciences*.

Pritchard, O.G., Hallett, S.H. and Farewell, T.S. (2013) *Soil movement in the UK – Impacts on critical infrastructure Soil movement in the UK – Impacts on Critical Infrastructure*.

Revil, A. (2012) Spectral induced polarization of shaly sands: Influence of the electrical double layer. *Water Resources Research*.

Reynolds, J.M. (1997) *An Introduction to Applied and Environmental Geophysics*.

Rinaldi, V. a. and Cuestas, G. a. (2002) Ohmic Conductivity of a Compacted Silty Clay. *Journal of Geotechnical and Geoenvironmental Engineering*, 128 (October): 824–835.

Robinson, D. a., Gardner, C.M.K. and Cooper, J.D. (1999) Measurement of relative permittivity in sandy soils using TDR, capacitance and theta probes: Comparison, including the effects of bulk soil electrical conductivity. *Journal of Hydrology*, 223: 198–211.

Robinson, D. a and Friedman, S.P. (2001) *Effect of particle size distribution on the effective dielectric permittivity of saturated granular media.*, 37 (1): 33–40.

Robinson, D.A., Jones, S.B., Wraith, J.M., et al. (2003) A review of advances in dielectric and electrical conductivity measurement in soils using time domain reflectometry. *Vadose Zone Journal*, 2 (4): 444–475.

Rogers, C.D.F., Chapman, D.N., Entwisle, D., et al. (2009) "Predictive Mapping of Soil

- Geophysical Properties for GPR Utility Location Surveys.” In *5th International Workshop on Advanced Ground Penetrating Radar*. Granada, Spain, 2009.
- Rogers, C.D.F., Hao, T., Costello, S.B., et al. (2012) Condition assessment of the surface and buried infrastructure - A proposal for integration. *Tunnelling and Underground Space Technology*, 28 (1): 202–211. doi:10.1016/j.tust.2011.10.012.
- Rosenbaum, M.S. (1976) EFFECT OF COMPACTION ON THE PORE FLUID CHEMISTRY OF MONTMORILLONITE. *Clays and Clay Minerals*, 24: 118–121.
- Rosine, T.N. and Sabbagh, T.T. (2015) The impact of the diameter to height ratio on the compressibility parameters of saturated fine-grained soils. *International Journal of Research in Engineering and Technology*, 4 (6): 2319–1163.
- Royal, A.C.D., Atkins, P.R., Brennan, M.J., et al. (2011) Site Assessment of Multiple-Sensor Approaches for Buried Utility Detection. *International Journal of Geophysics*, 2011: 1–19. doi:10.1155/2011/496123.
- RSK (2018) *Geophysical services*. Available at: https://www.environmental-geophysics.co.uk/documentation/info/RSK_Geophysical_Services.pdf (Accessed: 8 January 2018).
- Saarenketo, T. (1998) Electrical properties of water in clay and silty soils. *Journal of Applied Geophysics*, 40 (1–3): 73–88.
- Sadeghioon, A., Metje, N., Chapman, D., et al. (2014) SmartPipes: Smart Wireless Sensor Networks for Leak Detection in Water Pipelines. *Journal of Sensor and Actuator Networks*, 3 (1): 64–78. doi:10.3390/jsan3010064.
- Samouëlian, A., Cousin, I., Tabbagh, A., et al. (2005) Electrical resistivity survey in soil science: a review. *Soil and Tillage Research*, 83 (2): 173–193.
- Scheuermann, A., Hübner, C., Wienbroer, H., et al. (2010) Fast time domain reflectometry (TDR) measurement approach for investigating the liquefaction of soils. *Meas. Sci. Technol. Meas. Sci. Technol*, 21 (21): 25104–11.
- Schon, J.H. (2004) *Physical properties of rocks: fundamentals and principles in petrophysics*. Oxford: Elsevier.
- Schwartz, B.F., Schreiber, M.E. and Yan, T. (2008) Quantifying field-scale soil moisture using electrical resistivity imaging. *Journal of Hydrology*.
- Sénéchal, P., Perroud, H., Kedziorek, M.A., et al. (2005) Non destructive geophysical monitoring of water content and fluid conductivity anomalies in the near surface at the border of an agricultural field. *Subsurface Sensing Technologies and Applications*, 6 (2): 167–192.
- Shah, J., Jefferson, I. and Hunt, D. (2014) Resilience assessment for geotechnical infrastructure assets. *Infrastructure Asset Management*, 1 (4): 95–104.
- Shankland, T.J. and Waff, H.S. (1974) Conductivity in Fluid-Bearing Rocks. *Journal of Geophysical Research*, 79 (32): 4863–4868.
- Sivapullaiah, P.V., Sridharan, A. and Stalin, V.K. (2000) Hydraulic conductivity of

- bentonite-sand mixtures. *Canadian Geotechnical Journal*, 37 (2): 406–413.
- Skierucha, W. (2000) Accuracy of soil moisture measurement by TDR technique. *International Agrophysics*, 14 (i): 417–426.
- Skierucha, W. (2009) Temperature dependence of time domain reflectometry-measured soil dielectric permittivity. *Journal Of Plant Nutrition And Soil Science*, 172 (1): 186–193.
- Skierucha, W., Wilczek, a. and Walczak, R.T. (2004) Polowy system monitorowania parametrów fizykochemicznych gleb i gruntów. *Acta Agrophysica*, 4 (2): 533–545.
- Sridharan, A. and Jayadeva, M.S. (1982) Double layer theory and compressibility of clays. *Geotechnique*, 32 (2): 133–144.
- Sridharan, A. and Nagaraj, H.B. (2000) Compressibility behaviour of remoulded, fine-grained soils and correlation with index properties. *Canadian Geotechnical Journal*, 37 (JANUARY): 712–722.
- Sridharan, A. and Rao, G.V. (1973) Mechanisms controlling volume change of saturated clays and the role of the effective stress concept. *Géotechnique*, 23 (3): 359–382. doi:10.1680/geot.1973.23.3.359.
- Suwansawat, S. and Benson, C.H. (1999) Cell Size for Water Content-Dielectric Constant Calibrations for Time Domain Reflectometry. *Geotechnical Testing Journal*, 22 (1): 3–12.
- Tabbagh, A., Dabas, M., Hesse, A., et al. (2000) Soil resistivity: a non-invasive tool to map soil structure horization. *Geoderma*, 97 (3–4): 393–404.
- Terzaghi, K., Peck, R.B. and Mesri, G. (1996) *Soil Mechanics in Engineering Practice Third Edition*. John Wiley & Sons.
- Thomas, A. (2010) *Measurement of electromagnetic signal velocities in saturated fine-grained soils*. PhD thesis, University of Birmingham.
- Thomas, A.M., Chapman, D.N., Rogers, C.D.F., et al. (2010a) Electromagnetic properties of the ground: Part I – Fine-grained soils at the Liquid Limit. *Tunnelling and Underground Space Technology*, 25 (6): 714–722.
- Thomas, A.M., Chapman, D.N., Rogers, C.D.F., et al. (2010b) Electromagnetic properties of the ground: Part II – The properties of two selected fine-grained soils. *Tunnelling and Underground Space Technology*, 25 (6): 723–730.
- Thomsen, A., Hansen, B. and Schelde, K. (2000) Application of TDR to water level measurement. *Journal of Hydrology*.
- Thring, L.M., Boddice, D., Metje, N., et al. (2014) Factors affecting soil permittivity and proposals to obtain gravimetric water content from time domain reflectometry measurements. *Canadian Geotechnical Journal*, 51 (11): 1303–1317.
- Tiwari, B. and Ajmera, B. (2012) New Correlation Equations for Compression Index of Remolded Clays. *Journal of Geotechnical and Geoenvironmental Engineering*, 138: 757–762.

- Topp, C., Resource, L. and Canada, A. (1980) *Electromagnetic Determination of Soil Water Content*, 16 (3): 574–582.
- Topp, G.C., Zegelin, S. and White, I. (2000) Impacts of the Real and Imaginary Components of Relative Permittivity on Time Domain Reflectometry Measurements in Soils. *Soil Science Society of America Journal*, 64 (4): 1244.
- Turner, G. and Siggins, A.F. (1994) Constant Q attenuation of subsurface radar pulses. *Geophysics*.
- Valls-Marquez, M. (2009) *Evaluating the capabilities of some constitutive models in reproducing the experimental behaviour of stiff clay subjected to tunnelling stress paths*. PhD thesis, University of Birmingham.
- Valls-Marquez, M., Chapman, D.N. and Ghataora, G.S. (2008) Preparation of k0-consolidated reconstituted samples in the laboratory. *International Journal of Geotechnical Engineering*, 2: 343–354.
- Waxman, M.H. and Smits, L.J.M. (1968) Electrical Conductivities in Oil-Bearing Shaly Sands. *Society of Petroleum Engineers Journal*. 8.
- Wilkinson, P.B., Meldrum, P.I., Kuras, O., et al. (2010) High-resolution Electrical Resistivity Tomography monitoring of a tracer test in a confined aquifer. *Journal of Applied Geophysics*, 70 (4): 268–276.
- Yanuka, M., Topp, G.C., Zegelin, S., et al. (1988) Multiple reflection and attenuation of time domain reflectometry pulses: Theoretical considerations for applications to soil and water. *Water Resources Research*.
- Yu, X. and Drnevich, V.P. (2004) Soil Water Content and Dry Density by Time Domain Reflectometry. *Journal of Geotechnical and Geoenvironmental Engineering*, 130 (9): 922–934.
- Zambrano, C.. E., Drnevich, V.P., Yu, X., et al. (2006) “Soil Texture Characterization from TDR Waveform Analysis.” *In TDR 2006*. Purdue University.
- Zhou, W.-H. and Zhao, L.-S. (2014) One-Dimensional Consolidation of Unsaturated Soil Subjected to Time-Dependent Loading with Various Initial and Boundary Conditions. *International Journal of Geomechanics*, 14 (2): 291–301.